Development of Polymeric Nanostructures Using RAFT Polymerization

A Thesis Submitted for the Degree of

DOCTOR OF PHILOSOPHY

BY

S N Raju Kutcherlapati

School of Chemistry
University of Hyderabad
Hyderabad-500 046
INDIA

December 2016

Dedicated

to

My Family

“There comes a point in your life when you need to stop reading other people’s books and write your own.”

Albert Einstein

DECLARATION

I hereby declare that the matter embodied in the thesis entitled ***"Development of Polymeric Nanostructures using RAFT Polymerization"*** is the result of investigations carried out by me in the School of Chemistry, University of Hyderabad, Hyderabad, India under the supervision of **Prof. Tushar Jana** and it has not been submitted elsewhere for the award of any degree or diploma or membership, etc.

In keeping with the general practice of reporting scientific investigations, due acknowledgments have been made wherever the work described is based on the findings of other investigators.

December 2016

S N Raju Kutcherlapati

Regd. No: 10CHPH24

CERTIFICATE

This is to certify that the work described in this thesis entitled ***"Development of Polymeric Nanostructures using RAFT Polymerization"*** has been carried out by **Mr. S N Raju Kutcherlapati** bearing registration number 10CHPH24 in partial fulfillment of the requirements for award of Doctor of Philosophy in the School of Chemistry is a bonafide work carried out by him under my supervision and guidance and the same has not been submitted elsewhere for any degree.

This thesis is free from plagiarism and has not been submitted previously in part or in full to this or any other University or Institution for the award of any degree or diploma.

Parts of this thesis have been:

A. Published in the following publications:

1. Yeole, N.; **Kutcherlapati, S. N. R.;** Jana, T. *RSC Advances*, **2014**, *4*, 2382. **(Chapter 3)**
2. Yeole, N.; **Kutcherlapati, S. N. R.;** Jana, T. *J. Colloid Interface Sci.*, **2015**, *443*, 137. **(Chapter 4)**
3. **Kutcherlapati, S. N. R.;** Yeole, N.; **G**adi, M. R.; Perali, R.S.; Jana, T. *Polym. Chem.*, **2017,** (DOI: 10.1039/c6py02202b). **(Chapter 5)**

and

B. Presented in the following Conferences:

1. Asian Polymer Association **(APA 2013).** (National)
2. Recent Advances in Polymer Technology **(RAPT-2014).** (International)
3. 4th FAPS Polymer Congress **(4 FAPS-IPC 2015), Malaysia.** (International)

Further, the student has passed the following courses towards fulfillment of course work requirement for Ph.D.:

	Course code	Course Name	Credits	Pass/Fail
1.	CY-801	Research Proposal	3	Pass
2.	CY-805	Instrumental Methods A	3	Pass
3.	CY-806	Instrumental Methods B	3	Pass
4.	CY-842	Chemical Dynamics	3	Pass

Dean
School of Chemistry
University of Hyderabad
Hyderabad-500 046, India

Prof. Tushar Jana
(Thesis supervisor)

PREFACE

The present thesis entitled ***"Development of Polymeric Nanostructures using RAFT Polymerization"*** has been divided into seven chapters. ***Chapter 1*** includes a brief introduction about the importance of various types of polymeric nanomaterials and their synthetic procedures. In particular, an overview of the variety of methods published so far that are used for the preparation of these materials. It also discusses the properties and applications of different polymeric nanomaterials such as colloidal nanoparticles, graphene oxide/polymer nanocomposite, and glyco polymeric nanomaterials. ***Chapter 2*** describes the source of materials, methods and experimental techniques used for working chapters. ***Chapter 3*** deals with a synthetic procedure for the preparation of polystyrene (PS) nanoparticles with a functional polymeric shell on the surface of PS particle with a variation in particle size as well as core-shell dimensions. ***Chapter 4*** demonstrates an *in-situ* method for the development of polystyrene nanocomposites with graphene. ***Chapter 5*** describes the preparation of glycopolymeric particles with core-shell morphology where shell consist the functional glycomonomer with a variation in particle size as well as core-shell dimensions. ***Chapter 6*** deals with the preparation of glycopolymer grafted silica nanoparticles (SiNPs) with different (desired) chain lengths and chain densities and its protein binding investigations. ***Chapter 7*** deals with the preparation of poly(N-vinyl imidazole) grafted silica nanoparticles (SiNPs) with various chain lengths and chain densities and its nanocomposite with polybenzimidazole for the development of proton exchange membrane. ***Chapter 8*** summarizes the findings of the present investigations, presents a concluding remark and the future scopes with future tasks.

December-2016 **S N Raju Kutcherlapati**

ACKNOWLEDGEMENT

I take this opportunity to thanking one and all who were directly or indirectly involved in the successful completion of this thesis

Firstly, I would like to express my sincere gratitude to my advisor Prof. Tushar Jana for his continuous support during my Ph.D. study for his patience, motivation and immense knowledge. His guidance helped me in all the times throughout my doctoral studies. I could not have imagined having a better advisor and mentor for my Ph.D. study. I am also indebted to him for the work freedom during the last five years.

I would like to thank the former and present Deans, School of Chemistry, for their constant encouragement by allowing me to avail all the facilities. I am extremely thankful individually to all the faculty members of the school for their kind help and cooperation at various stages.

Besides my advisor, I would like to thank my doctoral committee members Prof. Anunay Samanta and Prof. Abani K Bhuyan for their insightful comments and encouragement, which incented me to widen my research from various perspectives.

I sincerely acknowledge Prof. Ramu Shridher and Prof. M. J. Swamy, School of Chemistry, University of Hyderabad for providing me the glyco monomers and helping me with protein binding studies for part of my thesis work. I thank Dr. Madhu, Umamaheswara Rao and Diparna Datta for helping for the same.

DST and UoH are acknowledged for providing financial assistance for attending an international conference in Malaysia during my research period. I also acknowledge CSIR-India for my fellowship.

I felt very lucky and proud to have lab mates like Dr. Arindam, Dr. Arun, Dr. Sandip, Dr. Murali, Dr. Mousumi, Dr. Shudhangshu Maity, Dr. Jorphin, Dr. Niranjan, Dr. Jayaprakash, Dr. Bikas, Dr. Shuvra Singha, Dr. Konda Reddy, Dr. Malkappa, Dr. Venkanna, Dr. Ramesh, Narasimha, Bala, Kishor, Rambabu, Moumitha, Suchismitha, Harilal and Nilanjan for stimulating discussions, encouragement and for all the fun we have had in the last five years. Also, I thank my friends in the School of Chemistry; in particular, I am very much thankful to the project assistants who have assisted me throughout my research days.

I also thank Chandu, Bala, Billa, Naidu, Azad and Harilal, who has shared the residence with me, made me joyful after long work hours and tensions after I reach the room. I render my thanks for them as they have supported me in every aspect.

I deeply express my sincere gratitude to all my teachers starting from the school, to the college and to the University for teaching me all the discipline, values and education throughout my academic career. My heartfelt gratitude to Rajendra sir (HM), Hanuman Raju sir, Ramesh Raju sir, KBR sir, Ramakrishna sir and Nagamani madam for their support and encouragement to reach this stage. Without their guidance, may be, I can't reach these heights.

I render my special thanks to all the non-teaching staff for their timely help. I thank Mr. Thurab Syed, Smt. Vijayalakshmi and Mr. Durgesh for their help in recording NMR spectra. I thank Mr. Shetty, Mr. Vijay Bhaskar, Mr. Dilip, Mr. Sai, Mr. Sharma, Mr. Jayaram, Mr. Sunil, Mr. Pankaz, Mr. Durgaprasad. Mr. Shetty, Mr. Joseph, Mr. Sambashiva Rao and Mr. Venkatesh for their cooperation during the tenure of my Ph. D.

I am really fortunate for have closest friends like Kishore Pawar, Chandu, Ashok, Sudheer, Naidu, Srinu, Keshav, Venky, Sunil, Durgaprasad, Sunil(FESEM), Shamugan, Edukondalu, TRN Prasad, Suresh, Krishna, Ramakrishna, Arjun anna, Krishna, Ramudu, Venkatesh, Murali, Ramana, Shekthivel, Ganesh, Obaiah, Sesi anna, Vikranth, Anup, Babu, Narendra, Srujana, Lasya, Hari, Guptha, Nabindo, Sudheer, Anil, Chaitanya, Geetha, Krishna Reddy, Rudra, Sugatho, Ramesh, Chitti, Uday, Ramakrishna, Yasin and Pavan in HCU with whom I have some wonderful memories in Hyderabad throughout my Ph.D. life.

I would also like to express my sincere thanks to all my close friends Vijay, Neela, Prudhvi, Nagaraju, Rudra, Suresh, Lalitha, Anji, Satish, Varma, jyothi, Pramila, Prasad Raju, Madhu, Ramakrishna, Varma, Venkatapathi, Satya Krishna, Srinu, Varma, Lakshman, Srinivasa Raju, Chittaranjan, Caitanya, Ram Varma, Munny, Vamsi, Gopi, Krishnam Raju, Siva, Arun, Rajesh, Harika, Madhu, Santosh, Durgarao, Vinay, Rachana, Hyndu, Pradeep, Venkat reddy, Arun, Shiva, Srinivas and Satynaraya for their help and encouragement in various stages of my life.

The list will not be completed without acknowledging my favorite place, Bhimavaram where I have stayed valuable five years for my graduation and post-graduation, I owe to my hostel, KVSS for giving me free accommodation and food for these five years with a top class infrastructure and also for giving me some best friends. I sincerely acknowledge Ramalinga Raju garu, Narasimha Raju garu, Ramachandra Raju garu, Venkata Ramaraju garu, Jagga Raju garu, Gokaraju Gangaraju garu, total Datla family members and KVS samithi Hyderabad as well as Chanti Raju garu, Gopi garu, Srinu garu, Murali garu, Surya Narayana garu and Peddiraju mamayya for helping financially and supporting me in various stages of my studies.

Above all, it is the endless love, sacrifice and prayers of Mother, Father, Brother(s), Sister(s), Brother-in-law(s), My darlings (Siri and Sai), Chinnanna, Pedananna, my in-laws, my love (My wife Vaishnavi) and all the family members and well-wishers. I must express my very profound gratitude to them for providing me with unfailing support and continuous encouragement throughout my years of study and through the process of researching and writing this thesis. This accomplishment would not have been possible without them.

December, 2016
University of Hyderabad
Hyderabad-500 046, India

S N Raju Kutcherlapati

Common Abbreviations

ATRP	Atom transfer radical polymerizations
CLRPs	Controlled/ Living radical polymerizations
DMAc	N,N-dimethyl acetamide
DMF	N,N-dimethyl formamide
DSC	Differential Scanning Calorimeter
DLS	Dynamic Light Scattering
FT-IR	Fourier Transform Infrared Spectroscopy
FESEM	Field Emission Scanning Electron Microscopy
GO	Graphene oxide
GP	Glyco polymer
GPC	Gel Permeation Chromatography
M_n	Number Average Molecular Weight
M_w	Weight Average Molecular Weight
MW	Molecular Weight
NMP	Nitroxide mediated polymerization
PS	Polystyrene
PDI	Polydispersity Index
PNVI	Poly(N-vinyl imidazole)
RAFT	Reversible addition-fragmentation chain transfer polymerization
RGO	Reduced graphene oxide
SiNP	Silica nanoparticles
TEM	Transmission Electron Microscopy
T_g	Glass transition temperature
TGA	Thermogravimetric analyzer
WAXD	Wide-angle X-ray diffraction

CONTENTS

Chapter 1

Introduction

INTRODUCTION

This thesis focuses on the development and investigation of polymer bound interfaces on nanoparticles with advanced architectures to tailor the properties of polymer for various applications. Reversible addition-fragmentation chain transfer (RAFT) polymerization and a toolbox of surface functionalization were utilized to prepare polymeric nanomaterials. The thread which connects all the chapters of this thesis is the RAFT polymerization. This introductory chapter describes various types of polymeric nanomaterials and the involved synthetic methodologies at the outset and then delves into the detailed utility of these materials in a variety of fields. In the following chapters, I will investigate the role of RAFT polymerization to construct different nanoscale materials. New synthetic procedures were established and exploited to understand the involved chemistry in detail.

1.1 History of Polymers

Polymers have been with us since the beginning of time. Though the word sounds complicated, they are a part of everyday life. Natural polymers such as tar and shellac, tortoise shell and horns, as well as tree saps that produce amber and latex exist in nature. The synthetic polymers are the polymers used by us for our day to day life which range from the plastic bags and bottles to materials which can protect astronauts while they are in space. The term polymer is obtained from the Greek words: poly means many, and mer means parts are built up by covalent linking of a large number of much smaller molecules generally called as monomers. A polymer may consist of hundreds, thousands, tens of thousands or more monomer (or more monomers) molecules.[1] Until World War II, natural substances were generally available and therefore synthetic polymers that were being developed were not an essential. The richness and sustainability of life have improved quite significantly due to the vast utilization of polymer science and technology.

1.2 Synthesis of Polymers

1.2.1 Free Radical Polymerization

Free-radical polymerization (FRP) is also called as conventional free radical polymerization (CFRP). In this polymerization, an initiator is used to produce free radicals that can initiate polymerization by the addition of monomeric units. Thermal dissociation of the initiator is the most widely used radical generation. In the initial stages of the polymerization reaction, the chain which is initiated by the initiator fragment continues to

propagate by the addition at monomeric units until chain growth is terminated. The termination may occur when two propagating chains meet and undergo bimolecular termination or when the propagating chain transfers its radical to another species (e.g. to monomer, polymer, solvent, chain transfer agent, etc.) resulting in the formation of dead chains. The term "dead" stems from the fact that these chains have lost their active center and cannot add monomer units unless chain transfer to these dead polymer chains takes place.[1,2]

1.2.1.1 Mechanism and Kinetics of CFRP

The mechanism of CFRP involves a series of chain reactions where the fast growth of polymer chains through subsequent addition of monomers to an active center (initiator fragment) at the end of the chain is the main characteristic feature. Four steps: initiation, propagation, chain transfer and termination which are involved in the CFRP is shown in Figure 1.1.[3,4]

Initiation involves the addition of the initiator radical (which comes from the dissociation of initiator) to the first monomer molecule to produce the chain initiating radical. ***Propagation*** occurs when an initiator activates the polymerization, monomer molecules are added one by one to the active chain in the propagation step and a new reactive site is generated after each addition of monomer. ***Transfer*** reactions can occur between a propagating chain and a molecule of monomer or transfer agent or initiator or solvent. The transfer reaction produces one dead chain and a new small radical that may or may not be efficient in reinitiating the polymerization. ***Termination*** occurs via coupling reactions of two active centers (referred to as combination), or atomic transfer between active chains (termed disproportion).

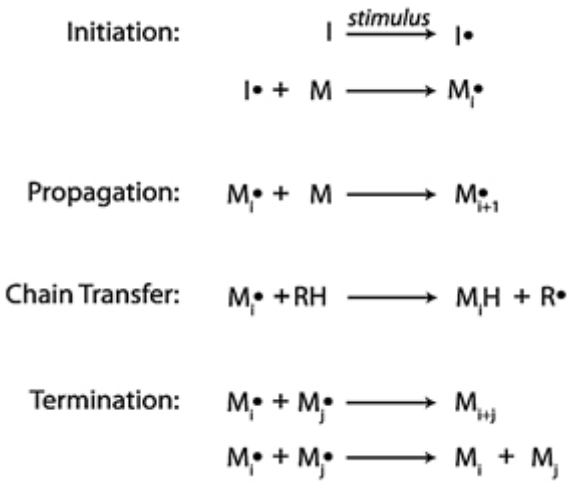

Figure 1.1. *Schematic representation of the free radical chain process* in CFRP.[3]

Where $M_i^{\bullet}$ represents a free radical capable of initiating propagation, M denotes monomer, $M_i^{\bullet}$ and $M_j^{\bullet}$ refer to propagating radical chains with degrees of polymerization of i and j, respectively. RH is a chain transfer agent, and $M_i + M_j$ represent terminated macromolecules. Because chain transfer may occur for every radical at any and all degrees of polymerization, the influence of chain transfer on the average degree of polymerization and on polydispersity, which cannot be neglected.

Furthermore, in CFRP, each chain grows very fast in the early stages of polymerization, and this eventually leads to the formation of the dead polymer as one of the chain stoppage events take place. The timescale for chain growth may be in the order of seconds or even less. Therefore, a variation of polymerization conditions over this short timescale for chain growth is very difficult, resulting in a poor or very limited control over the molecular weight, its distribution and polymer architecture.

1.2.2 Free Radical Polymerization Methods

The reactions through which free radical polymerizations are carried out are broadly divided into two main types, namely homogeneous and heterogeneous reactions.[5] Solution and bulk polymerizations are come under homogeneous processes, while emulsion polymerization is a heterogeneous process. These polymerization techniques are described in the following section.

1.2.2.1 Bulk and Solution Polymerizations

In bulk polymerization (also referred as mass polymerization), the ingredients are a monomer-soluble initiator, a monomer, and a polymer. All these are present in a single phase (homogeneous polymerization) without any solvents or dispersion media. Bulk polymerization offers the simplest polymerization process among the others with minimum contamination of the product. However, the combination of the highly exothermic nature of the free radical addition reaction as well as the gel effect makes the heat dissipation difficult[5] and therefore, a careful temperature control is required. Furthermore, the viscosity increases with monomer conversion making stirring and heat transfer inefficient. This may cause an auto-acceleration and reactor thermal runaway, which requires strong and elaborate stirring equipment to overcome such problems. Due to these difficulties, bulk polymerization is not commercially or widely used technique for chain polymerization. However, these difficulties can be bypassed by reducing the reaction conversion with the separation and recycling of unreacted monomer.

Solution polymerization (polymerization in a solvent) overcomes many of the difficulties faced by the bulk polymerization. In solution polymerization, solvent acts as a diluent to reduce the viscosity of the reactions and aiding good heat transfer. It ensures better heat control and proper mixing. On the other hand, the presence of the solvent may impart new difficulties such as chain transfer to the solvent may lead to reducing the degree of polymerization. Therefore, the careful selection of the appropriate solvent is crucial.[6] In addition, further processing is required in order to extract the solvent from the final products where complete extraction of the solvent is difficult and economically impractical. Thus solution polymerization is also commercially unattractive.

1.2.2.2 Emulsion Polymerization

Emulsion polymerization is an extensively used process for the production of polymer latex products and is an important polymerization process on industrial scale.[7] Emulsion polymerization produces approximately 90% of polymer dispersions in the industry and has been used since the 1930's. It is a preferred method of polymerization compared to other methods from an environmental perspective since the continuous phase is aqueous, and therefore uses less solvent and emits fewer volatile organic compounds (VOC). The low viscosity (water-based) provides excellent heat transfer for improved temperature control. High molecular weight polymers can easily be produced at higher polymerization rates compared to other methods of polymerization and the main interesting aspect is that the final product can be used as produced without any exhaustive purification or modification.[8]

Emulsion polymerization is a free-radical mechanism and it is a heterogeneous polymerization system. Oil-in-water is the most common type of emulsion polymerization where the monomer (oil phase) is emulsified within the continuous aqueous phase. The typical ingredients within a conventional emulsion polymerization system are the water-immiscible monomer(s), a water-soluble initiator (such as potassium persulfate, KPS), the dispersion medium (typically water), and the surfactant(s) (also termed as emulsifier).[9]

1.2.2.2.1 Mechanism and Kinetics of Emulsion Polymerization

At the start of emulsion polymerization, the surfactant is added to emulsify the monomer with agitation into droplets, having diameters of tens of micrometers in the continuous phase. With a surfactant concentration greater than the CMC, micelles will also form in the continuous phase and some monomer will diffuse into the hydrophobic centers of

the micelles. Although the monomer is considered hydrophobic, a small amount will still dissolve in the aqueous phase, which is crucial for emulsion polymerization to be successful. The decomposition of the water-soluble initiator from the rise in the temperature leads to the formation of primary radicals which react and propagate with the small amount of monomer dissolved in the aqueous phase. As these chains become longer, they become insoluble in water and are captured within the organic (hydrophobic) center of micelles leading to the formation of a polymer particle. The polymer particles continue to grow as the monomer continues to diffuse from the monomer droplets through the aqueous phase. The concentration of monomer within the particles continues to decrease as polymerization causes the conversion to increase, which is also accompanied by a drop in the rate of polymerization.[10] A schematic representation of the mechanism of emulsion polymerization is illustrated in Figure 1.2.

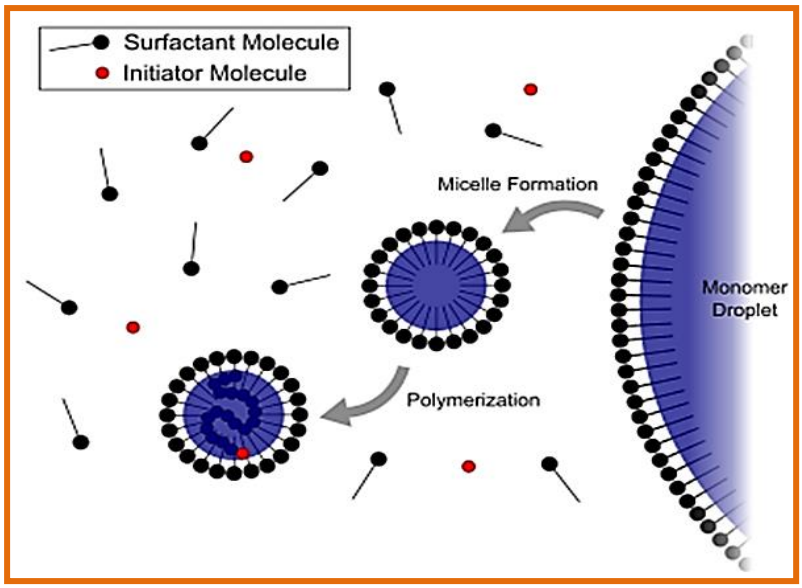

Figure 1.2. *Schematic representation of emulsion polymerization.*[9]

1.2.2.2.2 Advantages of Emulsion Polymerization

The advantages of emulsion polymerization over the other methods such as bulk or solution polymerization are as follows:

- At a given temperature, emulsion polymerization is faster than either bulk or solution polymerization.
- In a given conditions, the molecular weight increase is high in emulsion polymerization than similar bulk polymerization. The high molecular weight of

polymers are due to the initiator decomposes in one phase (the aqueous) while polymerization occurs in another (the micelles).

- Emulsion does not require a vigorous mechanical separation that is necessary for suspension polymerization.
- Unlike traditional bulk polymerization there are no (a very limited) unreacted monomer leftovers, means the latex can be used without vigorous further purification. This is very important for paints and coatings. Just some color needs to be added to the latex and it's ready to use.
- An excellent heat control than the other polymerizations
- Control over initiation, propagation, chain transfer and termination reactions are easy (when compared to other methods) due to low polymerization temperatures (0-80°C) are involved.
- High rates of polymerization can be obtained simultaneously with a high degree of polymerization.
- In contrast to solutions of polymers, thus high polymer concentrations can be obtained at low viscosity.
- Since the medium involved is invariable water, the uses of expensive solvent and consequent recovery problems are eliminated. A secondary factor in some cases is that the fire risk is reduced.
- Work up of the polymer when there is a need of solid polymer is very easy. The latex can be simply coagulated in an appropriate manner and then wash with water or other aqueous solutions, pressed and dried.

1.2.2.2.3 Disadvantages of Conventional Emulsion Polymerization

The main disadvantage of emulsion polymerization is the presence of emulsifier or surfactants which are added to the system to enable the formation of micelles and becomes the backbone of the system. Removal of the surfactant from the system is the main bottleneck and time consuming and needs to be done by repeated washings. Once the latex is formed and it hardens, some of the surfactant particles are entrapped and it becomes very difficult to remove them. Again, the high residual impurity level influences certain polymer properties. The presence of the surfactant is a disadvantage of certain applications of emulsion polymers such as those involving instrument calibration and pore size determination. The presence of

adsorbed surfactant can vary with the polymerization and application condition. Removal of the surfactant, on the other hand, can lead to coagulation or flocculation and destabilized latex. Thus, there is a need for an emulsifier-free (surfactant free) emulsion polymerization system where it should have advantages like emulsion process and should address the aforementioned issues.

1.2.2.3. Surfactant-free Emulsion Polymerization

Surfactant-free emulsion polymerization (SFEP) (also known as emulsifier-free emulsion polymerization or soap-free emulsion polymerization) is a type of emulsion technique that is executed without the addition of a surfactant in the formulation. The typical recipe for SFEP is generally similar to a conventional emulsion polymerization, involving the use of water-insoluble monomer(s), a water-soluble initiator, and an aqueous dispersion medium. In this type of system, it is generally agreed that the oligomers formed during the initial stages of polymerization act as "*in-situ* formed" surfactants, aiding in the stabilization of particles during and after polymerization. On the other hand, some systems of SFEP also use ionic comonomer(s) in the experimental formulation. After polymerization, stability can be provided solely by the electrostatic charge provided by the initiator's ionic groups, or an ionic comonomer can also be used to increase the latex stability during and after polymerization.[11]

It is observed that the nucleation mechanism of SFEP is more complex than conventional emulsion polymerization.[12] Without the use of surfactant, no micelles are present within the system initially, so it is disputed that the micelle nucleation is not considered as an appropriate mechanism for the generation of polymer particles at the start of the reaction. Given the complexity of the system, resolving the particle nucleation mechanisms continues to be a great challenge to scientists in this area of research.[13]

One theory, that commonly discussed is a coagulative nucleation theory, where nucleation occurs through the precipitation of oligomers/oligo radicals.[11] During the start of SFEP, the decomposition of the water-soluble initiator leads to the generation of hydrophilic radicals which then react to form oligomer radicals (oligo radicals). When these *in-situ* formed oligo radicals reach a critical chain length, they become insoluble in the water phase, and it is postulated that they coagulate together to form the initial polymer particles with very small

diameters.[14, 15] These unstable particles continue to coagulate together until the electrostatic charge at the surface is sufficient for particle stabilization.

1.2.2.3.1 Advantages of Surfactant-free Emulsion Polymerization

These can be summarized as

- The polymer synthesized has low viscosity and have high molecular weight at high rates.
- Latexes prepared by this process are stabilized by the chemically bound groups obtained from the initiator. Since the surface-active groups are chemically bound, the lattice can be easily purified without loss of stability.
- They have good thermal control and are operable with soft or waxy polymers.
- The particle number is generally lower by up to about two orders magnitude compared to the typical emulsion polymerization, typically 10^{12} versus 10^{14} particles per mL. This is a consequence of the lower total particle surface area that can be stabilized by the sulfate groups alone relative to that when added surfactant is present.

Although CFRP (as discussed above) is a very dominant, fast and economical technique for polymer synthesis, it permits very little control over the molecular weight and its distribution and the structure of the polymer chain. Also, the synthesis of sophisticated and complex macromolecular architectures such as block copolymers, star polymers or comb polymers or higher order is not possible with CFRP. A suitable way to control the polymer structure efficiently during its synthesis is a living process in which almost all of the growing radicals are protected from termination reactions.

1.2.3 Controlled/Living Radical Polymerization (CLRP)

Synthesis of polymers with well-defined architectures, compositions, and functionalities has long been of great interest to polymer chemists. Syntheses of polymers *via* radical routes are well studied and are being used extensively in academics and industries. Though the CFRP is of enormous industrial importance since approximately 50% of all commercial polymers are produced by using the CFRP method, [16] the high reactivity of the propagating radicals and there is a probability of undergoing bimolecular termination, transfer reactions to monomers, and other side reactions limit the applications of CFRP.

Although living anionic polymerization (LAP) method [17] offers high levels of control in terms of well-defined polymers as well as precise molecular architectures, but due to intolerant to functionality and impurities, this method is less flexible than radical

polymerization. Thus in the field of polymer chemistry, it has been a long-standing goal to develop a process that should have the strength as free radical polymerization with the control and precision offered by living anionic polymerization. Controlled radical polymerization (CRP) method or control living radical polymerization (CLRP), offers levels of control and precision almost as good as those of LAP method while maintaining the strength of a CFRP method in terms of tolerance and flexibility.

These CRPs are classified into three different subgroups: (1) stable free-radical polymerization such as nitroxide mediated polymerization (NMP),[8, 19] (2) degenerative transfer polymerization, such as iodine transfer polymerization (ITP),[20,21] single electron transfer-degenerative transfer living radical polymerization (SET-DTLRP),[22,23] reversible addition-fragmentation chain transfer (RAFT),[24,25] macromolecular design *via* the interchange of xanthates (MADIX)[26,27] polymerization, and (3) metal mediated polymerization, such as atom transfer radical polymerization (ATRP),[28,29] single electron transfer living radical polymerization (SET-LRP),[30] and organotellurium mediated living radical polymerization,[31] organostibine-mediated polymerization (SBRP),[32] organocobalt-mediated radical polymerization (CMRP).[33]

Among the existing CRP techniques, maximum work has been carried out using ATRP, NMP, and RAFT methods. Each of these techniques is briefly discussed below involving the use of an initiator, transfer agent, and terminators to control chain termination of the classical free radical process.

1.2.3.1 Atom Transfer Radical Polymerization (ATRP)

In ATRP, a transition metal complex is used as a controlling agent in the equilibrium process. Transition metal complex (Mt^nY/L) is used as an activator and is responsible for homolytic cleavage of alkyl halide bond (R-X) through a reversible redox process. The growing radicals ($R^{\bullet}$) react reversibly with the transition metal in its higher oxidation state ($X-Mt^{n+1}Y/L$) as a deactivator to form dormant species. This equilibrium is conducted with the rate constants of k_{act} and k_{deact} for activation and deactivation reactions, respectively. The probability of bimolecular termination reactions is reduced and polymerization resembles a living system when $k_{deact} >> k_{act}$ and the rate of initiation is much more than the rate of propagation (Figure 1.3). In this scheme, k_t and k_p represent the termination and propagation rate constants, respectively. Also, the dead chains resulted from the combination of radicals,

disproportionation between growing radicals, and abstraction of hydrogen atom by a growing radical are symbolized by R-R, $R^{=}$, and RH.[34]

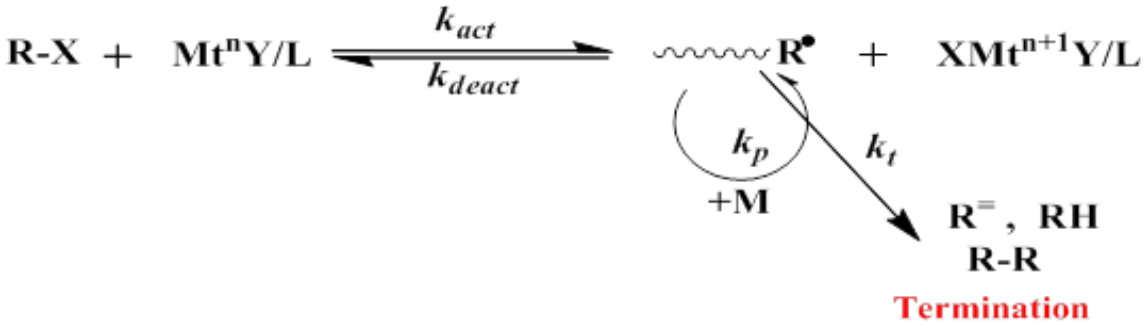

Figure 1.3. *Mechanism of Atom transfer radical polymerization.*[34]

1.2.3.2 Nitroxide-Mediated Polymerization (NMP)

In NMP, alkoxyamines are used as dormant species to control the polymerization process via a dynamic equilibration between them and propagating radicals. Stable free radicals like 2,2',6,6'- tetramethylpiperidinyloxyl (TEMPO) used in this technique, has to be stable to some extent and also should not participate in side reactions such as the abstraction of β-H atoms and also they should not react with themselves or monomers. Mechanistically, the formed active radicals after decomposition of dormant alkoxyamines with the rate constant k_d can propagate by adding monomer units or recombined with the stable nitroxide radicals to form dormant species with the rate constant of k_c (Figure 1.4). However, side reactions such as thermal initiation, biradical termination, and alkoxyamine decomposition to yield terminally unsaturated polymer and hydroxylamine are possible.[35]

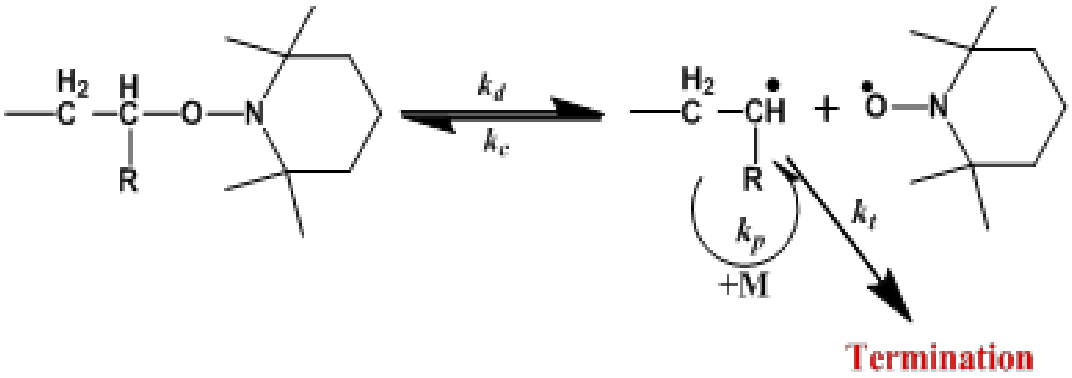

Figure 1.4. *Mechanism of Nitroxide mediated polymerization.*[35]

1.2.3.3 Reversible Addition-Fragmentation Chain Transfer (RAFT) Polymerization

The RAFT process was invented at the Commonwealth Scientific and Industrial Research Organization (CSIRO) in 1998 and became one of the most convenient and versatile techniques for preparing living polymers with low polydispersity and predictable molecular weights. [36-38] The RAFT process utilizes classic free radical initiators and monomers along with the presence of a RAFT agent based on the dithiocarboxylate moiety as shown in Figure 1.5.

In recent years RAFT polymerization has emerged as a very attractive method for producing pseudo-living free radical polymerizations. [39,40] The main potential of RAFT polymerization lies in its versatility towards the types of monomers which can be polymerized including styrenic, (meth)acrylamides, (meth)acrylates, acrylonitrile, vinyl acetates, vinyl formamide, vinyl chlorides as well as a range of other vinyl monomers. [41] Another advantage of the RAFT process is that it is carried out under the same conditions as a classic free radical polymerization except with the addition of a chain transfer agent (CTA, also referred as a RAFT agent). As a result, RAFT polymerization has been carried out in bulk, solutions (aqueous or organic), suspensions, emulsions, mini and microemulsions, and also ionic liquids and can be carried out at low temperatures.[42,43] In addition to simple homopolymers, a large variety of macromolecular structures have been synthesized via RAFT including statistical, block, multiblock, gradient, and comb copolymers, telechelic (co)polymers, star, hyperbranched, and network (co)polymers etc (Fig.1.6).[44-45]

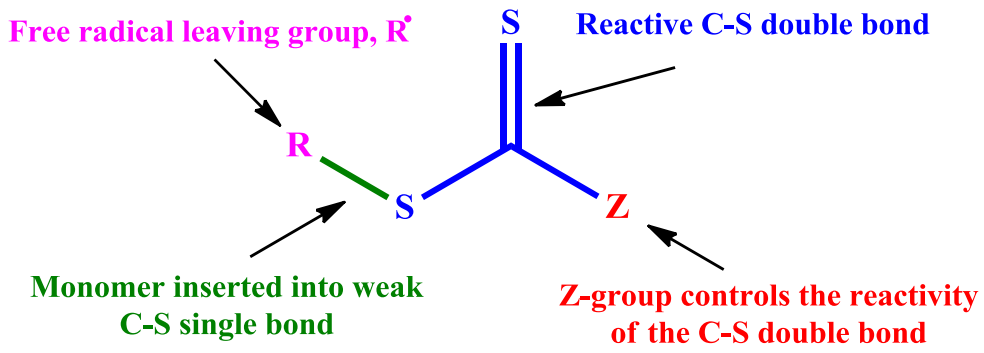

Figure 1.5. *The generic structure of Reversible addition fragmentation chain transfer (RAFT) polymerization moiety.*

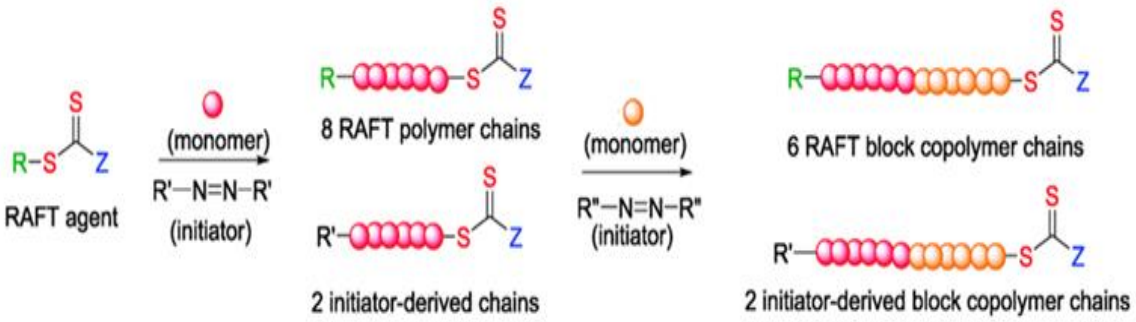

***Figure 1.6**. Synthesis of homo and block copolymers using Reversible addition fragmentation chain transfer (RAFT) polymerization.*[37]

1.2.3.3.1 The RAFT Mechanism

The RAFT mechanism is shown in Figure 1.7. Unlike other controlled free-radical polymerization techniques, RAFT polymerization uses a conventional free-radical initiator. Radicals initiated from this initiator can either add to the S=C moiety of RAFT agent or can add to the monomer to form a propagating radical which in turn can add to RAFT agent. A labile intermediate radical 2 is produced, which can fragment back towards the starting materials or, can form a temporarily deactivated dormant polymer species 3 together with a radical R• resulting from the RAFT agent. This radical should then add to monomer, thereby reinitiating the polymerization. An important feature in the RAFT mechanism is that the dithiocarboxylate moiety S=C(Z)S- which is present in the initial RAFT agent 1, is retained in the polymer chain 3. As the dithiocarboxylate moiety is retained in the polymer chain 3, the dormant polymer chains can act as transfer agents themselves (generally called as macro-RAFT) as is shown in reaction (c) of Figure 1.7.

Like in Figure 1.7 reaction (c), a propagating radical reacts with the polymeric RAFT agent 3. During this reaction, the propagating radical transforms into a dormant polymer, while the polymer chain from the polymeric RAFT agent is released as a radical capable of further growth and similar to reaction (a), the dithiocarboxylate moiety is retained and the newly formed dormant species can again be reactivated.

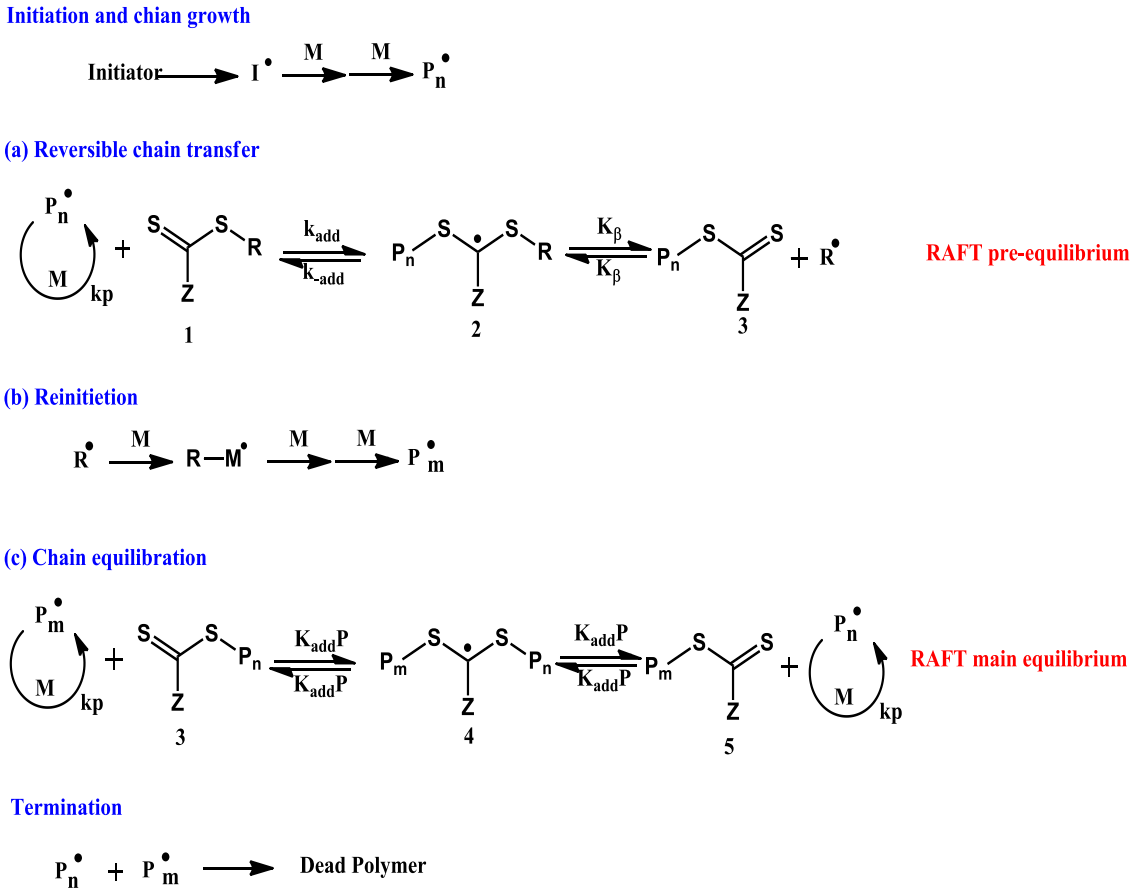

Figure 1.7. *Mechanism of Reversible addition fragmentation chain transfer (RAFT) polymerization.*[39]

For RAFT polymerizations to follow the rules of controlled/living polymerizations, a few aspects of the reaction scheme are very important. Exchange reaction (c) should be rapid compared with propagation. As it can be deduced from the symmetrical structure of intermediate species 4, there is no preference for the direction of fragmentation and the probability of formation of P_n• or P_m• is equal. Assuming that the transfer is fast compared to propagation the radical is exchanged rapidly among the chains and all chains have equal probability to add monomer, and thus all chains will grow at the same rate. To achieve the final molecular weight distribution with a low polydispersity, all chains should start growing at the start of the reaction. For this, the initial change of RAFT agent 1 into dormant polymer species 3 [exchange reaction (a) in Figure 1.7] should be rapid. In this reaction, the intermediate radical 2 is not symmetrical, so the R group needs to be chosen in such a way that

it should be a better homolytic leaving group than the oligomeric polymer chain. Another important aspect concerning the R group is its ability to reinitiate polymerization. If the barred radical R$^{\bullet}$ only adds to monomer slowly, then inhibition and retardation may occur. Most notably, during the early stages of the polymerization, the slow conversion of the transfer agent results in a broadened molecular weight distribution.

It is highly important that a constant number of chains are propagating throughout the reaction. If not, the chains that start growing at a later stage of the polymerization will have different chain lengths from the main part of the material. The concentration of chains at the beginning of the polymerization is equal to the initial concentration of RAFT agent. For all polymer chains to carry the RAFT moiety up to high monomer conversions, the initiator concentration needs to be considerably smaller than the RAFT agent concentration. In some cases, polymerization times can be significantly long due to this very low initiator concentration. This can be the case for recipes with very low RAFT agent concentration for getting higher molecular weights.

1.2.3.3.2 RAFT Moieties

The organic compounds that are used to mediate the RAFT polymerization are based on the dithiocarboxylate moiety. A wide variety of RAFT agents with different Z and R groups have been synthesized and evaluated for their effectiveness in controlling the polymerization of various vinyl monomers.[46,47] RAFT agents, in general, can be subdivided into four classes according to the activating Z-group. These are dithioesters[48,49] xanthates[50] dithiocarbamates[51] and trithiocarbonates[52] as shown in Figure 1.8. Some of the more versatile RAFT agents are 4-cyanopentanoic acid dithiobenzoate (CPDB) and benzylsulfanylthiocarbonylsufanylpropionic acid (BSPA) that were used in this thesis.

Figure 1.8. Various *types of RAFT agents.*[38]

Dithioesters, more specifically dithiobenzoates and dithioacetates were the first compounds to be used as RAFT agents.[48,49] Generally, dithioesters based RAFT agents exhibits higher activity than trithiocarbonates, xanthates, and dithiocarbamates but they suffer from some serious drawbacks compared to other RAFT agents. Dithioesters have an intense pink to dark red color and also have a very offensive odor. Moreover, dithiobenzoates cause severe retardation in the polymerization of monomers like styrene and acrylates [51, 53] Rhodia et al. firstly introduced xanthate based RAFT agents[50] which are easier to synthesize than dithioesters. Another advantage of xanthates is that they are colorless and have an odor that is far less offensive than that of dithioesters. However, their transfer constant is rather low, yielding polymers with higher polydispersy Index. Trithiocarbonates were designed as RAFT agents for the synthesis of triblock copolymers.[54,55] Only two polymerization steps are required to form triblock copolymers and chain extension. In trithiocarbonates, the role of the activating group is taken by the alkyl-S- moiety. Trithiocarbonate RAFT agents generally have a high transfer constant. The general guidelines for selection of RAFT agents for various polymerizations have been presented in Fig. 1.9.

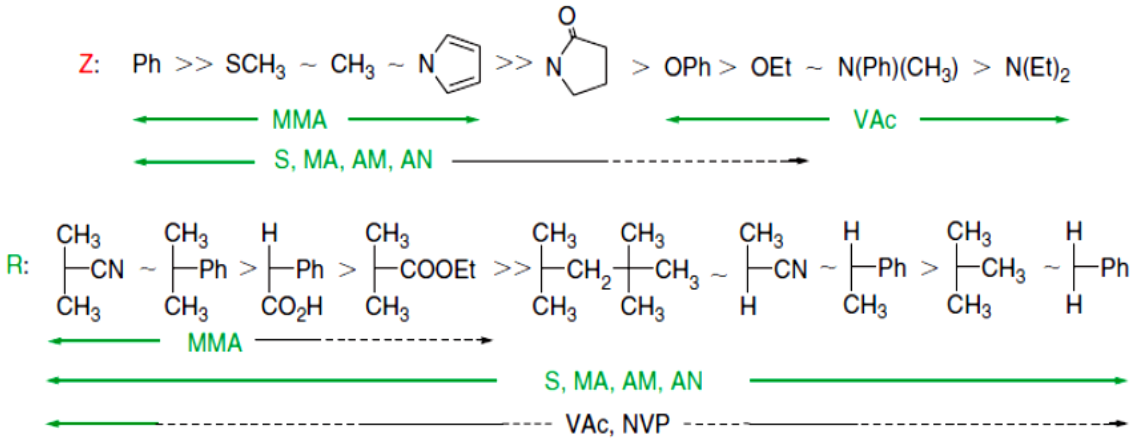

Figure 1.9. *The general guidelines for selection of RAFT agents for various polymerizations. For Z, addition rates decrease and fragmentation rates increase from left to right. For R, fragmentation rates decrease from left to right. Dashed line indicates partial control.*[49] *(i.e. control of molecular weight but poor polydispersity or substantial retardation in the case of VAc or NVP).*

1.2.3.3.3 The Major Strengths of the RAFT Technique

The advantage in terms of the major strength of RAFT are listed below

- ✓ An ability to control the polymerization of a number of monomers in various solvents, including water. It uses only chain transfer agents and common free radical initiators (without the need of metal catalysts).[14,48]
- ✓ Found tolerant to a wide variety of functional groups which allows the facile synthesis of polymers with pendant, and end-group functionalities at alpha and omega chain ends (important for biological applications).[56,57]
- ✓ A wide variety of architectures such as telechelic, block copolymers, graft copolymers, stars, gradient copolymers, and dendritic structures can be synthesized (as shown in Figure 1.10).[49]
- ✓ Found compatible with a variety of established polymerization methods such as bulk, solution, suspension,[58] emulsion,[49] and dispersion[59] polymerizations.
- ✓ RAFT method has the ability to perform polymerizations from a wide variety of substrates, allowing the modification of surfaces and the in situ generation of polymer conjugates.[60]

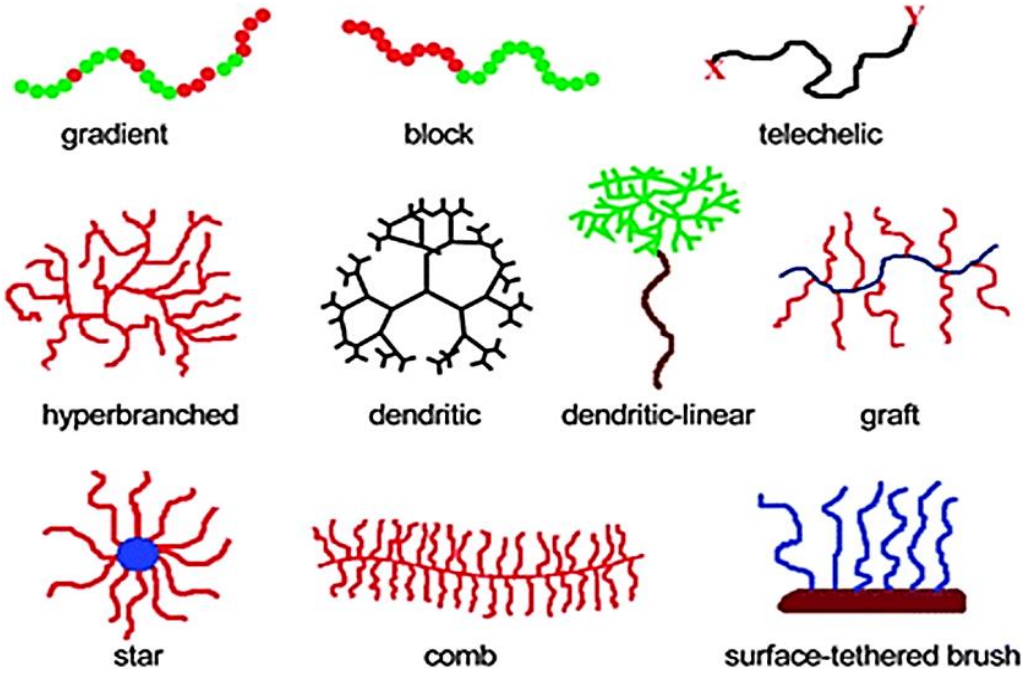

Figure 1.10. *A variety of architectures can be made using RAFT polymerization.*[49]

1.3 Nanomaterials

Nanoscience and nanotechnology deal with the development and understanding of materials with at least one of its dimensions in less than 100 nm and these are often called as nanomaterials (Figure 1.11). These nanomaterials have been found to have a better property which is significantly different than that of the compositional atoms as well as corresponding macroscopic materials.[61,62] The most interesting thing is that the properties of materials change as their size approaches the nanoscale as the percentage of atoms at the surface of material increases and it becomes more significant.

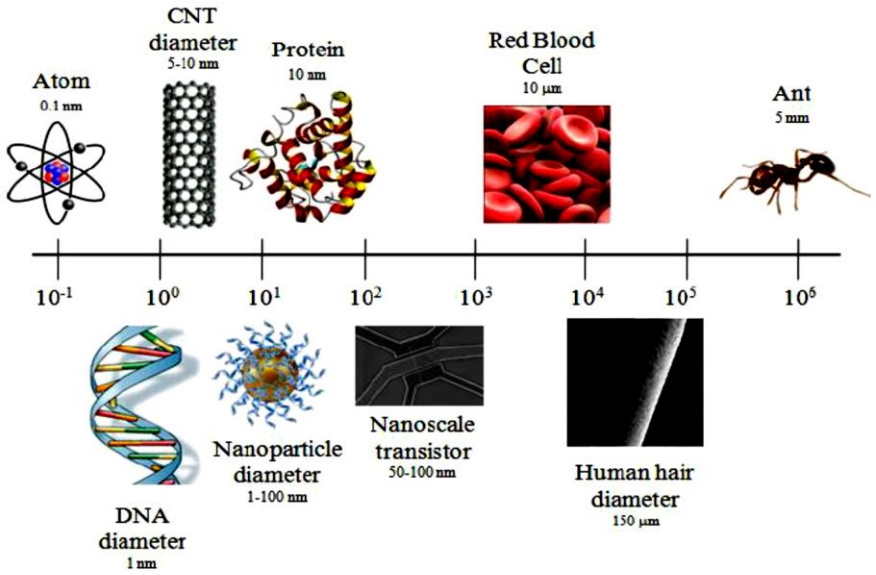

Figure 1.11.*The nanoscience scale length (1–100 nm) and its comparison with smaller (atomic) and larger (macroscopic) structures.* [63]

Nanoparticles, with all the three dimensions in nanoscale, is the most talked about current form of nanomaterials and their remarkable properties have been extensively utilized for various multidisciplinary applications in sensing, photonics, catalysis, biomedical, electronics etc (Fig. 1.12).[64-67] For example, gold nanoparticles are being used to enhance electroluminescence and quantum efficiency in organic light-emitting diodes,[68]palladium, and platinum nanoparticles are used as efficient catalysts,[69] glucose sensors are developed based on silver nanoparticles[70] and iron oxide nanoparticles are used as contrast agents in diagnosing cancer in Magnetic Resonance Imaging (MRI).[71] Even though the nanoparticles have its applications in various fields due to it's inherent properties, however, these properties have to

be modulated to another extent by the use of surface chemistry to improve the applicability or to make use these nanoparticles in many other fields.

The surface of the nanoparticles can be modified with ligands a molecule of interest such as antibodies, aptamers, and peptides to recognize specific receptors on the cell surface. These receptors should be overexpressed in the diseased cells but not on normal cells in order to increase specificity.

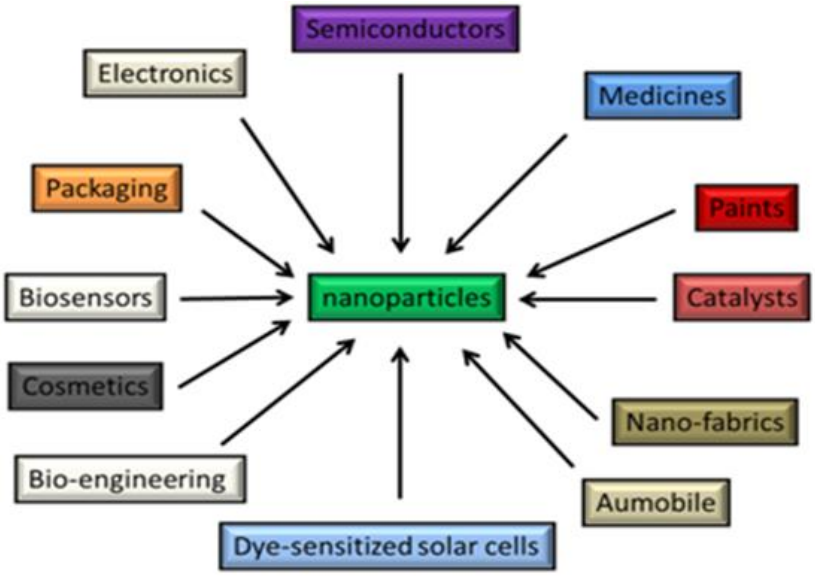

***Figure 1.12**. Applications of nanoparticles in different fields.*[64]

The surface of the nanoparticles can also be modified with synthetic polymers with well-defined properties for the target applications in various fields. Advances in the preparation, size control, surface modification and encapsulation capabilities of nanoparticles make them an ideal carrier for chemical drugs and biomolecules.

1.3.1 Nanoparticles in Drug Delivery

Most of the drugs, mainly anticancer drugs, are highly lipophilic, and unstable in aqueous media and hence become less potent because of its decomposition through hydrolysis. The use of such drugs can cause numerous side effects because of the diffusion of these small drugs a toxic side product across the cell membranes all over the body even though that is not the target of the drug. Therefore, researchers have been aiming for the development of polymeric materials especially in the form of nanoparticles to improve their properties like

solubility and to serve as drug carriers for targeted delivery. In order to protect the drug during circulation and release under specific conditions, polymeric drug carriers should (i) be capable of encapsulating lipophilic drug molecules within their core, (ii) possess a desirable size to achieve targeting through the Enhanced Permeability and Retention (EPR) effect, (iii) stably encapsulates the guest molecules to prevent premature release, (iv) release their contents in response to a specific stimulus triggered by the target cell environment (Fig. 1.13), (v) have an easily modified surface for conjugation of targeting ligands, (vi) exhibit low inherent toxicity and (vii) have reproducible synthetic methods.

The recent advances in the field synthetic methodologies to prepare nanoparticles with controlled size, surface modification, and encapsulation capabilities and advanced characterization techniques made possible for exploring its applications in numerous fields. In the current case, we have chosen silica nanoparticles as a model for exploiting its applicability to a step forward and will be discussed in the later section.

Figure 1.13. *Nanoparticle-based drug delivery with different stimuli.*[66]

1.3.2 Silica Nanoparticles

Among the numerous inorganic–organic hybrid materials, silica–polymer hybrid materials are the most studied in the literature. This may be ascribed to their wide use and in particular due to the ease of synthesis and precise control of the size and distribution of the particles.[72] Silica nanoparticles (SiNPs) have been used as fillers in the manufacturing of paints, rubber products,[73] and plastic binders. Silica particles coated with organic modifiers are used in applications that include stationary chromatography phases,[74] heterogeneous supported catalysts,[75] as well as in automotive, electronics, appliance, consumer goods,[76] aerospace and sensor[77] industries. SiNPs also hold a prominent interest in countless parts of biomedical

research, mainly for imaging, detection, and sensing to drug delivery and therapeutic uses. It is well known that silicon exhibits a low inherent toxicity when compared with the metal ions as well as several other types of semiconductor quantum dots which can pose significant risks to human health.[78] The overall combination of these properties of SiNPs opens up a new era of applications in various fields. Moreover, the hydroxyl groups on the surface of silica particles can be easily tailored with organic compounds such as initiators, ligands, metal ions or polymers by using well-established chemical modification procedures. Generally, these procedures involve the formation of an initiator layer on the surface of the silica followed by polymerization. Different polymerization techniques can be used to modify the surface of silica nanoparticles are explained in the following section.

1.3.3 Surface Functionalization of Nanoparticles

Surface functionalization of nanoparticles is very attractive and interesting due to their applications in coatings, biomedical engineering, organic light-emitting devices (OLEDs) and chemosensors.[79] Surface functionalization plays a crucial role in manipulating the properties of nanoparticles for desired applications, such as enhanced particle dispersion in polymer matrices and the resulting optoelectronic properties,[80] improved cellular internalizations,[81] enhanced binding ability for therapeutic delivery[82] and selective recognition to bio-systems.[83]

1.3.4 Grafting Methods

Functionalization of nanoparticles with polymeric materials or ligands is reported by using several methods.[84-87] These methods are highly effective for preventing aggregation of the nanomaterials by creating steric hindrance and large polymeric chains play a role in maintaining good dispersions of the nanomaterial.[88,89] Generally, surface functionalization of nanoparticles mainly includes three different strategies, namely “phisisorbtion”, “grafting from” and “grafting to” as shown in Figure 1.14.

1.3.4.1 Physisorption

In physisorption, polymers adsorb to the substrates with weak to strong electrostatic or hydrogen bonding.[91] The main problem in this case is that the adsorbed polymers can be completely removed by extensive washing and the rate of dissociation dependent upon the strength of the bounded ligand.

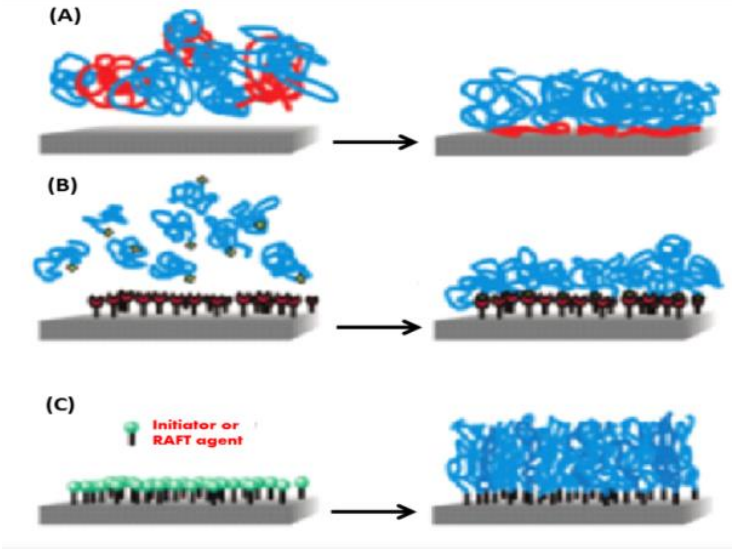

Figure 1.14. *Overview of grafting polymers to substrates (a) physisorption, (b) grafting-to and (c) grafting-from methods.*[90]

1.3.4.2 The *Grafting-to* Approach

In the *grafting-to* approach, the substrate should be modified previously with different end functional groups which should act as connecting points for the polymers with substrates. Recently, click chemistry has proven to be a popular strategy where polymers or substrates are functionalized with azide or alkyne moieties.[92,93] One disadvantage with this approach is that the post-modification yields are dependent upon the molecular weight of the polymer higher yield favors smaller molecular weight polymers and vice versa.

1.3.4.3 The *Grafting-from* Approach

This is the most adopted method for the grafting polymeric chains to the substrates than other two methods as mentioned above. In the grafting from the approach, substrates are generally anchored with CTAs followed by the growth of polymer chains from the surface. As polymer growth is outward direction from the substrates, it depends on the diffusion of monomers to the growing chain end. Generally, high dense brushes can be achieved by this method.

Controlled radical polymerizations are generally used for this purpose due to its inherent advantages than other CFRPs. In the current case, we have used RAFT technique. This grafting from method generally operated through either the Z-group or R-group approach.[94]

1.3.4.3.1 Z-group Approach

In the Z-group approach (Figure 1.15), the RAFT agent is attached to the surface via its stabilizing Z group. The polymeric radicals always propagate in solution before they attach to the surface of the substrate via the chain transfer reactions with attached RAFT agents. This approach resembles a "grafting to" approach. In the synthesis of star polymers, the Z-group approach has been proven to provide better control over the polymerization and molecular weights.[95,96] However, the Z-group approach suffers from the steric hindrance around the CTA unit which is due to the shielding effect of the previously grafted polymers and this may have negative influence on the control of the polymerization.[97,98] Stenzel *et al*. prepared HPC-*g*-PS copolymer utilizing the Z-group approach.[98,99]

The molecular weight of the PS grafts cleaved from the backbone showed a deviation from the theoretical molecular weight because of the reduced accessibility of the CTA unit with increasing conversion due to the propagating radicals were not able to reach the CTA unit and preferably terminated in solution.

1.3.4.3.2 R-group Approach

In the R-group approach (Figure 1.15), the RAFT agent is attached to the substrate surface via its leaving and reinitiating R group. The solid substrate acts as part of the leaving R group and thus the propagating radicals are located on the terminal end of the surface grafted polymer, which facilitates the growth of grafted polymer chains. This approach resembles a grafting from the approach. Davis and co-workers have first employed the R-group approach to graft polystyrene (PS) branches from a densely CTA-functionalized backbone with good control over the molecular weight (MW) and molecular weight distribution (MWD).[100] In the current work we have used the grafting from R group approach.

Even though CFRP and CLRP techniques used for grafting polymer onto the substrates, CLRP dominates over the CFRP due to its inherent properties making it ideal for this purpose. A variety of controlled radical polymerizations (CLRP), such as ATRP, NMP, and RAFT have been employed to graft a wide range of polymers from surfaces over a broad range of graft densities with controllable chain lengths, polydispersity, and morphology.[101-103] These surface-attached polymers have well-defined and advanced structures such as block copolymers, branch copolymers, and star-shaped polymers. Usually, NMP requires high reaction temperatures and ATRP generates residual copper or other metals after

polymerization which is extremely difficult to remove completely. Thus, both NMP and ATRP have not been widely applied on nanoparticle surfaces for biomedical applications.

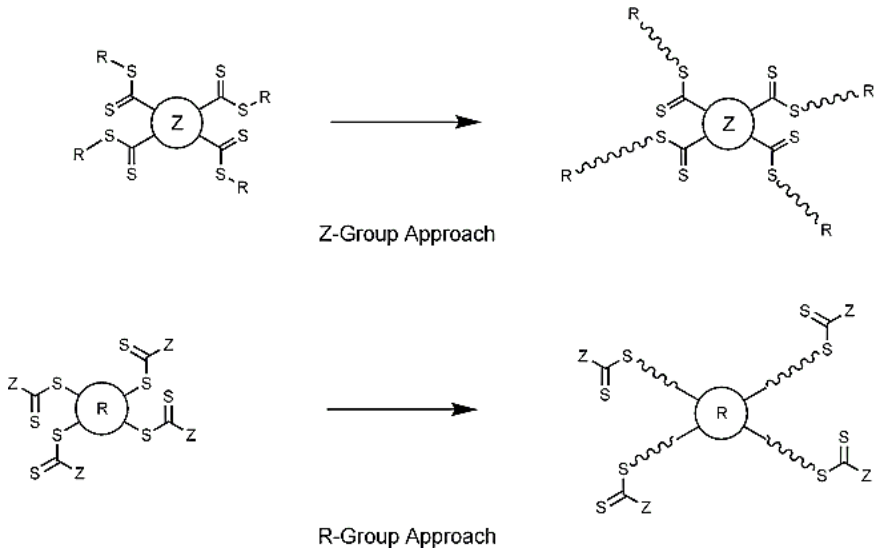

Figure 1.15. *Z-group and R-group approaches for surface-initiated RAFT polymerization.*[98]

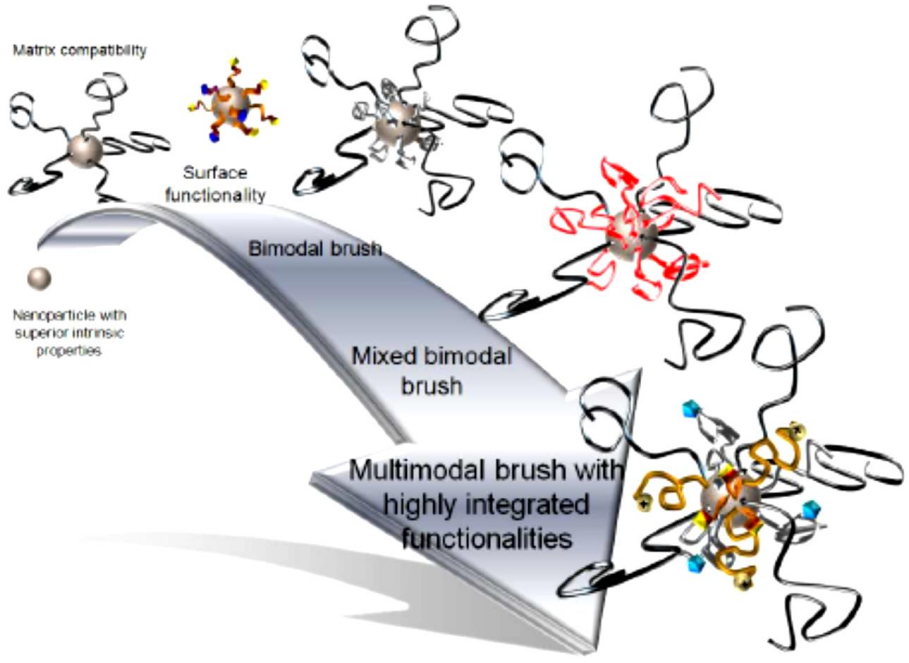

Figure 1.16. *Surface functionalization of nanoparticles: from simple to complex.*[109]

RAFT, generally employing mild reaction conditions without residual metal after polymerization is adaptable to a variety of functional monomers. Due to the advantages of the RAFT technique it has been widely applied for the surface functionalization of nanoparticles. Even though, both "grafting to" and "grafting from" have been demonstrated as effective methods to graft monomodal polymer brushes on surfaces, grafting from is extensively used. These methods have been reviewed by Benicewicz,[104] Brittain,[105] Matyjaszewski,[106,107] and Perrier.[108] In addition, these two strategies can work cooperatively to functionalize nanoparticles with ligands or polymers from the simple to the complex (as shown in Figure 1.16) with desired properties for various applications.

1.3.5 Characterization of Surface Functionalization Nanomaterials

The characterization of surface polymer functionalized nanoparticles is a crucial and tricky part of research on surface functionalities with monomodal, bimodal, mixed bimodal and multimodal distributions as shown in Figure.1.16. There are numerous factors that need to be well characterized in surface engineering.

The first one and the main is the graft density. A variety of surface functionalized nanoparticles has been analyzed using UV-vis spectroscopy[110, 111] and TGA analysis. The second factor is grafting distributions. The polymer length and its distribution can be easily characterized by GPC analysis of the cleaved polymer chains. However, the characterization of the three-dimensional distribution of the grafted brushes on particle surfaces is not easy. Recently, significant progress has been accomplished in the characterization of spatially symmetric and asymmetric distributions of surface functionalities.[112-114] Transmission electron microscopy so far is the main technique to qualitatively characterize the asymmetric distribution of surface functionalities.[115,116]

The third factor is the morphology of the grafted brushes. The morphology of the surface grafted brushes is influenced by the interactions between the brush and the dispersing solvent or polymer matrix. The dimensions of the brush usually characterized by dynamic light scattering as well as with theory and simulations.[117-118] In addition to this, Kumar,[119]Koo,[120] Mittal,[121] and Hussain[122] have reviewed various extensively about the characterizations of surface ligand engineering and polymer nanocomposites.

1.4 Glyconanoparticles

In the last decades, there has been an explosion in the synthesis, characterization, and applications of nanomaterials, which can potentially revolutionize the diagnosis and treatment of diseases.[123-126] The field is actively progressing towards using more specific and targeted nano-therapies at cellular and molecular level. Tremendous advances have been made to create sugar-functionalized nanomaterials for biological applications where carbohydrates play a significant role.[124,125,127, 128] Currently, glycol nanomaterials have attracted a great deal of attention owing to their multifaceted carbohydrate functionality, small size, biocompatibility, as well as their unique optical, electronic and magnetic properties because of which it finds applications in various fields (Figure 1.17).

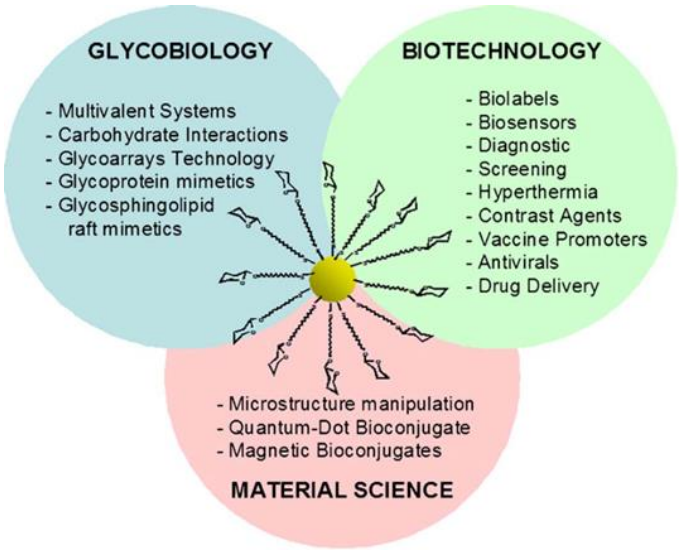

Figure1.17. *The prospective uses of glyconanoparticles in various fields.*[128]

1.4.1 Carbohydrates

Carbohydrates have the highest abundance of all biomolecules in nature. Naturally occurring carbohydrates, glycoproteins, and glycolipids present at the surface of cells play crucial roles in biological events such as recognition sites between cells and perform many biological process energy, storage and metabolic intermediates.[129-131] They can trigger various phenomena like cell growth, inflammatory responses to viral infections. The carbohydrates which are conjugated to proteins or lipids mediate many biological processes like molecular recognition, signal transduction, cell adhesion, inflammation and molecular trafficking.

Carbohydrate-mediated interactions at the cell surface range from hormones, enzymes, and antibodies to bacteria, viruses, and toxins (Figure 1.18).[138] Surface-exposed carbohydrate moieties that are characteristic of a given microbe may serve as key biomarkers for bacteria and pathogen identification, diagnosis and vaccine development. Carbohydrates, as a detection platform, have already demonstrated the tremendous potential to achieve superior sensitivity and selectivity.[132,133] At present, carbohydrate-functionalized glycol nanomaterials are finding many important applications in exploring carbohydrate-protein interactions and cell-cell communication.[134-137] Identifying, quantifying and imaging the carbohydrates, glycoproteins and glycolipids are critical both for elucidating their biological function, and for the evaluation and design of therapeutics.

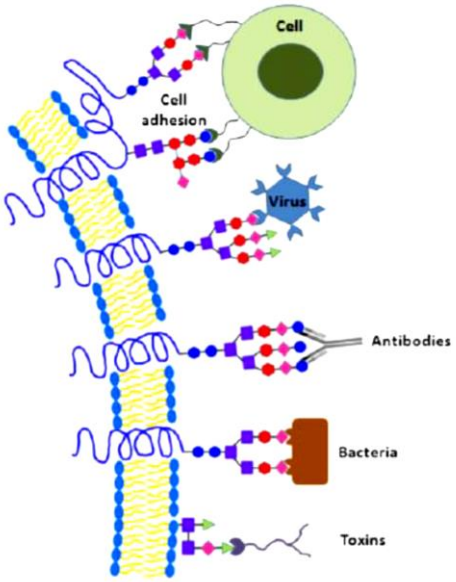

Figure 1.18. *Multivalent protein–carbohydrate interactions at the cell surface*.[138]

1.4.2 Lectins

Lectins are an important class of proteins that interact with carbohydrates in a non-covalent manner. Lectins are proteins that do not have inherent catalytic, antibody-like or enzymatic roles in the body[139] but they are highly sugar-specific and therefore take part in a variety of biological processes such as cell adhesion, migration, phagocytosis, cell differentiation and apoptosis (Figure 1.19).[140, 141] They also act as recognition agents in some processes such as the clearance of glycoproteins from the circulatory system, control of intracellular trafficking of glycoproteins. The nature of the interactions between lectins and

carbohydrates is mainly based on hydrophobic interactions and hydrogen bonds between the hydroxyl groups of the carbohydrates and the amino acid residues of the lectin proteins. Along with this metal-ion coordination and hydrophobic stacking of patches of sugar surface with the proteins are also responsible for lectin carbohydrate binding interactions.[139] While a variety of lectins have been researched in the past, Concanavalin A (Con A) has been of major importance especially for α-D-mannoside residues. It binds α-D-glucosyl residues and is a member of the legume lectin family. Con A exists in the form of a tetramer at near-neutral pH and has one binding site per subunit.

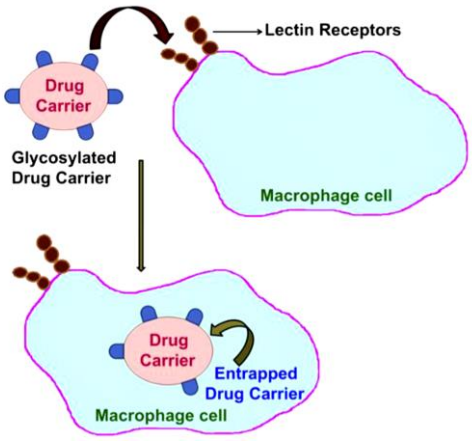

Figure 1.19. *Lectin receptor-mediated targeting to macrophages.*[141]

Despite all the developments, there are still some difficulties which need to be addressed in order to use the carbohydrates for diagnosis and therapeutic applications. Generally, carbohydrate-mediated molecular interactions have been shown to be weak and of with low affinity. In order to overcome this bottleneck, there is a need of making a suitable platform to display carbohydrates in a polyvalent system called as glycopolymer to increase the binding strength and selectivity. For example, a synthetic polymer of methyl-α-mannoside (which displays multiple mannose residues) shows an increase in binding affinity of about 10^5 when compared to its monomeric part.[142] The second challenge is that unlike the specific receptor interaction, there can be several receptors recognizing the same carbohydrate ligand thus strategies need to be developed to differentiate these receptors. The third challenge is to acquire pure carbohydrates for biological studies. This is due to the heterogeneity, it is difficult to purify large quantities of oligosaccharides from natural sources. Therefore, to

explore the utility of carbohydrates for biomedical applications involves a multi-disciplinary approach.

Since the last decade, carbohydrate-based interactions have been gained much attention but still the methodologies which can effectively probe these interactions. Efforts have been made to mimic the advantages of multivalent interactions to our requirements which led to the development of new strategies in the field of biochemistry.[125] The main reason for this is the multivalency of carbohydrate ligands show great potential through its strong chelating effects as well as the fine tuning of spatial and topological proximities. For this purpose, carbohydrate functionalized nanoparticles (GNPs) has been chosen as the best choice as these nanomaterials can serve as a promising platform for presenting carbohydrates in biological applications. The smaller sizes and a large surface to volume ratios of GNPs can enhance the receptor binding. Moreover functionalizing the NPs with multiple carbohydrate derivatives which can potentially enhance the binding affinities of individual ligands to their binding partners by many folds. Hence, the preparation of glyco-conjugated or bioconjugated nanoparticles have been a hot topic in material science and GNPs can be utilized in various fields of *in vivo* and *in-vitro* work.

1.5 Graphene

Graphene is a flat monolayer of carbon atoms tightly packed into a 2D honeycomb lattice.[146] The term graphene was coined by Hanns-Peter Boehm[147] who described single-layer carbon foils in 1962. Due to its single-atom-layer sp^2 structure, graphene has attracted many interests for its potential applications in electronics[148,149] and nanocomposites.[150] It is the basic structural unit of carbon allotropes including graphite, carbon nanotubes and fullerenes (Figure 1.20). Graphene is the most used among all the other nanofillers which are a two-dimensional carbon sheet with one molecular thickness and sp^2-hybridized carbons covalently bonding in a honeycomb structure which can be wrapped into 0D fullerenes, rolled into 1D nanotubes or stacked into 3D graphite. Graphene sheets stack to form graphite with an interplanar spacing of 0.335 nm.

As the basic building block for graphitic materials, graphene consists of only one monolayer of carbon atoms while graphite is composed of several to a few parallel graphene layers bonded by van der Waals forces. The carbon-carbon bond length in graphene is about 0.142 nm.[151] Graphene was first isolated in 2004 by physicists Andre Geim at the University

of Manchester and the Institute for Microelectronics Technology, Chernogolovka, Russia by using adhesive tape.[152]Graphene has been theoretically studied for over sixty years[153-155] and has been widely used to describe the properties of various carbon-based materials. Earlier, Graphene is assumed to be unstable and could not exist in the free state. According to the recent studies, graphene sheets have unusual electronic properties arising from the confinement of electrons in two dimensions and have attracted tremendous attention in recent years because of its exceptional thermal, mechanical and electrical properties.[157, 158] Graphene exhibits a strong ambipolar electric field effect.

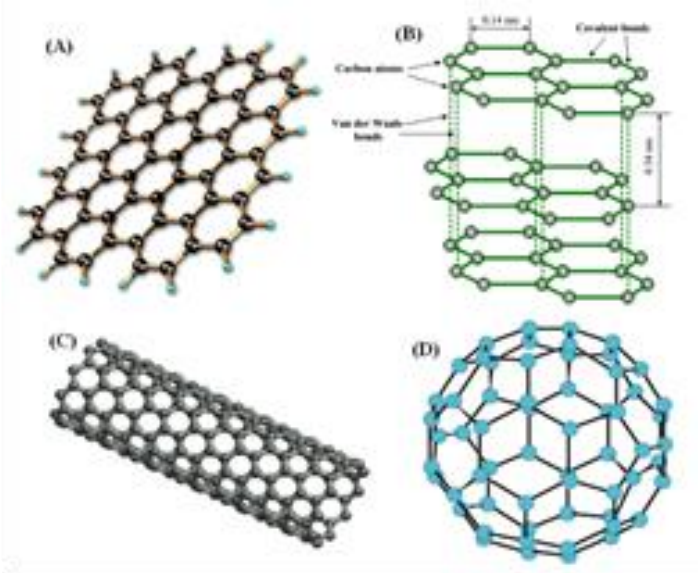

Figure 1.20. *Allotropes of carbon, (A) graphene (B) graphite (C) carbon nanotube and (D) fullerene.*[156]

Graphene is well known for its wide range of applications in various fields such as energy devices,[159,160]catalysts,[161,162] sensors,[163,164] conductive materials,[165] drug delivery[166] and polymer nanocomposites,[167,168] ultracapacitor[169] etc. Apart from its electronic properties, graphene displays several other unusual and desirable attributes. Graphene is a giant aromatic macromolecule that conducts both electricity and heat well in two dimensions. Also, their mechanical strength is comparable to that of CNTs. Since graphene consists of a single sheet of sp^2 carbon atoms, it can undergo a wide class of organic reactions. It can incorporate into polymers and inorganic systems to enhance mechanical strength, thermal and electrical conductivity. For reliable integration of graphene into practical electronic devices, it is essential to have a simple, reproducible and controllable technique to produce large-area

graphene sheets on a large scale. Micromechanical cleaving[170] exfoliation of individual graphene sheets via sonication in a solvent,[171] and growth of graphene on silicon carbide (SiC) or nickel substrates[172] have been reported as possible techniques to produce graphene.

In addition, functional polymers have enabled the preparation of polymer-graphene nanocomposites that demonstrate a variety of interesting properties. The properties of a graphene-based polymeric nanocomposite greatly depend on the dispersion of graphene in the polymeric matrix. The irreversible aggregation of graphene via π-π stacking can greatly hinder its production, storage, and processing[173]. Hence the functionalization and stabilization of graphene via modification are necessary in order to avoid the undesired aggregation to maximize properties for the intended end-use application.

Recently-developed polymerization methods, especially living free radical polymerization techniques allow for the preparation of polymers with precise control over composition, architecture, and molecular weight. Therefore, polymers on the surface of graphene sheets allows the preparation of composites that merge the properties of the polymer with the conductivity and strength of graphene. For these reasons, the polymer chemistry on the graphene surface has recently attracted lot of interest among polymer scientists.

1.6 Aims of the Thesis

In this chapter, we have discussed the importance of various types of polymeric nanomaterials and their synthetic procedures in detail. In particular, an overview of the variety of methods published so far that are used for the preparation of these materials is presented in this introduction chapter. We have also discussed the properties and applications of different polymeric nanomaterials such as colloidal nanoparticles, graphene oxide/polymer nanocomposite, and glyco polymeric nanomaterials. Throughout the discussion, we have seen that using a process which can control the preparation of these materials is necessary for the preparation of the polymers with desired properties. This thesis deals with the development and optimization of synthetic methods for preparation or surface modification of polymeric nanomaterials using RAFT polymerization and their physicochemical characterization. In addition, these materials were analyzed in detail to provide insights into their use for various possible applications in biology as well as in proton exchange membrane (PEM) fuel cell.

The polymeric core–shell particles with different shell thickness and functional groups could provide a unique advantage in encapsulating small molecules or inorganic nanoparticles

as well as in directing the self-assembly. Keeping this as our objective, in ***Chapter 3*** we have planned to develop a synthetic procedure for the preparation of polystyrene (PS) nanoparticles with a functional polymeric shell on the surface of PS particle. The knowledge and expertise generated in Chapter 3 encourage us to use the core-shell particles especially the shell functionality in developing polymer nanocomposite with inorganic fillers. In ***Chapter 4***, we have made an effort to develop the polystyrene nanocomposites with graphene and more interestingly we wanted to do it in an *in-situ* method.

Carbohydrates are implicated in a large number of biological processes ranging from cell-cell interactions to bacterial and viral infection. Lectins are carbohydrate-binding proteins that are generally specific for certain sugars. However, typical carbohydrate–lectin interactions tend to have very low monomeric binding affinities. In many cases, the binding of saccharide ligands by protein receptors can be improved significantly through the attachment of multiple saccharide residues to a common support. For this purpose in ***Chapter 5***, we have planned to prepare glycopolymeric particles with core-shell morphology where shell consist the functional glycomonomer. Even though, we have prepared the glycopolymer nanoparticles in chapter 5, the main problem faced by us is the very weak binding of these particles with corresponding proteins which is due to the short distance between the carbohydrate moiety and the polymeric backbone as well as the high glyco polymeric chain density on the formed particle surface. For this purpose, in ***Chapter 6*** we planned to graft a sugar monomer on particle surface with different (desired) chain lengths and chain densities. Since the particle size also plays a significant role as we noticed from chapter 5 work that we could not make very small particles based on polymeric core, thereby we planned to work with silica nano particles (SiNP) core which can be made very smaller in size. The expertise on surface grafting of polymeric chain as gained in chapter 6 has been further utilized in developing materials which are useful as nanofillers for this proportion of nanocomposites with polybenzimidazole for the development of PEM membrane. The aim of the ***Chapter 7*** mainly deals with addressing the serious drawbacks of phosphoric acid (PA) doped PBI membrane which are acid leaching, low mechanical strength, and oxidative stability during fuel cell operation. Therefore, the thesis mainly deals with the synthesis and characterization of various polymeric nanomaterials for various applications from biology to coatings to fuel cell. The aims and objectives of each chapter of this thesis are expanded at the end of the introductory part of the individual chapters.

References

1. IUPAC. Glossary of Basic Terms in Polymer Science. *Pure Appl. Chem.*, 1996, **68**, 2287.
2. R. Stepto, K. Horie, T. Kitayama, and A. Abe, *Pure and Applied Chemistry*, 2003, **75,** 1359.
3. D. Feldman, *Des. Monomers Polym.* 2008, **11**, 1–15.
4. W. P. Hohenstein and H. Mark, *J. Polym. Chem.*, 1946, **1,** 127.
5. G. Odian, *Principles of Polymerization*, 2004.
6. H. B. Yamak, *Polymer Science*, 2013.
7. C. –S. Chern, *Principles and Applications of Emulsion Polymerization*, 2008.
8. J. R. Fried, *American Chemical Society*, 2003.
9. C. S. Chern, *Prog. Polym. Sci.*2006, **31,** 443–486.
10. H. B. Yamak, *INTECH Open Access Publisher*, 2013.
11. Y.-M. Wang and C. Y. Pan, *Colloid Polym. Sci.*1999, **277,** 658–665.
12. A. -R. Mahdavian and M. Abdollahi, *Polymer.*2004, **45,** 3233–3239.
13. K. Tauer, R. Deckwer, I. Kühn and C. Schellenberg, *Colloid Polym. Sci.*1999, **277,** 607.
14. S. A. Chen and S. T. Lee, *Macromolecules*1992, **25,** 1530–1533.
15. S. A. Chen and S. T. Lee, *Macromolecules*1991, **24,** 3340–3351.
16. K. Matyjaszewski and K., Ed. Matyjaszewski, *ACS Symposium Series 854; American Chemical Society: Washington, DC*, **p2,** 2003.
17. M. Szwarc, M. Levy and R. Milkovich, *J. Am. Chem. Soc.*, 1956, **78,** 2656.
18. C. J. Hawker, A.W. Bosman and E. Harth, *Chem. Rev.*, 2001, **101,** 3661.
19. V. Sciannamea, R. Jerome and C. Detrembleur, *Chem. Rev.*, 2008, **108,** 1104.
20. C. Boyer, P. Lacroix-Desmazes, J.-J. Robin and B. Boutevin, *Macromolecules*, 2006, **39,** 4044.
21. G. David, C. Boyer, J. Tonnar, B. Ameduri and B. Boutevin, *Chem. Rev.*, 2006, **106,** 3936.
22. V. Percec, A. V. Popov and L.A.*J. Polym. Sci., Part A: Polym. Chem.*, 2005, **43,** 2276.
23. V. Percec and M. J. Sienkowska, *J. Polym. Sci., Part A: Polym. Chem.*, 2009, **47,** 628.
24. J. Chiefari, Y.K. Chong, F. Ercole, J. Krstina, R. T. A. Mayadunne, G. Moad, E. Rizzardo and S. H. Thang, *Macromolecules*, 1998, **31,** 5559.

25. T. P. Le, G. Moad, E. Rizzardo and S. H. Thang, *PCT Int. Appl. WO 9801478 A1 19980115*, 1998.
26. D. Charmot, P. Corpart, H. Adam, S. Z. Zard and G. Bouhadir, *Macromol. Symp.*, 2000, **150,** 23.
27. P. Corpart, D. Charmot and D. Michelet, *PCT Int. Pat. Appl. WO 9858974 A1 19981230*, 1998.
28. K. Matyjaszewski and J. Xia, *Chem. Rev.*, 2001, **101,** 2921.
29. N. V. Tsarevsky and K. Matyjaszewski, *Chem. Rev.*, 2007,**107,** 2270.
30. V. Percec, T. Guliashvili, J. S. Ladislaw, A. Stjerndahl, M. J. Sienkowska, M. J. Monteiro and S. Sahoo, *J. Am. Chem. Soc.*, 2006, **128,** 14156.
31. Y. Sugihara, Y. Kagawa, S. Yamago and M. Okubo, *Macromolecules*, 2007, **40,** 9208.
32. B. Ray, M. Kotani and S. Yamago, *Macromolecules*, 2006, **39,** 5259.
33. B. B. Wayland, C. H. Peng, Z. Lu and M. Fryd, *Macromolecules*, 2006, **39,** 8219.
34. N. Ayres, *Polym. Rev.*, 2011, **51,** 138.
35. K. Ohno, Y. Tsujii and T. Fukuda, *Macromolecules*, 1997, **30,** 2503.
36. J. Chiefari, Y. K. Chong, F. Ercole and T. P. T. Le, *Macromolecules*, 1998, **31,** 5559.
37. G. Moad, E. Rizzardo and S. H. Thang, *Aust. J. Chem.*, 2006, **59,** 669.
38. G. Moad, E. Rizzardo and S. H. Thang, *Aust. J. Chem.*, 2009, **62,** 1402.
39. G. Moad, E. Rizzardo and S. H. Thang, *Aust. J. Chem.*, 2012, **65,** 985.
40. D. J. Keddie, G. Moad, E. Rizzardo and S. H. Thang, *Macromolecules*, 2012, **45,** 5321.
41. G. Moad, D. Keddie, E. Rizzardo and S. H. Thang, *Macromol. Symp.*, 2015, **350**, 34.
42. G. Moad, E. Rizzardo and S. H. Thang, *Polymer*, 2008, **49,** 1079.
43. G. Moad, J. Chiefari, J. Krstina, A. Postma and E. Rizzardo, *Polym.. Intern*. 2000, **49,** 993.
44. G. Moad, Y. K. Chong, E. Rizzardo and S. H. Thang, *Polymer*, 2005, **46,** 8458.
45. G. Moad, *Progress in Polymer Science*, 1999, **24,** 81.
46. G. Moad, R. T. A. Mayadunne, E. Rizzardo and S. H. Thang, *Macromol. Sympo.*, 2003, **192**, 1.
47. M. Benaglia, J. Chiefari, E. Rizzardo and S. H. Thang, *J. Am. Chem. Soc.*, 2009, **131,** 6914.
48. J. Chiefari, Y. K. Chong, E. Rizzardo and S. H. Thang, *Macromolecules*, 1998, **31,** 5559.

49. T. P. T. Le, G. Moad, E. Rizzardo, and S. H. Thang, *Du Pont. PCT Int. Appl.*, WO9801478, 1998.
50. D. Charmot, P. Corpart, H. Adam and G. Bouhadir, *Macromol. Symp.*, 2000, **23,** 150.
51. M. J. Monteiro, and J. A. M. de Brouwer, *Macromolecules*, 2001, **34,** 349.
52. S. Motokucho, A. Sudo, F. Sanda and T. Endo, *Chem. Ccommun.*, 2002, **17,** 1946.
53. P. Vana and C. Barner-Kowollik, *Macromol. Theory and Simulations*, 2002, **11,** 823.
54. M. H. Stenzel and T. P. Davis, *J.Polym.Sci., Part A: Polym.Chem.*, 2002, **40,** 4498.
55. J. T. Lai, D. Filla and R. Shea, *Polym.Prepr.*2002, **43,** 122.
56. C. W. Scales, A. J. Convertine and C. L. McCormick, *Biomacromolecules*, 2006, **7,** 1389.
57. A. W. York, C. W. Scales, F. Huang and C. L. McCormick, *Biomacromolecules*, 2007, **8,** 2337.
58. J. D. Biasutti, T. P. Davis and J. P. A. Heuts, *J. Polym. Sci., Part A: Polym. Chem.*, 2005, **43,** 2001.
59. Y. Chan, V. Bulmus, L. Barner and M. Kavallaris, *J. Controlled Release*, 2006, **115,** 197.
60. M. Barsbay, O. Gueven, T. P. Davis, C. Barner-Kowollik and L. Barner, *Polymer*, 2009, **50,** 973.
61. D. L. Leslie-Pelecky and R. D. Rieke, *Chem. Mater*. 1996, **8**, 1770.
62. J Shi, S. Gider, K. Babcock and D.D. Awschalom, *Science* 1996, **271**, 937.
63. C. Le, J. Han,C.Y. Ryu, B.C Benicewicz, *Macromolecules* 2006, **39,** 3175.
64. S. H. Sun, C.B. Murray, D. Weller, L. Folks and A. Moser, *Science* 2000, **287**, 1989.
65. T.J. Hyeon, *Chem Soc Chem Commun* 2003, 927.
66. J. I. Martin, J. Nogues, K. Liu, J. L. Vicent, and I. K. Schuller, *J Magn Magn Mater* 2003, **256**, 449.
67. V. Provenzano, A. J. Shapiro and R.D. Shull, *Nature* 2004, **429**, 853.
68. H. Zou, S. Wu and J. Shen, *Chem. Rev*. 2008, **108**, 3893.
69. R. A. Vaia and J. F. Maguire, *Chem. Mater*. 2007, **19**, 2736.
70. L. S. Schadler, S. K. Kumar, B. C. Benicewicz, S. L. Lewis and S. E. Harton, *MRS bulletin* 2007, **32**, 335.
71. S. K. Kumar and R. Krishnamoorti, *Annu. Rev. Chem. Biomol. Eng.* 2010, **1**, 37.
72. W. Stober and A. J. Fink, *Colloid Interface Sci*. 1968, **26**, 62.

73. H. Hommel, A. Touhami and A. P. Legrand, *Makromol. Chem*., 1993**, 194,** 879.
74. Y. Wei, L. M. Fan and L. R. Chen, *Chromatographia*, 1997, **46**, 637.
75. J. P. Mathew and M. Srinivasan, *Polym. Int.*, 1992, **29**, 179.
76. M. Garcı´a, W. E. Zyl, M. G. J. Cate, J. W. Stouwdam, H. Verweij, M. S. Pimplapure and G. Weickert, *Ind. Eng. Chem. Res.*, 2003, **42,** 3750.
77. C. M. Stafford, A. Y. Fadeev, T. P. Russell and T. J. McCarthy, *Langmuir,* 2001, **17**, 6547.
78. Q. Wang, Y. Bao, J. Ahire, and Y. Chao, *Adv. Health. Mater*. 2013, **2**, 459.
79. H. Zou, S. Wu and J. Shen, *Chem. Rev*.2008, **108**, 3893.
80. Y. Li, T. M. Krentz, L. Wang, B. C. Benicewicz and L. S. Schadler, *ACS Appl.Mater. Interfaces.*2014, **6**, 6005.
81. S. K. Kumar, N. Jouault, B. Benicewicz and T Neely, *Macromolecules*.2013, **46**, 3199.
82. K. Saha, A. Bajaj, B. Duncan and V. M. Rotello, *Small*. 2011, **7**, 1903.
83. R. Elghanian, J. J. Storhoff, R.C. Mucic, R.L. Letsinger and C.A. Mirkin, *Science.* 1997, **277,** 1078.
84. O. Prucker and Ru¨he *J. Macromolecules*, 1998, **31,** 602.
85. B. Radhakrishnan, R. Ranjan and W. J. Brittain, *Soft Matter*, 2006, **2,** 386.
86. M. R. Bockstaller and E. L. Thomas, *Phys. ReV. Lett.* 2004, **93,** 166106.
87. K. Bridger, D. Fairhurst and B. J. Vincent, *Colloid Interf Sci*, 1979, **68,** 190.
88. A. Rungta, B. Natarajan, T. Neely, D. Dukes, L. S. Schadler and B. C. Benicewicz, *Macromolecules*, 2012, **45,** 9303.
89. Y. Li, P. Tao, A. Viswanath, B. C. Benicewicz, L. S. Schadler, *Langmuir*, 2013, **29,** 1211.
90. P. Mansky, Y. Liu, E. Huang, T. P. Russel and C. Hawker, *Science* 1997, **275,** 1458
91. T. B. Norsten, E. Jeoung, R. J. Thibault and V. M. Rotello, *Langmuir* 2003, **19,** 7089.
92. B. Helms, J. L. Mynar, C. J. Hawker and J. M. Fréchet, *J. Am. Chem. Soc.* 2004,**126,** 15020.
93. W. H. Binder and R. Sachsenhofer,*Macromol. Rapid Commun.* 2008, **29,** 952.
94. Hand book of RAFT polymerization; ISBN 978-3-527-31924-4 - Wiley-VCH, Weinheim, 2008; Vol. 12.
95. A. Gregory and M. H. Stenzel, *Prog. Polym. Sci*.2012, **37,** 38.

96. L. Barner, T. P. Davis, M. H. Stenzel and C. Barner-Kowollik, *Macromol. Rapid Commun.* 2007, **28,** 539.

97. M. Hernandez-Guerrero, T. P. Davis, C. Barner-Kowollik and M. H. Stenzel, *Eur. Polym. J.* 2005, **41,** 2264.

98. M. H. Stenzel and T. P. Davis,*J. Polym. Sci. Part A: Polym. Chem.*2002, **40,** 4498.

99. M. H. Stenzel, T. P. Davis and A. G. Fane, *J. Mater. Chem.*2003, **13,** 2090.

100. J. F. Quinn, R. P. Chaplin and T. P. Davis, *J. Polym. Sci., Part A: Polym. Chem.* 2002, **40,** 2956.

101. M. Husseman, E. E. Malmström, M. McNamara, M. Mate, D. Mecerreyes, D. G. Benoit and J. L. Hedrick, P. Mansky, E. Huang, T. P. Russell and C. J. Hawker, *Macromolecules*, 1999, **32,** 1424.

102. J. Gao, J. Li, B. C. Benicewicz, H. Hillborg and L and S. Schadler, *Polymers*, 2012,**4,** 187.

103. J. Gao, J. Li, S. Zhao, B. C. Benicewicz, H. Hillborg and L. S. Schadler, *Polymer*, 2013, **54,** 3961.

104. Y. Li, L. S. Schadler and B. C. Benicewicz, *Handbook of RAFT Polymerization.*; C., Ed. Barner-Kowollik, Wiley-VCH: *Weinham, Germany* 2008, p 423.

105. B. Radhakrishnan, R. Ranjan and W. Brittain, *J. Soft Matter*.2006, **2,** 386.

106. J. Pyun and K. Matyjaszewski, *Chem. Mater.* 2001, **13,** 3436.

107. J. Pyun, T. Kowalewski and K. Matyjaszewski, *Macromol. Rapid Commun.*2003, **24,** 1043.

108. J. Moraes, K. Ohno, T. Maschmeyer and S. Perrier, *Chem. Commun.*2013, **49,** 9077.

109. Y. Li, T. M. Krentz, L. Wang, B. C. Benicewicz and L. S. Schadler, *ACS Appl.Mater. Interfaces.* 2014, **6,** 6005.

110. J. Gao, J. Li, S. Zhao, B. C. Benicewicz, H. Hillborg and L. S. Schadler, *Polymer*, 2013, **54,** 3961.

111. N. Wu, L. Fu, M. Su, M. Aslam, K. C. Wong and V. P. Dravid, *Nano Lett.* 2004, **4,** 383.

112. M. Lattuada and T. A. Hatton, *Nano Today*, 2011, **6,** 286.

113. A. Walther and A. H. Muller, *Chem. Rev*., 2013, **113,** 5194.

114. J. Hu, S. Zhou, Y. Sun, X. Fang and L. Wu, *Chem. Soc. Rev.*,2012, **41,** 4356.

115. S.-H. Hu and X. Gao, *J. Am. Chem. Soc.*, 2010, **132,** 7234.

116. L. Y. Wu, B. M. Ross, S. Hong and L. P. Lee, *Small.*, 2010,**6,** 503.

117. F. L. Verso, L. Yelash, S. A. Egorov and K. Binder, *Soft Matter*, 2012, **8,** 4185.
118. D. Reith, A. Milchev, P. Virnau and K. Binder, *Macromolecules*, 2012, **45,** 4381.
119. C. Kumar, J. Jestin, D. Gigmes, R. Schweins, E. Di-Cola, F. Dalmas, D. Bertin, F and Boué, F., *Macromolecules*,2010, **43,** 4833.
120. J. H. Koo, Polymer nanocomposites: Processing, Characterization, and Applications; McGraw-Hill, New York, 2006.
121. V. Mittal, Wiley-VCH: Weinheim, Germany, 2012; Chapter 1, pp 1−12.
122. F. Hussain, M. Hojjati, M. Okamoto and R. E. Gorga, *J Compos Mater*, 2006, **40,** 1511.
123. Q. A. Pankhurst, N. T. K. Thanh, S. K. Jones and J. Dobson, *Applied Physic*, 2009, **42**, 224001.
124. X. Huang, S. Neretina and M. A. El-Sayed, *Adv. Mater.*, 2009**, *21***, 4880.
125. D. Peer, J. M. Karp, S. Hong, O. C. Farokhzad, R. Margalit and R. Langer, *Nat Nano*, 2007, ***2***, 751.
126. M. Ferrari, *Nat Rev Cancer*, 2005**, 5**, 161.
127. Q. A. Pankhurst, J. Connolly, S. K. Jones and J. Dobson, *J. Phy. D: Appl. Phy.*, 2003, ***36***, R167.
128. J. M. de la Fuente and S. Penadés, *Biochimica et Biophysica Acta (BBA) - General Subjects*, 2006**, 1760,** 636.
129. X. Michalet, F. F. Pinaud, L. A. Bentolila, J. M. Tsay, S. Doose, J. J. Li, G.Sundaresan, A. M. Wu, S. S. Gambhir and S. Weiss, *Science*, 2005, **307**, 538.
130. R. Kikkeri, B. Lepenies, A. Adibekian, P. Laurino and P. H. Seeberger, *J. Am. Chem. Soc.*, 2009,**131,** 2110.
131. H. Lis and N. Sharon, *Chem. Rev.*, 1998, **98**, 637.
132. P. Babu, S. Sinha and A. Surolia, *Biocon. Chem.*, 2006, **18**, 146.
133. T. K. Dam, C. F. Brewer, *Chem. Rev.*, 2002, **102**, 387.
134. D. M. Ratner, E. W. Adams, M. D. Disney and P. H. Seeberger, *ChemBioChem*, 2004, **5**, 1375.
135. E. Oh, D. Lee, Y. P. Kim, S. Y. Cha, D.-B. Oh, H. A. Kang, J. Kim, H.-S. Kim, *Angew. Chem. Int. Ed.*, 2006, **45,** 7959.
136. T. K. Lindhorst, *Weinheim*, 2003.
137. Y. C. Lee, R. T. Lee, *Acc. Chem. Res.*, 1995, **28,** 321.

138. X. Zeng, C. A. Andrade, M. D. Oliveira, X. L. Sun, *Anal. Bioanal. Chem.*, 2012, ***402,*** 3161.
139. H. Lis and N. Sharon, *Chem. Rev.*, 1998, **98**, 637.
140. R. Kikkeri, X. Liu, A. Adibekian, Y. H. Tsai and P. H. Seeberger, *Chem. Comm.*, 2010, **46**, 2197.
141. K. Jain, P. Kesharwani, U. Gupta and N. K. Jain, *Biomaterials*, 2012, **33**, 4166.
142. K. H. Mortell, R. V. Weatherman, L. L. Kiessling, *J. Am. Chem.Soc.*, 1996, **118,** 2297.
143. J.H. Ahire, I. Chambrier, A. Mueller, Y.P. Bao, Y.M. Chao, *ACS Appl. Mater. Interfaces*, 2013, **5**, 7384.
144. Q. Wang, Y. Bao, J. Ahire, Y. Chao, *Adv. Health. Mater.* 2013, **2**, 459.
145. Y. Zhai, M. Dasog, R. B. Snitynsky, T. K. Lowary nad J. G. C. Veinot, *J. Mater. Chem. B*, 2014, **2**, 8427.
146. A. K. Geim and K. S. Novoselov, *Nat. Mater.*, 2007, **6**, 183.
147. H. –P. Boehm, R. Setton and E. Stumpp, *Pure & Appl. Chem.*1994, **66,** 1893.
148. Y. Zhu, S. Murali, X. Li, J. R. Potts and R. S. Ruoff, *Adv. Mater*. 2010, **22,** 3906.
149. A. K. Geim and K. S. Novoselov, *Nat. Mater*. 2007, **6**, 183.
150. F. Yavari, C. Kritzinger, C. Gaire, P. M. Ajayan and N. Koratkar, *Small* 2010, ***6,*** 711.
151. R. Heyrovska, *"Atomic Structures of Graphene, Benzene and Methane with Bond Lengths as Sums of the Single, Double and Resonance Bond Radii of Carbon"*.http://arxiv.org/ftp/arxiv/papers/0804/0804.2488.pdf, 2008. (59-73)
152. http://en.wikipedia.org/wiki/Graphene
153. P. R. Wallace, *Phys. Rev.*, 1947, **71,** 622.
154. J. W. McClure, *Phys. Rev.*, 1956, **104**, 667.
155. J. C. Slonczewski and P. R. Weiss. *Phys. Rev.*, 1958, **109,** 272,.
156. T. Kuilla, S. Bhadra, D. Yao and J. H. Lee, *Prog. Polym. Sci.* 2010, **35**, 1350.
157. Y. Zhu, S. Murali, W. Cai, X. Li, J. W. Suk, J. R. Potts and R. S. Ruoff, *Adv. Mater.*, 2010, **22,** 3906.
158. A. K. Geim and K. S. Novoselov, *Nat. Mater.* 2007, **6,** 183.
159. N. Park, S. Hong, G. Kim and S. H. Jhi, *J. Am. Chem. Soc.* 2007, **129,** 8999.
160. M. H. Liang and L. J. Zhi, *J. Mater. Chem.* 2009, **19**, 5871.
161. R. I. Jafri, N. Rajalakshmi and S. Ramaprabhu, *J. Mater. Chem.* 2010, **20,** 7114.
162. J. Pyun, *Angew. Chem., Int. Ed.* 2011, **50,** 46.

163. J. T. Robinson, F. K. Perkins, E. S. Snow, Z. Q. Wei and P. E. Sheehan, *Nano Lett*. 2008, **8,** 3137.

164. G. P. Keeley, A. O'Neill, J. N. Coleman and G. S. Duesberg, *J. Mater. Chem.* 2010, **20,** 7864.

165. J. P. Zhao, S. F. Pei, W. C. Ren, L. B. Gao and H. M. Cheng, *ACS Nano* 2010, **4**, 5245.

166. R. Y. Zhang, M. Hummelgard, G. Lv and H. Olin, *Carbon* 2011, **49,** 1126.

167. R. Verdejo, M. M. Bernal, L. J. Romasanta and M.A. Lopez-Manchado, *J. Mater. Chem*. 2011, **21**, 3301.

168. D. Y. Cai and M. Song, *J. Mater. Chem*. 2010, **20,** 7906

169. E. Yoo, J. Kim, E. Hosono, H. Zhou, T. Kudo and I. Honma, *Nano Lett.* 2008, **8,** 2277.

170. L. L. Zhang, R. Zhou and X. S. Zhao, *J. Mater. Chem*. 2010, **20,** 5983.

171. M. H. Liang and L. J. Zhi, *J. Mater. Chem*. 2009, **19,** 5871.

172. L. Valentini, M. Cardinali, S. B. Bon, D. Bagnis, R. Verdejo, M. A. Lopez-Manchado and J. M. Kenny, *J. Mater. Chem.* 2010, **20,** 995.

173. J. S. Cheng, G. C. Zhang, J. H. Du, L. Y. Tang, J. Y. Xu and J. H. Li, *Mater. Chem*. 2011, **21,** 3485.

Chapter 2

Materials, Methods & Instrumentation

This chapter describes the source of materials, experimental procedures, all the characterization techniques and the corresponding instruments used in chapters 3 to 7.

2.1 Source of Materials

Styrene (St) (Sisco Chem., India) and hydroxyethyl methacrylate (HEMA) (Acros, India) was vacuum distilled prior to use. 4,4'-Azobis (4-cyanopentanoicacid) (ACP, Sigma-Aldrich) was purified by recrystallization from methanol HPLC grade water (Fisher Scientific) and AR grade ethanol (Changshu Yangyuan Chemical, China), Graphite powder, 1,3-dicyclohexyl carbodiimide (DCC), 4-dimethyl amino pyridine (DMAP), styrene sulfonate sodium salt (SS-Na) were purchased from Sigma–Aldrich. Potassium persulfate (KPS), hydrogen chloride (HCl 35%), potassium permanganate and phosphoric acid were purchased from Merck India. Dimethyl formamide (DMF), dichloromethane (DCM) were purchased from Fluka. Sulfuric acid (99%) and hydrogen peroxide (30%) were purchased from Fisher Scientific. Tetraethylorthosilicate (TEOS, 99%), (3-Aminopropyl)triethoxysilane (APTES, 99%), Sodium bicarbonate (NaHCO3), ammonium hydroxide (NH4OH , 28%), ethyl alcohol (EtOH, 99%), dry toluene (AR grade), dry dimethylformamide (AR grade) and N-Hydroxysuccinamide were purchased from Finar chemicals Ltd, India. N-Vinyl imidazole (NVI) (99.9%) and 2,2′-Azobis(2-methylpropionitrile) (AIBN, 98%) purchased from Sigma-Aldrich was freshly recrystallized from methanol and kept under nitrogen until use. Formic acid (FA) (99%) was purchased from Qualigens, India. All the other chemicals were reagent grade unless otherwise mentioned.

2.2. Preparation of Materials

2.2.1. Synthesis of Benzylsulfanylthiocarbonylsufanylpropionic acid (BSPA) RAFT agent

Benzylsulfanylthiocarbonylsufanylpropionic acid (BSPA) RAFT agent was synthesized using the previously reported method as shown in scheme 2.1.[1, 2] Briefly, potassium hydroxide (3.366g, 60 mmol) was added in distilled water (30 mL) followed by the addition of mercaptopropionic acid (2.614g, 30mmol) in a dried 250 mL round bottom flask. Then carbon disulphide (3.988g, 66 mmol) was added with an addition funnel at a rate of 0.1ml/min, formation of an orange colour solution was observed and it was stirred for 5 hours at room temperature. Then benzyl bromide (5.131g, 30 mmol) was added and the reaction mixture was stirred at 80°C for 12 hours. After completion of the reaction, it was cooled to room temperature followed by the addition of chloroform (30 mL) and then the reaction

mixture was acidified with aqueous hydrochloric acid (1N) until the organic layer become yellow. The water phase was extracted with chloroform (30 mL) twice and dried over anhydrous magnesium sulphate overnight. After the evaporation of the solvent, the remaining product was purified by silica gel column chromatography with a 7:3 hexane/ethyl acetate mixture as an eluent. Then the product was recrystallized from 7:3 hexane/ethyl acetate and dried in vacuum overnight. Yellow colour solid (6.69g, 82%) was obtained. The detail of its characterization is included in corresponding chapter.

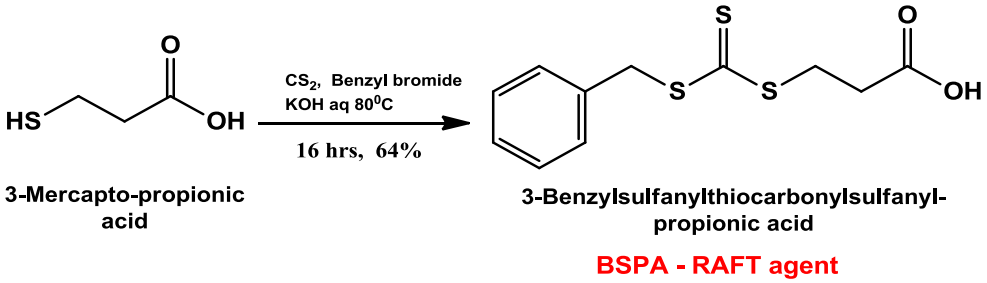

Scheme 2.1 *Synthesis of BSPA RAFT agent.*

2.2.2. Synthesis of 4-cyanopentanoic acid dithiobenzoate (CPDB).

4-cyanopentanoic acid dithiobenzoate (CPADB) was synthesized as reported elsewhere as shown in scheme 2.2.[3,4] Briefly, the dithiobenzoic acid (DTBA) was firstly prepared using sodium methoxide (30 % solution in methanol, 45 g, 250 mmol), elemental sulphur (8.0 g, 250 mmol), anhydrous methanol (62.5 g) and benzyl chloride (15.75 g, 125 mmol). The reaction mixture was heated in an oil bath at 67 ºC for 10 h. After this time, the reaction mixture was cooled to 7 ºC using an ice bath. The precipitated salt was removed by filtration and the solvent removed in vacuum. The residue was dissolved in deionized water (125 mL). The crude sodium dithiobenzoate solution was acidified with 1.0 N HCl (125 mL) and extracted with diethyl ether (50 mL). Deionized water (75 mL) and 1.0 N NaOH (150 mL) were added, and sodium dithiobenzoate was transfered to the aqueous phase. The sodium dithiobenzoate solution (87.5 mL) and potassium ferricianide (III) (8.23 g, 25 mmol) were mixed in deionized water (150 mL) under vigorous stirring. The red precipitate was filtered and washed with deionized water until the washings became colourless. The solid was filtered and dried in vacuum at room temperature overnight. The product, di(thiobenzoyl) disulphide, was recrystallized from ethanol. Finally, the synthesis of 4-cyanopentanoic acid dithiobenzoate (CPADB) was carried out by dissolving 4,4'-azobis(4-cyanopentanoic acid)

(2.92 g, 11.5 mmol) and di(thiobenzoyl)disulfide (2.13 g, 7 mmol) in 40 mL of distilled ethyl acetate. The reaction solution was heated at reflux for 18h and ethyl acetate was removed in vacuum. The crude product was isolated by column chromatography (silica gel 60 Å, 70-230 mesh) using ethyl acetate hexane (2:3) as eluent. Fractions that were red in colour were combined and dried over anhydrous sodium sulphate overnight. The solvent mixture was removed in vacuum, and the red oily residue placed in a freezer at -20 ºC, whereupon it crystallized. The target compound was recrystallized with an ethyl acetate:hexane (2:3) mixture, Dark red colour solid (78%) was obtained. The detail of its characterization is included in corresponding chapter.

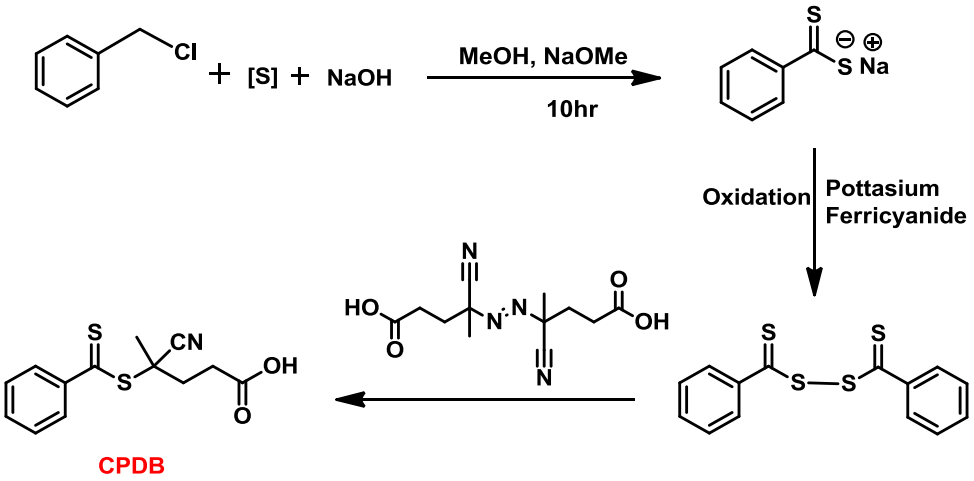

Scheme 2.2. *Synthesis of CPDB RAFT agent.*

2.2.3. Synthesis of Activated CPDB

The activation of CPDB was carried out by using NHS as described elsewere.[5] CPDB (2.04 g, 7.3 mmol), N-Hydroxysuccinamide (0.84 g, 7.3 mmol) were dissolved in dry dichloromethane (15 mL) and then N,N'-Dicyclohexylcarbodiimide (DCC, 1.51 g, 7.3 mmol) was added to the above reaction mixture under nitrogen atmosphere, stirred at room temperature for 18 h the dark condition. The insoluble by-product was filtered; the remaining solution was concentrated and was purified by using silica column chromatography in 4:1 (v/v) *n*-hexane/ethyl acetate giving red solid. (2.28 g, 83% yield). The detail of its characterization is included in corresponding chapter.

2.2.4. Synthesis of Silica Nanoparticles (SiNP)

The widely adopted Stöber method was used to prepare SiNPs from TEOS by way of a hydrolysis and condensation reaction.[6] Briefly the method as follows: ammonium hydroxide (28 wt% in water, 10 mL) and ethanol (400 mL) were added to a 1000 mL round bottomed flask at room temperature. To this tetraethylorthosilicate (TEOS, 10 mL) and HPLC water (10 mL) were added dropwise under vigorous stirring. After stirring for 24 h at room temperature, the formed SiNPs were isolated by using centrifugation 10,000 rpm for 30 min. The sediments were redispersed in ethanol (one time) and water (3 times) followed by centrifugation at a rate of 10,000 rpm for 30 min, respectively. The obtained SiNPs were dried under vacuum at 50 °C for 48 h. The yield obtained was 3.2 g.

2.2.5. Synthesis of Amine Modified SiNPs (SiNP-NH_2)

The above synthesized SiNPs (3 g) was transferred into round bottom flask containing dry toluene (70 mL) and dispersed by using ultrasonication for 45 min, followed by the dropwise addition of (3-Aminopropyl)triethoxysilane (APTES, 0.4 mL, 0.0009 mmol) under vigorous stirring in presence of N2 atmosphere and the reaction is continued for 24 h at 90°C. After the reaction the reaction mixture was cooled to room temperature, the reaction mixture was precipitated in hexane (300 mL). The amine functionalized SiNPs were isolated by using centrifugation at 5000 rpm for 30 min. The sediments were redispersed in acetone and isolated by centrifugation at 5000 rpm for 15 min. This purification cycle was repeated three times. The obtained amine modified SiNPs (SiNP-NH_{2H}, where H indicates higher degree of modification) were dried under vacuum at 70 °C for 48 h, obtained 2.85 g (95% yield). A low surface density of amine modified SiNPs (SiNP-NH_{2L}, where L indicates low modification) was also prepared using the same way (3g of SiNPs with 0.2 mL of APTES) and obtained 2.73 g (91% yield).

2.2.6. Synthesis of RAFT Modified SiNPs (SiNP-CPDB)

The high surface modified SiNP-NH_2 (SiNP-$NH_{2H,}$ 2.75 g) were dispersed in dry THF (50 mL) and ultrasonication for 30 min followed by nitrogen bubbling for 20 min while stirring. To this activated CPDB (CPDB-NHS, 0.5g, 1.3 mmol) was added under stirring and the mixture was stirred for 24 h at room temperature by closing the reaction vessel with aluminum foil. After the reaction, the reaction mixture was precipitated from 4:1 mixture of cyclohexane and diethyl ether (400 mL) and isolated by using centrifugation 7000 rpm for 20

min. The sediments were redispersed in THF followed by the precipitation from 4:1 mixture of cyclohexane and diethyl ether (400 mL) and isolated by using centrifugation 7000 rpm for 20 min for purification. This purification cycle was repeated four times and the obtained RAFT functionalized SiNPs were dried under vacuum at 50 °C for 24 h, and 2.45 g (89% yield, called as SiNP-$CPDB_H$, H indicates high modification) sample was collected. The low surface CPDB anchored SiNPs (SiNP-$CPDB_L$, L indicates low modification) were prepared by using the same way (2.5g low amine modified SiNPs (SiNP-NH_{2L}) with 0.25 g, (0.65 mmol) of CPDB-NHS and obtained 2.3 g (92% yield) of samples. The relative amount of RAFT (CPDB) agent which is covalently attached on the SiNPs was estimated by using TGA analysis[7] and will be discussed in the corresponding chapters.

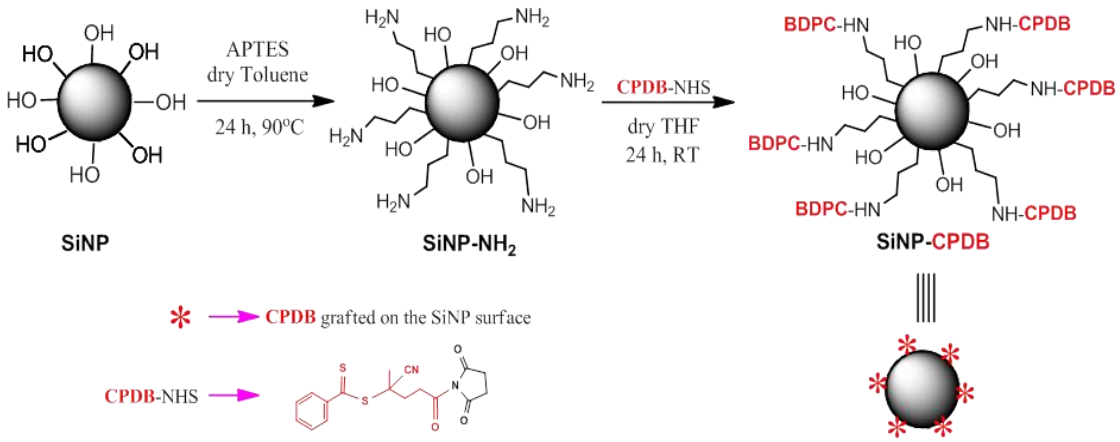

Scheme 2.3. *Synthesis of 4-Cyanopentanoicacid dithiobenzoate modified SiNPs (SiNP-CPDB).*[7]

2.3. Characterization Methods

2.3.1. Spectroscopic Studies

2.3.1.1. FT-IR Study

Fourier transform infrared (FT-IR) spectra of all the powdered samples were recorded on a Nicolet 5700 FTIR spectrometer at a resolution of 0.5 cm^{-1} with an average of 64 scans in the form of KBr pellet.

2.3.1.2. ^{1}H and ^{13}C NMR Study

The NMR spectra the samples were recorded using Bruker AV 400/500 MHz spectrometer in different deuterated solvents or mixture of solvents and will be mentioned in each chapter.

2.3.1.3. UV-Visible Study

Electronic absorption spectra were recorded on a Cary-100Bio (VARIAN) UV-visible spectrometer. Appropriate solvents are used and mentioned in corresponding chapter when required.

2.3.1.4. Wide Angle X-ray Diffraction

The wide angle X-ray diffraction patterns (WAXD) of all the samples were obtained from Philips powder diffraction instrument (model PW 1830). The diffractograms were recorded with nickel-filtered Cu Kα radiation source operated at 40kV and 30mA in the 2θ range 5-40º with a scanning rate of 0.6° 2θ/min.

2.3.2. Microscopy Study

2.3.2.1. FESEM Study

The morphology of all the samples were examined in the Field Emission Scanning Electron Microscope (FESEM, Zeiss Ultra 55 model) instrument operated at 5 kV. A drop of the polymer nanocomposite/ nanoparticles dispersion in water was placed on glass plate, dried at room temperature and gold coated before imaging in FESEM.

2.3.2.2. Transmission Electron Microscopy (TEM)

The morphology of all the samples was studied using transmission electron microscope (TEM) FEI Tecnai Model no. 2083. A drop of the polymer nanocomposite/ nanoparticles dispersion in water was placed on carbon coated copper grid (200 mesh), dried at room temperature and observed under TEM with an acceleration voltage of 200kV.

2.3.2.3. Confocal Raman Study

Confocal Raman microscopic analysis was carried on Alpha300 RA microscope (WITec GmbH, Ulm, Germany) equipped with a frequency NdYAG laser (λ = 532 nm) and a 100X (NA = 0.9) air objective.

2.3.3. Thermal analysis

2.3.3.1. TG-DTA Study

Thermo gravimetric analysis (TGA) of glyconanoparticles was carried out on TG-DTA, (Netzsch STA 409PC) from 30 to 800 ^{o}C with a scanning rate of 10 °C/min in presence of nitrogen flow.

2.3.3.2. DSC Analysis

A differential scanning calorimetry (DSC) instrument (Pyris Diamond DSC, Perkin Elmer) was used to measure the glass transition temperature (T_g) and melting temperature (T_m) of the powder sample by scanning the sample from 20 to 150 °C with a scanning rate of 5 °C min^{-1}. Before scanning, the DSC was calibrated using In and Zn.

2.3.4. Gel Permeable Chromatography

The molecular weights and its distribution (PDI) of the samples were measured at 30 °C using a gel permeation chromatography (GPC, Waters 515 HPLC) with an RI detector (Waters 2414) in various solvents and flowrates and will be discussed in each chapter separately. All the polymer solutions were filtered through 0.45 μm PTFE filter paper. Then 20 μL of these filtered polymer solutions were injected for GPC analysis. Narrow molecular weight distribution polystyrene standards (Polymer Standards Service) with polydispersity index ≤ 1.1 were used for GPC molecular weight calibration.

2.3.5. Particle Size and Zeta Potential Analysis

The hydrodynamic radius, polydispersity and zeta potential of the samples (dispersed in water) were measured using a Dynamic light scattering based Zetasizer (Nano-S90 or Nano-S90, Malvern) instrument. The samples were diluted with water before measurements for making proper concentration.

2.3.6. Dynamic Mechanical Analysis (DMA)

The temperature dependent dynamic mechanical analysis of all membranes samples was carried out using dynamic mechanical analyzer (DMA), model Q-800 TA Instruments. The membranes were cut in 25 mm × 5 mm × 0.15 mm dimension and clamped on to the fixed tension clamp of the instrument and were first annealed at 400°C for 30 minutes followed by equilibration at 100ºC for 20 minutes and then scanned from 100°C to 450°C at a scanning

rate of 4°C/min. The storage modulus (E'), loss modulus (E'') and tan δ values were measured at a constant linear frequency of 1 Hz with a preload force of 0.01 N.

2.3.7. Proton Conductivity

Proton conductivity of all the PA doped membranes was measured with Autolab impedance analyzer (PGSTAT302N) over the frequency range 1 Hz to 100 kHz. The membranes were fixed to a homemade Teflon conductivity cell with four platinum electrodes; two outer electrodes 1.5 cm apart supply current to the cell, while the two inner electrodes 0.5 cm apart on opposite sides of the membrane measure the potential drop across the electrodes. The cell along with the membrane was heated at 100º C for 2 hours to remove water completely after which it was allowed to cool inside a desiccator. The conductivity was measured from room temperature to 160° C at 20° C intervals. The samples were held for 30 minutes at each temperature to reach equilibrium and after which impedance was measured. The proton conductivity was calculated using the equation

$$\sigma = \frac{D}{RBL}$$

where, σ is the proton conductivity (S/cm), D is the distance between the electrodes, B and L are the thickness and width of the membranes, respectively and R is the resistance obtained from Nyquist plots.

References

1. S. Bhattacharjee and D. Bong, *J. Polym. Environ.*, **2011,** *19*, 203.
2. N.M. Huang, H.N. Lim, C.H. Chia, M.A. Yarmo and M.R. Muhamad, Int. *J. Nanomed.* **2011**, *6*, 3443.
3. Y. Mitsukami, M. S. Donovan, A. B. Lowe and C. L. McCormick, *Macromolecules*, **2001**, *34*, 2248.
4. C. L. McCormick and A. B. Lowe, *Acc. Chem. Res.*, **2004**, *37*, 312.
5. N. J. Warren, O. O. Mykhaylyk, D. Mahmood, A. J. Ryan and S. P. Armes, *J. Am. Chem. Soc.*, **2014**, *136*, 1023.
6. W. Stöber, A. Fink and E. Bohn, J. *Colloid. Interface Sci.*, 1968, **26**, 62.
7. C. Li, J. Han, C. Y. Ryu and B. C. Benicewicz, *Macromolecules*, 2006, **39**, 3175.

Chapter 3

Tunable Core-Shell Nanoparticles: Macro-RAFT Mediated One-Pot Emulsion Polymerization

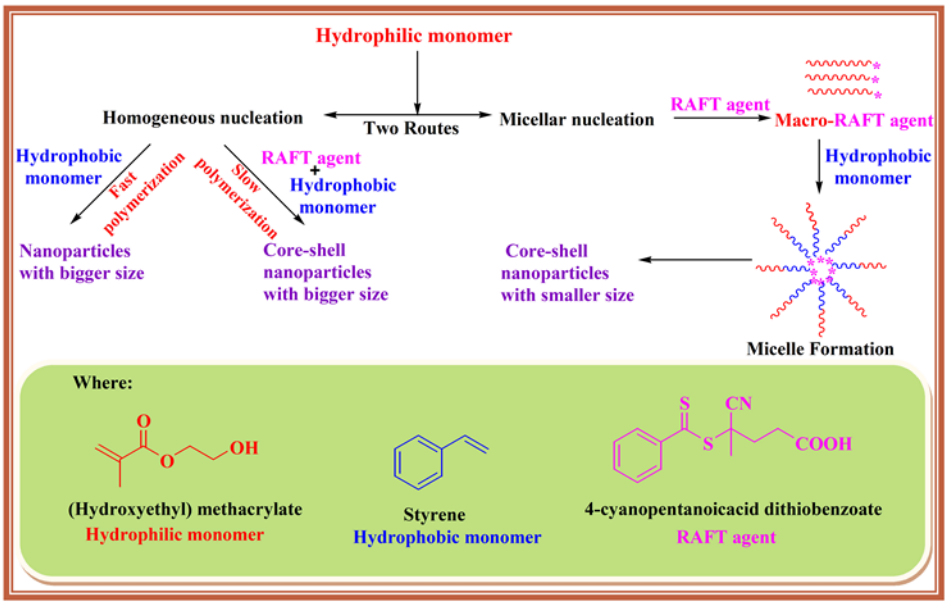

Simple and robust one-pot procedure for the preparation of polystyrene (PS) nanoparticles with a functional polymeric shell on the surface of PS particle with a variation in particle size as well as core-shell dimensions.

RSC Adv., 2014, 4, 2382-2388.

3.1. Introduction

RAFT (Reversible Addition Fragmentation Chain Transfer) polymerization has received a continuous interest from scientific community and widely accepted for the development of novel polymeric materials in very simple experimental conditions.[1,2] Due to ease in reaction condition, it is successful in complex system such as dispersion and emulsion polymerizations.[3] RAFT polymerization became the focus of intensive research since method allows synthetic tailoring of macromolecules with complex architectures and applicable to wide range of vinyl monomers under variety of experimental conditions including the preparation of water-soluble materials. Hydrophilic or amphiphilic macromolecular RAFT agent (macro-RAFT agent), which acts as both the macro-RAFT agent and the steric/electrosteric stabilizer can undergo RAFT polymerization in aqueous heterogeneous system.[4-9] The use of water soluble RAFT agent allowed for the synthesis of water soluble macro-RAFT agent which on chain extension leads to formation of surfactant-like polymer molecules which on further polymerization leads to nanoparticles with least polydispersity. The process appeared to have all advantages associated with the conventional emulsion polymerization process. The formation of a predetermined morphology under these simple reaction conditions is appealing but requires clean and homogeneous growth throughout the process.

Series of aqueous dispersion RAFT polymerizations mediated with different macro-RAFT agents, and morphologies like spheres, worms, vesicles, or lumpy rods have been reported.[10-16] Among different morphology, the core-shell nanoparticles have advantage of combining multiple functionalities on nanoscopic scale.[17] Nanoparticles designing mainly focus on more complex nanoscopic polymer core-shell architectures potentially useful in material science for paints, coatings, adhesives, and impact modifiers.[18,19] Ho et. al. explained several methods for the formation of core-shell particles such as grafting-to, grafting-from, layer by layer technique but these all processes are multistep and graft polymerization even though one pot process but needs water-soluble polymer containing amino groups.[20] However, tuning the core-shell dimensions of polymer nanoparticles is not achieved yet but manipulation of the shell size was carried out in case of poly-(N-isopropylacrylamide) (PNIPAM) coated gold clusters because of thermo responsive nature of PNIPAM.[21]

In our earlier publications,[22-24] we have synthesized polymer particles with core–shell morphology by using hydrophilic polystyrene sulfonate-sodium (PSS-Na) based macro-RAFT

agent in surfactant-free emulsion polymerization.[22] The hydrophilic macro-RAFT agent forms the shell material and the size along with dispersity of nanoparticles is increased as the molecular weight of hydrophilic macro-RAFT agent is increased.[23] The influence of different hydrophobic monomers on the morphology and emulsion stability was investigated. Colloidal particles of polystyrene showed a spherical morphology while colloidal particles of PMMA were observed with an oval structure.[24] In this article we have used HEMA as hydrophilic monomer to generate macro-RAFT agent. However, we realized that PHEMA based macro-RAFT cannot be utilized as surfactant like molecule in the emulsion owing to its insolubility in aqueous environment. Therefore in this article we have found out a new strategy, a one pot process to generate core-shell nanoparticles based on PHEMA macro-RAFT agent. Also, the present article focuses on use of controlled radical polymerization based on macro-RAFT agent under surfactant-free emulsion conditions for tuning the core-shell dimensions of polymer nanoparticles. Here, our special focus is to simplify the process for the generation of core-shell nanoparticles using common monomers. In addition to that, we propose tuning the dimensions of core-shell nanoparticles which can be achieved by one-pot procedure where PHEMA based macro-RAFT are formed first and followed by in-situ chain extension with hydrophobic monomer such as styrene. By tuning the nanoparticles size, it would be possible to control interstitial pore size between nanoparticles. Adjustable shell wall thickness in hybrid nanoparticles may enhance capability for chemical encapsulation, storage and release application.[25]

The surfactant free emulsion polymerization using macro-RAFT agent is not aimed for controlled free radical polymerization in an aqueous dispersed system rather we have used the advantages of well-defined hydrophilic macro-RAFT agent with high chain-end reactivity. The initial idea was to stabilize classical latex particles (not necessarily under controlled conditions), but it then appeared to be good over control of the polymerization which would allow the in situ creation of well-defined nanostructures.[26-28] Recently, the one pot synthesis of amphiphilic block copolymers based on poly(methacrylic acid) based macro-RAFT agent have been carried out in water medium.[29,30] This one pot method provides the advantage to skip the often time-consuming step of preparation and purification of the hydrophilic macro-RAFT agent leading to in-situ formation hydrophilic and hydrophobic segments.

3.2 Experimental Section

3.2.1 Materials and Methods

All information about the materials used in this study and the synthetic procedure for the preparation of RAFT agent are discussed in Chapter 2. The experimental methods and the characterization techniques which include molecular weight measurements by GPC (DMAc, 0.5 mL/min flow rate), thermal analysis by DSC, microscopic analysis by FE-SEM and TEM are discussed in Chapter 2.

3.2.2 One-pot surfactant free emulsion polymerization

3.2.2.1 Step one: Synthesis of Poly (HEMA) based Macro-RAFT Agent

In a typical recipe, HEMA, ACP (I) and RAFT (R) agent were added in a round bottom flask containing 30 ml water–ethanol mixture (90:10 by weight). The flask was deoxygenated by bubbling N_2 through solution for 15 min. Then the flask is immersed into an oil bath at 75 ^{o}C and polymerization allowed to proceed for 2 to 6 hours by continuous stirring using a magnetic stirrer. Three different weights of HEMA namely 60 mg, 150 mg and 300 mg which are 2, 5 and 10 wt.% with respect to styrene weight (3g), respectively were used to prepare PHEMA macro-RAFT agent.

Table 3.1 summarizes all reaction condition to make PHEMA macro-RAFT agent in 6 hours. HEMA weight percentage with respect to styrene are numbered as 1 (2 wt.%), 2 (5 wt.%) and 3 (10 wt.%). The reaction for different molecular weight for generation of macro-RAFT are labeled as A, B and C for theoretical molecular weight 8400, 5600 and 2800, respectively. Whereas, the Table 3.2 summarizes concentration and first step reaction time effect where 4, 5 indicates 2 wt.% and 10 wt.% HEMA with respect to styrene, respectively while X, Y and Z represents 2, 4 and 6 hours first step reaction time, respectively.

3.2.2.2 Step two: Surfactant free emulsion polymerization

In a typical second step, 30 mg of NaHCO3 was added into the step one followed by addition of ACP making total initiator concentration 30 mg (1.07 X 10-1 mmol) which is considering both steps kept constant at 1% (by weight) relative to styrene for all reactions. The flask was then deoxygenated by bubbling N_2 through the solution for 10 min. Styrene (3 g, 28.84 mmol) was then added into the flask. The whole reaction mixture was continued at 75ºC and stirred for 20 hours which leads to nanostructure formation (Scheme 3.1).

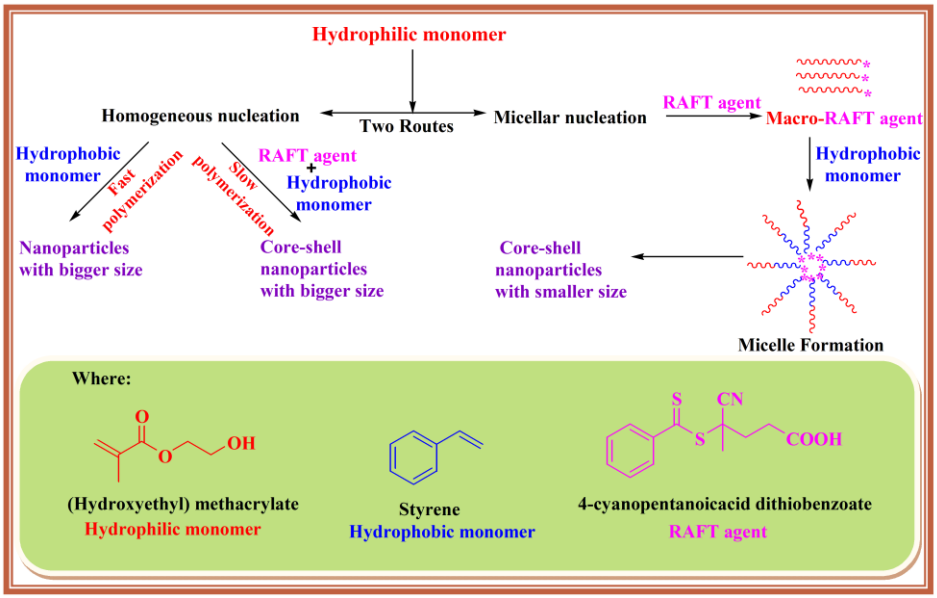

Scheme 3.1. *Macro-RAFT mediated surfactant free emulsion polymerization leading to nanostructure formation*

3.3 Results and Discussion

In series of experiments, the RAFT polymerization of HEMA was conducted in water-ethanol mixture using 4-cyanopentanoicacid dithiobenzoate as a RAFT reagent (R) and 4,4′-azobis (4-cyanopentanoicacid) (ACP) as an initiator (I), followed by chain extension using styrene as hydrophobic monomer (Scheme 3.1). The first step aqueous RAFT polymerization for PHEMA synthesis were under the similar conditions with the weight ratio of [R]/[I] is set to 3 for evaluating the effect of PHEMA molecular weight. It is well known that the molar ratio of the RAFT agent to initiator ([R]/[I]) is a key parameter for RAFT polymerization.[32] In general, RAFT polymerization under high [R]/[I] values runs slow and leads well-controlled RAFT polymerization. Considering this advantage, the weight ratio of [R]/[I] is set to 5/1 in evaluating effect of first step reaction time (Table 3.2).

To our knowledge, there is no report on the polymerization of HEMA in water as well as with block copolymerization with styrene using RAFT polymerization leading to nano-sized core-shell particle morphology. It is difficult to determine progress of HEMA polymerization as its concentration is too low (0.2 to 1 wt.%) with respect to overall reaction media. However, our intention is not to control polymerization by macro-RAFT agent but to utilize its chain end reactivity which will play active role in tuning the morphology explained briefly by different nucleation mechanism.

Table 3.1: RAFT agent concentration (which is related to molecular weight of PHEMA) and comonomer (HEMA) concentration variation

	First Step				Second Step
Expt. No.	HEMA	$M_{n,theory}$ [a]	RAFT	ACP	ACP
1A	60 mg (2 wt.% w.r.t. St)	8400	2 mg (0.0071mmol)	0.7 mg	29.3 mg
1B		5600	3 mg (0.0107 mmol)	1 mg	29 mg
1C		2800	6 mg (0.0214 mmol)	2 mg	28 mg
2A	150 mg (5 wt.% w.r.t. St)	8400	5 mg (0.0178 mmol)	1.6 mg	28.4 mg
2B		5600	7.5 mg (0.0267 mmol)	2.5 mg	27.5 mg
2C		2800	15 mg (0.0535 mmol)	5 mg	25 mg
3A	300 mg (10 wt.% w.r.t. St)	8400	10 mg (0.0357 mmol)	3.3 mg	26.7 mg
3B		5600	15 mg (0.0535 mmol)	5 mg	25 mg
3C		2800	30 mg (0.0178 mmol)	10 mg	20 mg

3.3.1 Effect of RAFT agent concentration

Theoretical molecular weight (M_n, theory) varies with the RAFT agent concentration (Table 3.1). We consider change in RAFT agent concentration as molecular weight effect which controls molecular weight of polymer (PHEMA) formed through RAFT polymerization. The weight ratio of the hydrophilic PHEMA based macro-RAFT agent to styrene usually kept in the range from 2% to 10%. Table 3.1 shows the recipe for the nine batches. Expt. 1A, 1B and 1C are carried out by using 2 wt.% of HEMA; Expt. 2A, 2B and 2C by using 5 wt.% of HEMA and 3A, 3B and 3C by using 10 wt.% of HEMA with respect to styrene. From FESEM images [Figure 3.1] it is clear that, high RAFT agent concentration i.e. low molecular weight of PHEMA leads to good small spherical particle formation with narrow particle size distribution (Batches 1C, 2C and 3C); whereas batches low RAFT agent concentration i.e. high molecular weight A and B (1A, 2A, 3A and 1B, 2B, 3B) show bigger particle size with high particle size distribution. This may be due to several reasons (1) more availability of thiocarbonylthio moiety having more chain end reactivity. (2) more number of small chains of PHEMA based macro-RAFT agent leading to more number of micelle. This is

in good agreement with earlier report for the different molecular weight PSSNa based macro-RAFT agent prepared separately and then used in surfactant-free emulsion polymerization.[23] Considering these observation, we focused mainly on lower chain length hydrophilic macro-RAFT i.e. higher RAFT agent concentration where very good results are obtained in terms of controlling particle size as well as morphology tuning.

Table 3.2. *One-pot synthesis of core–shell polymer nanoparticles using poly(HEMA) macro-RAFT*

First Step					Second step with final colloid characterization				
Expt. No.	[HEMA]	[RAFT]	[ACP]	Reaction Time (hr)	[ACP]	Final Conversion	Particle Size (nm)	Core diameter (nm)	Shell thickness (nm)
4X	60 mg	6 mg	1.2 mg	2	28.8 mg	86%	96	No core-shell morphology observed.	
4Y	(2 wt.% w.r.t. St)			4		88%	100		
4Z				6		84%	155		
5X	300 mg	30 mg	6 mg	2	24 mg	58%	230	126	52
5Y	(10 wt.% w.r.t. St)			4		54%	144	98	23
5Z				6		60%	85	59	13

3.3.2 Effect of reaction time for the PHEMA based macro-RAFT agent formation

Table 3.2 shows the recipe and characterizations for the six batches. Expt. 4X, 4Y and 4Z are carried out by using 2 wt.% of HEMA and Expt. 5X, 5Y and 5Z by using 10 wt.% of HEMA with respect to styrene. To determine the monomer conversion, small quantity of final emulsion were taken and quenched by using hydroquinone (0.01% solution in water) and measured gravimetrically. Final conversion decreases (Table 3.2) from 80% to 60% when weight percent of HEMA increased from 2 to 10 wt.%, this may be because of more chain transfer due to increase in thiocarbonylthio moiety from the RAFT reagent.

From FESEM images (Figure 3.2), we observed that the large and less uniform particle size for the first step reaction timing i.e. 2hr and 4 h which cannot form such well-ordered array which is in good agreement with previous report.[33] Soft and hydrophilic shell is necessary in the formation of three-dimensional colloidal crystals. The shell with least

functionalities on polymer particles forms close packed structures while hydrophilic shells adjusts interaction among the microspheres and facilitates self-assembly

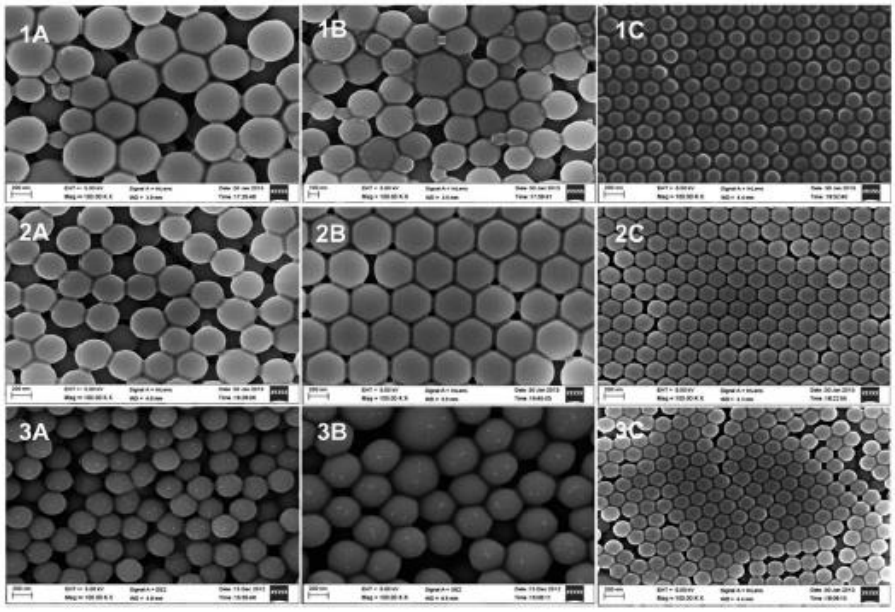

Figure 3.1. *FESEM images for colloids 1A, 1B, 1C using 2 wt% of HEMA; 2A, 2B, 2C using 5 wt% of HEMA; and 3A, 3B, 3C using 10 wt% of HEMA, respectively, where A, B and C indicate PHEMA theoretical molecular weights of 8400, 5600 and 2800, respectively.*

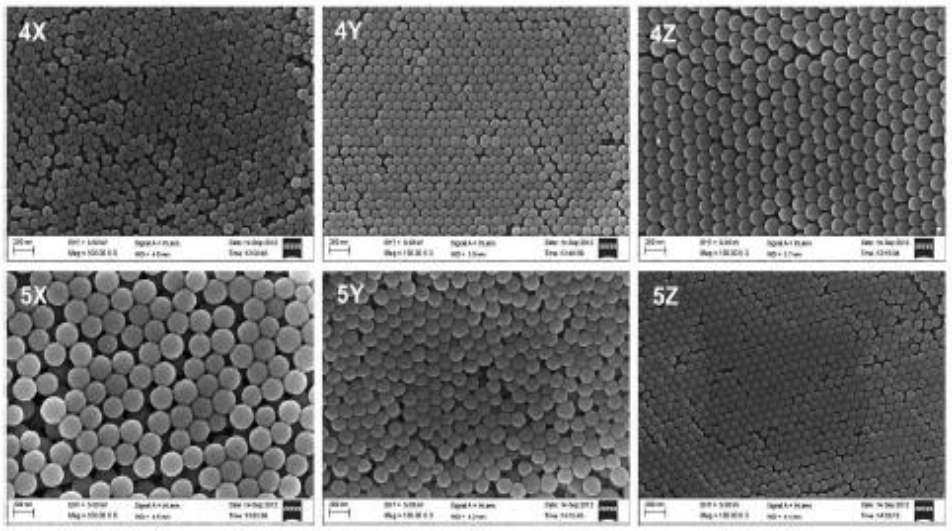

Figure 3.2. *FESEM images for colloids 4X, 4Y, 4Z using 2 wt% of HEMA and 5X, 5Y, 5Z using 10 wt% of HEMA, respectively. Where X, Y, Z indicates first step reaction time 2 h, 4 h and 6 h, respectively.*

On careful observation of morphology from TEM images (Figure 3.3), we found that the particle size goes on increasing for the expt. 4X to 4Y to 4Z i.e. for 2 wt.% of HEMA (Table 3.2). This may be because of enrichment of full HEMA conversion in the first step due to increase in first step reaction time from 2 h to 6 h ultimately leading to bigger final particle size. While the case is exactly reverse when we increase HEMA concentration from 2 wt.% to 10 wt.%. Due to increase in hydrophilic monomer there is possibility of forming more number of surfactant like molecule which lead to more number of micelle formation i.e. more number of polymer nanoparticles. For Expt. 5X, 5Y and 5Z the overall particle size decreases from 230 nm to 85 nm (Table 3.2).

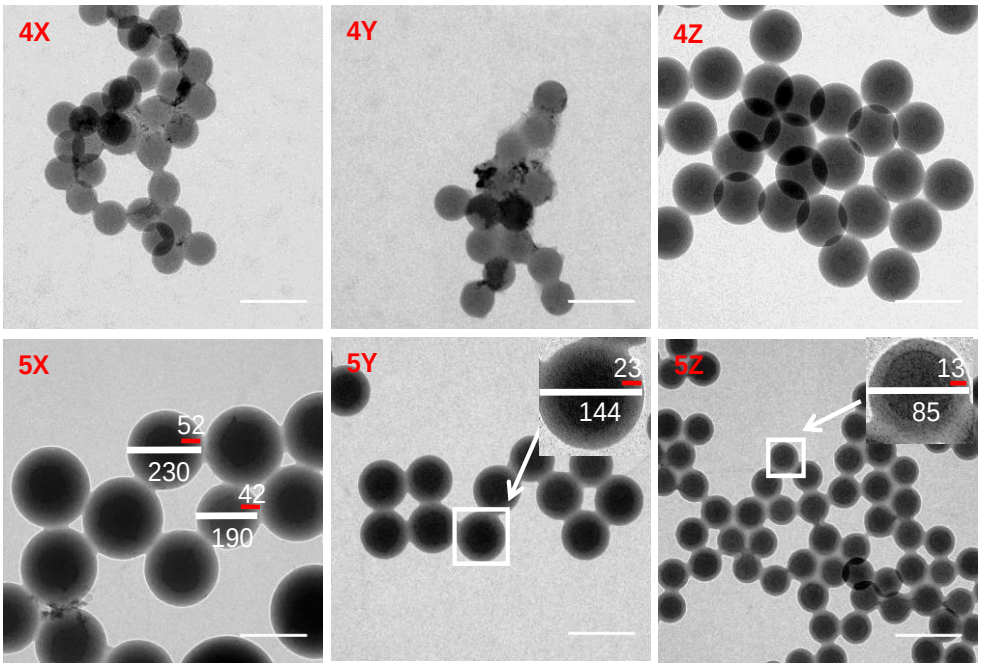

Figure 3.3. *TEM images for colloids 4X, 4Y, 4Z using 2 wt.% of HEMA 5X, 5Y, 5Z using 10 wt% of HEMA, respectively. Where X, Y, Z indicates first step reaction time 2 h, 4 h and 6 h, respectively. TEM scale bar is 200 nm in all the cases.*

Also we observed from Table 3.2 and Figure 3.3 that in Expt. 5Z least shell thickness (~13 nm) on particle can form comparatively good self-assembly among the particles compared to Expt. 5X (shell thickness ~ 52 nm) and Expt. 5Y (shell thickness ~ 23 nm). Even though we cannot observe the shell layer in TEM image for 4X, 4Y and 4Z but still there is presence of very less poly(HEMA) based macro-RAFT, which also leads to close packing of

polymer nanoparticles. The shell thickness has influence on self-assembly of polymer nanoparticles.

The proposed reason for this observations may be due to different nucleation theories that are accepted to different degrees, propose different particulate entities as the reaction locus for the reaction to occur. Micellar nucleation theory proposes the monomer swollen micelles as the main nucleation locus while the homogeneous nucleation considers the precipitated oligomeric radicals as the main nucleation locus. The homogeneous nucleation mechanism considers the precursor particles as the main nucleation locus. Thus, identification of the main nucleation loci in macro-RAFT mediated surfactant-free emulsion polymerization reactions constitutes to the particle formation as well as its dimension tuning. For a homogeneous nucleation polymerization mechanism, the free radicals were generated in the aqueous phase and then propagated with the joining of the monomer units until the oligomeric radicals exceeded their solubility and precipitated (in time zero condition). On the other hand, for the micellar nucleation mechanism, both the monomer initiation and polymer chain growing period occurred inside a micelle.

The nucleation mechanism is an important factor which affects the size of the nanoparticles. PHEMA based macro-RAFT agent exhibited obvious advantages over unreacted HEMA. A great number of smaller polymer particles would be generated in macro-RAFT mediated micellar nucleation predominated system compared with unreacted HEMA homogeneous nucleation polymerization system. In addition, the particle sizes of the latexes were marginally affected by the PHEMA based macro-RAFT agent and unreacted HEMA concentration; higher PHEMA percentage gave rise to smaller size nanoparticles while higher unreacted HEMA content give rise to bigger particle size. These phenomena possibly illustrate three completely different mechanisms represented by micellar nucleation mechanism (PHEMA macro-RAFT), partially homogeneous nucleation mechanism (PHEMA with unreacted HEMA) and homogeneous nucleation mechanism (only HEMA) In homogeneous nucleation process, the monomer transfer was inevitable and led to the formation of larger particles that of the micellar nucleation system, in which the mass transfer is prevented. More number of macro-RAFT chain without any unreacted HEMA in the reaction medium leads to more number of amphiphilic block copolymer which proceed through micellar nucleation to form more number of particles with smaller size (in case of 5Z). While for 5X and 5Y the less HEMA conversion causes more unreacted HEMA at the surface of nanoparticles leading to

partial homogeneous nucleation which shows increase in shell thickness. For 5X the more polydispersity is observed among particle size due to unreacted HEMA at the surface leading to disproportion of polymer particles. Incomplete HEMA conversion leads to advantage of tuning shell thickness but unreacted HEMA leads to comparatively more polydispersity among the final particle size. If the concentration of the PHEMA based macro-RAFT agent is adequate to provide a sufficient number of micelles to encapsulate all the generated and newly formed precursors, the particle size will become stable and will be minimized (PHEMA with 10 wt.% after six hours).

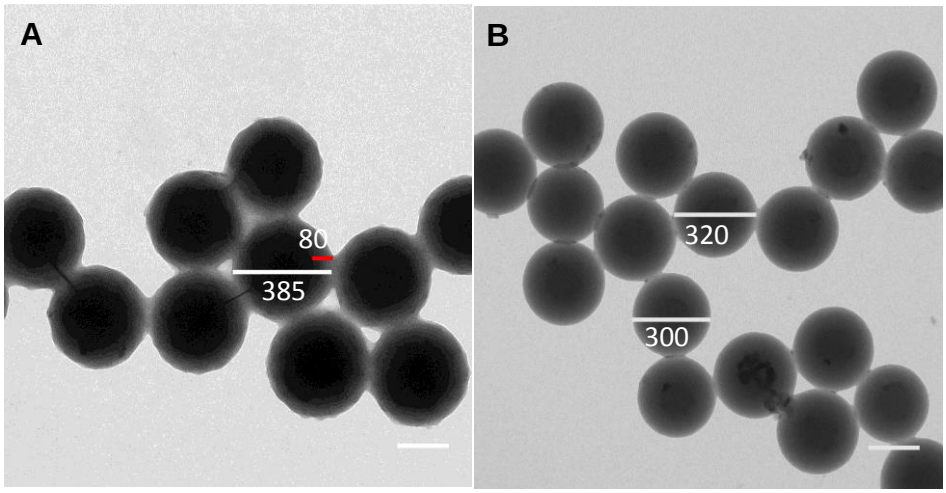

Figure 3.4. *TEM images for colloids A and B with and without using a RAFT agent, respectively, in time zero condition with 10 wt% of HEMA. TEM scale bar is 200 nm in both cases.*

3.3.3 Homogeneous nucleation at zero time condition for surfactant-free emulsion polymerization

To confirm the effect of RAFT agent and zero time condition we did several other experiments by using and without using RAFT reagent at zero hours which ultimately has role on the nucleation process. At zero hours there is no possibility of micellar nucleation and reaction goes through homogeneous nucleation only. From the TEM images Figure 3.4, we observe there is no core-shell morphology (with 72 % final monomer conversion after 6 hrs) observed for the emulsion nanoparticles formed without using RAFT agent. While there is effective role of RAFT agent concentration as reaction proceeds slowly (with 68% final monomer conversion after 20 h) giving core-shell morphology to the nanoparticles. From

these results we summarize there is effect of not only RAFT agent but also reaction time for first step HEMA polymerization.

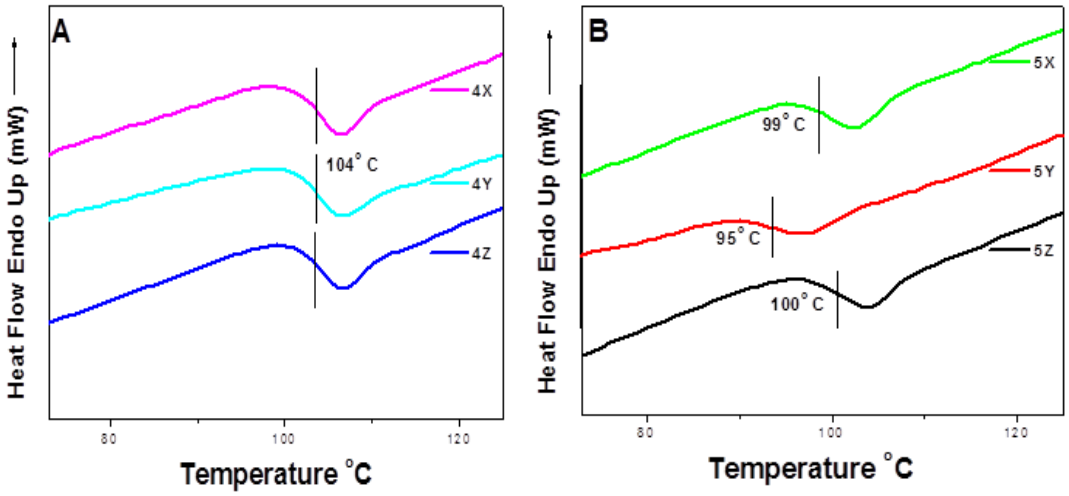

Figure 3.5. *DSC thermograms for colloids 4X, 4Y and 4Z using 2 wt% of HEMA shown in [A] and 5X, 5Y and 5Z using 10 wt% of HEMA shown in [B], respectively. Where X, Y and Z indicate the first step reaction time 2 h, 4 h and 6 h, respectively.*

PHEMA has glass transition temperature of about 86°C,[34] while PS shows 105°C.[35] DSC thermograms of colloidal nanoparticles are shown in Figure 3.5. The glass transition temperature of PHEMA component not observed due to very small block lengths with respect to polystyrene component. However, the T_g values for polystyrene segment in nanoparticles differs with the T_g value of homo polystyrene due to the PHEMA content. There is clear decrease in Tg value from 104°C to 95-100°C as concentration of PHEMA increased from 2 wt.% to 10 wt.% due to soft and flexible segment of hydroxyethyl group of PHEMA. GPC of the final colloids is given in Fig.3.6 where it shows bimodal peaks for the 5X, 5Y and 5Z colloids which may be due to blocky nature. Table 3.3 lists the MW and PDI obtained from GPC traces.

Table 3.3. j;dfmgkolf dhgmjcvfhmkjkg [,oljg5mtikh6

Sample Name	Mn	PDI
4X	371872	2.27
4Y	145082	1.46
4Z	277637	2.51
5X	269112	5.59
5Y	128930	5.99
5Z	163397	3.02

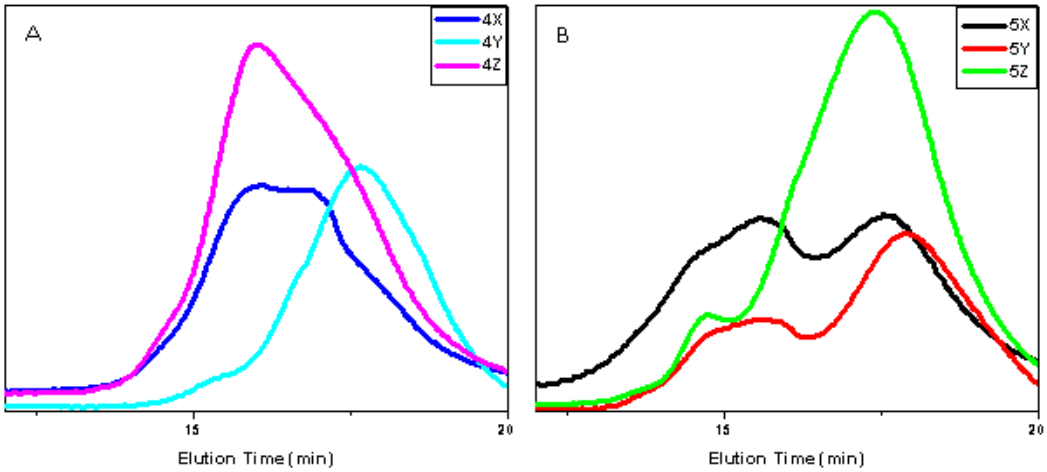

Figure 3.6. *GPC traces of colloids 4X, 4Y, 4Z [A] and 5X, 5Y, 5Z [B].*

3.4 Conclusion

A new method to achieve well-controlled surfactant-free aqueous RAFT polymerization of styrene in the presence of hydrophilic macro-RAFT agents for synthesis of core-shell nanoparticles is proposed. This strategy further utilized for tuning the core-shell dimensions. These core-shell particles with different shell thickness with hydroxyl functional groups could provide a unique advantage in encapsulating small molecules or inorganic nanoparticles (NPs) as well as in directing the self-assembly. This development may promote the interdisciplinary researchers among nanotechnology, functional materials and paint industry.

REFERENCES

1. G. Moad, E. Rizzardo and S. H. Thang, *Aust J Chem*, 2006, **59**, 669.
2. G. Moad, E. Rizzardo and S. H. Thang, *Aust J Chem*, 2012, **65**, 985.
3. C. Barner-Kowollik C. "Handbook of RAFT Polymerization", Wiley-VCH, Weinheim 2008.
4. J. Rieger, W. J. Zhang, F. Stoffelbach and B. Charleux, *Macromolecules*, 2010, **43**, 6302.
5. J. Xu, X. Wang, Y. Zhang, W. Zhang and P. Sun, *J Polym Sci Part A Polym Chem*, 2012, **50**, 2484.
6. C. Grazon, J. Rieger, N. Sanson and B. Charleux, *Soft Matter*, 2011, **7**, 3482.
7. W. Shen, Y. Chang, G. Liu, H. Wang, A. Cao and Z. An, *Macromolecules*, 2011, **44**, 2524.
8. Z. An, Q. QiuG and M. Liu, *Chem Commun*, 2011, **47**, 12424.
9. G. Liu, Q. Qiu, W. Shen and Z. An, *Polym Chem*, 2012, **3**, 504.
10. A. Blanazs, J. Madsen, G. Battaglia, A. J. Ryan and S. P. Armes, *J Am Chem Soc*, 2011, **133**, 16581.
11. A. Blanazs, A. J. Ryan and S. P. Armes, *Macromolecules*, 2012, **45**, 5099.
12. P. Chambon, A. Blanazs, G. Battaglia and S. P. Armes, *Macromolecules*, 2012, **45**, 5081.
13. Y. Li and S. P. Armes, *Angew Chem Int Ed*, 2010, **49**, 4042.
14. S. Sugihara, S. P. Armes, A. Blanazs and A. L. Lewis, *Soft Matter*, 2011, **7**, 10787.
15. S. Sugihara, A. Blanazs, S. P. Armes, A. J. Ryan and A. L. Lewis, *J Am Chem Soc*, 2011, **133**, 15707.
16. M. Semsarilar, V. Ladmiral, A. Blanazs and S. P. Armes, *Langmuir*, 2012, **28**, 914.
17. W. Schärtl, *Nanoscale*, 2010, **2**, 829.
18. O. Kalinina and E. Kumacheva, *Macromolecules*, 2001, **34**, 6380.
19. A. K. Khan, B. C. Ray and S. K. Dolui, *Prog Org Coat*, 2008, **62**, 65.
20. K. M. Ho, W. Y. Li, C. H. Wong and P. Li, *Colloid Polym Sci*, 2010, **288**, 1503.
21. J. Shan and H. Tenhu, *Chem Commun*, 2007, **44**, 4580.
22. N. R. Yeole, D. G. Hundiwale and T. Jana, *J Colloid Interface Sci*, 2011, **354**, 506.
23. N. R. Yeole and D. G. Hundiwale, *Colloids Surf A*, 2011, **392**, 329.

24. N. R. Yeole and D. G. Hundiwale, *RSC Adv.*, 2013, **3**, 22213.
25. H. G. Bagaria, S. B. Kadali and M. S. Wong, *Chem Mater*, 2011, **23**, 301.
26. M. Manguian, M. Save and B. Charleux, *Macromol Rapid Commun*, 2006, **27**, 399.
27. A. M. Dos Santos, J. Pohn, M. Lansalot and F. D'Agosto, *Macromol Rapid Commun*, 2007, **28**, 1325.
28. J. Bernard, M. Save, B. Arathoon and B. Charleux, *J Polym Sci Part A Polym Chem*, 2008, **46**, 2845.
29. I. Chaduc, W. Zhang, J. Rieger, M. Lansalot, F. D'Agosto and B. Charleux, *Macromol Rapid Commun*, 2011, **32**, 1270.
30. I. Chaduc, M. Girod, R. Antoine, B. Charleux, F. D'Agosto and M. Lansalot, *Macromolecules*, 2012, **45**, 5881.
31. Y. Mitsukami, M. S. Donovan, A. B. Lowe and C. L. McCormick, *Macromolecules*, 2001, **34**, 2248.
32. A. Goto and T. Fukuda, *Prog Polym Sci*, 2004, **29**, 329.
33. Q. Meng, Z. Li, G. Li and X. X. Zhu, *Macromol Rapid Commun*, 2007, **28**, 1613.
34. M. C. Shen, J. D. Strong and F. J. Matusik, *J Macromol Sci Phys*, 1967, **B1**, 15.
35. G. Reiter, M. Sferrazza and P. Damman, *Eur Phys J E*, 2003, **12**, 133.

Chapter 4

Polystyrene–Graphene Oxide (GO) Nanocomposite Synthesized by Interfacial Interactions between RAFT Modified GO and Core–Shell Polymeric Nanoparticles

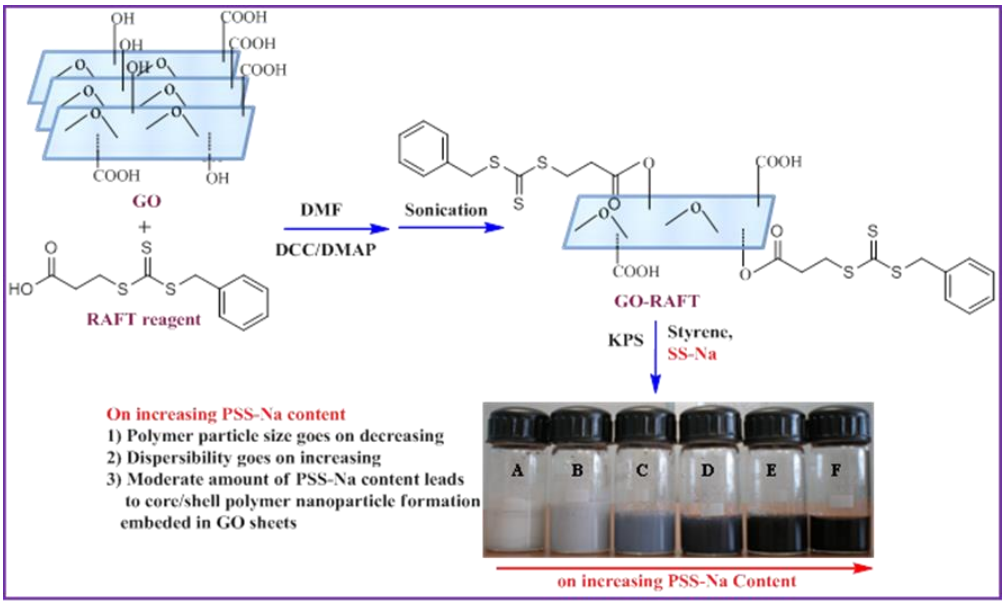

A simple and robust one-pot method for the preparation of polystyrene (PS)/graphene oxide (GO) nanocomposite using reversible addition fragmentation chain transfer (RAFT) modified GO in surfactant free emulsion polymerization.

J. Colloid Interface Sci., 2015, 443, 137–142

4.1. Introduction

Graphene, two-dimensional carbon nanostructure,[1,2] has attracted huge attention recently since it holds great potential applications in many technological fields.[3-8] However, lack of efficient synthetic method for the preparation of processable graphene sheets in large quantities has been the bottleneck for exploiting most useful applications. Chemical oxidation is considered to be one of the suitable methods in preparing large scale of exfoliated graphene oxide sheets which on reduction lead to graphene synthesis. [9] In this method, graphene oxide (GO) obtained by oxidation of graphite followed by exfoliation of graphite oxide layers using ultrasonic wave and on further reduction by hydrazine gives graphene. GO has several functional groups such as hydroxyl, carbonyl, epoxy also carboxylic groups mainly at the edges of carbon sheets, which enables the modification, and formation of nanocomposites of graphene with varieties of other materials including functional polymers.

The incorporation of small amount of graphene into polymers[10-14] can achieve substantial enhancement in properties like reinforcement, damage tolerance, electrical and thermal conductivity, corrosion protection, abrasion resistance, flame retardancy, etc. It is well known fact that graphene nanocomposites properties strongly depend on effective dispersion of graphene in the polymer matrix and good interfacial adhesion between polymer and graphene.

Researchers in the field of composites have grabbed the opportunity to develop multi-functional polymer nanocomposites (PNCs) filled with graphene oxide. Functionalized graphene (FG) has its natural advantages to be ideal nanofiller for PNCs since the FG still possesses most physical properties of graphene although it has a partly damaged carbon structure; and the functionalities on the surface of graphene can enhance the dispersion of graphene in polymeric matrices and the interfacial interaction between graphene and polymeric matrices. Recently, GO coated with PS was prepared using different methods via pickering emulsion polymerization,[15] mini emulsion polymerization[16] and several controlled radical polymerization (ATRP,[17] RAFT[18]), electrostatic interactions and π-π accumulations[19], etc.

Controlled/living radical polymerization (CLRP) such as RAFT polymerization[20], ATRP[21] with grafting-from and grafting-to methods leading to the route for post modification and improvement of final GO hybrid structures, shows great scope for materials applications. Among several CLRP, RAFT polymerization is often used method for designing different architectures due to its several advantages such as use of wide range of monomers as well as it

works in simple reaction conditions[22-26]. Combination of RAFT process and GO practically may lead to exfoliated GO tailor-made polymer nanocomposites with core-shell morphology. The hydroxyl groups of GO on esterification with carboxylic group of RAFT agent lead to formation of RAFT modified-graphene oxide (RGO)[16].

As per our knowledge, synthesis of GO modified with core-shell polymer nanoparticles via one pot process along with improved dispersibility in aqueous media has not been reported in literature. Here we report, the successful synthesis of core-shell polystyrene-polystyrene sulfonate (PS-PSS-Na) particles with GO sheets forming "smart-composite" using surfactant free emulsion polymerization. The approach developed presents a smart route to produce novel GO-based polymeric nanostructures with potential as important building blocks in nanocomposite materials.

4.2 Experimental Section:

4.2.1 Materials and Methods:

All information about the materials used in this study and the synthetic procedure for the preparation of RAFT agent is discussed in the Chapter 2. The experimental methods and all the characterization techniques which include spectroscopic characterization by UV-Vis and FT-IR, thermal analysis by TGA, microscopic analysis by FE-SEM and TEM, zeta potential DLS study are discussed in Chapter 2.

4.2.2. Preparation of highly oxidized graphene oxide (GO)

Natural graphite powder was oxidized to graphene oxide (GO) by using a simplified Hummer's method. The procedure is as follows: The graphite powder (1 g) was mixed with concentrated H_2SO_4:H_3PO_4 (320:80 ml) and potassium permanganate (3 g) using magnetic stirrer. All materials were added very slowly and the mixture was stirred for next 3 days. The mixture color changed from dark green to dark brown. Then to stop reaction, 30% H_2O_2 was added into the solution until the color of the mixture changed into brilliant yellow indicating fully oxidized graphite. Then the mixture was washed three times with dil. HCl and millipore water until pH in the range of 4-5 was achieved. The washing was carried out by centrifugation followed by decantation. Finally the highly oxidized graphene oxide product was dried under vacuum.

4.2.3. Synthesis of GO-RAFT agent

GO (125 mg) was stirred in DMF (25 ml) for 15 min, after which it was sonicated for a further 15 min by using ultra sonicator. The sonication was done to allow effective dispersion of the GO sheets in the solvent DMF. RAFT agent (125 mg) was then added and the resultant mixture stirred for 5 min at room temperature. After that DCC (125 mg) and DMAP (25 mg) were added to the solution and the mixture was stirred at room temperature for 24 hours (Scheme 4.1). The solvent was removed under vacuum and the solid was washed with DCM until the washings are free of the RAFT agent. The coupling of GO and RAFT was monitored by UV-Vis spectroscopy. The washings after the reaction were done to remove the unattached RAFT agent. The resultant product was then dried under vacuum to yield GO-RAFT.

4.2.4. In-situ emulsion polymerization for nanocomposites preparation using GO-RAFT

In 25 mL round bottom flask, 10 mL of water was taken. After 15 min of N_2 purging, 5 mg of GO-RAFT was added into the water and dispersed using sonication for 5 min. Initiator KPS (10 mg) was added to it. Then ionic monomer styrene sulfonate sodium salt (SS-Na) 1g was added to the reaction mixture, followed by hydrophobic monomer [styrene (1.1 ml)]. This mixture was refluxed at 70°C at 500 rpm stirring speed for 20 hours (Scheme 4.1). Finally we collected colloidal juice. We altered the SS-Na concentration for Expt. A, B, C, D, E with 0, 2, 6, 10, 15 wt.% with respect to styrene, respectively. Whereas Expt. F was carried out with 100 wt.% SS-Na without any hydrophobic monomer styrene.

4.3 Results and Discussion:

4.3.1. Synthesis of PS/GO nanocomposite by in-situ polymerization

Initially, natural graphite powder was oxidized to graphene oxide (GO) by using a modified Hummer's method.[28] RAFT reagent further modifies GO by esterification process forming GO-RAFT agent using 1,3-dicyclohexyl carbodiimide (DCC), and 4-dimethyl amino pyridine (DMAP) as coupling agent at room temperature (Scheme 4.1). The coupling of GO and RAFT was monitored by UV-Vis spectroscopy (Figure 4.1 and 4.2). The washings after the reaction were done to remove the unattached RAFT agent. The resultant product was then dried under vacuum to yield GO-RAFT.

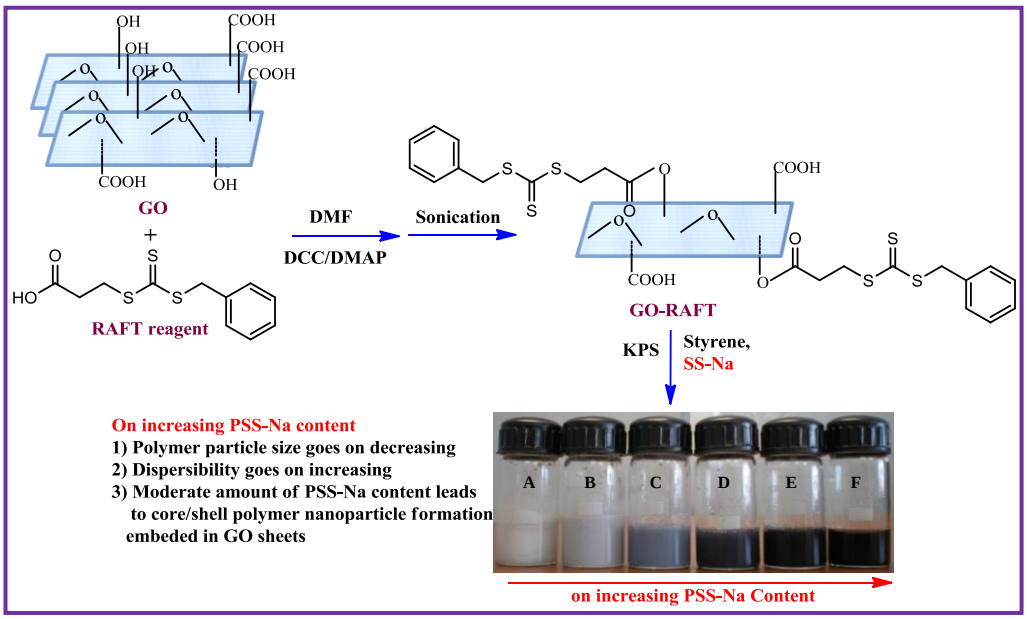

Scheme 4.1. *Schematic representation of PS/GO nanocomposite synthesis.*

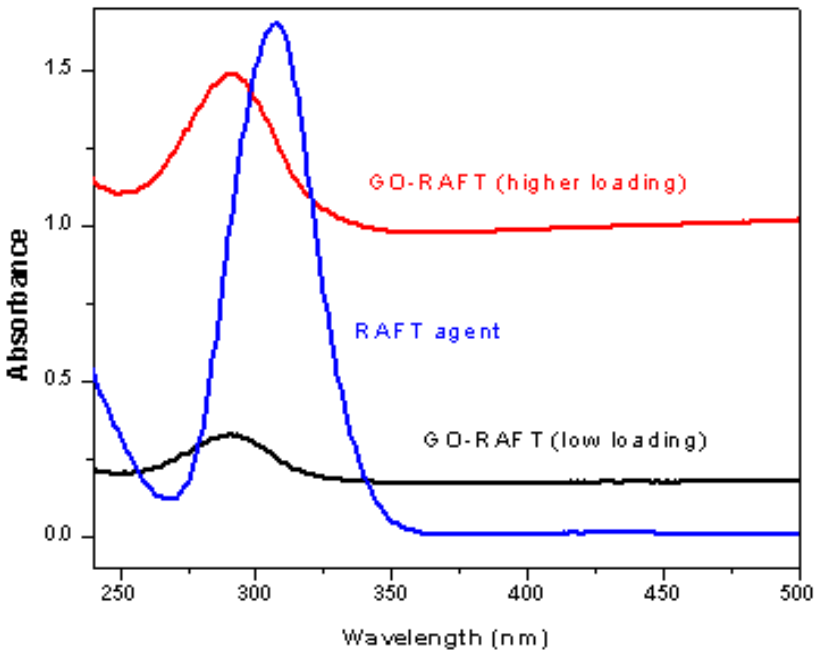

Figure 4.1. *Absorption spectra of RAFT and GO-RAFT agent with low and high loadings.*

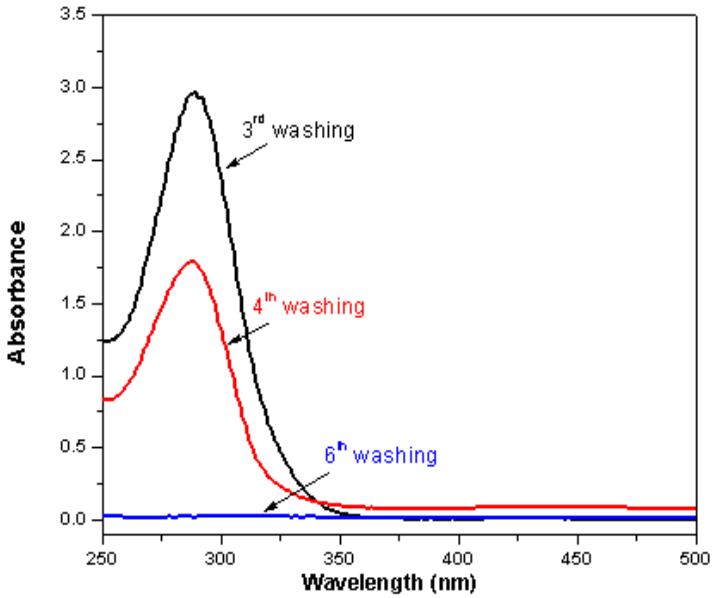

Figure 4.2. *Washing of extra RAFT agent from GO-RAFT after reaction between GO & RAFT agent to ensure that no unreacted RAFT agent is not absorbed on the GO-RAFT. After 6th washing no more RAFT agent is found in washing liquid proving the absence of unreacted RAFT agent in GO-RAFT.*

FTIR spectra of GO, RAFT and GO-RAFT agent are shown in Figure 4.3. The GO spectrum shows bands at 3000-3600, 1740, 1630 and 1058 cm^{-1} which are assigned to vibration frequencies of -OH, C=O, C=C and C-O bonds, respectively, of functional groups present in the GO. RAFT agent shows the bands at 3060, 2950, 1416 and 1060 cm^{-1} because of the vibration of aromatic hydrogen, saturated C-H, saturated C-H bending and C=S bonds, respectively. The presence of both the GO and RAFT agents above mentioned bands in case of GO-RAFT sample, and the peak shifting and broadening of these bands attribute the bond formation between the functional groups of GO and RAFT agent. It is to be noted that the carbonyl peak of RAFT agent at 1695 cm^{-1} shifted to 1732 cm^{-1} in GO-RAFT. This clearly confirms the formation of ester bond in GO-RAFT. Therefore, both UV-Vis and FTIR data proved that the formation of GO-RAFT and absence of any free RAFT agent in the GO-RAFT.

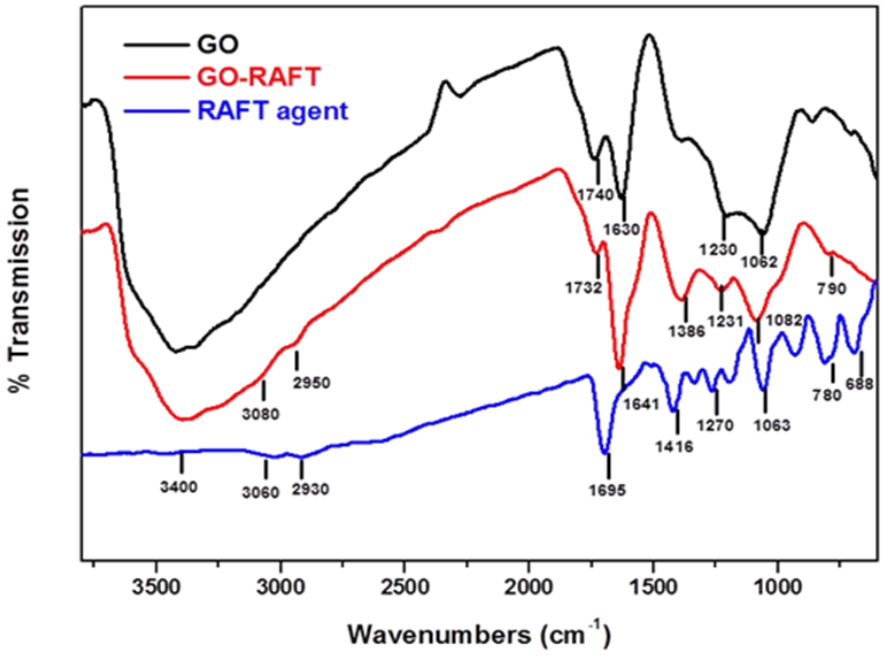

Figure 4.3. *FTIR spectra for GO, GO-RAFT and RAFT agent.*

Earlier it has been reported [29] that GO behaves as a radical inhibitor to polymerization due to its inherent structure, which possesses a high concentration of phenolic hydroxyl groups (similar to many polymerization inhibitors, such as tert-butylcatechol) as well as higher GO loadings give rise to ill-defined morphologies. Therefore, we carried out current polymerization keeping very low GO concentration (0.5 wt.% with respect to styrene) to check effective role of PSS-Na with well-retained morphology. Here PSS-Na provides unique benefit to graphene oxide in providing good dispersion as well as thermal stability with various combine advantages. PSS-Na reduces or eliminates hydrophobic interactions between the hydrophobic side walls of GO sheets and which further triggers interaction closely towards side walls of GO sheets and ionic salt component helping dispersibility in aqueous medium.

Synthesis of polymer nanocomposites was carried out in one pot by combining RAFT process and the surfactant free emulsion polymerization condition. The GO-RAFT agent was added into water as solvent followed by sonication for next 5 minutes owing to exfoliation of GO sheets. The process is preceded further by adding styrene (monomer), SS-Na (ionic comonomer) and potassium peroxisulphate (KPS) together at 70°C and the polymerization was continued for 20 h by stirring the reaction mixture. Several batches of polymerization were

carried out by altering SS-Na concentration in reaction, however all other conditions remain constant. The polymerization scheme of nanocomposite synthesis is shown in Scheme 4.1.

All obtained latexes are shown in Figure 4.4a (immediately after synthesis) and Figure 4.4b (after 1 week standing). From these images, we could clearly observe on increasing the SS-Na content very good interaction among GO sheets and water medium with interfacial polymer particle growth. On increasing SS-Na content the dispersibility also increases along with stability period depending on PS segment. Du *et. al*.[30] reported PSS-Na coupling with GO lead to form super capacitors which retains higher specific capacitance which widens the applications in electrochemical energy storage devices. Hence, the use of PSS-Na may also be highly beneficial in regards to its applications.

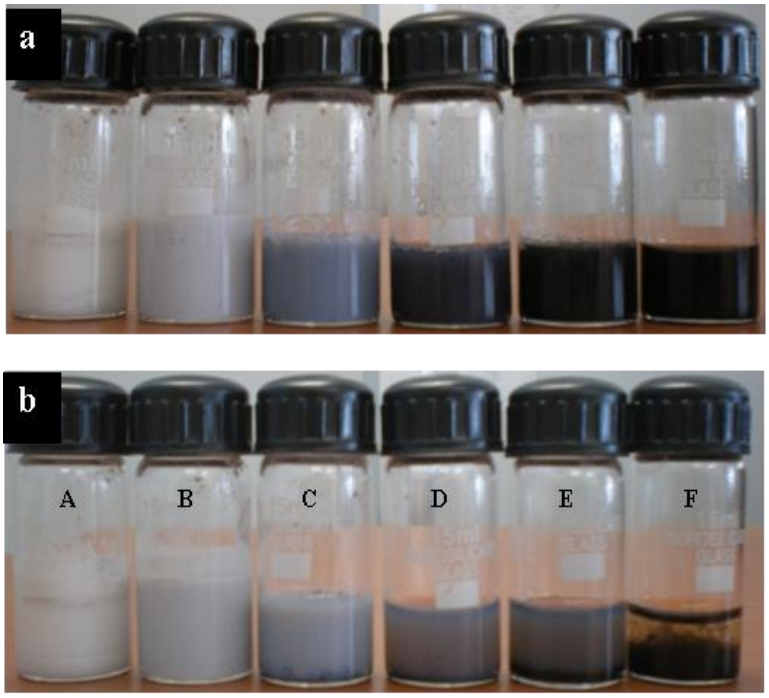

Figure 4.4. *Latexes images obtained immediately after synthesis (a) and after 1 week standing (b).*

Here, one pot strategy is applied since all the reactants undergo successive reactions in just one vessel which avoids separation and purification processes of the inter-mediate compounds. Therefore, it would save much time and resources. Purpose of this work is to establish one pot graphene oxide exfoliation with distinct polymer morphology in surfactant free emulsion polymerization. Recently, Thickett et. al.[29] proposed method to prepare

composite material using graphene oxide in ab initio emulsion polymerization systems. Surfactant and polyelectrolyte have effective role as a dispersing agent. The ionic polystyrene sulfonate sodium salt (PSS-Na) has its own role in stabilizing dispersion. Hassam et. al.[31] reported enhancement in dispersion stability of carbon nanotubes (MWCNT and SWCNT) using PSS-Na.

4.3.2. TEM and WAXD studies

The polymer particle formation takes place up to 10 wt.% of SS-Na with respect to styrene, where the size ranging from 400 nm to 4-5 nm is observed from TEM images as shown in Figure 4.5. We observed from TEM images that beyond 15 wt.% and more there is no polymer particle formation and as a result flocculation of GO sheets is observed (Figure 4.5E and F). By increasing the SS-Na concentration, the polymer particle size decreases from 400 nm (Figure 4.5A) to 5 nm (Figure 4.5D and Figure 4.6). At 6 wt.% of SS-Na, well defined core-shell nanoparticle is observed in which GO sheets are embedded as shown in inset of Figure 4.5C (also in Figure 4.6).

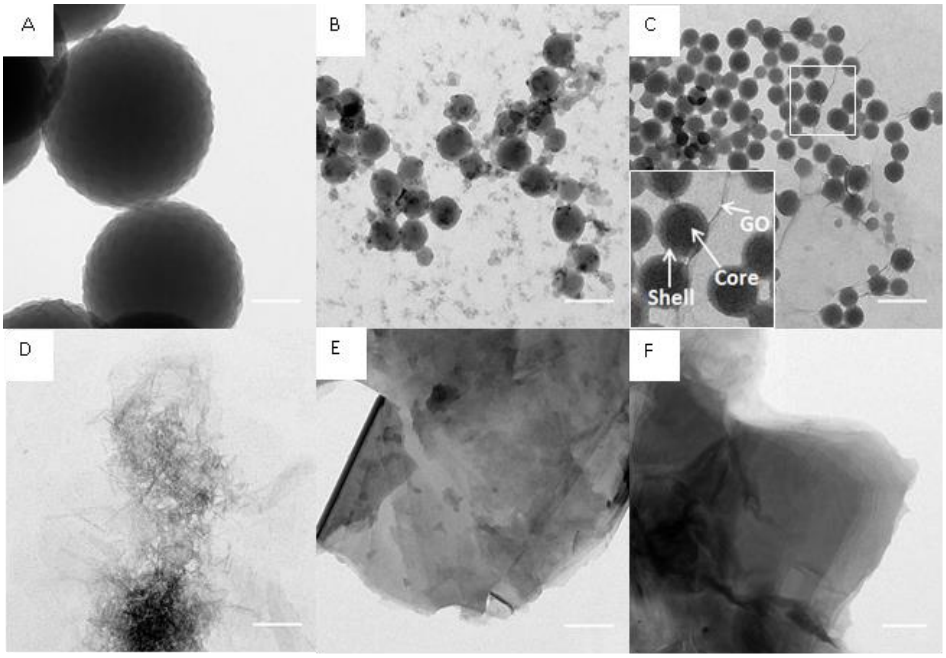

Figure 4.5. *TEM images A, B, C, D, E and F for colloids having 0, 2, 6, 10, 15 and 100 wt.% comonomer (SS-Na) concentration, respectively. Inset of Figure C shows the core-shell morphology along with clear graphene oxide layer. TEM scale bar is 150 nm in all the cases except for F with 500 nm.*

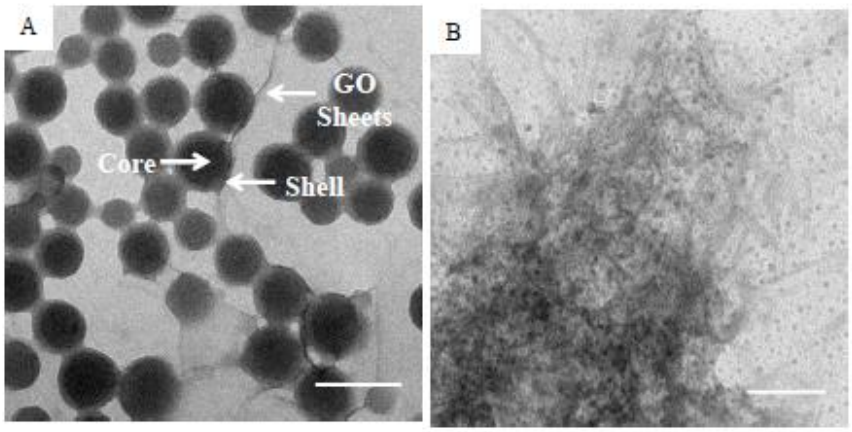

Figure 4.6. *High resolution TEM images of nanocomposites with 6 wt.% (A) and 10 wt.% (B) of comonomer(SS-Na) concentration. TEM scale bar for both the images is 50 nm.*

The interlayer distance of GO has increased slightly from 0.79 nm (2θ =11.07°) to 0.97 nm (2θ = 9.06°) after GO-RAFT formation (Figure 4.7). PS/GO nanocomposites with fixed GO-RAFT (0.5% with respect to styrene weight) loading and varying SS-Na concentrations are used dis-play different XRD patterns depending on the SS-Na concentrations. Figure 4.7 clearly shows that when SS-Na loading is very low (0 and 6 wt.%), the GO interlayer spacing is completely absent. On the other hand when SS-Na loading is high (15, 100 wt.%), the peak for GO interlayer spacing at 20 wt.% is observed, although this peak is very low intense peak. These observations suggest that the influence of PSS-Na on the formation of nanocomposites. When PSS-Na loading is only 6 wt.% , since core-shell morphology forms (Figure 4.5C) which allow stronger interaction with GO and as result GO layers are completely exfoliated. However, at higher PSS-Na the core shell morphology do not form and hence less interaction between PS or PSS-Na with GO, therefore GO layers could not be exfoliated completely. The peak at 2θ = 20° observed for high PSS-Na content is due to the amorphous halo of PS-PSS-Na, copolymer. Similarly observation we have made from diffraction pattern obtained from TEM study (Figure 4.8). As we can see till 6 wt% PSS-Na, there is no diffraction pattern indicating complete exfoliation of GO, however at higher PSS-Na loading different diffraction pattern (rings in case of 10 wt.% and rings with bright spot in case of 100 wt.%) are obtained attributing partial recombination of GO layer. These above discussion clearly indicate that presence of appropriate amount of SS-Na concentration in the

polymerization mixture leads to the formation of exfoliated GO sheets in nanocomposites due to the occurrence of PS-PSS-Na core-shell nanoparticles which generate some kind of interface which interfere the process of recombination of GO sheets.

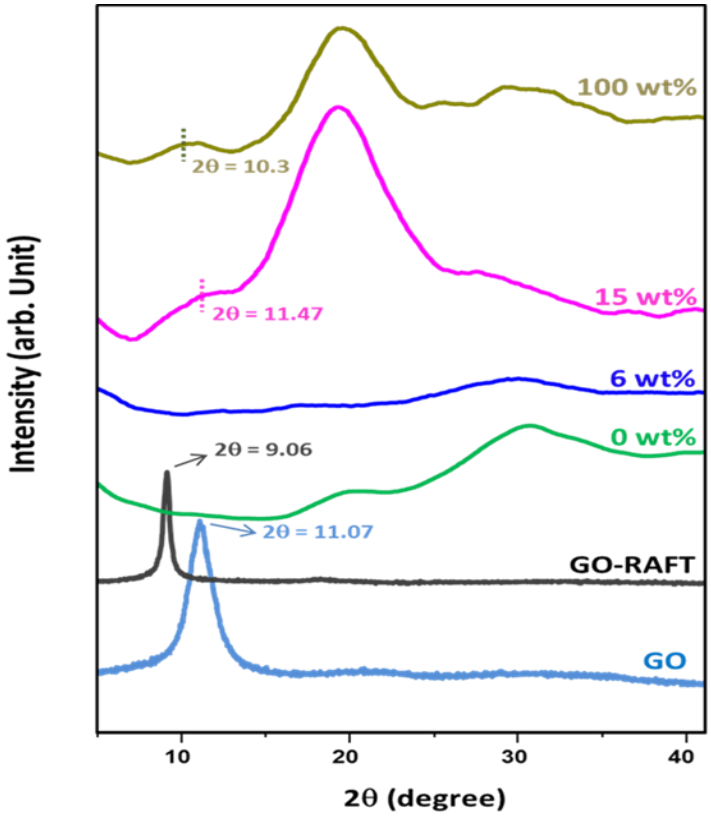

Figure 4.7. *XRD patterns A, B, C, D, E and F for nanocomposites having 0, 2, 6, 10, 15 and 100 wt.% comonomer (SS-Na) concentration, respectively.*

It is well-known that the dispersion and interface are two key parameters in the evaluation of PNCs.[32] In polymer/GO nanocomposites, interfaces typically create much larger volume fractions than in conventional particle-filled composites.[33] This factor plays important role to minimize the enthalpic interaction so that the distribution occurs between carbon backbone layers. For such GO-polymer systems, the moderation of polymer chains largely depends on characteristics of the interface. In this case, the interaction between polymer and graphene layers can be tuned by changing interface parameters, like ionic comonomer concentration. Thus, in order to optimize the performance of GO based nanocomposites, an effective method to tailor the interface structure is developed.

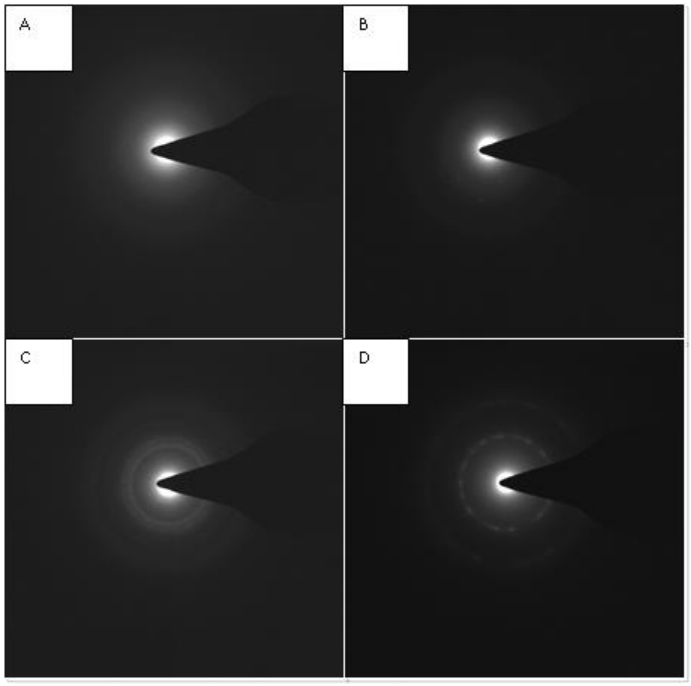

Figure 4.8. *Diffraction patterns of nanocomposites with 0 wt.% (A), 6 wt.% (B), 10 wt.% (C) and 100 % (D) of comonomer concentration.*

4.3.3. Colloidal stability study by zeta potential

A zeta potential study reveals the efficacy of SS-Na content in stabilizing emulsion shown in Figure 4.9. In absence of SS-Na content there is no interaction among GO sheets and polymer particles in water medium. At 2 wt.% there is some kind of interaction between GO sheets and polymer particles but shows less zeta potential value due to some kind of coalescence startup which can be seen from TEM images (Figure 4.5B). But on increasing PSS-Na content up to 6 wt.% the stability is very good and hence higher zeta potential value as observed. On further SS-Na increment, the zeta potential value reduces due to no proper polymer particle formation causing inertia for emulsion stability. At only SS-Na (sample F) there is very low zeta potential value ultimately leading to destabilize emulsion is due to no proper polymer particle formation. From this we can conclude that, there is role of not only SS-Na content but also polymer nanoparticles which supports the entire emulsion system. From diffraction and XRD studies (Fig 4.9), we confirm the non-assembly of GO sheets together for upto uniform concentration of SS-Na.

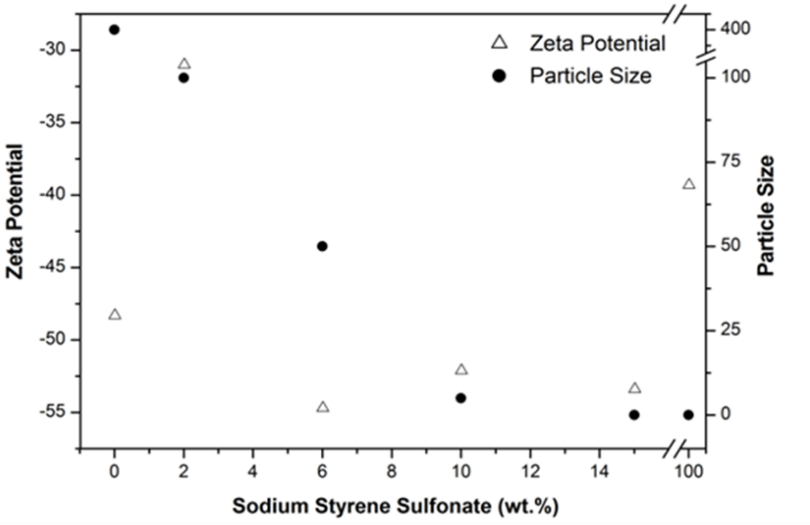

Figure 4.9. *Zeta potential and particle size of colloids as function of SS-Na concentration.*

4.3.4. Thermal study

Thermo gravimetric studies (Figure 4.10) reveal that SS-Na content has an influence on thermal stability of PS/GO nanocomposites. The graphite is stable without any degradation even at 600 ^{o}C whereas GO degrades in two stages: first around 100 ^{o}C due to moisture and second around 175 ^{o}C due to oxygen functionality elimination. The amount of residual remained even after 600 ^{o}C is due to carbon ash. The PSS–Na has high thermal stability with three stages of degradation regions: first ~100 °C due to elimination of moisture adsorbed on sulfonate group and second at 430 °C for polystyrene segment and the third degradation at 515 °C for sulfonate groups. The PS/GO nanocomposites show better thermal stability compared to PSS-Na and graphene oxide. The nanocomposite helps to modify thermal stability in initial temperature by reducing effect of moisture due to less hydrophilic nature of polystyrene. Thermal stability increases with increasing loading of PSS-Na. The onset decomposition temperature of nanocomposites is much higher than that of graphite oxide whereas improvement in hydrophobic character (less moisture loss) at initial stage if less content of SS-Na is used. It is thus very favorable to use moderate SS-Na concentration to improve the overall thermal stability of nanocomposites.

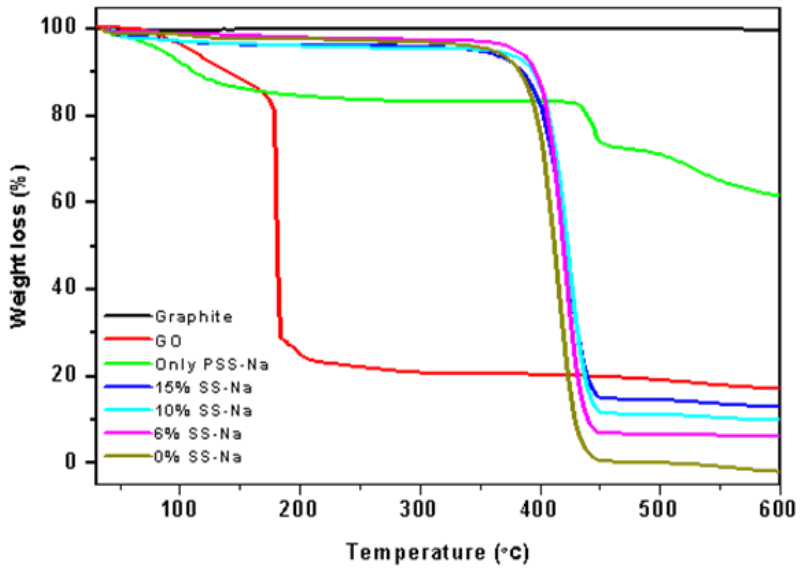

Figure 4.10. *TGA plots of graphite, graphene oxide (GO) and PS/GO nanocomposites with different SS-Na loading as indicated in the figure.*

4.4. Conclusions

In conclusion, we report PS/GO nanocomposite formation using one pot RAFT process with the help of core-shell PS nanoparticles in presence of ionic comonomer SS-Na. At zero SS-Na concentration there is no proper surface interaction among polymer particle and GO sheets whereas increased surface activity is observed at moderate ionic strength due to moderate SS-Na concentration forming small, stable nanoparticles with core-shell morphology, but at only SS-Na concentration without PS there is no particle formation which limits colloidal stability and potential hetero-coagulation giving rise to little stacking among GO sheets. Efficient dispersibility of GO in water is expected under conditions where the ionic strength due to PSS-Na is low enough to allow polymer particle formation but high enough to provide a sufficient driving force for GO sheets to disperse and forming PS/GO sheet interface.

References

[1]. K. Geim and K. S. Novoselov, *Nat. Mater*, 2007, **6**, 183.

[2]. A. K. Geim, *Science*, 2009, **324**, 1530.

[3]. R. Hassan, Graphene Nanoelectronics: Metrology, Synthesis, Properties and Applications, *Springer Publisher*, 2012.

[4]. L. K. Randeniya, H. Shi, A. S. Barnard, J. Fang, P. J. Martin and K. K. Ostrikov, *Small*, 2013, **9**, 3993.

[5]. J. R. Potts, D. R. Dreyer, C. W. Bielawski and R. S. Ruoff, *Polymer*, 2011, **52**, 5.

[6]. L. Oakes, A. Westover, J. W. Mares, S. Chatterjee, W. R. Erwin, R. Bardhan and C. L. Pint, *Sci. Rep.*, 2013, **3**, 3020.

[7]. C. Ataca, E. Akturk, S. Ciraci and H. Ustunel, *Appl. Phys. Lett.*, 2008, **93**, 043123.

[8]. Y. Wu, H. Luo, H. Wang, C. Wang, J. Zhang and Z. Zhang, *J. Colloid Interface Sci.*, 2013, **394**, 183.

[9]. D. R. Dreyer, S. Park, C. W. Bielawski and R. S. Ruoff, *Chem. Soc. Rev*., 2010, **39**, 228.

[10]. M. Hazarika and T. Jana, *Compos. Sci. Technol*.,2013, **87**, 94.

[11]. V. Singh, D. Joung, L. Zhai, S. Das, S. I. Khondaker, and S. Seal, *Prog. Polym. Sci.*, 2011, **56**, 1178.

[12]. H. Kim, A. A. Abdala and C. W. Macosko, *Macromolecules*, 2010, **43**, 6515.

[13]. Y. H. Yu, Y. Y. Lin, C. H. Lin, C. C. Chan and Y. C. Huang, *Polym. Chem.* 2014, **5**, 535.

[14]. A. L. Higginbotham, J. R. Lomeda, A. B. Morgan and J. M. Tour, *ACS Appl. Mater. Interfaces*, 2009, **1**, 2256.

[15]. G. Yin, Z. Zheng, H. Wang, Q. Du and H. Zhang, *J. Colloid Interface Sci.*, 2013, **394**, 192.

[16]. H. M. Etmimi, M. P. Tonge and R. D. Sanderson, *J. Polym. Sci., Part A: Polym. Chem.*, 2011, **49**, 1621.

[17]. H. Roghani-Mamaqani, V. Haddadi-Asl, K. Khezri, E. Zeinali and M. Salami-Kalajahi, *J. Polym. Res.*, 2014, **21**, 333.

[18]. F. Beckert, C. Friedrich, R. Thomann and R. Mülhaupt, *Macromolecules*, 2012, **45**, 7083.

[19]. S. Li, T. Qian, S. Wu and J. Shen, *Chem. Commun.*, 2012, **48**, 7997.

[20]. G. Moad, E. Rizzardo and S. H. Thang, *Aust. J. Chem*., 2005, **58**, 379.

[21]. K. Matyjaszewski, *Macromolecules*, 2012, **45**, 4015.

[22]. C. Barner-Kowollik, Handbook of RAFT Polymerization, Wiley-VCH, Weinheim 2008.

[23]. N. Yeole, D. Hundiwale and T. Jana, *J. Colloid Interface Sci*, 2011, **354**, 506.

[24]. N. Yeole and D. Hundiwale, *RSC Adv.*, 2013, **3**, 22213.

[25]. N. Yeole and D. Hundiwale, *Colloids Surf. A*, 2011, **392**, 329.

[26]. N. Yeole, S. N. R. Kutcherlapati and T. Jana, *RSC Adv.*, 2014, **4**, 2382.

[27]. S. Bhattacharjee and D. Bong, *J. Polym. Environ.*, 2011, **19**, 203.

[28]. N. M. Huang, H. N. Lim, C. H. Chia, M. A. Yarmo and M. R. Muhamad, *Int. J. Nanomedicine*, 2011, **6**, 3443.

[29]. S. C. Thickett and P. B. Zetterlund, *ACS Macro Lett.*, 2013, **2**, 630.

[30]. F. P. Du, J. J. Wang, C. Y. Tang, C. P. Tsui, X. P. Zhou, X. L. Xie and Y. G. Liao, *Nanotechnology*, 2012, **23,** 475704.

[31]. C. Hassam and D. A. Lewis, *Aust. J. Chem.*, 2014, **67**, 66.

[32]. H. S. Khare and D. L. Burris, *Polymer*, 2010, **51**, 719.

[33]. M. Fang, K. Wang, H. Lu, Y. Yang and S. Nutt, *J. Mater. Chem.*, 2010, **20**, 1982.

Chapter 5

RAFT Mediated One-Pot Synthesis of Glycopolymer Particles with Tunable Core–Shell Morphology

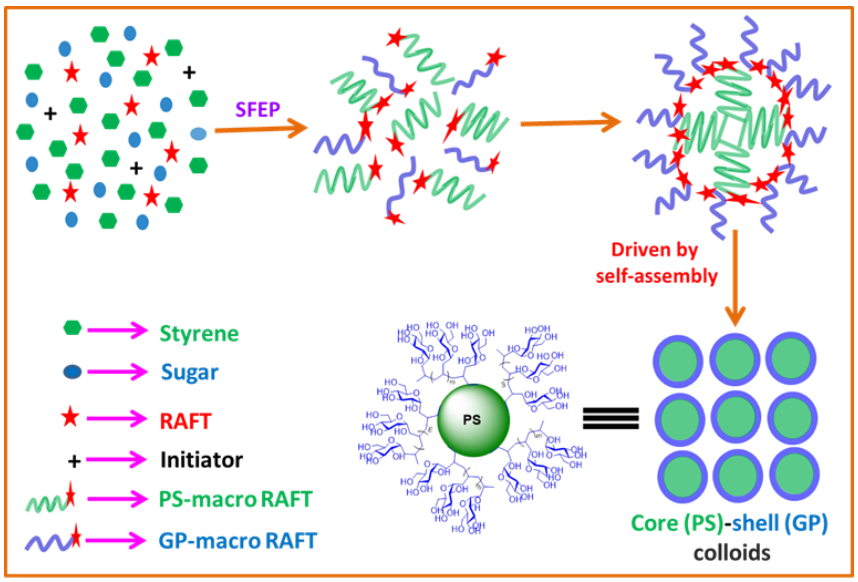

A simple and one-pot method for the synthesis of glycopolymer based colloidal particles with tunable core–shell morphology using reversible addition fragmentation chain transfer (RAFT) polymerization.

Polym. Chem., 2017, DOI: 10.1039/c6py02202b

5.1. Introduction

Carbohydrates in the form of glycoproteins, proteoglycans and glycolipids play significant role in a large number of biological processes.[1-6] Hence, study of interactions between carbohydrates and lectins (proteins with carbohydrate binding sites) can reveal the complex biological mechanisms which are essential in developing new therapeutics for a range of diseases.[7] However, the weak interactions between carbohydrates and lectins, as observed from the low association constant, is the main bottleneck for designing carbohydrates based therapeutics which are generally very site-specific. However, this binding can be enhanced by either crowding a large number of carbohydrates on a substrate, generally called as multivalent approach, or bringing different sugar moieties in a sequence. This process of clustering is termed as the "glycoside-cluster effect".[8] In principle, this effect can be realized by synthesizing a polymer (can be called as glycopolymer) chain in which carbohydrates (similar or different) are part of either main or side chains. Glycopolymers have been reported with various morphologies and structures e.g. linear glycopolymers, glycodendrimers, and spherical glycopolymers etc.[9, 10] Therefore, demand of synthesizing novel glycopolymers with varied sugar structure remains attractive and challenging.[11-13]

Synthesis of glycopolymers has been reported using two strategies: (1) the polymerization of sugar containing monomers (called as glycomonomers) by conventional polymerization techniques and/or (2) modification of preformed polymers with sugar bearing functional groups. Often, glycopolymer synthesis was carried out with protected glycomonomer so that unnecessary hydrolysis/ reaction can be avoided during polymerization and deprotection is carried out after polymerization.[14-16] This whole process of protection-deprotection is a tedious job, and hence, there is need to develop a method/technique for the polymerization of unprotected glycomonomer. Moreover, the majority of the glycopolymer syntheses have been carried out in an organic solvent which is not desirable because the product is intended to be used for the biological applications. There are only very few reports where unprotected glycomonomers have been used for the synthesis of glycopolymers in aqueous solvents[17-19] and also these unprotected glycopolymers have been utilized to stabilize the gold nanoparticles.[20]

The morphology of glycopolymers in solution (aqueous medium) can have vital role in binding capacity with proteins.[21-25] For example, if a glycopolymer is self-assembled into nano/colloidal particles with carbohydrate groups exposed on the particle surface, then one

might expect greater binding with proteins since density and accessibility of binding groups are high. Based on this concept, several reports have appeared where glycopolymers are decorated on silica,[26-28] magnetic,[29] quantum dots[29, 30] and gold nanoparticles,[31-33] and their interactions with lectins have been studied. The majority of the reported glycopolymers have been synthesized using conventional polymerization process and hence resulting in a broad range of molecular weight.[34] As a result, the robust self-assembly with uniform morphology cannot be obtained which in turn hamper the interactions with lectins.

The above discussion clearly highlights three major issues: (1) protection-deprotection of glycomonomer, (2) use of organic solvents and (3) difficulty in achieving uniform morphology owing to broad polymer molecular weight, in the context of the synthesis and development of glycopolymers. Recently, glycopolymers have been synthesized using living ionic,[35] ring opening,[36] and ring opening metathesis[37] polymerizations by few groups to overcome these issues and yet there are certain disadvantages associated with these techniques. However, there is no report on the synthesis of glycopolymers with a designed morphology using living radical polymerization such as Reversible Addition Fragmentation Chain Transfer (RAFT) polymerization.[38-43] The robustness of RAFT method against wide range of monomers and functional groups can be very useful for the synthesis of glycopolymers with very specific and designed morphology.[44-47]

Herein, we report the synthesis of glycosylated core-shell colloidal nanoparticles by using RAFT method through surfactant-free emulsion copolymerization of sugar as hydrophilic monomer and styrene as a hydrophobic monomer in an aqueous solvent. This current approach addresses all the three major obstacles, which are highlighted here, for the synthesis and development of glycopolymer which may have high protein binding capability.

5.2 Experimental Section:

5.2.1 Materials and Methods:

All information about the materials used in this study and the synthetic procedure for the preparation of RAFT agent is discussed in the Chapter 2. The experimental methods and all the characterization techniques which include molecular weight measurements by GPC, spectroscopic characterization by UV-Vis, FT-IR and NMR, thermal analysis by TGA and DSC, microscopic analysis by FE-SEM, TEM and Confocal Raman, light scattering and Zeta potential by DLS study are discussed in Chapter 2. The glyco monomer or sugar 1-(α-D-

glucopyranosyl)-prop-2-ene (α-Glu) (Scheme 5.1) was synthesized [48,49] and provided by Dr. P. Ramu Shridher, School of Chemistry, University of Hyderabad.

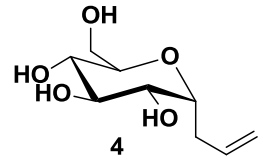

1-(α-D-Glucopyranosyl)-2-propene

(Sugar)

Scheme 5.1. *1-(α-D-glucopyranosyl)-prop-2-ene (glycomonomer or sugar)*

5.2.2 One-pot synthesis of glycopolymer core-shell nanoparticles by surfactant-free emulsion polymerization

In a 25 mL round bottom flask, 9 mL of water was taken containing 10 mg (1 wt %) of $NaHCO_3$. After N_2 purging for 30 min, calculated amount of RAFT agent dissolved in 1 mL of ethanol was added to this followed by the addition of initiator ACP (10 mg, 356 mmol). Then hydrophilic sugar monomer (calculated amount) was added to the reaction mixture followed by 1 g (1.1 mL, 9.601 mmol) styrene (hydrophobic monomer). Finally, the reaction mixture was purged with N_2 for another 10 min followed by immersing the reaction vessel into a preheated oil bath at 70°C. The reaction continued for 20 hours with 500 rpm stirring speed. After the completion of the polymerization reaction, the reaction mixture kept outside the oil bath and opened for air to flow inside and stop the reaction. Finally, we have collected colloidal juice and stored in a 30 mL glass bottle. Polymerization mixtures were collected in different time interval during the course of the reaction to find out the monomer conversion gravimetrically. We have altered 1) the sugar concentration (2, 5, 7.5 and 10 wt %) with respect to styrene for a series of experiments to check the effect of sugar on the formation of glycopolymer core-shell nanoparticles and 2) the hydrophilic macro-sugar chain length (2K, 4K, 5K and 8K, where K represents the kilo Dalton (KD) with fixed styrene by changing the RAFT agent to sugar monomer concentration. The chain length of macro-sugar is theoretically calculated using eq1.

$$\bar{M}_{n,\,theory} = \frac{[\text{Mass of Monomer}] * X_{monomer}}{[RAFT]_0} + MW_{RAFT} \text{ ---- eq (1)}$$

Where $X_{monomer}$ is the fractional conversion, MW_{RAFT} is the molecular weight of the RAFT agent and $[RAFT]_0$ is the initial concentration of RAFT agent.

We have also carried out the reaction without sugar / RAFT agent to check the importance of the RAFT process in the formation of core-shell structure. Finally, we have carried out several controlled reactions to achieve smaller particles size without compromising the core-shell nanoparticle structure of glycopolymer.

5.3 Results and Discussion

Often emulsion polymerization is used for synthesizing polymeric colloidal particles; however, use of surfactant-free emulsion polymerization technique is not so common. To the best of our knowledge, the one pot synthesis of the glycosylated polystyrene (PS) core-shell nanoparticles where the core is the PS and shell is the glycopolymer (GP) in surfactant-free emulsion polymerization using RAFT method has not been reported. In this work, we have chosen the allyl group containing sugar (Scheme 5.1) as a model glycomonomer (comonomer) which has been polymerized using BSPA, which act as a RAFT agent, ACP as an initiator and styrene as a main hydrophobic monomer by the RAFT polymerization technique. A schematic representation of the core (PS)-shell (GP) particle formation is shown in Scheme 5.2. The reason behind choosing the RAFT method can be ascribed to the intrinsic characteristics of the controlled/living polymerization mechanism of RAFT method.49 Here, we have prepared a series of core (PS)-shell (GP) colloidal particles by varying the amount of sugar (2-10wt %) with respect to hydrophobic monomer styrene and also altering the chain length of sugar macro-RAFT (2K, 4K, 5K and 8K) by changing the RAFT agent amount in reaction mixture to prepare a well-defined core-shell particles by keeping all the other reaction conditions unchanged.

5.3.1 Particle size and colloidal stability

The morphology and the particle size of the colloidal particles were examined by FESEM and TEM. The FESEM images of glycopolymer particles prepared with a sugar macro-RAFT chain length of 4000 Daltons (4K) for various weight % of sugar with respect to styrene monomer are presented in Fig. 5.1. As seen from the images, the particles are essentially perfectly spherical, monodisperse and the sizes vary from 460 nm (2 wt %) to 130 nm (10 wt%) in diameter. The sizes obtained from TEM analysis (Fig. 5.1) are in well agreement with the FESEM results. We have made a series of glycopolymer particles with the

variation in macro sugar chain length (2K, 4K, 5K and 8K) and in that we have also varied the wt% of sugar (2, 5, 7.5 and 10 wt%) as discussed in the experimental section earlier.

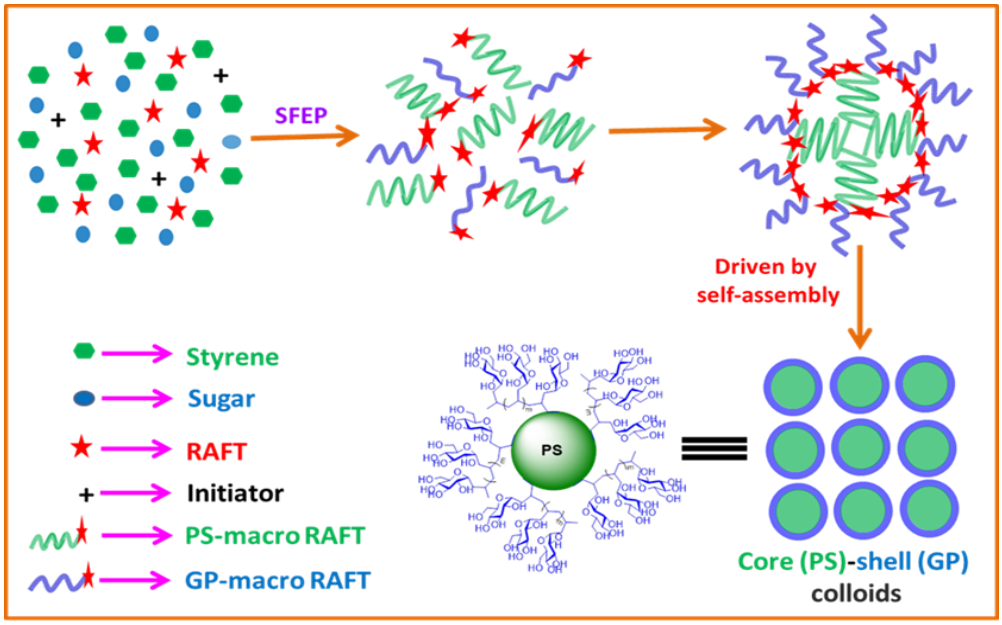

Scheme 5.2*. Schematic representation of the core (PS)-shell (GP) particle formation using RAFT mediated surfactant free emulsion polymerization (SFEP).*

The FESEM and TEM images of all the above mentioned glycopolymer particles are presented in Fig.5.2 to Fig. 5.4. It is very clear from all the images that the synthesized particles are highly monodisperse and spherical. The particle size measured from both FESEM and TEM images for all the cases matches each other very well. All the particle sizes obtained from these measurements for various macro-sugar chain lengths are plotted as a function of sugar concentration in the polymerization feed and shown in Fig. 5.5. It is quite clear that the size decreases as sugar content increases in the polymerization feed.

The size of the glycopolymer particles is decreasing with increasing wt% of sugar is the result of the formation of more number of growing macro-sugar radical which acts as an emulsifier in the polymerization. Formation of more number of emulsifier (similar like micelles) due to more number of macro-sugar radicals (when the amount of the sugar is high in the reaction medium) yields the smaller size micelle and hence smaller particles are obtained.

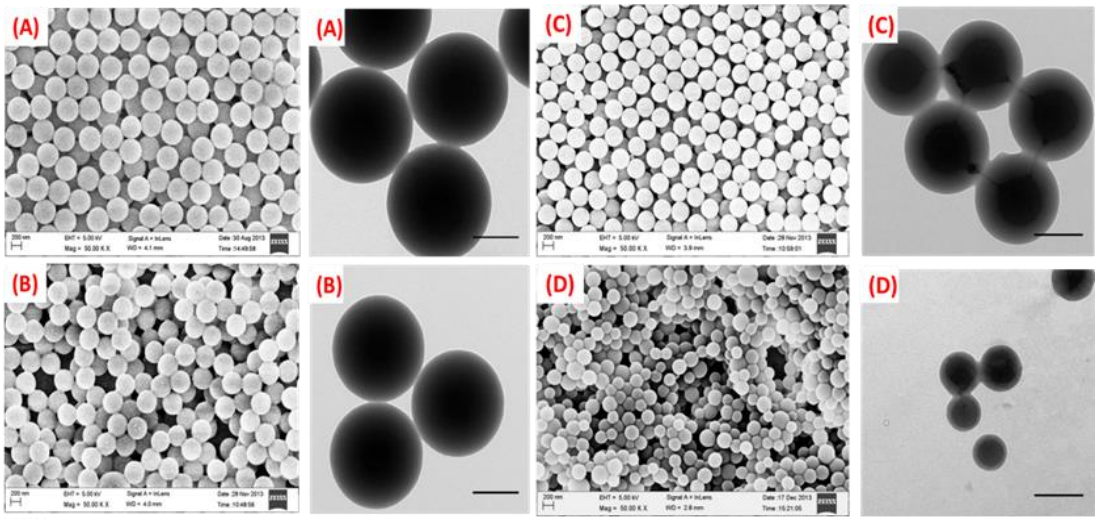

Figure.5.1. *FESEM and TEM images of glycopolymer particles prepared with a macro-sugar chain length of 4K with the variation of sugar content (A) 2 wt%, (B) 5 wt%, (C) 7.5 wt% and (D) 10 wt% in the polymerization. The scale bar for all the TEM images is 200 nm.*

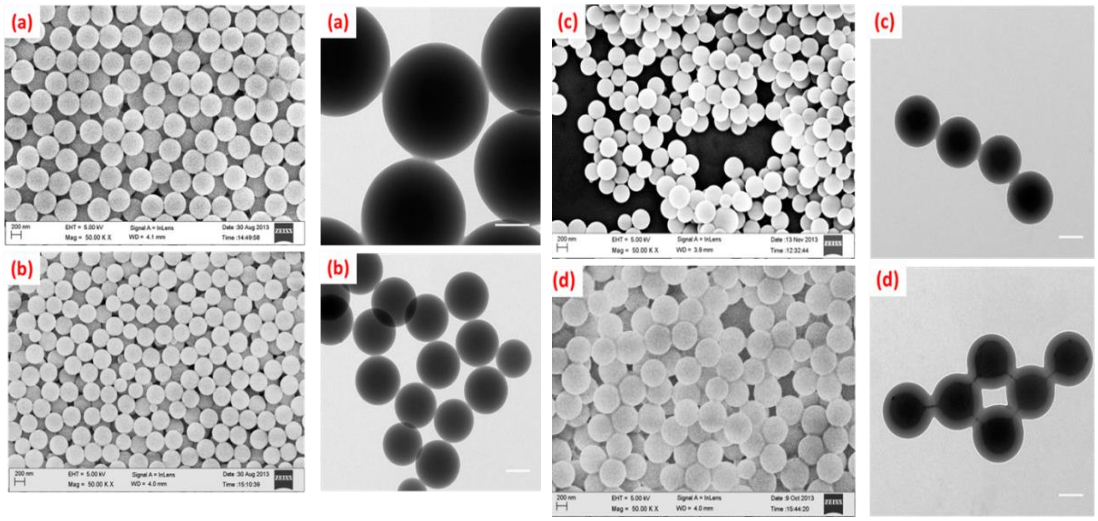

Figure 5.2. *FESEM and TEM images glyconanoparticles with a macro sugar chain length of 2K with a variation of sugar content (a) 2 wt%, (b) 5 wt%, (c) 7.5 wt% and (d) 10 wt% in the reaction. The scale bar for TEM images is 200 nm.*

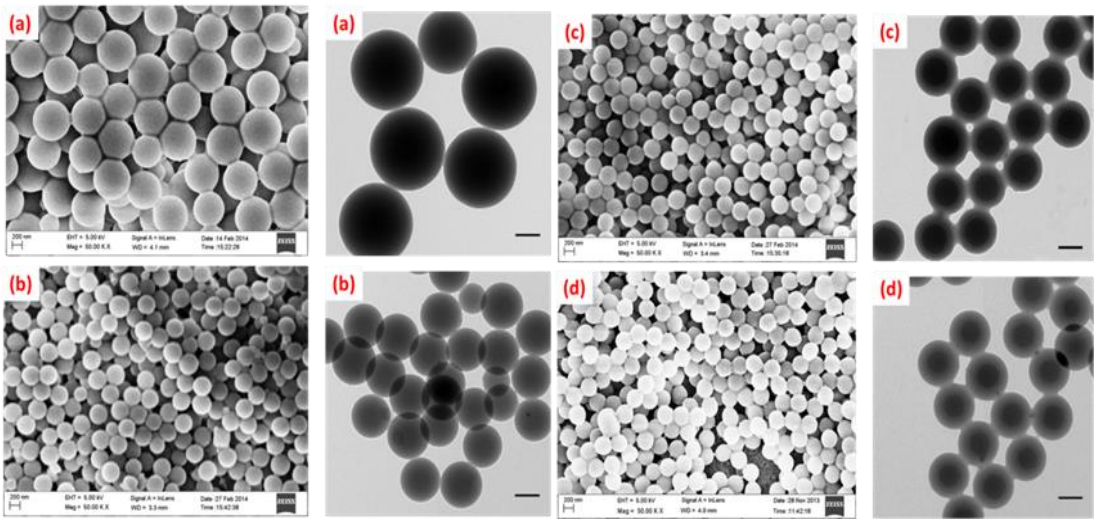

Figure 5.3. *FESEM and TEM images glyconanoparticles with a macro sugar chain length of 5K with a variation of sugar content (a) 2 wt%, (b) 5 wt%, (c) 7.5 wt% and (d) 10 wt% in the reaction. The scale bar for TEM images is 200 nm.*

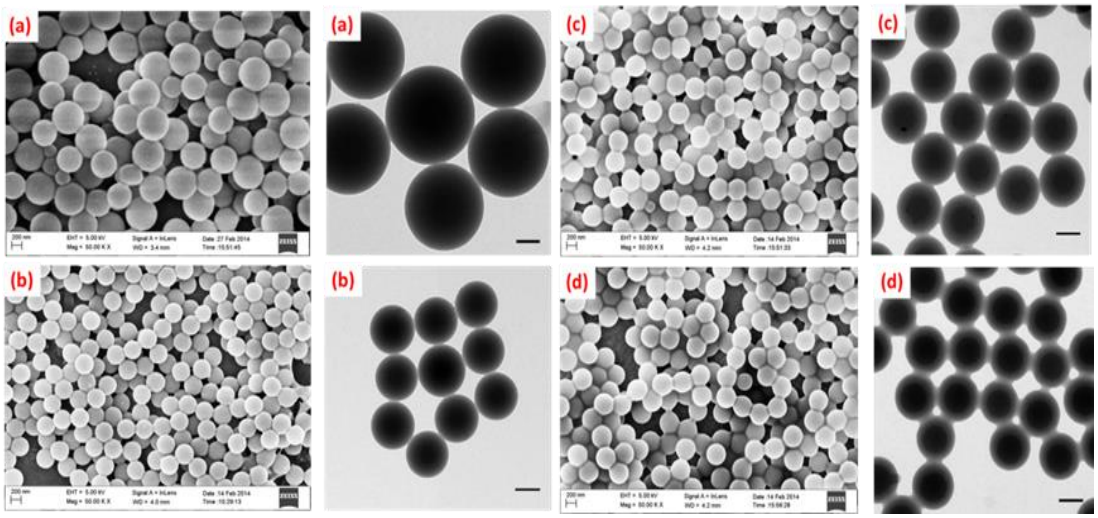

Figure 5.4. *FESEM and TEM images glyconanoparticles with a macro sugar chain length of 8K with a variation of sugar content (a) 2 wt%, (b) 5 wt%, (c) 7.5 wt% and (d) 10 wt% in the reaction. The scale bar for TEM images is 200 nm.*

From the TEM images of the entire series, one can easily conclude that if the amount of sugar is on higher side i.e. more than 5 wt% then we can clearly see the core-shell morphology- the darker inner part is the core, and the lighter outer part is the shell. The core part is the PS and the shell part is the glycopolymer. The reason behind the formation of core (PS)-shell (GP) can be understood from the self-assembly behavior of hydrophobic PS and hydrophilic GP chains. Self-assembly driven core-shell morphology formation has been explained and demonstrated by us and many others in case of PS and sulfonated PS (SPS) pair where hydrophobic PS formed core and hydrophilic SPS yields shell.[40, 41, 50, 51] We did not observe the shell for lower sugar content (2, 5 wt % sugar), but we believe there may be a very thinner shell which could not be detected. A comparison of core-shell thickness (Table 5.1) clearly attributes that core/shell thickness ratio decreases with increase in sugar content in the polymerization and also with increasing macro-sugar chain length. This means that thicker glycopolymer shell can be obtained when more sugar is added to the polymerization feed or a bigger hydrophilic chain (macro-sugar) is part of the PS-GP copolymer chain.

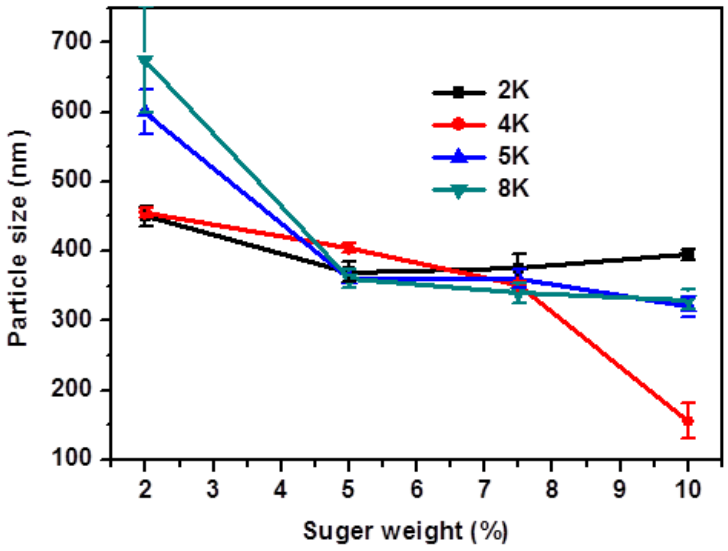

Figure 5.5. *Variation of particle size as a function of % of sugar in the polymerization feed for various macro-sugar chain lengths. Each data in the plot is the average particle size measured from at least five particles.*

Table 5.1. *Core and shell thickness as obtained from the TEM images and their ratio for various samples having different macro-sugar chain length.*

Macro-sugar chain length	Sugar (wt%)	Core size (nm)	Shell size (nm)	Core / shell ratio
2K	7.5	315	60	5.25
	10	269	126	2.13
5K	7.5	280	80	3.5
	10	207	113	1.83
8K	7.5	195	145	1.34
	10	157	173	0.9

To study the stability of the resulting core-shell glyconanoparticles, we have carried out the zeta potential studies of all the samples and the data plotted against the sugar wt% for various macro-RAFT chain lengths (Fig. 5.6). All the samples zeta potential are below -20 mV which is sufficient enough for the stability. The values are found to depend on both particle size and the sugar content in the reaction. The decrease in zeta potential and hence the higher stability of the emulsion is observed till 7-8 wt% of sugar content, and after that zeta potential increases and hence the stability decreases. The decrease in stability in case of high sugar content may be due to the more and more hydrophilic attraction between particles which makes them slightly unstable. It is also important to note that the variation of zeta potential and stability also highly dependent on the macro-sugar chain length as seen from Fig. 5.6.

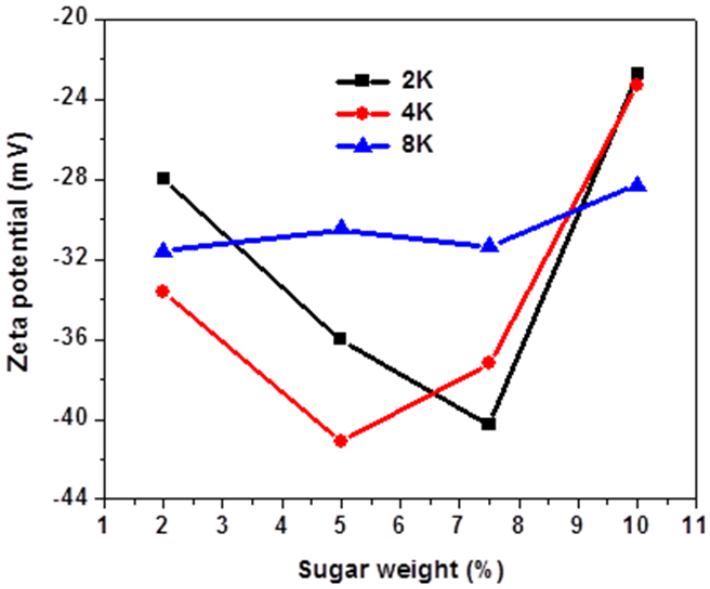

Figure 5.6. *Zeta potential analysis of glyconanoparticles prepared with a macro sugar chain length of 2K, 4K and 8K and with a variation in sugar content (2-10 wt %) with respect to monomer styrene.*

5.3.2 Spectroscopic characterization of polystyrene-glycopolymers

^{1}H NMR spectra presented in Fig .5.7 and Fig. 5.8 clearly indicate the complete disappearance of vinyl protons (4.5-6.0 ppm) of sugar monomer after the polymerization and the gradual appearance of proton signals at 3.0-4.5 ppm for sugar in the resulting glycopolymer. There is also increase in the peak intensity around 1.2-2 ppm for the saturated carbon chain after the polymerization with an increase in sugar wt% and macro-sugar chain length. These results suggest that there is an explicit incorporation of sugar moiety on the polystyrene chain.

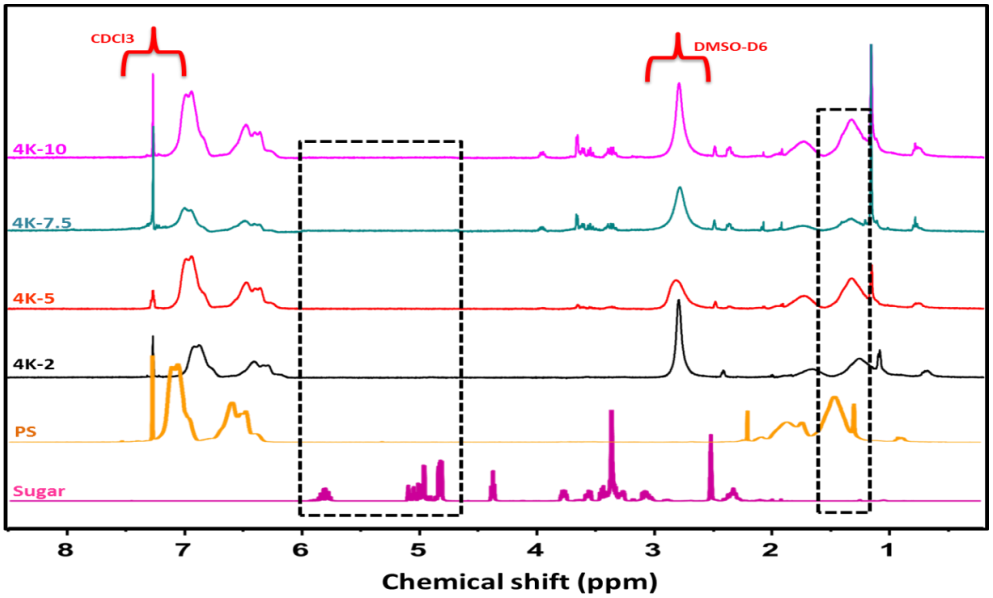

Figure 5.7. *^{1}H NMR spectra of PS-glycopolymers prepared using macro-sugar chain length of 4K by varying sugar wt% with respect to monomer styrene along with pure sugar and polystyrene(PS).*

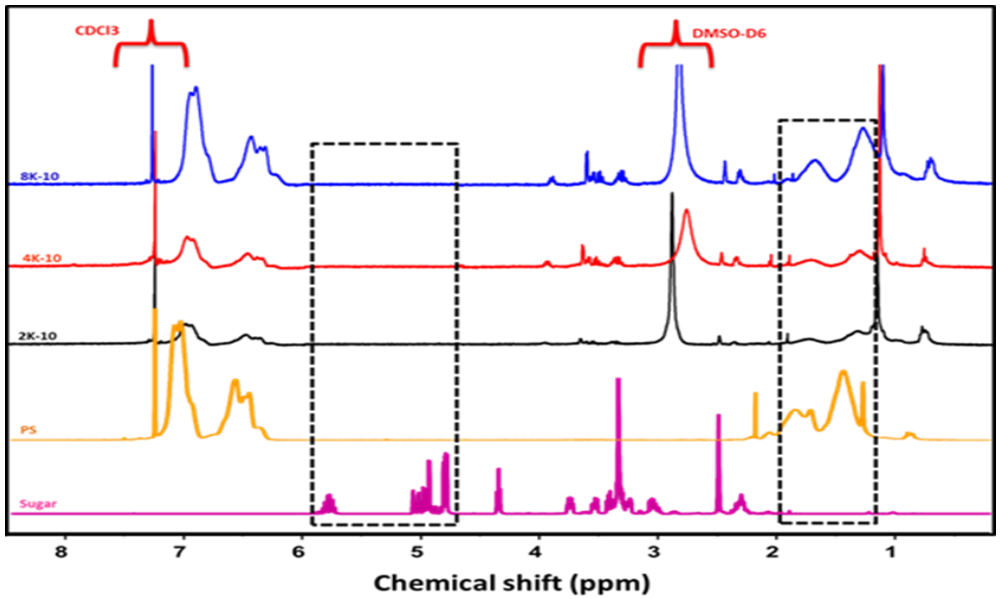

Figure 5.8. *^{1}H NMR spectra of PS-glycopolymers prepared using 10 wt% sugar with respect to main monomer styrene by varying macro sugar chain length (2K,4K and 8K) along with pure sugar and polystyrene (PS).*

UV-Vis absorption spectra (Fig. 5.9) of sugar monomer, polystyrene and PS-glycopolymer were recorded in a mixture (50/50) of DMSO and $CHCl_3$ solvents. Sugar monomer and polystyrene absorbs at around 312 nm and 269 nm, respectively. Glycopolymer absorbs both at 316 nm as well as 269 nm, the former peak is due to sugar moiety and later is for polystyrene. The shift 4 nm (312 nm to 316 nm) of sugar moiety peak in the case of glycopolymer is attributed due to the presence of sugar moiety on the PS-sugar glycopolymer. Thus the glycopolymer spectrum consists of both the components and a 4 nm shift in sugar absorbance confirm the formation of glycopolymer which contains both sugar and PS chains.

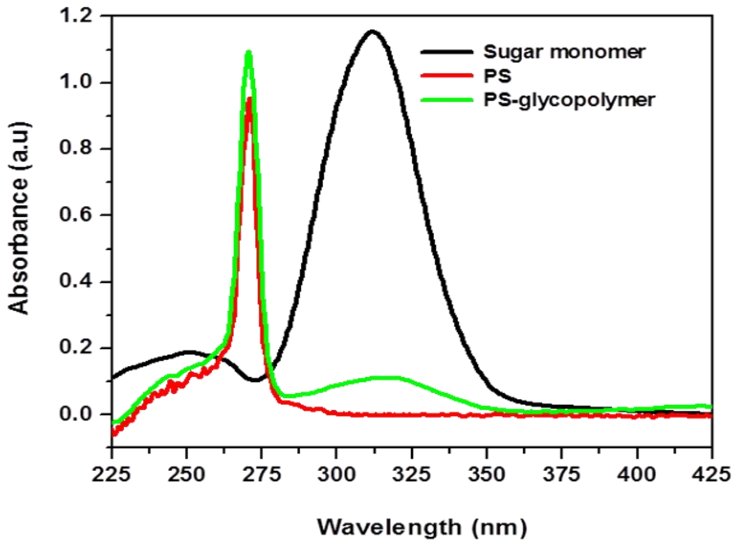

Figure 5.9. *UV-Vis spectra of glycopolymer along with sugar monomer and PS.*

5.3.3 Molecular weight of glycopolymer and kinetics of polymerization

Number average molecular weight ($\bar{M}_n$) and polydispersity index (PDI) of synthesized PS-glycopolymers obtained from GPC traces (Fig. 5.10) are tabulated in Table 5.2. The results clearly show that the $\bar{M}_n$ decreases with increase in sugar content in the reaction feed for any given macro-sugar chain length (only 4K macro sugar data is shown here). The decrease in the $\bar{M}_n$ values with increase in sugar wt% is due to a lesser hydrodynamic volume of the glycopolymer chains when compared to the low sugar content in the reaction medium. The more number of macro-sugar chains are present in the reaction medium when amount of sugar present is high, thus resulting in decrease of the molecular weight of polymer chains with increasing wt% of sugar. We can also observe a shoulder (elution time at about 14 min) in the Fig. 5.10A which becomes bigger with increase in sugar content and thus may be the result of

cross-terminated chains because of cross-coupling of growing sugar and polystyrene macro radicals. On the other hand, $\bar{M}_n$ increases with increasing the macro sugar chain length for the same amount of sugar. PDI also increases with increasing macro-sugar chain length indicating broader molecular weight distribution. The cross-terminated peak is presented in all the GPC chromatograms is due to the cross-coupling reaction between the polymerizable macroradicals and this peak becomes more prominent with increase in macro-sugar chain length also. Cross-coupling reaction is may be due to the complex mechanisms associated with the synthesis of PS-glycopolymer architectures without any surfactant and use of unprotected glycomonomer.[21]

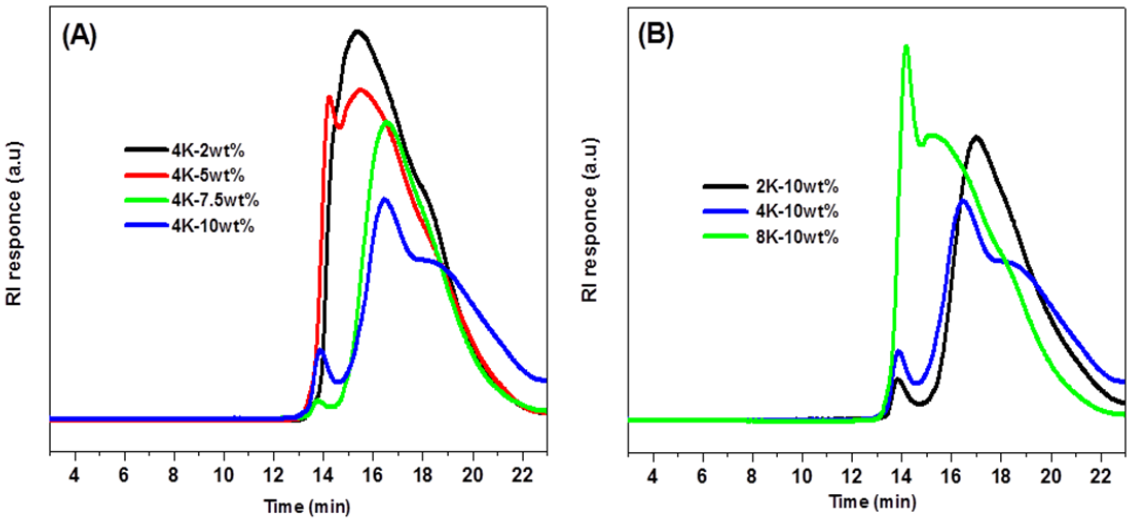

Figure 5.10. *GPC traces of PS-glycopolymers synthesized with (A) macro sugar chain length of 4K and variation of sugar content 2 wt%, 5 wt%, 7.5 wt% and 10 wt% with respect to styrene and (B) 10 wt% sugar with respect to monomer styrene by varying macro-sugar chain length (2K,4K and 8K).*

In order to study the living nature of the polymerization as well as the reaction kinetics, we have measured % of conversion as a function of polymerization time for various sugar wt% during the course of the polymerization reaction and the results are shown in Fig. 5.11. The linear relation of monomer conversion with time as observed in Fig. 10(A) indicates that the polymerization followed first order rate kinetics which proves the living nature of the polymerization and there is a retardation period (as frequently observed in RAFT polymerization) in each case up to 45 minutes at the start of the reaction, the exact reason of which is still a topic of debate.[52-54] From the Fig. 5.11(A), we can clearly observe that the presence of co-monomer sugar increases the rate of overall monomer conversion as well as the

rate of the reaction. The final monomer conversion also increases with increase in the wt% of sugar in the polymerization [Fig. 5.11(B)]. This may be due to the formation of both the blocks simultaneously in the medium and probably the exchange of oligomeric radical chains between sugar and styrene macro-radicals via RAFT mechanism. The reaction is steadier when higher sugar content is present (as well as RAFT) which effectively balances the final macro-sugar chain length.

Table 5.2. *Molecular weight and PDI of PS-glycopolymers obtained from GPC measurements*

Sample identity	$\bar{M}_n$	PDI
4K-2wt%	82×10^3	2.34
4K-5wt%	71×10^3	3.05
4K-7.5wt%	55×10^3	1.60
4K-10wt%	45×10^3	2.08
2K-10wt%	40×10^3	1.62
4K-10wt%	45×10^3	2.08
8K-10wt%	83×10^3	3.05

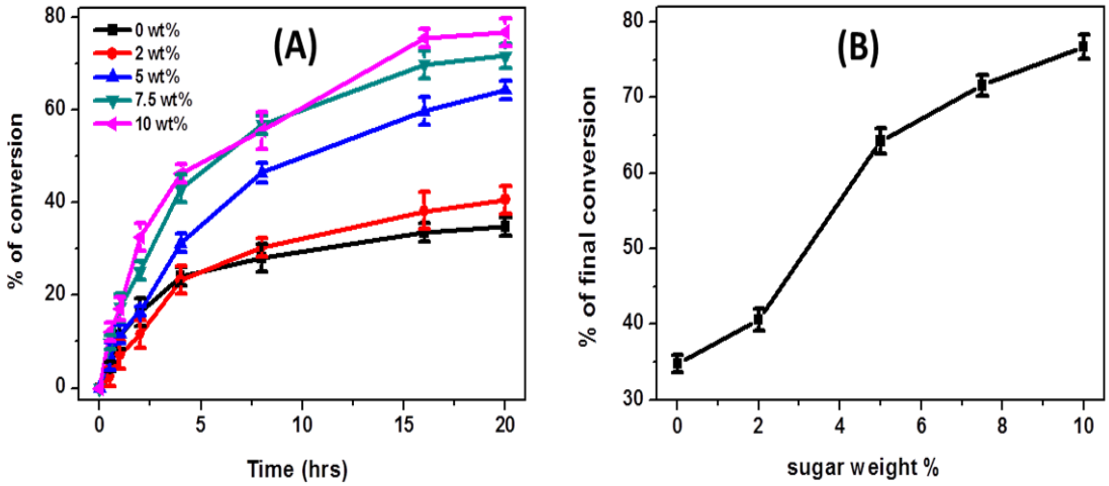

Figure 5.11. *Kinetic (A) and final % of conversion (B) plots of glycopolymers with variation of sugar content in the polymerization mixture when macro-sugar chain length is 4K.*

5.3.4 Control polymerization and particle size optimization

The results presented so far clearly indicate two important observations: (I) addition of sugar monomer is necessary for forming the glycosylated core-shell nanoparticles and (II) RAFT method is essential for the preparation of well-defined particles with core-shell morphology, as presented in the current system. We have further carried out several control experiments which will be discussed in the following section to prove our claim further and to check the importance or necessity of RAFT method, and to optimize the reaction conditions.

The RAFT function in the one-pot polymerization for the synthesis of glyco core-shell nanoparticles has been verified by conducting a reaction without any added RAFT in the reaction medium, but the added amount of sugar is 10% (like in the case of 4K-10 wt% but without RAFT) and all the other reaction conditions are kept unchanged. The resulted particles are polydisperse in nature though the formation of core-shell glyconanoparticles is seen (Fig. 5.12). Hence, it can be concluded that RAFT agent in the medium is playing a crucial role and without that the polymerization is heterogeneous in nature yields polydisperse particles and also the sugar monomer conversion was less as unreacted sugar monomer can be seen from FESEM and TEM images (Fig. 5.12).

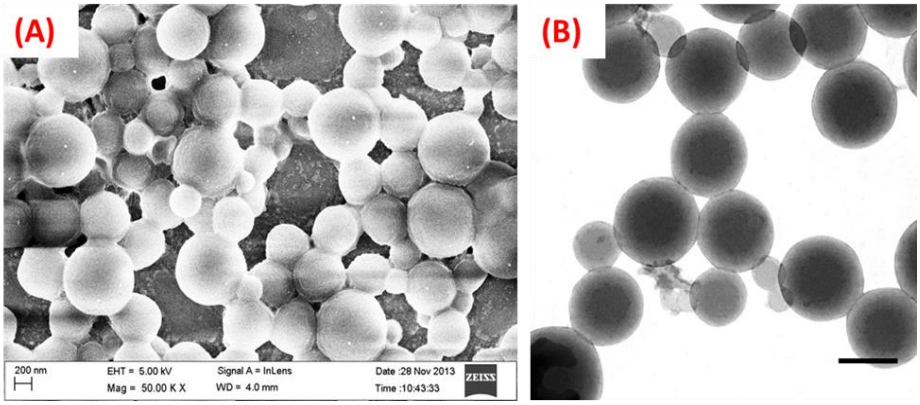

Figure 5.12. *FESEM (A), TEM (B) images of glycopolymers prepared using 10 wt% of sugar (as in the case of 4K-10 wt%) but without any added RAFT reagent. TEM scale bar is 200 nm.*

We have carried out another set of reaction in which we added neither RAFT agent nor sugar and the results are presented in Fig. 5.13. It clearly indicates that no core-shell morphology formation due to the lack of sugar comonomer along with the formation of polydisperse particles due to the absence of RAFT agent. To further confirm the role of RAFT agent and sugar, we have also carried out an experiment without any sugar but an added

amount of RAFT reagent. One can observe monodisperse particles (Fig. 5.14) due to the role of added RAFT reagent (like in the case of 4K-10 wt% but without sugar) in the reaction medium. It makes the polymerization in a well-controlled manner, therefore, makes a monodisperse particle. However, we do not observe any core-shell nature of particles which is attributed for the nonexistence of the sugar monomer in the reaction medium (Fig. 5.14). Thus these results (Fig. 5.12, 5.13, 5.14) support our claims that both the RAFT reagent and sugar are necessary for the formation of well-defined monodisperse particles with core-shell morphology.

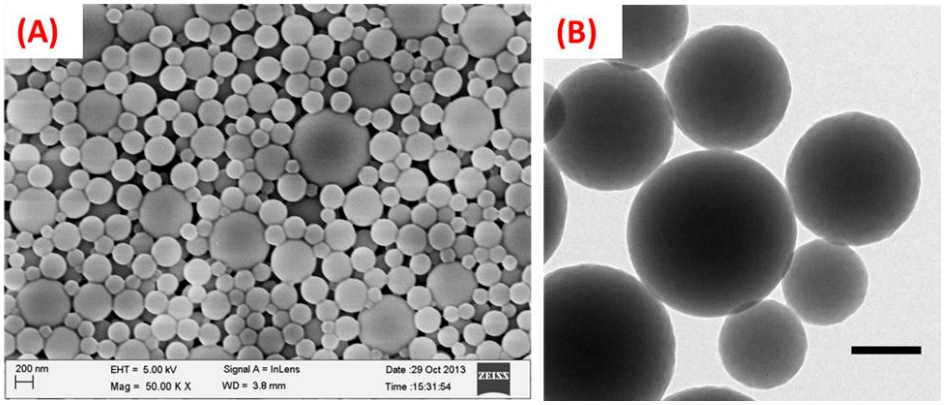

Figure 5.13. *FESEM (A), TEM (B) images of glycopolymers prepared without RAFT reagent and sugar in the reaction. TEM scale bar is 200 nm.*

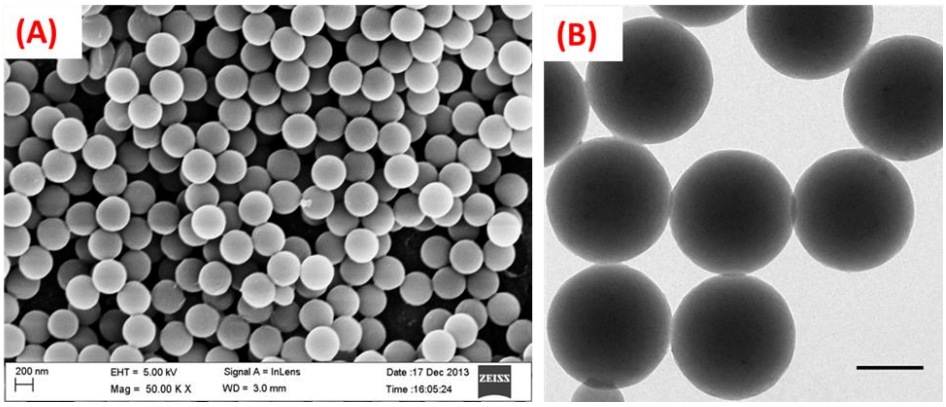

Figure 5.14. *FESEM (A), TEM (B) images of glycopolymers prepared by adding RAFT agent (amount is equal to 4K-10 wt %) but without any addition of sugar monomer. TEM scale bar is 200 nm.*

Along with the above mentioned controlled experiments, we have carried out polymerization experiments with an objective to decrease the size of glyco core-shell nanoparticles by increasing the wt% of sugar to 20 wt% in case of 4K macro-RAFT series since earlier we observed that increase in wt% of sugar decreases the particle size. Although we observed the well-defined formation of glyco core-shell monodisperse particles, but the size increases (instead of decreasing) from 130-150 nm (Fig 5.1D-both FESEM and TEM) to 280-290 nm (Fig. 5.15). This increase in the size explains that up to certain sugar content (10 wt%), there is a clear balance between hydrophilic (sugar) and hydrophobic (PS) chains (propagating macroradicals) which may alter by adding more sugar into the medium and gives rise to a clear increase in the particle size. In another experiment, we have carried out the reaction with 10 wt% of sugar and 4K macro-sugar chain length and with sonication for 15 minutes before polymerization. Unfortunately, there is no decrease in the particle size was observed rather size increased to 220-230 nm in (Fig. 5.15B).

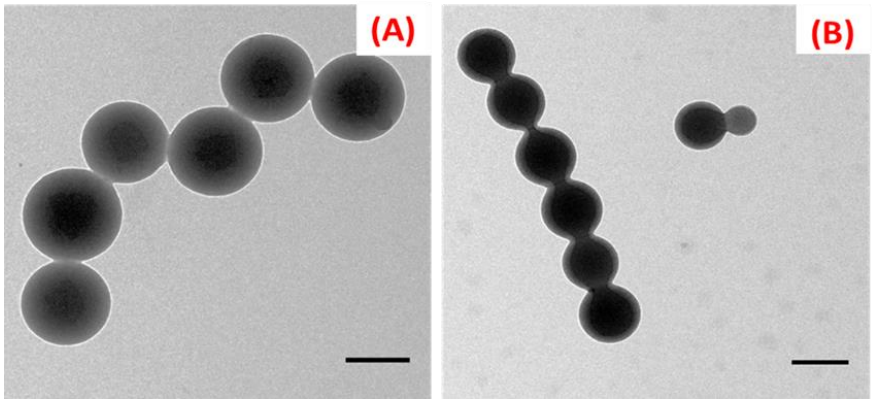

Figure 5.15. *TEM images of glyconanoparticles prepared with (A) macro sugar chain length of 4K with 20 wt% sugar (with respect to monomer styrene) and (B) macro sugar chain length of 4K with 10 wt% sugar (with respect to monomer styrene) along with a sonication for 15 min before starting reaction. The scale bars are 200 nm.*

The sugar layer on the polymer particle surface has been decreased in this case may be due to the more homogenous reaction mixture owing to the sonication. In conclusion, we can say that the optimized reaction conditions which are presented in the Table 5.1 and Fig. 5.1 are

the best to obtain monodisperse core-shell particles and sizes cannot be decreased further in the current system.

5.3.5 Thermal studies

Thermo gravimetric analysis (TGA) of PS-glycopolymer nanoparticle powder which was obtained after evaporation of the emulsion was performed, and data are presented in the Fig. 5.16. The single decomposition temperature for sugar and polystyrene are found around 210 °C and 350 °C, respectively (Fig. 5.16A). Whereas in the case of glycosylated nanoparticles, two degradation temperatures are observed (around 210 °C and 350 °C) corresponding to both sugar and polystyrene blocks. This once again confirms the presence of both sugar and polystyrene in the particle. Thermal degradation at a place corresponding to sugar degradation (210 °C) increases with the increase in the wt% of sugar in the reaction mixture. The increase in chain length of macro-sugar in the polymerization mixture clearly increases the content of sugar moiety on the particle surface as decomposition of sugar content in the TGA thermogram increases. This concludes that the higher wt% or bigger chain length of macro sugar chains gives highly sugar dense core-shell nanoparticles as also seen from TEM images in earlier section.

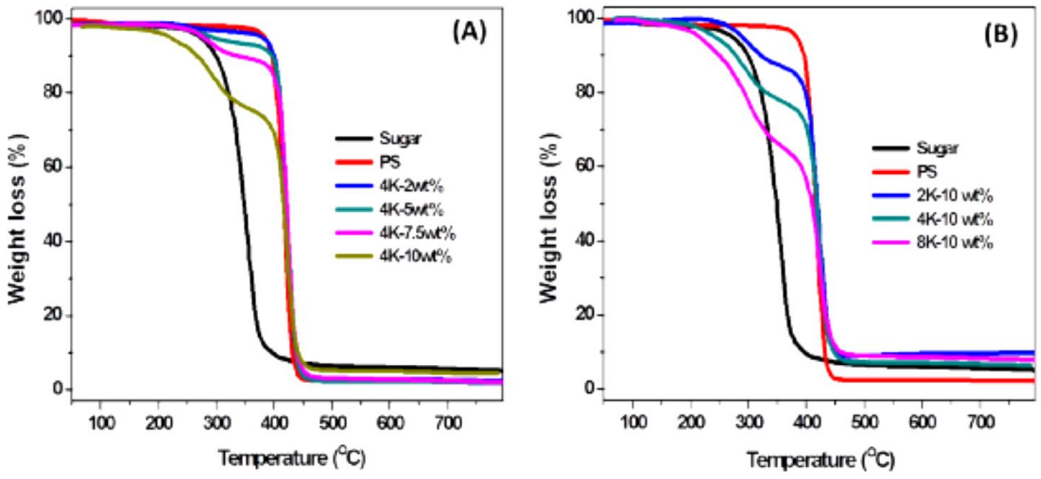

Figure 5.16. *TGA thermograms of PS-glycopolymers prepared using (A) macro sugar chain length of 4K by varying sugar wt% and (B) 10 wt% sugar with respect to monomer styrene by varying macro sugar chain length (2K,4K and 8K) along with pure sugar and polystyrene.*

Differential scanning calorimetry (DSC) analysis shows single melting temperature (T_m) at 141.09°C for the sugar monomer and glass transition (T_g) at 103.9°C for PS (Fig. 5.17). PS–glycopolymers display a T_g at around 100°C which corresponds to polystyrene in it, and the T_g also decreases with increase in the wt% of sugar. A small endothermic peak at a higher percentage of sugar (7.5 and 10 wt%) is observed at around 137 °C to 139 °C which is in a similar temperature region to that of the monomeric sugar melting peak at 141.09 °C. We believe that this is due to the polymeric sugar content in the glycopolymer indicating that the PS–glycopolymers (particularly higher sugar content polymers) may have a partial crystalline character. In fact the wide angle X-ray diffraction studies (Fig. 5.18) of the higher sugar content sample (4 K-10 wt%) display several small crystalline peaks in the PS amorphous halo region. The relatively smaller glycopolymer chain length in comparison to the PS chain may be the reason behind the small enthalpy endothermic peak (Fig. 5.17) and low intensity X-ray diffraction peak (Fig. 5.18) in the case of PS–glycopolymers. Earlier, the crystalline behaviour of carbohydrate-based copolymers with a high composition of glycomonomer has been studied extensively.[59]

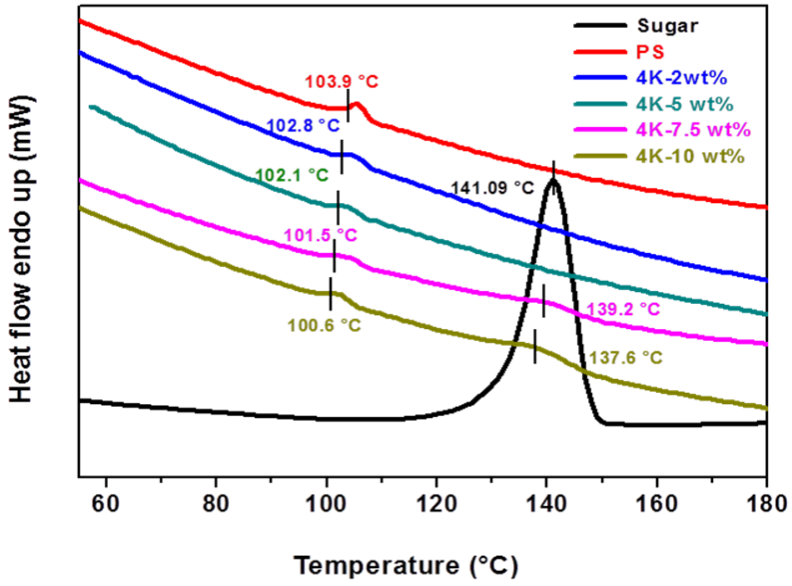

Figure 5.17. *DSC thermograms of PS-glycopolymers prepared using macro sugar chain length of 4K by varying sugar wt%. Also DSC of sugar monomer and PS are shown in the figure for comparison.*

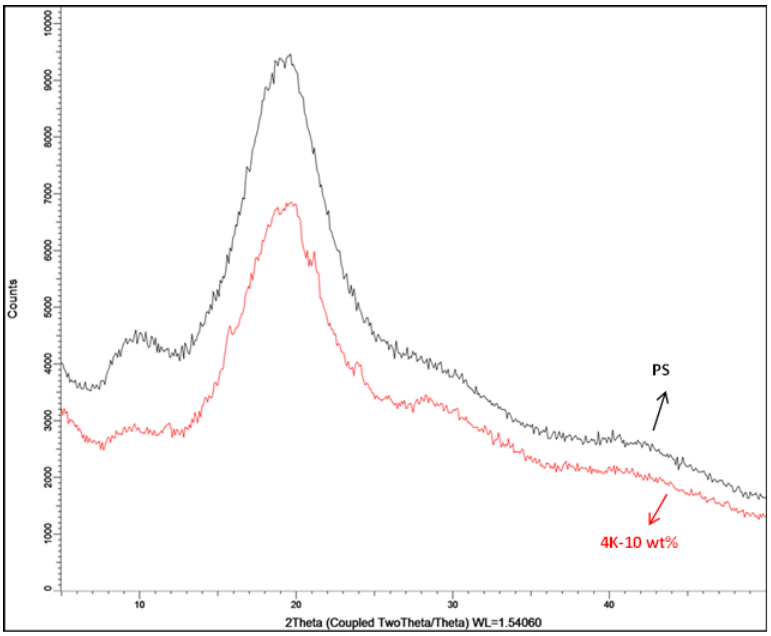

Figure 5.18. *WXRD patterns of PS and PS-glycopolymer prepared using macro sugar chain length of 4K with 10 wt% sugar monomer.*

5.3.6 Closer look at the core-shell region

We have conducted confocal Raman imaging studies along with the collection of Raman spectra from selected area for core-shell nanoparticles to strengthen our claim of core-shell structure and to understand the interfacial region of core-shell. Different colour code (red for sugar chain and blue for polystyrene chain) are used in Raman studies to see the difference between polystyrene and sugar chain (Fig. 5.19). A clear core-shell nature of nanoparticles, where sugar chain (red) on the surface of the PS (blue) in the core of particles are observed. The size of the particles almost matches with the size obtained from TEM. The spectra collected from red and blue region are also shown in Fig. 5.19A. The Raman signal corresponding to the colour coding of the particles indeed confirmed that the red part is the sugar containing chain whereas the blue part is the PS chain. It must be noted that the core-shell do not possess very sharp interface rather a diffused interface between core and shell is observed.

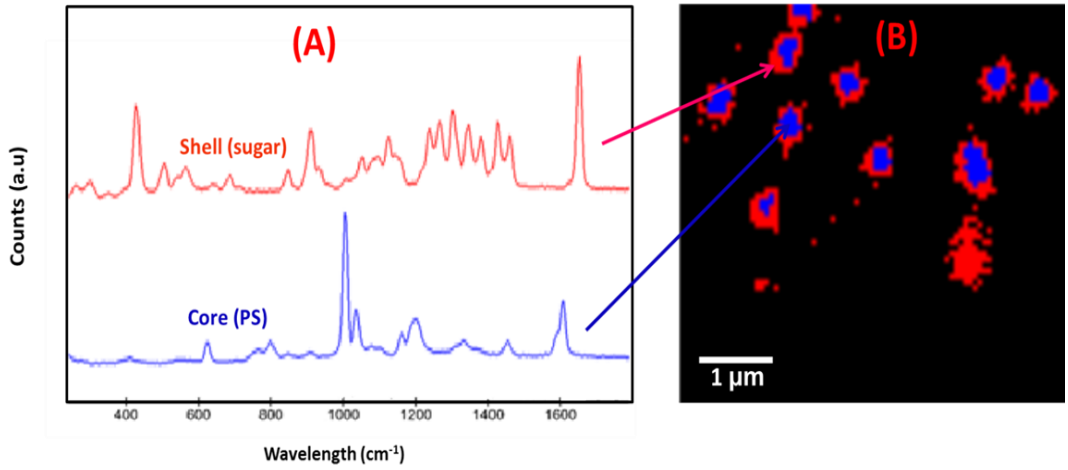

Figure 5.19. *Confocal Raman spectra (A) and images (B) of glycopolymer prepared using 10 wt% sugar with a macro sugar chain length of 8K.*

5.4 Conclusion

In summary, we have demonstrated the RAFT mediated one-pot synthesis of polymeric core-shell colloidal particles in which shell consist glycopolymer and polystyrene is in the core. The resulting core-shell particles displays a narrow size distributions and the size of the formed particles can be readily controlled by changing the macro sugar chain length as well as the sugar content with respect to styrene content in the polymerization feed. The size of the particles decreases with increase in the sugar content in the medium, and the shell thickness increases with sugar content and macro sugar chain length. Zeta potential data reveals that all the formed emulsions are stable for several months. The microscopic, spectroscopic studies unequivocally confirm the formation of polystyrene (core) - glycopolymer (shell) particles. Molecular weight obtained from GPC studies also confirms the formation of PS-GP copolymer. The present methodology delivers a controlled synthesis of well-defined core-shell colloidal particles with protein binding glycopolymer on the surface of the particles which may have potential use in designing and developing new carbohydrate based therapeutics.

References

1. S. L. Flitsch and R. V. Ulijn, *Nature*, 2003, **421**, 219.
2. K.-A. Karlsson, *Curr. Opin. Struct. Biol.*, 1995, **5**, 622.
3. H. Lis and N. Sharon, *Chem. Rev.*, 1998, **98**, 637.

4. J. J. Lundquist and E. J. Toone, *Chem. Rev.*, 2002, **102**, 555.
5. Y. Miura, *J. Polym. Sci.: Part A: Polym. Chem.*, 2007, **45**, 5031.
6. A. Varki, *Glycobiology*, 1993, **3**, 97.
7. T. K. Ritter and C.-H. Wong, in *Carbohydrate-Based Drug Discovery in the Battle against Bacterial Infections: New Opportunities Arising from Programmable One-Pot Oligosaccharide Synthesis, in Carbohydrate-Based Drug Discovery*, Wiley-VCH Verlag GmbH & Co, Malden, MA, Editon edn., 2003, vol. 1, pp. 899–932.
8. Y. C. Lee and R. T. Lee, *Acc. Chem. Res.*, 1995, **28**, 321.
9. R. J. Pieters, *Org. Biomol. Chem.*, 2009, **7**, 2013.
10. W. Ye, S. Wwlls and J. M. Desimone, *J. Polym. Sci.: Part A: Polym. Chem.*, 2001, **39**, 3841.
11. O. Leon, V. Bordege, A. Munoz-Bonilla, M. Sanchez-Chaves and M. Fernandez-Garcia, *J. Polym. Sci.: Part A: Polym. Chem.*, 2010, **48**, 3623.
12. A. Muñoz-Bonilla, O. León, V. Bordegé, M. Sánchez-Chaves and M. Fernández-García, *J. Polym. Sci.: Part A: Polym. Chem.*, 2013, **51**, 1337.
13. Q. Zhang, P. Wilson, A. Anastasaki, R. McHale and D. M. Haddleton, *ACS Macro Lett.*, 2014, **3**, 491.
14. H. Arslan, O. Zırtıl and V. Bütün, *Eur. Polym. J.*, 2013, **49**, 4118.
15. A. B. Lowe and R. Wang, *Polymer*, 2007, **48**, 2221.
16. Y. Wang, X. Li, C. Hong and C. Pan, *J. Polym. Sci.: Part A: Polym. Chem.*, 2011, **49**, 3280.
17. J. Bernard, X. Hao, T. P. Davis, C. Barner-Kowollik and M. H. Stenzel, *Biomacromolecules*, 2006, **7**, 232.
18. T. Serizawa, S. Yasunaga and M. Akashi, *Biomacromolecules*, 2001, **2**, 469.
19. T. Taniguchi, M. Kasuya, Y. Kunisada, T. Miyai, H. Nagasawa and T. Nakahira, *Colloids Surf. B Biointerfaces*, 2009, **71**, 194.
20. S. C. Abeylath and E. Turos, *Carbohydrate Polymers*, 2007, **70**, 32.
21. C.-S. Cho, A. Kobayashi, R. Takei, T. Ishihara, A. Maruyama and T. Akaike, *Biomaterials*, 2001, **22**, 45.
22. Z. Mouline, E. Mahon, E. Gomez, V. Barragan-Montero, J.-L. Monterob and M. Barboiu, *Chem. Commun.*, 2014, **50**, 731.

23. J. Rojo, V. Díaz, J. M. d. l. Fuente, I. Segura, A. G. Barrientos, H. H. Riese, A. Bernad and S. Penadés, *ChemBioChem*, 2004, **5**, 291.
24. Y. Wang, C.-Y. Hong and C.-Y. Pan, *Biomacromolecules*, 2013, **14**, 1444.
25. J. H. Ahire, M. Behray, C. A. Webster, Q. Wang, V. Sherwood, N. Saengkrit, U. Ruktanonchai, N. Woramongkolchai and Y. Chao, *Adv. Healthcare Mater.*, 2015, **4**, 1877.
26. J. H. Ahire, I. Chambrier, A. Mueller, Y. Bao and Y. Chao, *ACS Appl. Mater. Interfaces*, 2013, **5**, 7384.
27. T.-Y. Guo, P. Liu, Y.-Q. Xia and M.-D. Song, *J. Appl. Polym. Sci.*, 2010, **116**, 1611.
28. X.-L. Sun, W. Cui, C. Haller and E. L. Chaikof, *ChemBioChem*, 2004, **5**, 1593.
29. X. Jiang, M. Ahmed, Z. Deng and R. Narain, *Bioconjugate Chem.*, 2009, **20**, 994.
30. C. Boyer, A. Bousquet, J. Rondolo, M. R. Whittaker, M. H. Stenzel and T. P. Davis, *Macromolecules*, 2010, **43**, 3775.
31. K. M. Halkes, A. C. d. Souza, C. E. P. Maljaars, G. J. Gerwig and J. P. Kamerling, *Eur. J. Org. Chem.*, 2005, **17**, 3650.
32. C.-C. Lin, Y.-C. Yeh, C.-Y. Yang, G.-F. Chen, Y.-C. Chen, Y.-C. Wu and C.-C. Chen, *Chem. Commun.*, 2003, **23**, 2920.
33. S. Liu, H. Yan, M. Wang and L. Wang, *J. Agric. Food Chem.*, 2013, **61**, 11974.
34. S. Loykulnant and A. Hirao, *Macromolecules*, 2001 **34**, 8434.
35. K. Tsutsumiuchi, K. Aoi and M. Okada, *Macromolecules*, 1997, **30**, 4013.
36. C. W. Cairo, J. E. Gestwicki, M. Kanai and L. L. Kiessling, *J. Am. Chem. Soc.*, 2002, **124**, 1615.
37. M. R. Hill, R. N. Carmean and B. S. Sumerlin, *Macromolecules*, 2015, **48**, 5459.
38. S. M. Jung and V. G. Gomes, *Polym. Plast. Technol. Eng.*, 2013, **52**, 854.
39. G. Wang, X. Li, D. Yang, Y. Gao and H. Li, *Design. Monom. Polym.*, 2014, **17**, 132.
40. N. Yeole, S. N. R. Kutcherlapati and T. Jana, *RSC Adv.*, 2014, **4**, 2382.
41. N. Yeole, S. N. R. Kutcherlapati and T. Jana, *J. Colloid Interface Sci.*, 2015, **443**, 137.
42. G. Moad, E. Rizzardo and S. H. Thang, *Aust. J. Chem.*, 2012, **65**, 985.
43. M. Destarac, I. Gauthier-Gillaizeau, C.-T. Vuong and S. Z. Zard, *Macromolecules*, 2006, **39**, 912.
44. A. B. Lowe and C. L. McCormick, *Aust. J. Chem.*, 2002, **55**, 367.
45. A. B. Lowe, B. S. Sumerlin and C. L. McCormick, *Polymer*, 2003 **44**, 6761.

46. G. Moad, E. Rizzardo and S. H. Thang, *Aust. J. Chem.*, 2009, **62**, 1402.
47. D. Horton and T. Miyake, *Carbohydr. Res.*, 1988, **184**, 221.
48. R. Y. Tam, S. S. Ferreira, P. Czechura, J. L. Chaytor and R. N. Ben, *J. Am. Chem. Soc.*, 2008, **130**, 17494.
49. C. Gonzato, M. Courty, P. Pasetto and K. Haupt, *Adv. Funct. Mater.*, 2011, **21**, 3947.
50. D. Arunbabu, Z. Sanga, K. M. Seenimeera and T. Jana, *Polym Int.*, 2009, **58**, 88.
51. N. Yeole, D. Hundiwale and T. Jana, *Journal of Colloid and Interface Science*, 2011, **354**, 506.
52. Y. Kwak, A. Goto, K. Komatsu, Y. Sugiura and T. Fukuda, *Macromolecules*, 2004, **37**, 4434.
53. J. B. McLeary, M. P. Tonge and B. Klumperman, *Macromol. Rapid Commun.*, 2006, **27**, 1233.
54. R. Venkatesh, B. B. P. Staal, B. Klumperman and M. J. Monteiro, *Macromolecules*, 2004, **37**, 7906.
55. A. Pfaff, V. S. Shinde, Y. Lu, A. Wittemann, M. Ballauff and A. H. E. Müller, *Macromol. Biosci.*, 2011, **11**, 199.
56. Y. Kwak, A. Goto, K. Komatsu, Y. Sugiura and T. Fukuda, *Macromolecules*, 2004, **37**, 4434.
57. J. B. McLeary, M. P. Tonge and B. Klumperman, *Macromol. Rapid. Commun.*, 2006, **27**, 1233.
58. R. Venkatesh, B. B. P. Staal, B. Klumperman and M. J. Monteiro, *Macromolecules*, 2004, **37**, 7906.
59. M. L. Cerrada, V. Bordegé, A. Muñoz-Bonilla, O. León,R. Cuervo-Rodríguez, M. Sánchez-Chaves and M. Fernández-García, *Carbohydr. Polym.*, 2013, **94**, 755.

Chapter 6

Glycopolymer Grafted Silica Nanoparticles: Synthesis using *Grafting from* RAFT Polymerization and Binding Study with Lectin

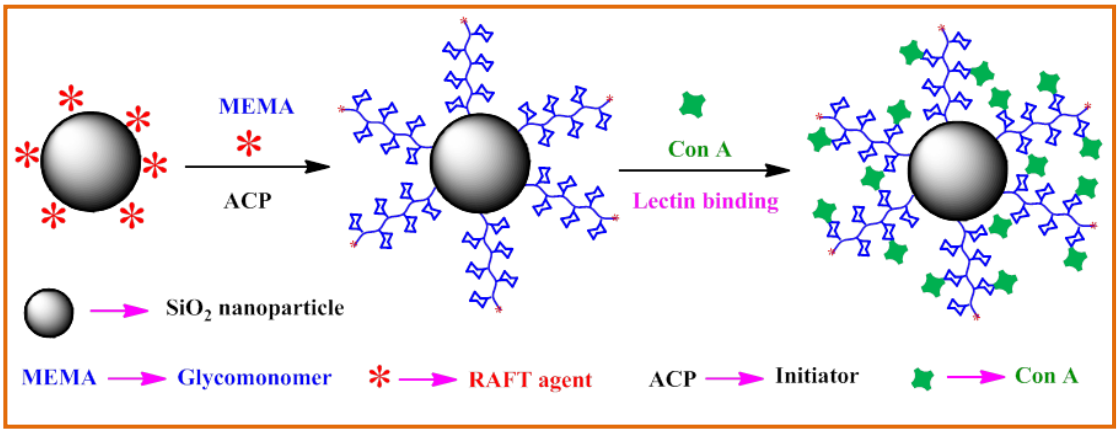

Synthesis of glycopolymer (GP) grafted silica nanoparticles (SiNP) by using reversible addition fragmentation chain transfer (RAFT) polymerization through grafting from approach with a variable chain lengths and densities.

6.1. Introduction

Often, the interaction between carbohydrates and proteins is recognized as low affinity binding and can be enhanced by creating a multivalent interaction using multiple carbohydrate ligands. This approach can lead to increase in the interaction of carbohydrate with their corresponding receptors (proteins) by manifold than that of corresponding monovalent interaction.[2-6] A polymeric chain in which carbohydrate groups are hanging from the main backbone can act as a multiple carbohydrate ligands and termed as glycopolymer (GP).

The synthesis of glycopolymers with different morphologies is an important step towards the understanding of interactions between GPs and proteins, and more importantly unravelling the influence of GP morphology on the binding with proteins.[6] Hence, there is need to develop a versatile method for the preparation of GPs especially in such a structural form (morphology) which enables the conjugation with proteins readily. One can hypothesise that the GP chains grafted on the surface of nanoparticles might be the right choice for easy and strong conjugation with protein/lectin. This objective can be realized if one can grow the GP chains on the nanoparticle surface.

Among several nanoparticles surface which can be used to graft GP chain,[7-14] silica nanoparticles (SiNP) in particular provides several interesting advantages like biocompatibly, low toxicity and readily functionalizable surface when compared with heavy metals and other types of metallic/ semiconducting surfaces.[15-18] Moreover, uniformly sized SiNP can be easily prepared from inexpensive starting materials using simple synthetic protocols.[19] In literature, carbohydrate modified SiNPs have recently attracted much attention for understanding lectin-carbohydrate interactions and find applications in a variety of biological processes including fertilization, cell migration, cancer therapy, and host-pathogen interactions.[13, 14, 20-22] Very recently, carbohydrate modified SiNPs were used to target the site of tumor cells, multi-drug resistance cells with high precision.[16, 23, 24]

Grafting of carbohydrates on SiNPs surface has been carried out using varieties of conjugation techniques which include CuAAC, amide coupling, nucleophilic substitution, and photo coupling methods.[6, 23-25] Majority of these methods typically involve laborious multi-step procedures as well as costly and potentially toxic metal catalysts. Also, these methodologies cannot be used to graft GPs since GPs are synthesized with protected glycomonomer to avoid unnecessary hydrolysis during polymerization and deprotection is

carried out after polymerization.[26-28] The whole process of protection-deprotection on the SiNP surface can become very tedious and hence, there is need to develop a method for grafting of GP chain on SiNPs surface. Two methods namely *grafting–to* and *grafting-from* are mostly used for modification of nanoparticle surfaces with polymers.[29-34] In case of *grafting-to* method, polymer chains are grafted to the nanoparticle surface and in case of *grafting-from*, the grafting reaction is conducted by polymerizing monomers from the nanoparticle surface. In both the cases, a thin polymer layer can be formed on the nanoparticle surface. Though *grafting-to* method is simple to be performed, but the obtained graft density is fairly low since the diffusion of polymer chains to the particle surface is sterically hindered. Therefore, we believe the *grafting-from* method to grow the GP chain onto the SiNPs surface would be the correct choice for obtaining high density GP on SiNP surface. Among the controlled radical polymerizations (CRPs), reversible addition fragmentation chain transfer polymerization (RAFT) is found to be highly popular for grafting polymers on SiNP surface owing to the advantages on being compatible with a wide range of monomers including functional monomers, free of transition metal ion contamination and moreover reactions can be conducted in mild conditions. [25, 35-42]

With this background as discussed above and to the best of our knowledge no report has appeared till now on the grafting of GP chains on the SiNP surface using *grafting from* RAFT polymerization method which will allow control over molecular weights, chain length and hence the morphology of resulting materials, which in turn can have significant influence on protein binding. Therefore, In this work, we report the synthesis of structurally well-defined, glycopolymer-grafted-SiNP hybrid materials by modifying the surface of SiNPs with suitable RAFT agent and then chain extended with glycomonomer to produce GP grafted SiNPs (SiNP-g-GP). The monomer used in this study is the mannose derivative (mannosyloxyethyl methacrylate, MEMA) which has strong lectin binding activity. In addition to synthesis, characterization and structural elucidation of SiNP-g-GP, we have studied the lectin binding of this nanomaterial with Con A using isothermal titration calorimetry (ITC).

6.2 Experimental Section

6.2.1 Materials and Methods

All information about the materials used in this study and the synthetic procedure for the preparation of RAFT agent as well as silica nanoparticles (SiNPs) are discussed in the

Chapter 2. The experimental methods and all the characterization techniques which include molecular weight measurements by GPC, spectroscopic characterization by FT-IR and NMR, thermal analysis by TGA and DMA, microscopic analysis by FE-SEM and TEM, light scattering by DLS study are discussed in Chapter 2. The glyco monomer used in this study is the mannose derivative (mannosyloxyethyl methacrylate, MEMA) (Scheme 6.1) was synthesized and provided by Prof. Ramu Shridher, School of Chemistry, University of Hyderabad and the lectin binding studies for the synthesized GNPs has been done in Prof. M. J. Swamy laboratory, School of Chemistry, University of Hyderabad, India.

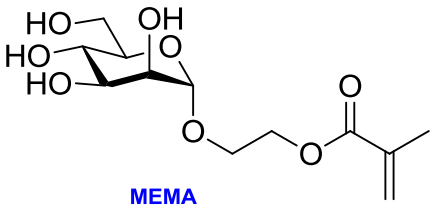

Scheme 6.1. *Structure of the used glyco monomer mannosyloxyethyl methacrylate (MEMA).*

6.2.2 Polymerization of MEMA using SiNP-CPDB

We have carried out the polymerizations in two different solvents namely (mixture of water: ethanol (7:3) and DMF, to check the suitability of solvent so as to get good amount of GP loading on the SiNP surface. We have also executed many controlled reactions to check the role of free CPDB (RAFT agent) in the reaction mixture.

6.2.3 Water based reactions

Into a series of Schlenk tubes containing 7:3 mixture of water and ethanol (1.4 mL), SiNP-CPDB (0.1 g, which has 7.607 μmol of CPDB), MEMA (calculated amount, we have varied for different chain lengths), $NaHCO_3$ (2 mg), free CPDB (2.13 mg, 7.607 μmol), ACP (0.426 mg, 1.521μmol) were added by keeping the ratio of [SiNP-CPDB]: [free CPDB]: [ACP] = 1:1:0.2 constant for all the reactions, only the amount of MEMA were altered. These reaction vials were then sealed and subjected to three freeze-pump-thaw cycles followed by sonication for 10 min and stirred for 16 h in preheated oil bath at 70 ^{o}C. After completion of the reaction, the reaction mixture was quenched using liquid nitrogen. The glycopolymer grafted silica particles (SiNP-g-GP) were precipitated from large excess of hexane and isolated by using centrifugation at 7000 rpm for 30 min. The obtained precipitate was redispersed in methanol (40 mL) and centrifuged at 7000 rpm for 30 min. This step was

repeated for thrice and the obtained SiNP-G-GP was dried under vacuum at 70 ^{o}C for 48 h. We have altered the amount of glyco monomer (MEMA) in the reaction medium by keeping all the other reagents constant so as to obtain different chain length of GP chain on the SiNP surface.

6.2.4 DMF based reactions

The polymerization reactions were conducted using the identical protocols as described above in DMF solvent.

6.2.5 Homopolymerization of MEMA monomer using CPDB as RAFT agent

In a 10 mL Schlenk tube containing DMF (3 mL), MEMA (300 mg, 1.0273 mmol), CPDB (4.189 mg, 15 μmol) and ACP (0.42 mg, 1.5 μmol) were added. The reaction tube was sealed and subjected to three times freeze-thaw cycles followed by sonication for 10 min and stirred for 16 h in preheated oil bath at 70 °C. After completion of 16 h, the reaction mixture was quenched using liquid nitrogen; the GP was precipitated from large excess of cold hexane/diethyl ether mixture and isolated by filtration. This precipitation step was repeated twice and the obtained GP was dried under vacuum at 60 °C for 24 h.

6.2.6 Cleaving of the GP from the SiNP-g-GP

The GP was cleaved from the SiNP-g-GP according to the procedure described elsewhere.[48, 49] Briefly the process is as follows: in a polyethylene tube, the SiNP-g-GP (30 mg) was dissolved in 6 ml DMF. Aqueous Hydrofluoric acid (HF, 48 wt%, 0.6 ml) was added into this solution and the reaction mixture was stirred at room temperature for 6 h. The polymer was precipitated by adding the polymer solution into 20-fold of excess cold hexane/diethyl ether mixture in a polyethylene beaker and then the precipitate was collected by filtration. The GP obtained was dried in a vacuum oven at 80 °C for 24 h. The recovered GP was then subjected to molecular weight analysis.

6.3 Results and Discussion

6.3.1 Polymerizable SiNP surface

In this article, we report the successful grafting of glycopolymers (GP) on silica nanoparticles (SiNP) surface using *grafting from* RAFT polymerization technique. A multistep process has been developed to prepare glycopolymer grafted SiNP (SiNP-g-GP). First, the well-known Stober method was followed to prepare monodisperse SiNPs from tetraethyl

orthosilicate [$Si(OEt)_4$] through a hydrolysis and condensation reaction.[19] The measured particle size obtained from FE-SEM and TEM is 47 (±2) nm in diameter as displayed in Fig. 6.1 and these particles are highly monodisperse and the size of these nanoparticles can be readily controlled by altering the mole ratio of the reactants used in the synthesis. In the second step of SiNP-g-GP preparation the amine functionalized silica nanoparticles (SiNP-NH_2) were prepared by refluxing (3-aminopropyl)triethoxysilane (APTES) with silica nanoparticles as shown in Scheme 2.3 and the measured particle size of SiNP-NH_2 is 47 (±2) nm (FESEM & TEM) and 65 nm (DLS).

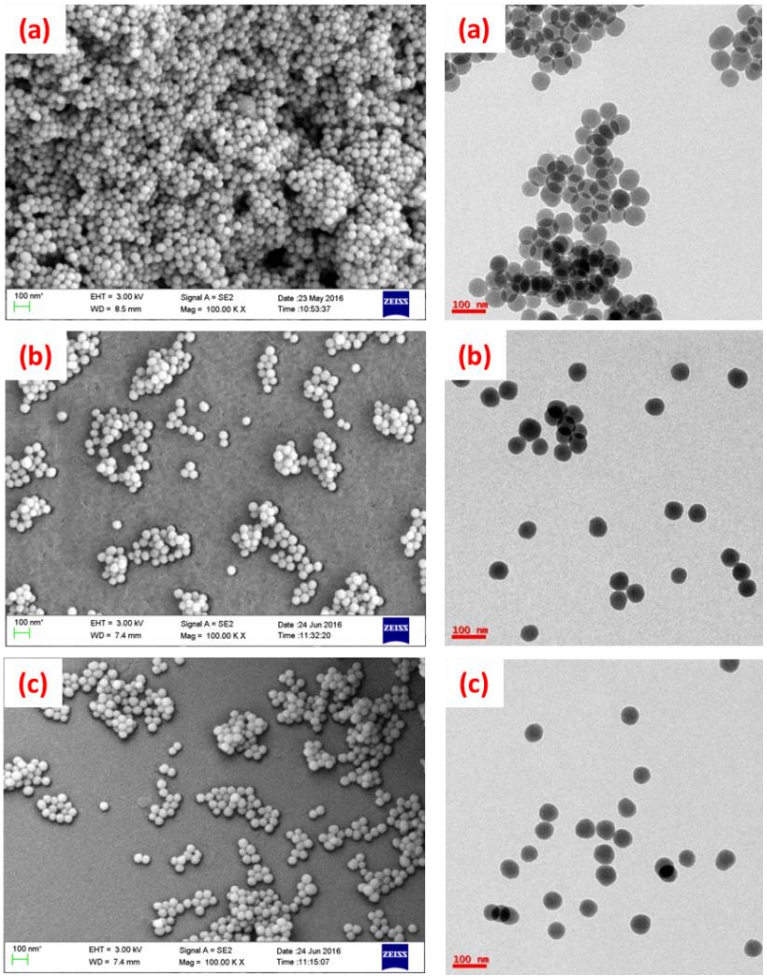

Figure. 6.1. *FE-SEM (left panel) and TEM images (right panel) of (a) bare SiNP, (b) SiNP-NH_2 and (c) SiNP-CPDB.*

It is well known that dithiobenzoate based RAFT agents can control the radical polymerization of a wide range of monomers including methacrylates, acrylates and styrene to provide polymers with predictable molecular weight and narrow polydispersities. By keeping this in mind, we have chosen a carbonyl group containing dithiobenzoate RAFT agent namely CPDB (4-cyanopentanoic acid dithiobenzoate) for our purpose and the further advantage with the carboxyl group of CPDB is that, this –COOH group can be readily utilize to immobilize CPDB on particle surface through a covalent bond with SiNP-NH_2. Accordingly in the third step of SiNP-g-GP preparation, we tried to couple CPDB with SiNP-NH_2 which is the crucial step. However, the simple condensation between the carboxylic acid of CPDB and amine group of SiNP-NH_2 did not work due to the weak stability of these dithiobenzoate (CPDB) under reaction conditions owing to the aminolysis of dithiobenzoate group.[48] Therefore, the carboxyl group of CPDB was first activated using N-hydroxysuccinamide (NHS) to get CPDB-NHS as shown in Scheme 2.3[47] and then this activated RAFT agent (CPDB-NHS) was successfully attached to silica nanoparticles by reacting with amine modified SiNP. The FESEM and TEM images of SiNP-CPDB are presented in Fig 6.1 along with bare SiNP and SiNP-NH_2. The measured particle size is 48 (±3) nm (FESEM & TEM) and 59 nm (DLS).

FT-IR and TGA analysis provide clear evidence for the step-by-step surface modification of SiNPs. Fig. 6.2 compares the FT-IR spectra of the SiNP-CPDB with the bare SiNP. The sharp band at 1645 and at 1552 cm^{-1} are due to C=O and N-H stretching of amide group, respectively. Bands at 2948, 1450 and 2254 cm^{-1} are the functional groups stretching of CPDB. This indicates that the dithiobenzoate group of CPDB RAFT agent is covalently attached to the surface of the SiNPs. TGA plots shown in Fig. 6.2 display that the final weight loss increases from bare SiNP to SiNP-NH_2 to SiNP-CPDB attributing that the attachment of organic groups (propyl amine or CPDB) to the surface of the SiNPs. The amount of RAFT (CPDB) which is covalently attached to the SiNPs was calculated from the TGA plots and found to be equal to 21.3 mg/g (76 µmol/g).[30, 50] ^{13}C NMR also gives the clear evidence of the successful surface grafting of CPDB.

The ^{13}C NMR spectrum of SiNP-CPDB was recorded using $CDCl_3$ dispersion and presented in Fig. 6.3(A). The chemical shift at 168,144 and 120 ppm are due to the amide carbonyl carbon, anomeric carbon of phenyl ring in CPDB and the cyano group in CPDB, respectively. The peaks around 124 -130 ppm and between 18-40 ppm are due to the phenyl

ring carbon atoms and for the alkyl carbons from CPDB RAFT agent and SiNP-NH_2, respectively. These results confirm a covalent attachment of CPDB with SiNPs.

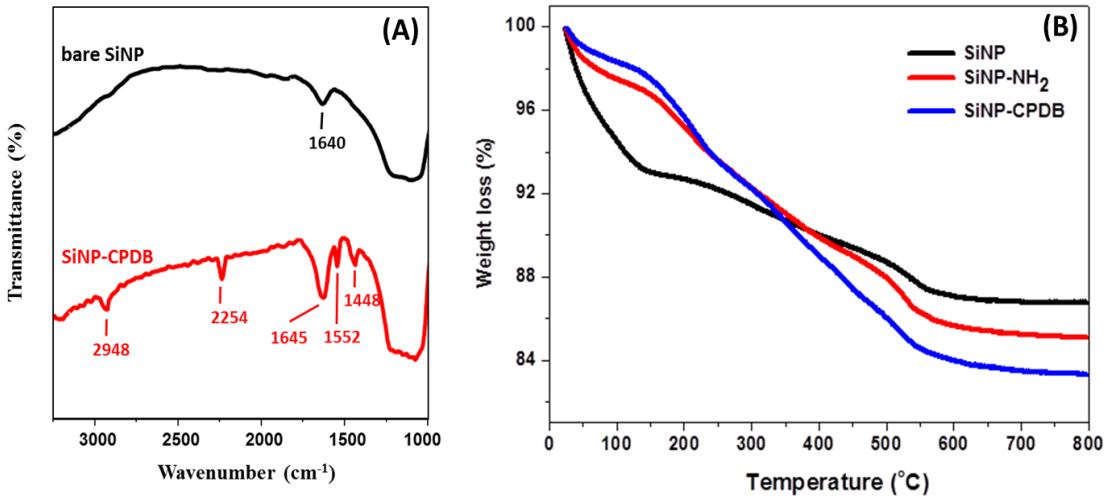

Figure. 6.2. *FT-IR spectra (A) and TGA plots (B) of bare SiNPs and RAFT modified SiNPs.*

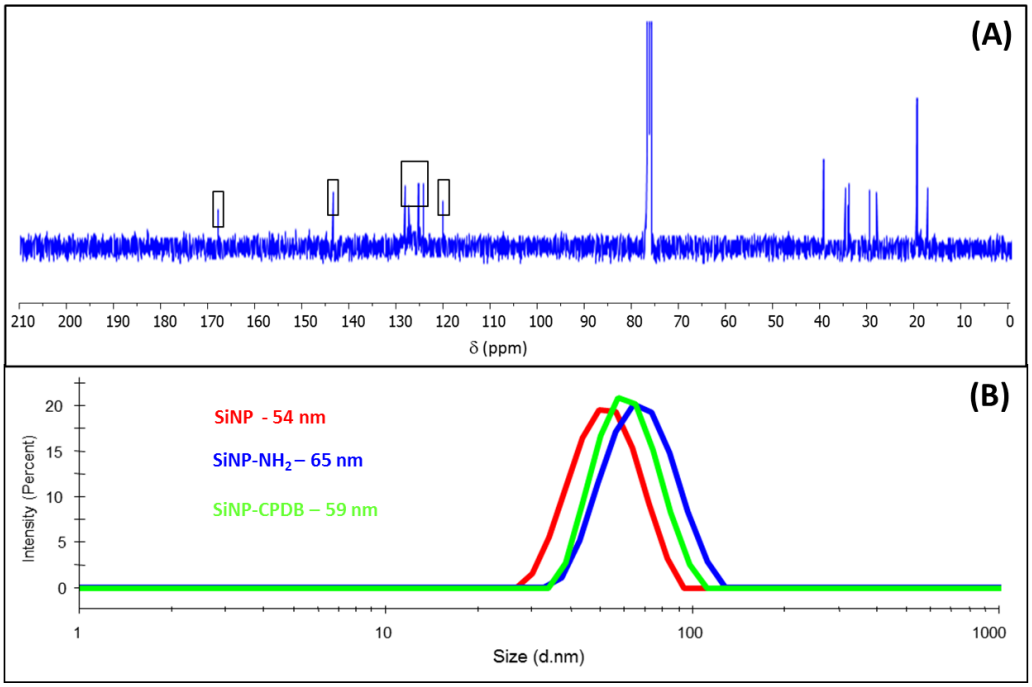

Figure. 6.3. *^{13}C NMR spectra of SiNP-CPDB (A) and DLS graphs of bare SiNP, SiNP-NH_2 and SiNP-CPDB.*

The particle size and size distribution of SiNPs were measured in water by using DLS and presented in Fig. 6..3(B). The mean diameter of bare SiNP is 53 nm and increased to 64 nm upon the amine modification which is due to the formation of hydrophilic amine shell and then decreased to 58 nm after attaching CPDB on SiNP particle surface. The decrease in the diameter may be due to decrease in hydration shell of particle after CPDB attachment owing to the attached alkyl chain and phenyl ring. Hence, the above discussions clearly proved that the SiNP surface is now ready for further grafting of polymer chain.

6.3.2 Growth of mannose based glycopolymer chain on the SiNP surface

Polymer chains can be grown on any solid (particle) surface using RAFT mediated grafting-from approach. There are two methods namely 'arm-first' and 'core-first' by which polymer chain be grown using *grafting from* RAFT method.[51-53] The relatively lower grafting density in the particle surface is usually achieved in the arm-first way,[51] where Z-group of RAFT agent is attached to the particle surface compared to core first method where R-group of RAFT agent is attached to the particle surface. The SiNP-CPDB has R-group on the SiNP surface; therefore any growth of chain in the current surface is expected to yield higher grafting density of polymer chain.

MEMA monomer (Scheme 6.1) was synthesized in multiple steps and characterized by Dr. P. Ramushidher. The polymerizable SiNP-CPDB surface was used to grow the Poly (mannosyloxyethyl methacrylate) (pMEMA) chain to produce the SiNP-g-GP where GP in pMEMA and hence this point onwards we refer it as SiNP-g-pMEMA. The reaction scheme is pictorially presented in Scheme 6.2. The polymerization was carried out in two different solvents: water/ethanol mixture (7:3) and DMF. The polymerization of MEMA in the presence of SiNP-CPDB was performed using additional amount of CPDB as a free chain transfer agent and ACP as a thermal initiator at 70 °C by keeping the reactant ratio as [SiNP-CPDB]: [free CPDB]: [ACP] = 1:1:0.2 and this ratio was kept constant for various sets of reaction with a variation of MEMA to get different chain lengths of pMEMA on the SiNP surface. After polymerization, reaction was stopped by quenching the tubes in liquid nitrogen and the particles were precipitated by centrifugation at 7000 rpm for 30 min. The impurity SiNP-g-pMEMA was obtained by repeated centrifugation-redispersion procedure until no free polymer was detected in the methanol solution. Finally the particles were dried in a vacuum oven at 80 °C for 24 h to yield SiNPs-g-pMEMA. All the characterizations of the prepared sample were carried out using this dry SiNPs-g-pMEMA. Table 6.1 summarizes all the

physical details of the all the synthesized polymers. To check the suitability of solvents, we have synthesized series of polymers with variable chain lengths of pMEMA and this has been achieved by varying the feed of MEMA monomer in the polymerization. P1, P2 and P3 samples (refer Table 6.1) are obtained in water/ethanol (7:3) mixture and P4, P5, P6 (refer Table 6.1) are obtained using DMF solvents. P7 is also obtained using DMF solvent without any SINP core. The number of repeated unit is calculated from the molecular weight data which was measured using GPC and will be discussed in the later section.

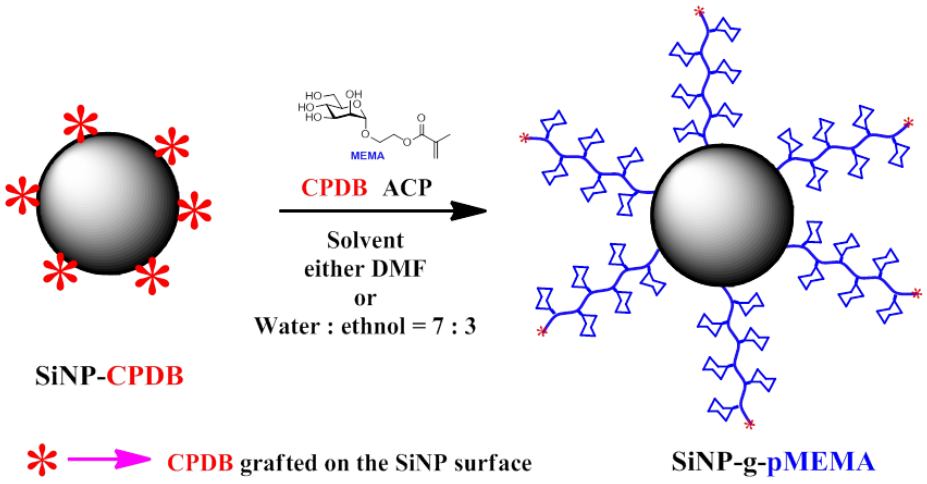

Scheme 6.2. *Synthesis of GP (pMEMA) grafted SiNPs (SiNP-g-pMEMA) from RAFT modified polymerizable SiNP.*

The relative amount of pMEMA (GP) grafted to SiNPs in the final products can be estimated from the TGA results. Fig. 6.4 shows the TGA curves for the SiNP-CPDB, SiNPs-g- pMEMA along with pMEMA (homopolymer without grafting on to the SiNP surface) prepared using two different solvents and obtained after purification. The decomposition temperature range for all the samples is 250-600 °C as shown in Fig. 6.4. The pure pMEMA (without SiNP, P7) is decomposed completely as can be seen from the TGA graphs (Fig. 6..4B). The TGA data clearly show that with increase in pMEMA chain length, the final weight loss is increasing (P4 to P6 weight loss increases significantly) attributing that the more amount of GP loading on the SiNP surface.

Table 6.1: *Summary of various physical data of SiNP-g-pMEMA*

Sample identity	Sample type	Solvent [a]	Addition of free RAFT	Amount of pMEMA grafting (wt% / g [b] of SiNP)	$\bar{M}_n$ [d]	Targeted $\bar{M}_n$ [e]	PDI[e]	Size (TEM) (nm) [f]	Size (DLS) (nm) [g]
-	SiNP-CPDB	-	-	-	-	-	-	48	58
P1	SiNP-g-$pMEMA_{18}$	S1	Yes	2.7	5500	5000	1.22	49	105
P2	SiNP-g-$pMEMA_{24}$	S1	Yes	4.2	7100	10000	1.19	50	122
P3	SiNP-g-$pMEMA_{16}$	S1	No	2.8	4900	10000	1.19	49	117
P4	SiNP-g-$pMEMA_{9}$	S2	Yes	9.5	2700	2500	1.17	51	91
P5	SiNP-g-$pMEMA_{32}$	S2	Yes	19.4	9400	10000	1.19	53	141
P6	SiNP-g-$pMEMA_{138}$	S2	Yes	38.1	40400	50000	1.37	57	164
P7	$pMEMA_{74}$ (GP)	S2	Yes	100	21700	20000	1.06	-	-

[a] the polymerization of MEMA was carried out in two different solvents in which, S1 is water/ethanol (7:3) mixture and 2 mg of $NaHCO_3$ is added to dissolve ACP initiator and S2 is dry DMF, [b] estimated from the TGA analysis, targeted $\bar{M}_n$ is calculated based on the calculations which is generally used for RAFT polymerization (also explained in chapter 5). [d and e] determined by gel permeation chromatography, [f] with a standard deviation of ±2 until P4 and ±4 for P5 and P6, [g] Size polydispersity obtained from DLS is less than 0.1

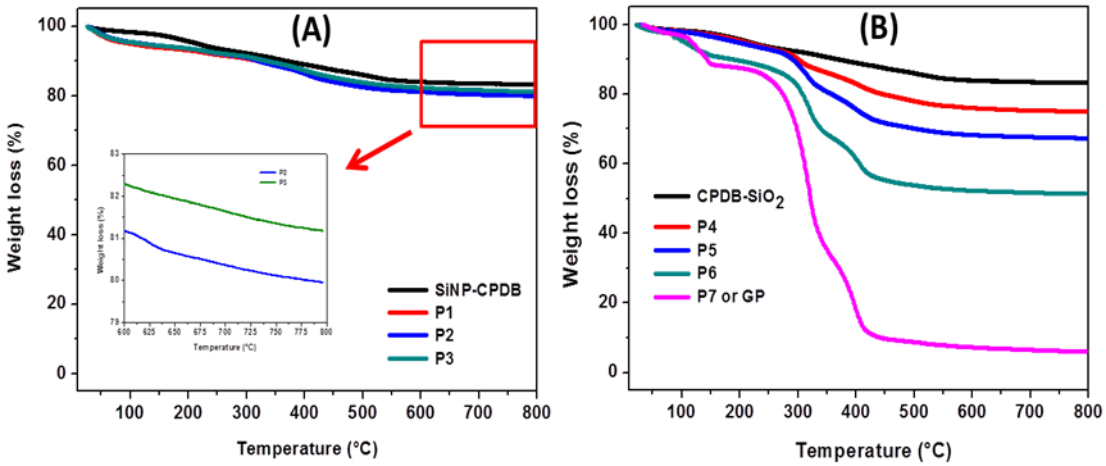

Figure. 6.4. *TGA analysis of SiNP-g-pMEMA samples of different chain lengths obtained from two different solvents water/ethanol (A), DMF (B). The details of individual samples identification are shown in the figure. Inset: The weight loss difference in case of P2 to P3.*

6.3.3 Role of solvent and free RAFT agent in the polymerization

We have carried out the polymerization in two different solvents to check the role of solvent in the polymerization of MEMA in *grafting from* approach. Two similar reactions (P2 and P5) in two different solvents (water/ethanol mixture and DMF) and identical targeting M.W (10 K) by keeping all other reaction conditions identical were conducted. The relative amount of GP which is grafted to SiNP is analysed from TGA data and the TGA plots are presented in Fig. 6.5. As seen from the TGA graph, the final weight loss is more when polymer prepared from DMF solvent (P5) than in water solvent (P2) may be due to the higher reinitiation capacity of the formed oligomeric radicals in DMF compared to water solvent. Table 6.1 data also shows higher GP loading in case of P5 than P2. Therefore, we can conclude that DMF is a better solvent for MEMA polymerization and to graft higher amount of pMEMA on SiNP surface.

Further, we want to check the role of free CPDB (RAFT agent) in the polymerization of MEMA using *grafting from* RAFT approach. For this reason, we have conducted a set of same reactions with identical targeted M.W (P2 & P3, details are presented in the Table 6.1) where we have taken all the ingredients in the same proportion except that free CPDB is not added in case of P3 and to maintain the [M]:[R]:[I] ratio, we have also halved the monomer as well as initiator in case of P3. The TGA data of isolated P2 and P3 sample (inset of Fig 6.4A) clearly shows less weight loss in case of P3 compared to P2. This attributes higher grafting of

pMEMA on SiNP in presence of free CPDB as also can be verified from the GP grafting amount as shown in Table 6.1. The excess CPDB in the polymerization mixture helps in exchanging oligomeric radicals and therefore the polymerization goes more steady which leads to high GP grafting. Hence, we have conducted remaining reactions (P4-P6) with the addition of similar amount of free CPDB and in DMF so that we can achieve better GP grafting.

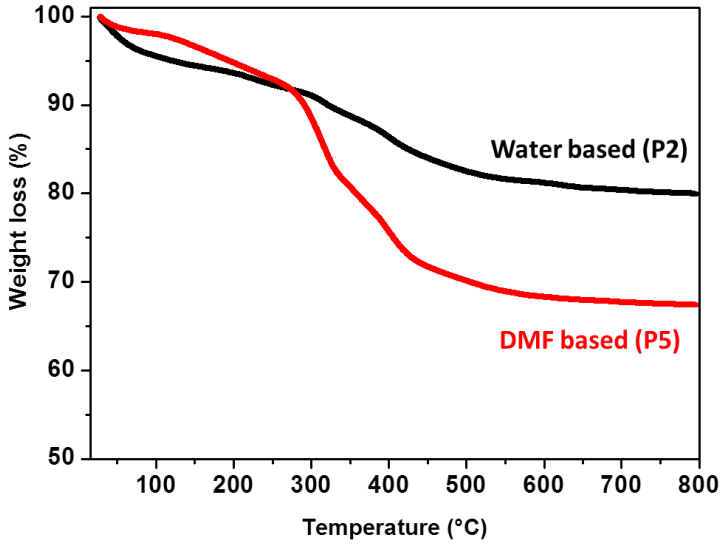

Figure. 6.5 *TGA thermogram showing the role of solvent for the synthesis of SiNP-g-GP. Refer to the Table 1 for sample identification.*

6.3.4 Spectroscopic evidence of poly MEMA grafting on SiNP

The grafting of pMEMA on the particle surfaces is confirmed by comparing the FT-IR spectra of SiNP-CPDB, SiNP-g-pMEMA and pMEMA (Fig 6.6). SiNP-g- pMEMA spectrum shows a peak at around 1217 cm^{-1} which correspond to C-O bond stretching of the mannose moiety which is apparent in the pMEMA spectrum at 1210 cm^{-1}. The bands observed at 1379 cm^{-1} and 1735 cm^{-1} are assigned to the C-O-C group and C-O ester double bond of the mannose sugar, respectively and these are also seen in pMEMA. The presence of characteristic bands of SiNP-CPDB on the spectrum of SiNP-g-pMEMA clearly proves that pMEMA is grafted on the SiNP-CPDB surface.

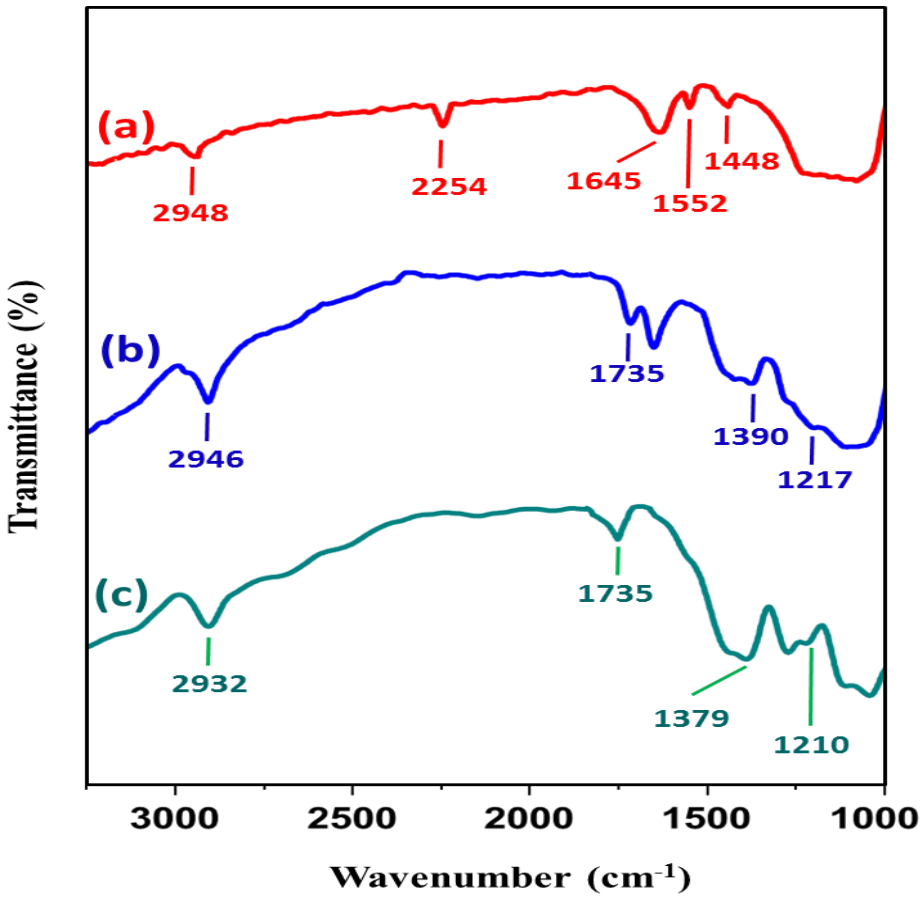

Figure. 6.6. *FT-IR spectra of (a) SiNP-CPDB, (b) SiNP-g- pMEMA and (c) pMEMA*

The grafting of GP on SiNP surface was further confirmed by ^{13}C NMR spectroscopy. Fig. 6.7 represents the ^{13}C-NMR spectra of SiNP-g-GP recorded in D_2O solvent. A peak at 170.9 ppm attributes the carbonyl carbon (C=O) of the ester from the pMEMA. The peak at 105.8 ppm is due to the anomeric carbon of mannose in MEMA. Several peaks between 64 ppm to 77 ppm are attributed to the five remaining carbon from the mannose ring and the remaining two peaks are due to the ethylene part of MEMA. Two peaks at 48.6 ppm and 29.2 ppm are due to the polymer backbone indicating the successful grafting of pMEMA on the SiNP nanoparticle surface.

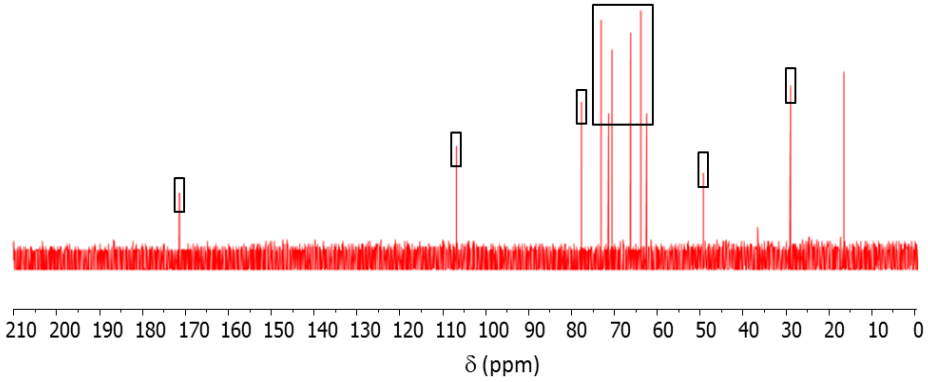

Figure. 6.7. *^{13}C NMR spectra of SiNP-g- pMEMA. Spectra was recorded in D_2O by dispersing the solid particles of the sample.*

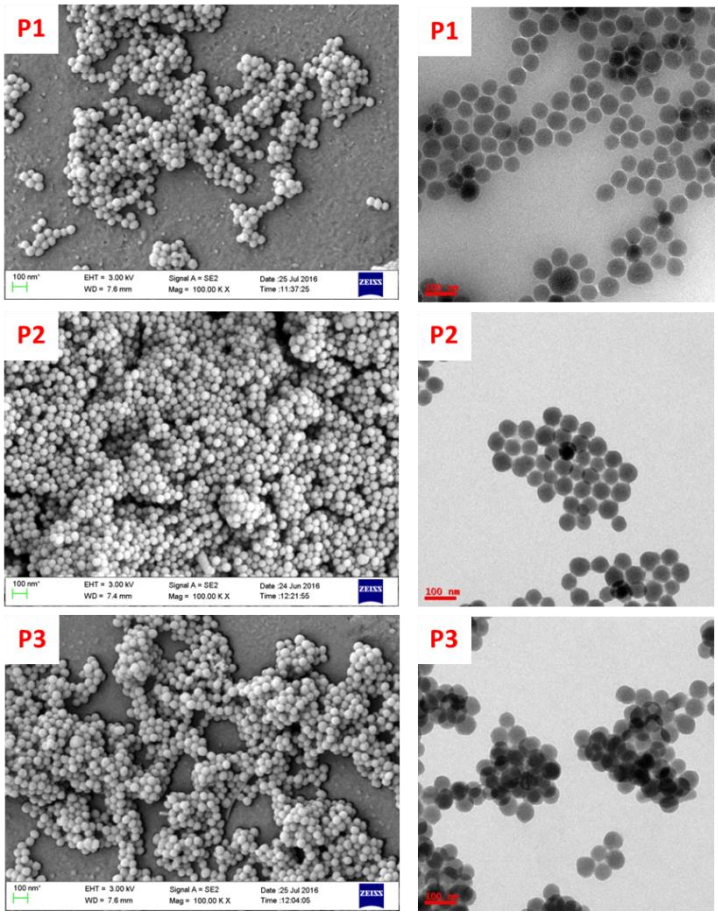

Figure. 6.8. *FE-SEM images (left panel) and TEM images (right panel) of SiNP-g-GP obtained after purification for different chain lengths prepared using water/ethanol (7:3) as a solvent. The description of sample identity (P1, P2 and P3) are described in Table 1.*

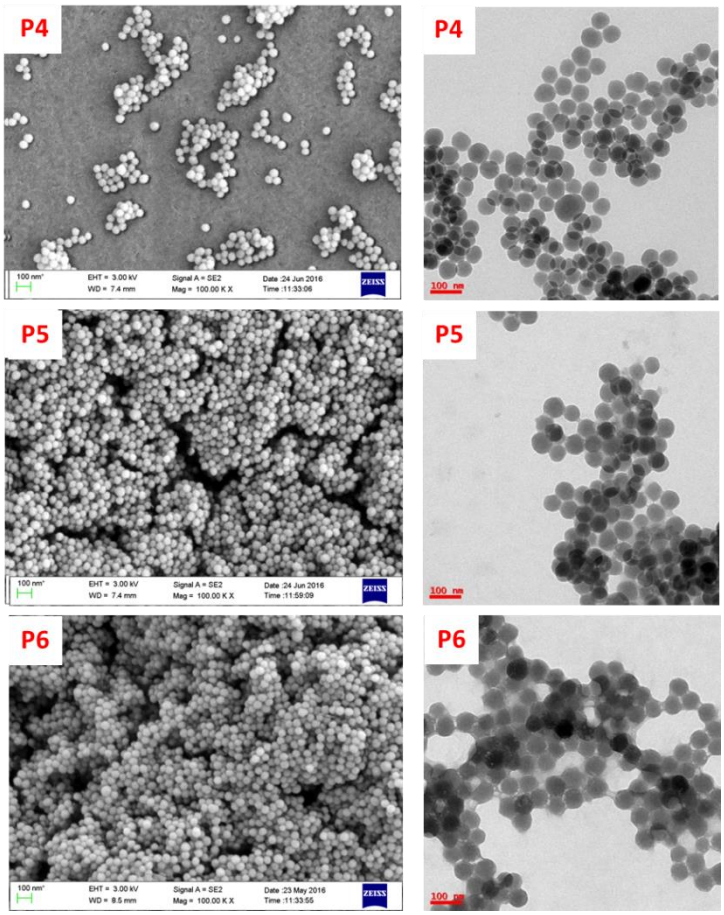

Figure. 6.9. *FE-SEM images (left panel) and TEM images (right panel) of SiNP-g-pMEMA nanoparticles obtained after purification for different chain lengths prepared using DMF as a solvent. The sample identification (P4, P5 and P6) can be found in Table 6.1.*

The particle size and size distribution of SiNP-g-pMEMA samples also were measured in water by using DLS and presented in Fig. 6.10, and the size obtained are listed in Table 6.1. Even though the core (SiNP-CPDB) diameter of all the particles are same (as prepared from the same sample of SiNP-CPDB), the hydrodynamic diameter of SiNP-g-pMEMA has increased by two to three fold indicating that the SiNP-g-pMEMA possesses the graft pMEMA chains which are highly hydrophilic and are in the swollen state as shown in the Fig 6.11. The size from DLS is proportional to the GP chain length on the particle surface or in other words size of the particles increases with increasing chain length of pMEMA (Table 6.1). The core reason for the increase in the hydrodynamic diameter is a result of surface grating of pMEMA chains on SiNP and similar results are obtained by others when particles

coated with a hydrophilic polymer chain.[54] These above results indicate that the grafting of pMEMA on the SiNP surface was successfully achieved by RAFT mediated controlled radical polymerization of MEMA using SiNP-CPDB. A comparison of size measured from microscopic and DLS technique clearly reveals that pMEMA chain is in swollen state in solvent (DLS measurement) but in collapsed state in dry condition (microscopic measurement). It must be noted from Table 6.1 data that the changes in particle size is almost insignificant with increasing GP chain length in case of data obtained from microscope technique, however it is very significant increase with increasing GP chain length. These observations once again reiterate the swelling nature of hydrophilic pMEMA chain as pictorially shown in the Fig. 6.11. It should be mentioned that all the particles are highly monodisperse in nature as seen from both microscopic and light scattering data.

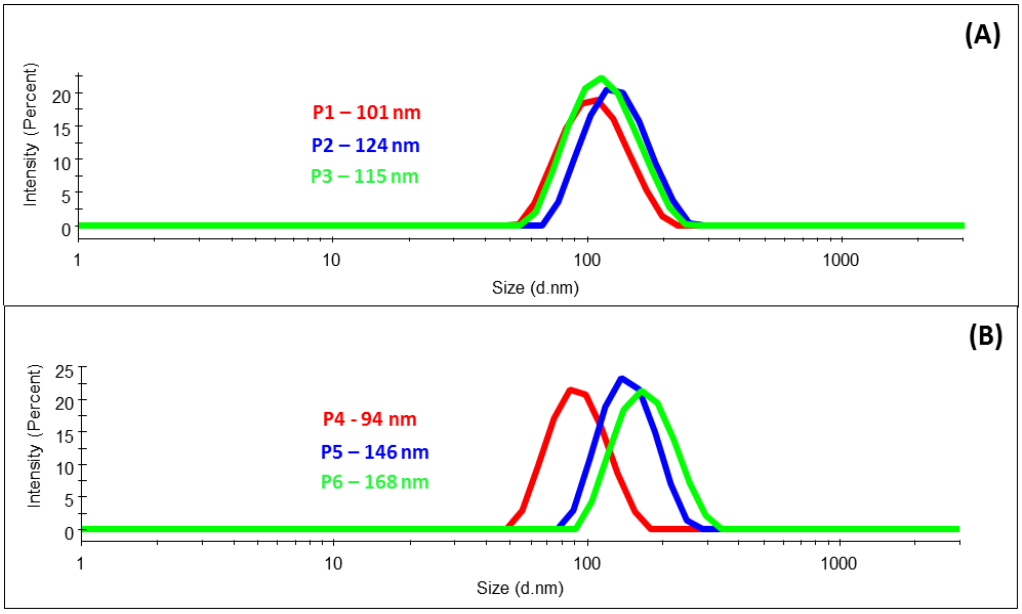

Figure. 6.10. *DLS plots of SiNP-g-pMEMA obtained from the polymerization conducted in (A) water/ethanol (7:3) and (B) DMF solvents.*

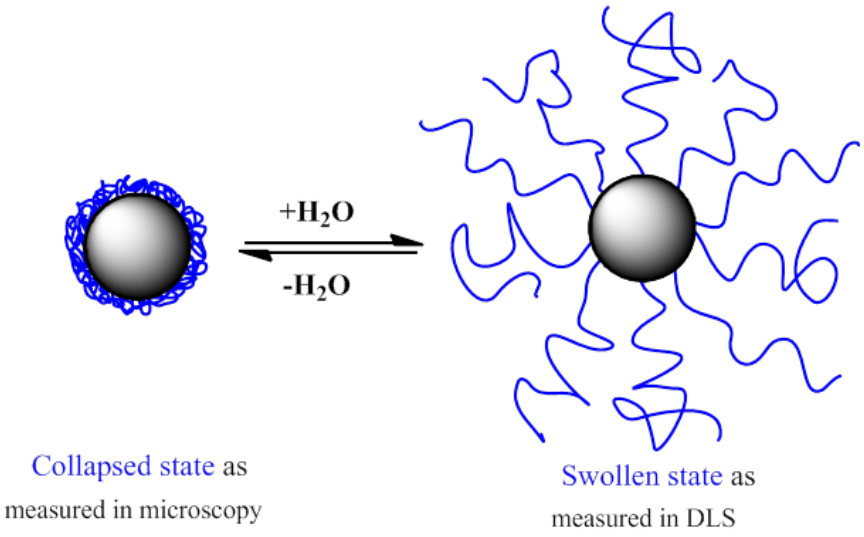

Figure. 6.11. *Schematic representation of SiNP-g-GP size measured using different methods.*

6.3.5 Molecular weight of grafted pMEMA on SiNP surface

The molecular weights and molecular weight distributions of grafted polymer chains, the pMEMA chains, were measured by GPC after cleaving the polymer from SiNP by treating the SiNP-g-pMEMA with aqueous HF solution. Fig. 6.12 shows the GPC chromatograms of all the samples which are obtained after the cleaving from SiNP surface. The GPC curves are all symmetric, unimodal and narrow, which indicate that the polymerization proceeded in a controlled manner. The number average molecular weight ($\bar{M}_n$) and polydispersity index (PDI) and the number of pMEMA chain (calculated from $\bar{M}_n$) and other details of all the polymers are tabulated in Table 6.1. The narrow PDI values (<1.3) indicated that the polymerization proceeded in accordance with a controlled/living radical polymerization mechanism as expected from RAFT method. The number average degree of polymerization (DP) are calculated from $\bar{M}_n$ and presented in Table 6.1 with the sample identification. It must be noted that the $\bar{M}_n$ obtained from GPC is tallying very well with the $\bar{M}_n$ (Table 6.1) values theoretically calculated from monomer and RAFT agent concentration in the polymerization feed. This indicates higher degree of conversion and well controlled reaction. Another interesting observation from Table 6.1 and Fig. 6.12A is that the $\bar{M}_n$ value of P3. The calculated $\bar{M}_n$ (targeted) is 10,000, however $\bar{M}_n$ from GPC is only 4900. This is simply because of the absence of free RAFT agent. This once again reconfirms the necessity of addition of free RAFT agent (CPDB) in the polymerization feed.

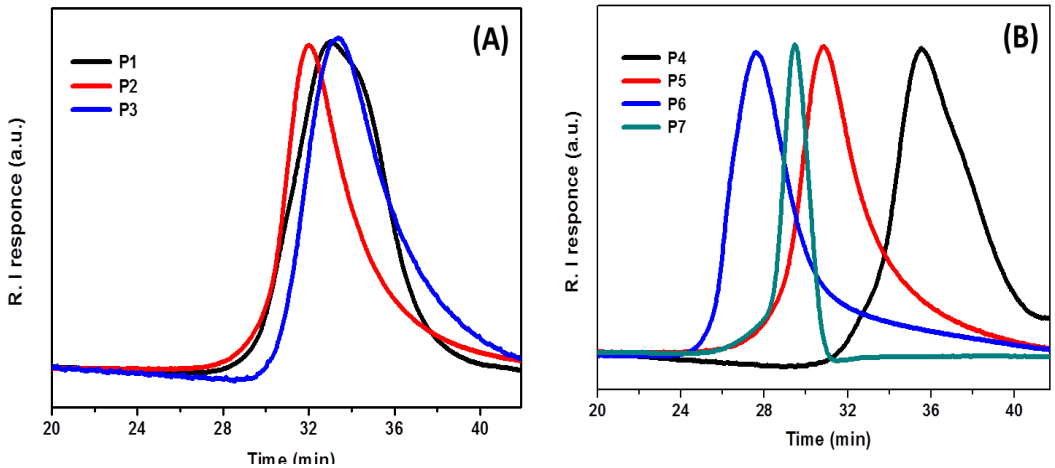

Figure. 6.12. *GPC curves of pMEMA chains cleaved from SiNP-g-pMEMA by using aqueous HF. Polymers obtained using water/ethanol (A) and DMF (B) as solvent for the polymerization.*

6.4 Conclusion

In summary, we have demonstrated a simple method to covalently graft glycopolymers (carbohydrates) on the surface of silica nanoparticles. Initially, CPDB RAFT agent anchored SiNPs were prepared, and then a mannose containing glycopolymer chain was grown on the surface of SiNPs using a *grafting from* RAFT polymerization method. The chain length of the GP on the SiNPs surface has been varied in order to graft higher amount of GP. The resulting SiNP-S-GP particles display a narrow size distributions and the size of the GP chain on the particle surface can be readily controlled by changing the monomer amount in the polymerization feed. Molecular weights obtained from GPC analysis after cleaving the GP from the SiNP confirms the formation of SiNP-g-GP. The microscopic, spectroscopic, thermal and DLS studies unequivocally confirms the formation of SiNP-g-GP particles. The mannose containing SiNP-g-GP shows the binding affinity and selectivity towards lectin Con A. The utility of this method can be extended to graft multiple carbohydrates on the single nanoparticle surface. The present methodology delivers a controlled synthesis of well-defined core-shell nanoparticles with protein binding glycopolymer on the surface of the particles which may be useful for delivering new carbohydrate based therapeutics.

References

1. X. Jiang, M. Ahmed, Z. Deng and R. Narain, *Bioconjugate Chem.*, 2009, **20**, 994.
2. G. B. Sigal, M. Mammen, G. Dahmann and G. M. Whitesides, *J. Am. Chem. Soc.*, 1996, **118**, 3789.
3. Y. C. Lee and R. T. Lee, *Acc. Chem. Res.*, 1995, **28**, 321.
4. J. J. Lundquist and E. J. Toone, *Chem. Rev.*, 2002, **102**, 555.
5. X. L. Sun, W. Cui, C. Haller and E. L. Chaikof, *ChemBioChem*, 2004, **5**, 1593-1596.
6. S. R. S. Ting, G. Chen and M. H. Stenzel, *Polym. Chem.*, 2010, **1**, 1392-1412.
7. C. Boyer, A. Bousquet, J. Rondolo, M. R. Whittaker, M. H. Stenzel and T. P. Davis, *Macromolecules*, 2010, **43**, 3775.
8. M. Toyoshima and Y. Miura and W. J. Parak, *Nano letters*, 2006, **5**, 531.
9. C.-C. Lin, Y.-C. Yeh, C.-Y. Yang, G.-F. Chen, Y.-C. Chen, Y.-C. Wu and C.-C. Chen, *Chem. Commun.*, 2003, **23**, 2920.
10. X. Jiang, A. Housni, G. Gody, P. Boullanger, M.-T. Charreyre, T. Delair and R. Narain, *Biocon. Chem.*, 2010, **21**, 521.
11. S. Sangabathuni, R. Vasudeva Murthy, P. M. Chaudhary, M. Surve, A. Banerjee and R. Kikkeri, *Nanoscale*, 2016, **8**, 12729.
12. M. Álvarez-Paino, V. Bordegé, R. Cuervo-Rodríguez, A. Muñoz-Bonilla and M. Fernández-García, *Macromol. Chem. Phy.*, 2014, **215**, 1915.
13. T. D. Farr, C.-H. Lai, D. Grünstein, G. Orts-Gil, C.-C. Wang, P. Boehm-Sturm, P. H. Seeberger and C. Harms, *Nano Letters*, 2014, **14**, 2130.
14. X. Wang, O. Ramström and M. Yan, *Chem. Commun.*, 2011, **47**, 4261.
15. C. Kirchner, T. Liedl, S. Kudera, T. Pellegrino, A. Muñoz Javier, H. E. Gaub, S. Stölzle, N. Fertig and W. J. Parak, *Nano letters*, 2005, **5**, 331.
16. Q. Wang, Y. Bao, J. Ahire and Y. Chao, *Adv. Healthc. Mater.*, 2013, **2**, 459.
17. M. De, P. S. Ghosh and V. M. Rotello, *Adv. Mater.*, 2008, **20**, 4225.
18. N. L. Rosi and C. A. Mirkin, *Chem. Rev.*, 2005, **105**, 1547.
19. W. Stöber, A. Fink and E. Bohn, *J. Colloid Interface Sci.*, 1968, **26**, 62.
20. T.-Y. Guo, P. Liu, Y.-Q. Xia and M.-D. Song, *J. Appl. Polym. Sci.*, 2010, **116**, 1611.
21. L. Wang and B. C. Benicewicz, *ACS Macro Letters*, 2013, **2**, 173.
22. K. Jiang, X. Wang, H. Geng, T. M. Beer, D. Z. Qian, O. Ramström and M. Yan, *Adv. Sci. Lett.*, 2015, **4**. 1621.

23. J. H. Ahire, I. Chambrier, A. Mueller, Y. Bao and Y. Chao, *ACS Appl. Mater. Interfaces*, 2013, **5**, 7384.
24. J. H. Ahire, M. Behray, C. A. Webster, Q. Wang, V. Sherwood, N. Saengkrit, U. Ruktanonchai, N. Woramongkolchai and Y. Chao, *Adv. Healthcare Mater.*, 2015, **4**, 1877.
25. S. N. Raju Kutcherlapati, N. Yeole, M. R. Gadi, R. S. Perali and T. Jana, *Polym. Chem.*, 2017. **DOI:** 10.1039/C6PY02202B.
26. H. Arslan, O. Zırtıl and V. Bütün, *Eur. Polym. J.*, 2013, **49**, 4118.
27. A. B. Lowe and R. Wang, *Polymer*, 2007, **48**, 2221.
28. Y. Wang, X. Li, C. Hong and C. Pan, *J. Polym. Sci.: Part A: Polym. Chem.*, 2011, **49**, 3280.
29. D. Li, X. Sheng and B. Zhao, *J. Am. Chem. Soc.*, 2005, **127**, 6248.
30. C. Bartholome, E. Beyou, E. Bourgeat-Lami, P. Chaumont, F. Lefebvre and N. Zydowicz, *Macromolecules*, 2005, **38**, 1099.
31. R. Yokoyama, S. Suzuki, K. Shirai, T. Yamauchi, N. Tsubokawa and M. Tsuchimochi, *Eur. Polym. J.*, 2006, **42**, 3221.
32. B. Radhakrishnan, R. Ranjan and W. J. Brittain, *Soft Matter*, 2006, **2**, 3866.
33. E. Glogowski, R. Tangirala, T. P. Russell and T. Emrick, *J. Polym. Sci. A Polym. Chem.*, 2006, **44**, 5076.
34. J. Liu, T. Tanaka, K. Sivula, A. P. Alivisatos and J. M. J. Fréchet, *J. Am. Chem. Soc.*, 2004, **126**, 6550.
35. N. Yeole, S. N. R. Kutcherlapati and T. Jana, *RSC Adv.*, 2014, **4**, 2382.
36. N. Yeole, S. N. R. Kutcherlapati and T. Jana, *J. Colloid Interface Sci.*, 2015, **443**, 137.
37. G. Moad, E. Rizzardo and S. H. Thang, *Aust. J. Chem.*, 2005, **58**, 379.
38. G. Moad, E. Rizzardo and S. H. Thang, *Aust. J. Chem.*, 2009, **62**, 1402.
39. G. Moad, E. Rizzardo and S. H. Thang, *Aust. J. Chem.*, 2012, **65**, 985.
40. K. Matyjaszewski, *Controlled/Living Radical Polymerization: Progress in RAFT, DT, NMP & OMRP*, American Chemical Society, 2009.
41. D. Pissuwan, C. Boyer, K. Gunasekaran, T. P. Davis and V. Bulmus, *Biomacromolecules*, 2010, **11**, 412.
42. Z. Wei, X. Hao, Z. Gan and T. C. Hughes, *J. Polym. Sci. A Polym. Chem.*, 2012, **50**, 2378.

43. M. Tosin and P. V. Murphy, *J. Org. Chem.*, 2005, **70**, 4107.
44. E.-H. Song, M. J. Manganiello, Y.-H. Chow, B. Ghosn, A. J. Convertine, P. S. Stayton, L. M. Schnapp and D. M. Ratner, *Biomaterials*, 2012, **33**, 6889.
45. Y. Mitsukami, M. S. Donovan, A. B. Lowe and C. L. McCormick, *Macromolecules*, 2001, **34**, 2248.
46. C. L. McCormick and A. B. Lowe, *Acc. Chem. Res.*, 2004, **37**, 312.
47. N. J. Warren, O. O. Mykhaylyk, D. Mahmood, A. J. Ryan and S. P. Armes, *J. Am. Chem. Soc.*, 2014, **136**, 1023.
48. C. Li, J. Han, C. Y. Ryu and B. C. Benicewicz, *Macromolecules*, 2006, **39**, 3175.
49. J. Pyun, S. Jia, T. Kowalewski, G. D. Patterson and K. Matyjaszewski, *Macromolecules*, 2003, **36**, 5094.
50. C. Bartholome, E. Beyou, E. Bourgeat-Lami, P. Chaumont and N. Zydowicz, *Polymer*, 2005, **46**, 8502.
51. V. Darcos, A. Dureault, D. Taton, Y. Gnanou, P. Marchand, A.-M. Caminade, J.-P. Majoral, M. Destarac and F. Leising, *Chem. Commun.*, 2004, **41,** 2110.
52. A. Duréault, D. Taton, M. Destarac, F. Leising and Y. Gnanou, *Macromolecules*, 2004, **37**, 5513.
53. Q. Zheng and C.-y. Pan, *Macromolecules*, 2005, **38**, 6841.
54. T. Taniguchi, Y. Kunisada, M. Shinohara, M. Kasuya, T. Ogawa, M. Kohri and T. Nakahira, *Colloids. Surf. A: Physicochem. Eng. Aspects*, 2010, **369**, 240.

Chapter 7

Control Synthesis of Poly(N-Vinyl imidazole) grafted Silica Nanoparticles using *Grafting from* RAFT Polymerization: Tunability of Chain Length and Density

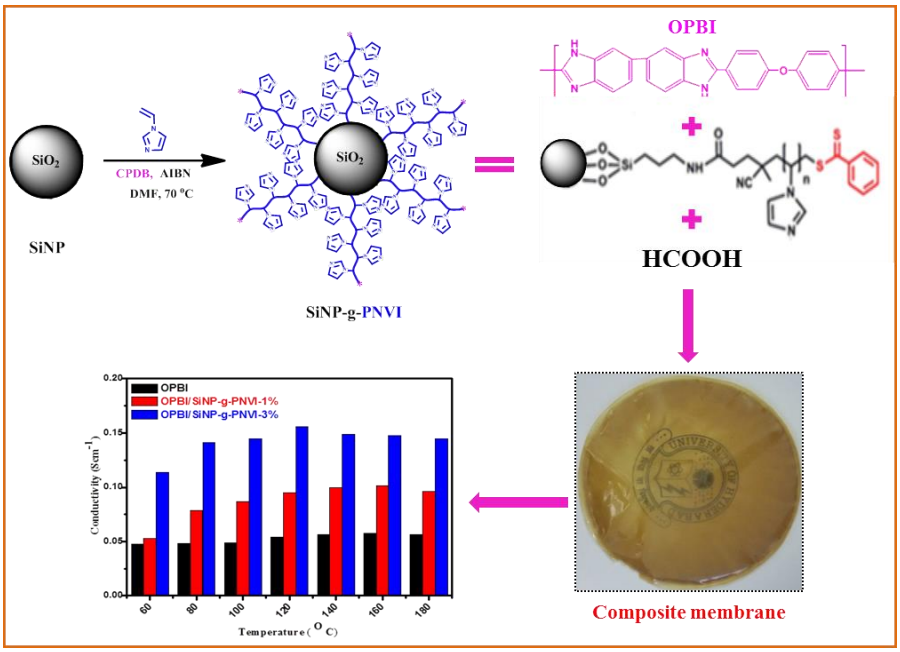

Synthesis of poly(N-vinyl imidazole) (PNVI) grafted silica nanoparticles (SiNPs) by using Reversible Addition Fragmentation chain Transfer (RAFT) polymerization through grafting from approach and its nanocomposite with PBI. Superior mechanical, proton conductivity and less acid leaching properties are obtained in case of nanocomposite which is useful for PEM fuel cell.

7.1. Introduction

Vinyl imidazole (VI) is one of the derivative of imidazole moiety which exhibits donating properties with a loan pair of electrons on N atom (3rd position) as well as withdrawing properties due to unsaturated heterocyclic ring.[1] Such mixed acidic and basic components in a polymer [poly(vinyl imidazole), also called as PVI] chain can impart acid-base complexing properties with other molecules [2] due to which polymers with imidazole derivatives along with its copolymers have attained a great interest in various fields.[3-13]

The most widely used monomer that consists of dangling imidazole functionalization is N-vinyl imidazole (NVI). However, it is well known that the polymerizations of N-vinylic monomers like N-vinyl imidazole (NVI), N-vinylpyrazole (NVP) and N- vinylcarbazole (NVC) is challenging task since propagating N-vinyl radicals present during the polymerization are highly reactive and unstable owing to the absence of resonance stabilization and thereby propagating radicals are responsible for chain transfer as well as chain termination events. As a result of this, polymerization of these monomers yields polymers with a broad molecular weight distribution as well as control over the polymerization process is very limited and hence the resulting morphology is very uncontrolled. Thereby, synthesis of narrow molecular weight distribution polymer with a control over the polymerization for these N-vinylic (heterocyclic) monomers is necessary and still challenging for their use in the desired areas.

In this context, controlled radical polymerizations (CRPs) may be a wise choice since they enable the synthesis of well-defined functional polymers with pre-determined molecular weights with narrow polydispersity and desired functional chain ends. Even though tremendous progress in the field of CRPs such as nitroxide-mediated polymerization (NMP),[14] atom transfer radical polymerization (ATRP)[15] and reversible addition–fragmentation chain transfer (RAFT)[16-18] polymerizations in the last decade, controlling the polymerization of NVI is still a challenging task and not attempted by anyone in the literature. Recently, Long *et al.* even stated that the "controlled radical polymerization of N-vinyl imidazole is not achievable"[19] citing the reason that the propagating radicals are highly reactive because they are not stabilized by resonance and therefore tend to undergo chain termination and chain transfer reactions very readily.

All the literature efforts to polymerize NVI using ATRP was not successful, they failed either with very low or no conversion.[20] The NVI polymers which are grown on solid

surfaces were not further characterized for their molecular weight, end functionalization and molecular structure.[21] The main problem to polymerize imidazole with ATRP is that, the monomers as well as its resulting polymers have high tendency to form complex with the metal ions [22, 23] which is used as ATRP catalysts in the polymerization medium. Even if well-defined poly(N-vinyl imidazole) (PNVI) are produced from ATRP, it becomes very difficult to remove metals ions from the resulting polymers for its strong binding with metal ions which may cause unwanted colour to the polymer product obstructing its use in biomedical applications due to the toxicity of transition metal ions and hamper the polymer properties when used for electronic, energy, or filtration applications. The controlled radical polymerization of NVI using Nitroxide mediated radical polymerization (NMP) is also quite challenging because of the high reaction temperatures (~120°C or more) which may lead to the addition of propagating radical to the internal double bond of the heterocyclic ring (imidazole ring) resulting in formation of a kind of gel which is generally called as "degradative addition".[24] Reversible addition–fragmentation chain transfer (RAFT) polymerization has been utilised for the polymerizations of N-heterocyclic monomers (NVI, NVP, and NVC) by xanthate type of chain transfer agents (CTA) to from well-defined polymers and copolymers.[11, 19, 25, 26]

Grafting of polymer chains onto the solid (particle) surfaces is an emerging process and gaining interest for its practical applications and fundamental studies of interfacial phenomena.[27] This technique gives opportunity to take advantage of a solid support as well as functionalized polymer giving a material with mixed properties.[28]

Recently, polybenzimidazole (PBI), a polymer in which imidazole groups are part of the main backbone, is found to serve as an excellent proton exchange membrane (PEM) material when doped with phosphoric acid (PA) for the use in PEM fuel cell (PEMFC). Many limitations which include low PA loading, PA leaching, weak mechanical strength of PA doped PBI membrane have been partially addressed by making nanocomposites of PBI with clays, graphenes, hetero polyacids, silica nanomaterials and acidic surfactants [29-32] etc. Very recently, we have demonstrated that the surface modification of the silica particle can significantly affect the properties of PBI nanocomposites and hence above mentioned limitation can be fine-tuned. [30, 32] In the present chapter, we are addressing the above issues by using *N*-heterocyclic compounds such as poly(N-vinyl imidazole) (PNVI) grafted on SiNP as a nano filler which we believe can be obtained by a surface-initiated RAFT polymerization of

PVI with RAFT agent modified SiNP. Since both the silica and imidazole would be present in our nanofiller hence we can expect better dispersion and reinforcement in mechanical strength.[33] In addition, imidazole, which is a strong Bronsted base (pKa is 6.50)[34] when mixed with PBI can increase the basic group number in the composite membrane which is useful for improving the acid doping level of the membrane. Along with this, we can except less PA leaching due to higher basicity and also interaction between nitrogen atom from imidazole group and H_3PO_4, $H_2PO_4^-$ or HPO_4^{2-} will be useful in increasing the acid uptake and decreasing leaching.

To the best of our knowledge, grafting of PNVI on the surface of SiNP using RAFT polymerization with different chain length and chain density has not been reported so far. With this background, in this chapter, we are presenting a method in which grafting of PNVI on the surface of SiNP for different chain length and chain density using *grafting from* RAFT method is developed. Then SiO_2-g-PNVI is employed as a nanocomposite material (nanofillers) with poly(4,4'-diphenylether-5,5'-bibenzimidazole) (OPBI) (Scheme 7.1) to prepare the anhydrous proton conducting membranes to address the problems which are raised earlier and are the bottle neck for successful use of PEM.

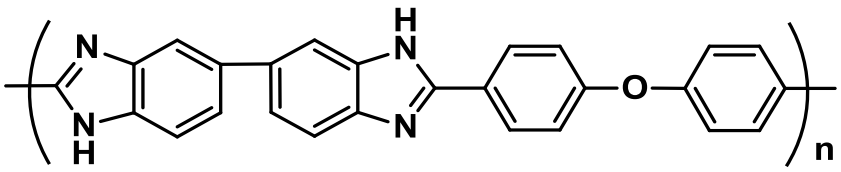

Scheme* 7.*1. *Poly*(4,4'-diphenylether-5,5'-bibenzimidazole) (referred as OPBI).

7.2 Experimental Section:

7.2.1 Materials and Methods:

All information about the materials used in this study and the synthetic procedure for the preparation of RAFT agent as well as silica nanoparticles (SiNPs) are discussed in the Chapter 2. The experimental methods and all the characterization techniques which include molecular weight measurements by GPC, spectroscopic characterization by FT-IR and NMR, thermal analysis by TGA, DSC and DMA, microscopic analysis by FE-SEM and TEM, light scattering by DLS study are discussed in Chapter 2.

7.2.2 Polymerization of NVI using SiNP-CPDB

We have carried out the reactions with two different SiNP-CPDBs: one is SiNP-$CPDB_L$ (with low RAFT density) for less chain density and second is with SiNP-$CPDB_H$ (with high RAFT density) for higher chain density on the SiNP surface. For details refer chapter 2.

Into a series of Schlenk tubes containing DMF (5 mL), SiNP-$CPDB_H$ (0.3g, 22.82 μmol by RAFT), NVI (calculated amount, we have varied the amount to prepare for different chain lengths of PNVI), CPDB (6.39 mg, 22.82 μmol) and AIBN (0.749mg, 4.564 μmol) were added by keeping [SiNP-CPDB]: [CPDB]: [ACP] = 1:1:0.2 constant throughout all the reactions. These reaction vials were then sealed and subjected to three freeze-pump-thaw cycles followed by sonication for 10 min and stirred for 20 h in preheated oil bath at 75^oC. After completion of the reaction, the reaction mixture was quenched using liquid nitrogen, the PNVI grafted SiNPs (SiNP-g-PNVI) were precipitated from a large excess of THF: hexane (8:2) mixture and isolated by using centrifugation. The obtained precipitate was redispersed in methanol (40 mL) and centrifuged at the rate 7000 rpm for 30 min. This step was repeated thrice, and the obtained PNVI grafted SiNPs were dried under vacuum at 90 ^oC for 48 h. We have altered the amount of NVI monomer in the reaction medium by keeping all the other reagents constant so as to obtain different chain length of PNVI chain on the SiNP surface. We have also conducted the reactions with SiNP-$CPDB_L$ for less surface grafting of PNVI chains on SiNP surface, and the concentration of all reagents were calculated with respect to the CPDB on the SiNP-$CPDB_L$ by keeping the identical final molar ratio as mentioned above.

7.2.3 Removal of SiNP core from SiNP-g-PNVI to obtain PNVI

Cleavage of the PNVI from PNVI grafted SiNPs was carried out according to the similar procedure described elsewhere.[40] In a polyethylene (PE) tube, the PNVI grafted SiNPs (50 mg) was dispersed in 6 ml methanol. Into this solution, aqueous HF (48 wt%, 1.5 ml) was added, and the reaction mixture was stirred at room temperature for 12 h, the excess HF was neutralized with $NaHCO_3$ and the polymer was extracted with methanol. The polymer (PNVI) was precipitated by adding the polymer solution into an excess of dry acetone and then the precipitate was collected by filtration. The PNVI obtained was dried in a vacuum oven at 80 °C for 24 h. The recovered PNVI was then subjected to Gel permeation chromatography (GPC) analysis.

7.2.4 Preparation of PBI/SiNP-g-PNVI nanocomposite

Homogenous nanocomposite membranes were prepared by solution blending method by adding 1 wt % and 3 wt % (with respect to polymer concentration) of SiNP-g-PNVI dispersion in formic acid to 2 wt % OPBI solution in formic acid. The final OPBI concentration in solution was 1 wt %. Then the solution was stirred vigorously at room temperature for 24 h to form a homogeneous mixture after which it was poured on to glass Petri dish and the solvent was evaporated at 70 °C inside an oven slowly (for 2 h). The formed membrane was peeled off from the petridish and then dried in a vacuum oven at 100 °C to remove the traces amount of solvent molecules. The thicknesses of the nanocomposite membranes were approximately 0.03-0.04 mm.

7.3 Results and Discussion

7.3.1 Surface functionalization of SINP

In this chapter, we report the successful grafting of poly(N-vinyl imidazole) (PNVI) on SiNP surface using *grafting from* RAFT polymerization technique. To achieve this, we have followed a multi-step procedure as described below and this kind of methodology has been used by us and others for the functionalization of various nanoparticles.[41, 42] The commonly used Stöber method was followed to prepare monodisperse SiNPs from tetraethylorthosilicate (TEOS) through a hydrolysis and condensation reaction.[39] The particle size was measured and found to be 47 (±2 nm) in diameter by FE-SEM and TEM, (Fig. 7.1) and 54 nm from DLS. The amine functionalized SiNPs were prepared by refluxing different amounts of (3-Aminopropyl)triethoxysilane (APTES) with SiNPs to obtain low (SiNP-$NH_{2L)}$ and high (SiNP-NH_{2H}) surface amine densities as described in experimental section.

Well known dithiobenzoate based RAFT agent CPDB which has been used for RAFT polymerization of a variety of monomers including methacrylates, acrylates, and styrene based monomers to prepare polymers with predictable molecular weight and narrow polydispersities was used in our current study. The presence carboxyl group in CPDB is very useful and can be readily be immobilized on SiNP particle surface through a covalent bond. Owing to the weak stability of the CPDB under the reaction condition, it is not easy to install CPDB on the SiNP surface by a simple condensation reaction due to the aminolysis of the dithiobenzoate group, a well reported phenomenon by many authors.[40, 43-45] Therefore, the carboxyl group of CPDB was first activated using NHS to get CPDB-NHS as explaines in chapter 2 and then the activated RAFT agent was attached to SiNPs by reacting with amine modified SiNPs. We

have prepared the different amine functional (-NH_2) loading SiNP particles: a SiNP-NH_{2H} (higher loading of –NH_2) and SiNP-NH_{2L} (lower loading of –NH_2) as discussed in the experimental part by changing the APTES concentration. Therefore, after CPDB-NHS attachment with thsese two particles, we obtain high loading of CPDB on SiNP particle which is denoted as SiNP-$CPDB_H$ and low loading of CPDB on SiNP particle which is denoted as SiNP-$CPDB_L$. The representative microscopic images of particles are shown in Fig 7.1. The relative amount of RAFT (CPDB) agent which is covalently attached on the SiNPs was calculated using TGA analysis[43] (Fig. 7.2) and found to be 21.3 mg/g for SiNP-$CPDB_H$ and 10.6 mg/g for SiNP-$CPDB_{L,}$ respectively.

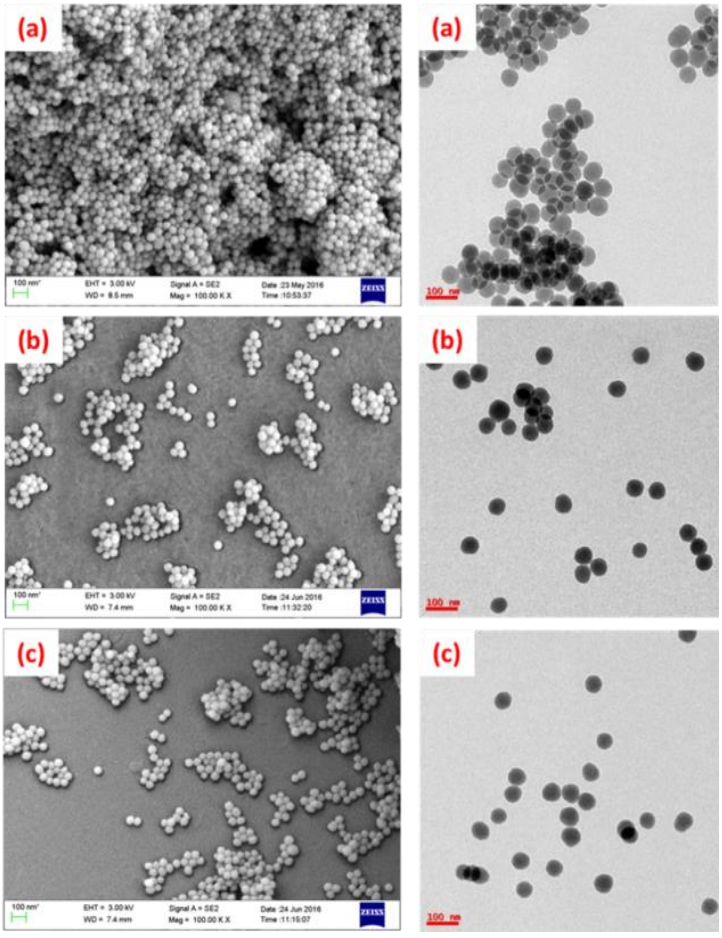

Figure. 7.1 *FE-SEM images (left panel) and TEM images (right panel) of (a) SiNP, (b) SiNP-NH_{2H} and (c) SiNP-$CPDB_H$.*

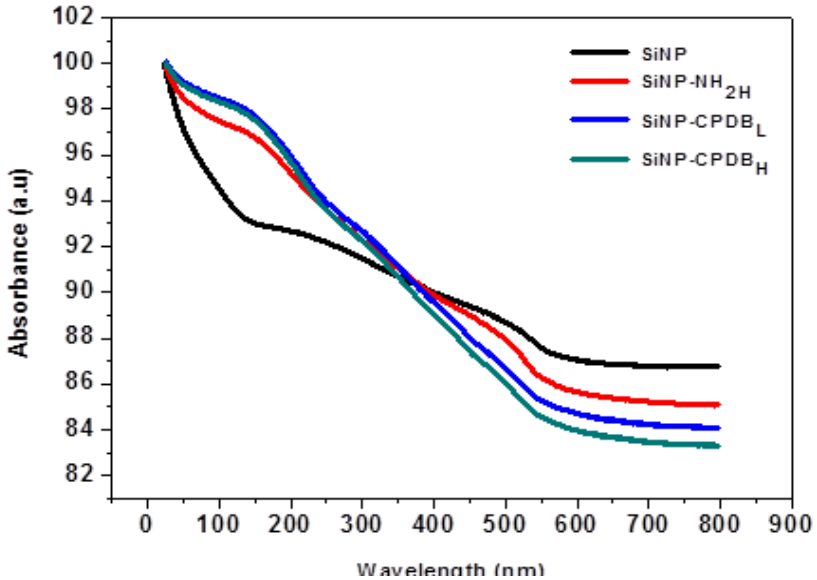

Figure. 7.2 *TGA analysis of SiNP, SiNP-$NH_{2H,}$ SiNP-$CPDB_L$ and SiNP-$CPDB_H$.*

The FT-IR spectrum of SiNP-CPDB (Fig. 7.3A) shows a sharp band at 1645 cm^{-1} which is attributed to the C=O stretching of the amide carbonyl and also a peak at 1551 $cm^{-1}$is attributed to the C-N stretching and N-H bending from the amide group. A band at 2254 cm^{-1} is attributed to cyano group in the CPDB. These bands clearly proved that the dithiobenzoate group of CPDB RAFT agent is covalently attached to the surface of the SiNPs. ^{13}C NMR gives the clear information about the surface grafted materials. The ^{13}C NMR spectrum of CPDB modified SiNPs dispersed in $CDCl_3$ and presented in Fig. 7.3B. The ^{13}C NMR spectra of SiNP-CPDB shows a chemical shift at 168 ppm which is due to the amide carbonyl carbon, a peak at 144 ppm represents anomeric carbon of phenyl ring in CPDB, a peak at 120 ppm is due to the cyano group in CPDB, and the peaks around 124-130 ppm are due to the phenyl ring carbon atoms. The peaks between 18-40 ppm are from the alkyl carbons from CPDB RAFT agent and SiNP-$NH_{2.}$ These results confirm a covalent attachment of CPDB with SiNPs.

The particle size and size distribution of these SiNPs were measured in water by using DLS and presented in Fig. 7.4. The mean diameter of bare SiNPs is 54 nm and increased to 65 nm upon the amine modification, which is due to the formation of hydrophilic amine shell and then decreased to 59 nm after attaching CPDB on SiNP particle surface. In this case, the decrease in the diameter is explained by decreasing the hydration shell of the particle after

CPDB attachment due to the attached alkyl chain and phenyl ring. All the particle sizes measured by DLS has shown less PDI (<0.1) indicating the monodispersity of the formed particles. The sizes which are obtained from the DLS data are comparatively larger than the sizes that are obtained from FESEM and TEM measurements because of the attachment of hydrophilic groups on particle surface makes the particles more hydrophilic due to the presence of hydration cell on the surface of particle and DLS measures the hydrodynamic diameter. But, TEM and FESEM measure only the dry particles with collapsed surface which is the reason for the increased size of particles in DLS. These above characterizations clearly indicate that the covalent attachment of CPDB on the SiNP surface.

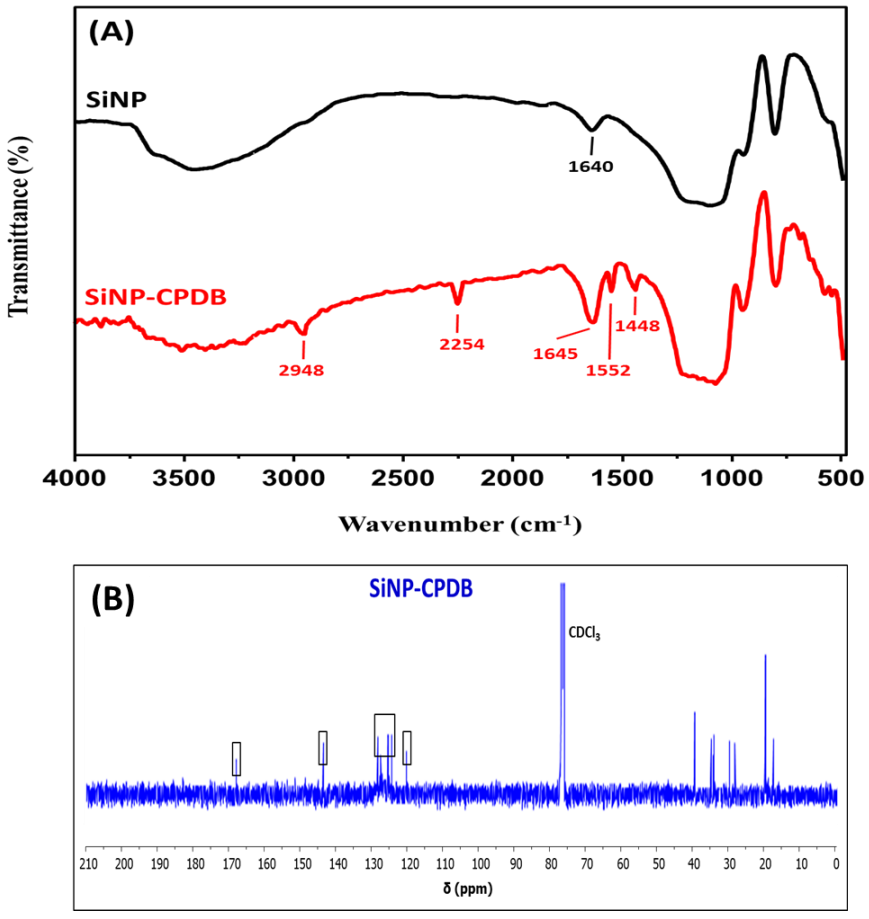

***Figure. 7.3**. FT-IR (A) and ^{13}C NMR (B) spectra of SiNP and SiNP-CPDB.*

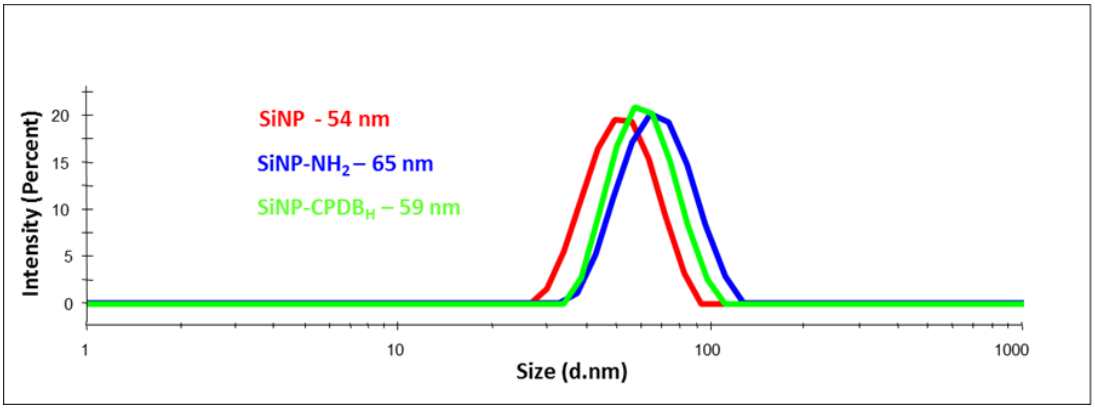

Figure. 7.4. *DLS graphs of bare SiNP, SiNP-NH_{2H} and SiNP-$CPDB_H$.*

7.3.2. Grafting of NVI chain on the SiNP surface

A *grafting from* RAFT polymerisation having core-first type approach was utilized to polymerize NVI on the SiNP surface. SiNP-CPDBs was used for the RAFT-mediated controlled radical polymerization of NVI (Scheme 7.3) in DMF solvent. We have performed the polymerization of NVI in the presence of two SiNP-CPDBs (SiNP-$CPDB_H$ with high RAFT density and SiNP-$CPDB_L$ with low RAFT density) and CPDB as a free chain transfer agent using AIBN as thermal initiator at 75 °C by keeping [SiNP-$CPDB_x$]:[CPDB]:[ACP] = 1:1:0.2 constant (where x indicates L or H), with the variation of NVI content in the raction feed to get different chain lengths of PNVI on the surface of the SiNP. The addition of free CPDB in polymerization helps in decreasing the cross termination of the polymeric radicals in the solution as well as increasing the loading of PNVI on SiNP surface by balancing/exchanging the oligomeric radicals with grafted ones.[40, 46, 47] Therefore, the polymerization goes more steady which leads to high PNVI loading. After polymerization, the reaction was stopped by quenching the tubes in liquid nitrogen, and the particles were precipitated by centrifugation at 7000 rpm for 30min. The pure PNVI grafted SiNPs were obtained by repeated centrifugation-redispersion procedure until no free polymer was detected in the methanol solution. Finally, the particles were dried in a vacuum oven at 90 °C for 48 h to yield PNVI grafted SiNPs (SiNP-g-PNVI). TGA, FT-IR, NMR, DLS, FESEM, and TEM were used to characterize the PNVI grafted SiNPs (SiNP-g-PNVIs) and Table 7.1 summarizes all the physical details of the all the synthesized polymers.

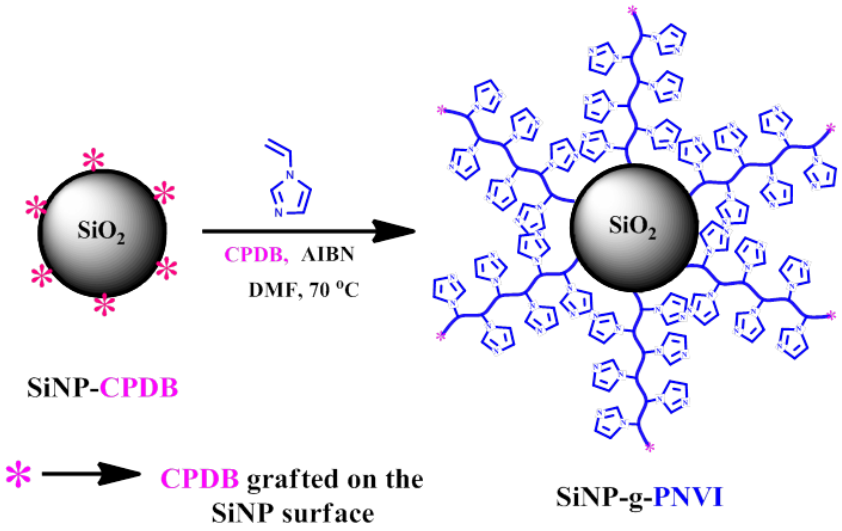

Scheme 7.3. *Synthesis of PNVI grafted SiNPs from SiNP-CPDB.*

Table.7.1: *Summary of various physical data of synthesized SiNP-g-PNVI*

Sample name[a]	Sample type	Grafting amount of PVI/SiO_2 (%)[b]	$\bar{M}_n$ [c]	PDI[d]	Size(nm)		PDI[f]
					TEM	DLS[e]	
-	SiNP-CPDB	-	-	-	48±2	58	0.18
P1	SiNP-g-$PNVI_{71}$	9.6	6700	1.43	52±3	105	0.23
P2	SiNP-g-$PNVI_{395}$	32.2	37200	1.52	57±2	141	0.31
P3	SiNP-g-$PNVI_{755}$	60.6	71100	1.49	61±4	190	0.34
P4	SiNP-g- $PNVI_{78}$	4.8	7300	1.31	50±3	98	0.28
P5	SiNP-g-$PNVI_{432}$	17.1	40700	1.36	54±3	126	0.36

[a] the polymers P1 to P3 are prepared using SiNP-$CPDB_H$, P4 and P5 are prepared using SiNP-$CPDB_L$, [b] estimated from the TGA analysis, [c and d] determined by gel permeation chromatography after removing SiNP core by aqueous HF treatment, and [e,f] obtained from DLS analysis. The number of repeat unit present in PNVI chain has been calculated from the M_n and repeat unit mass values.

The relative amount of PNVI grafted to SiNPs in the products was estimated by TGA analysis and presented in Fig 7.5 and Table 7.1. Fig. 7.5 shows the TGA curves for the PNVI grafted SiNPs prepared using two different loading of CPDBs on SiNP surface and cleaved PNVI obtained after removal of the SiNP core using aqueous HF treatment. The decomposition temperature range is around 400 °C for all the TGA curves shown in Fig. 7.5. Assuming that the PNVI is decomposed completely, as can be seen from the TGA graphs with an increase in PNVI chain length as well as chain density, the weight loss is increasing attributing that the more amount of PNVI loading on the SiNP surface. This result can be better understand by keeping it in mind that the same number of initiating groups on the particle surface, the amount of PNVI grafted to the particle surface increases with increasing PNVI chain length. On the other hand, the amount of PNVI grafted to the particle surface (PNVI chain density) increases with increase in the CPDB loading on the SiNP surface. As can be seen from the graph that the PNVI grafted to silica particles have higher thermal stability than the cleaved PNVI (without SiNP).

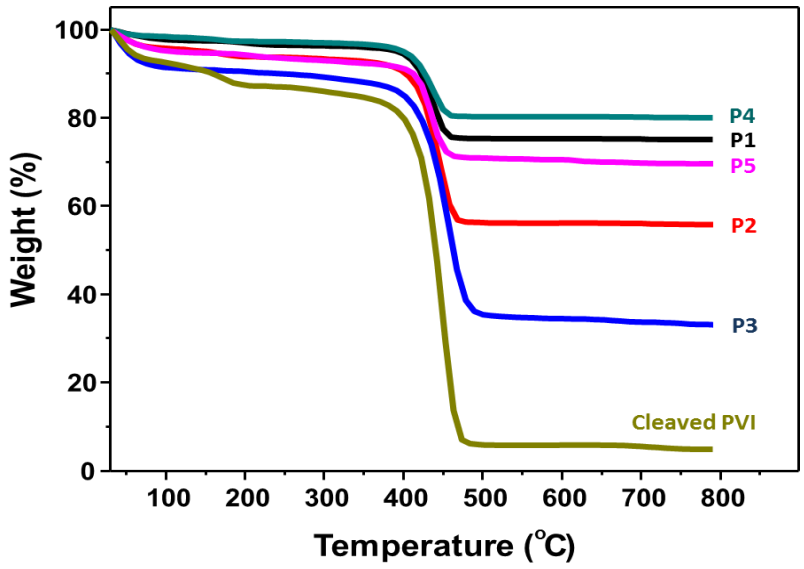

Figure. 7.5. *TGA analysis of PNVI grafted SiNPs for different chain lengths and chain densities.*

The FTIR spectra of SiNP (a), PNVI grafted SiNP (b) and cleaved PNVI (c) are compared in Fig. 7.6. The FTIR spectra of the cleaved PNVI (Fig. 7.6c) shows the absorption bands at 1651, 1502, 1419, and 1235 cm^{-1} are due to the C=N, C=C, C-H/C-N and N-C-N

stretching vibrations of imidazole ring, respectively. Band aapeared in Fig. 7.6C at 3113 cm^{-1} is attributed to C–H stretching mode vinyl imidazole ring, 2935 and 2859 cm^{-1} are due to CH and CH_2 stretching modes of the polymeric backbone as well as the stretching vibrations of azole C-H at 1090 cm^{-1}, the bending vibrations of heterocycles at 920, 828 and 749 cm^{-1} are seen. Moreover, the rocking vibration of imidazole rings at 667 cm^{-1} is also can be seen. These values are matching with the literature reports of pure PNVI structure.[48, 49] The grafting of PNVI on SiNPs (Fig. 7.6b) caused a slight shifting on several bands of PNVI but overall these bands are matching with the pure PNVI. This result suggests that the successful grafting of PNVI on SiNPs.

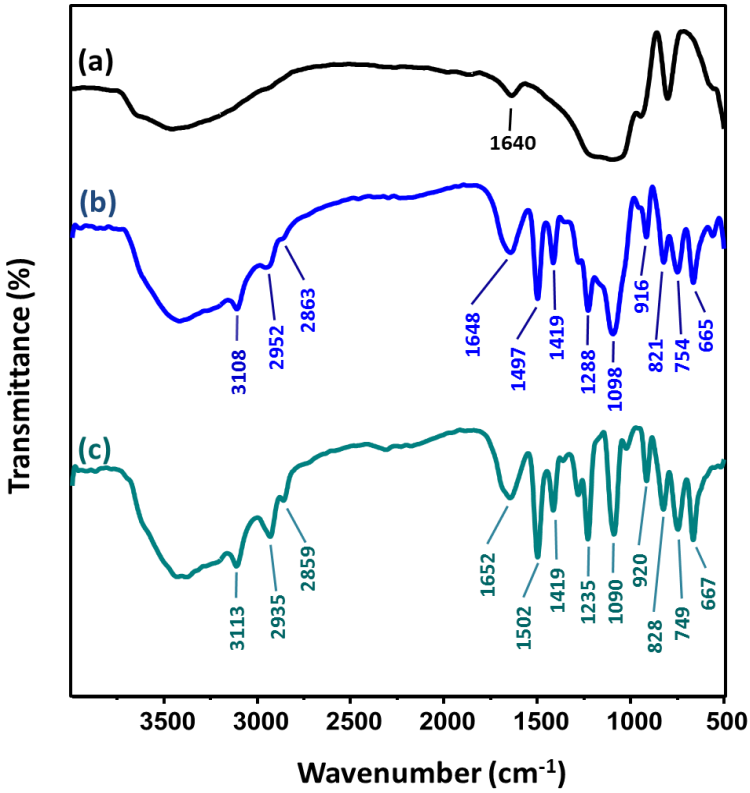

Figure. 7.6. *FT-IR spectra of (a) bare SiNP, (b) PNVI grafted SiNPs and (c) cleaved PNVI.*

The grafting of PNVI on SiNPs was further confirmed by ^{1}H NMR and ^{13}C NMR (Fig. 7.7) spectroscopy. The resonances of protons in the imidazole ring (c, d and e) are clearly observed in the range of 6.6–7.6 ppm. The peaks at 1.7–2.3 ppm and 2.9–3.2 ppm can be attributable to CH_2 and CH backbone of PNVI indicating the successful grafting of PNVI on the SiNP surface. The observed splitting of backbone CH and CH_2 groups of PNVI is due

to the chain configuration (different tacticities) of PNVI chains.[49, 50] similarly, ^{13}C NMR spectra (Fig. 7.7B) clearly confirm the structure of PNVI as seen from the peak assignments.

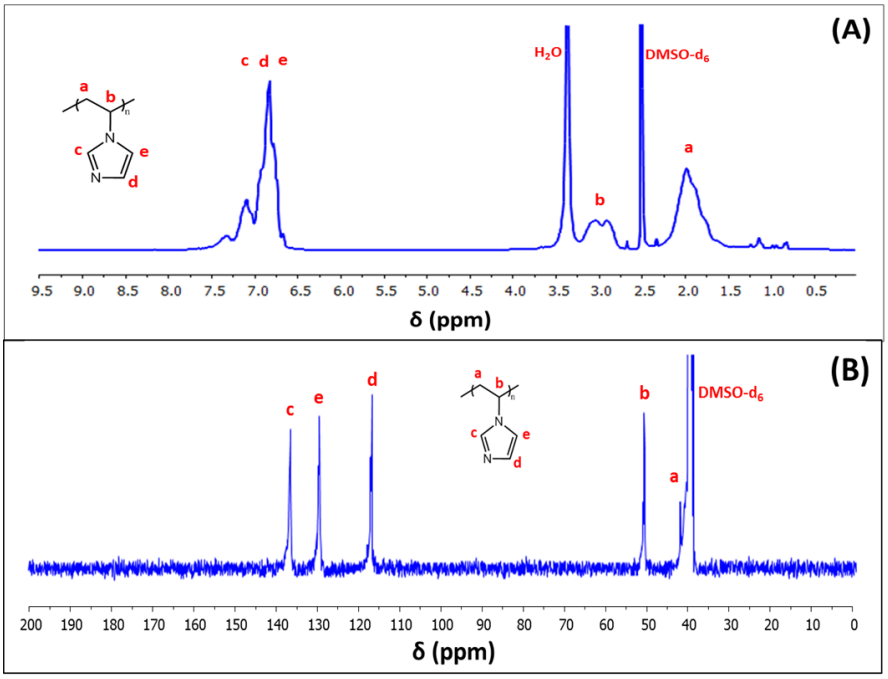

Figure. 7.7. *^{1}H (A) and ^{13}C NMR (B) spectra of PNVI grafted SiNPs.*

FESEM and TEM images of PNVI grafted SiNPs are presented in Fig. 7.8. A comparision of the SiNP-CPDB (Fig. 7.1c) surface and SiNP-g-PVNI surface (Fig. 7.8) clearly distinguished the morphological features. In the former case the surface is smooth and without roughness, but in case of PNVI grafted SiNPs rough surface is observed and also the grey surface layer (clearly visible from the inset images of TEM) of the silica particles is visible clearly which is attributed to the PNVI formed on the surface of SiNPs and this can be seen more prominently when the grafting density is more in case of P3 and P5. The increase in particle agglomeration with chain length as well as chain density in PNVI grafted SiNPs when compared with their precursor SiNP-CPDBs (Fig. 7.1c) and the increase in particle size (Table 7.1) from 48 (±2) nm ($SiNP\text{-}CPDB_H$) to 61 (±4) nm (P3) or 54 (±3) (P5) after grafting the PNVI chains uneqvovocally confirmed that the PNVI chains are chemically bound to the SiNPs. FE-SEM and TEM analysis of the SiNPs before and after reaction showed that the shape and size distribution of the particles remained unchanged indicating that the SiNPs were stable under the used conditions.

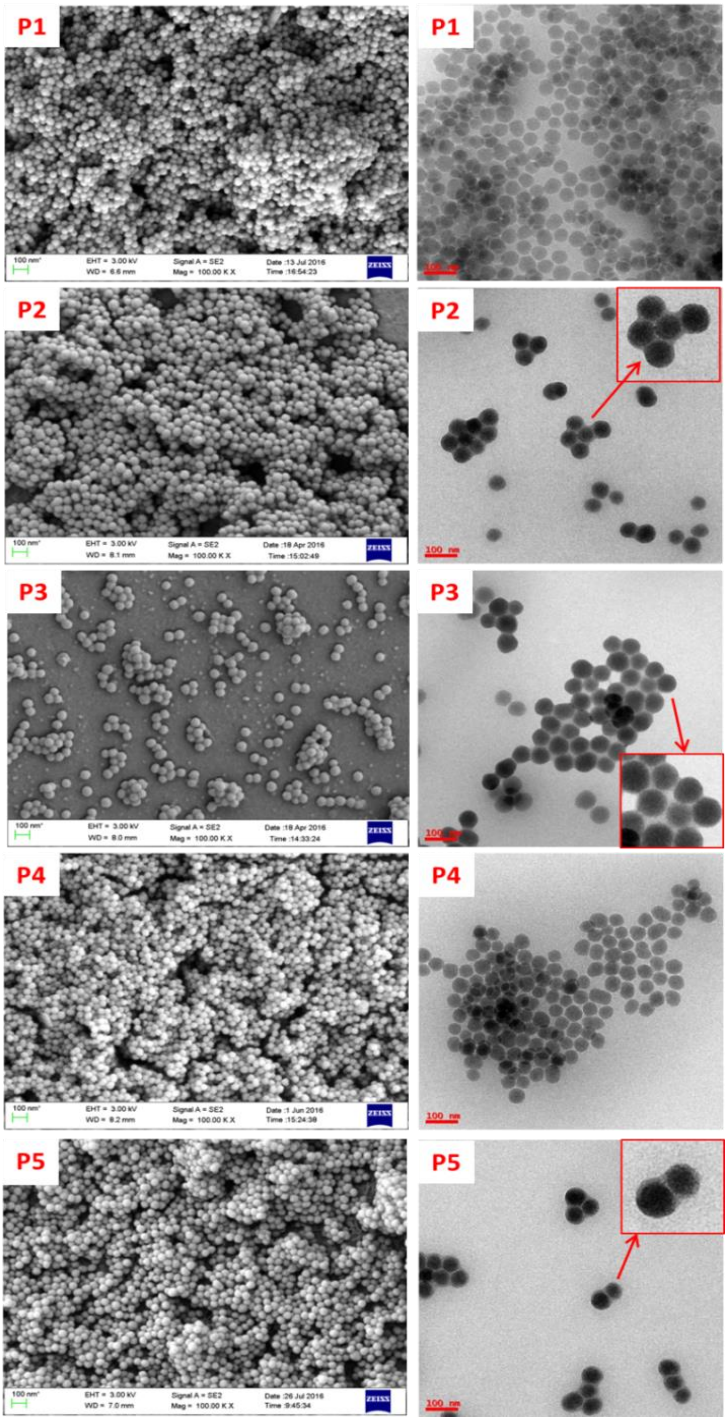

Figure 7.8. *FESEM (left panel) and TEM (right panel) images of PNVI grafted SiNPs obtained after purification for different chain lengths as well as chain density. For sample identity refer Table 7.1*

The particle size and size distribution of PNVI grafted SiNPs were also measured in water by using DLS and presented in Fig. 7.9 and Table 7.1. Even though the core (SiNP-CPDBs) diameter of all the corresponding particles are same (as prepared from the same sample of SiNP-CPDBs), the hydrodynamic diameter of PNVI grafted SiNPs are increased by two to three fold indicating that the PNVI grafted SiNPs possesses the graft PNVI chains which are highly hydrophilic and are in the swollen state and the size from DLS in proportional to the PNVI chain length on the particle surface as can be seen from the Table 7.1. The core reason for the huge increase in the hydrodynamic diameter is a result of the surface grating of PNVI chains on SiNPs, and similar results are obtained by us and others when particles coated with hydrophilic polymer chains.[51] These above results indicate that the grafting of PNVI on the SiNP surface was successfully achieved by RAFT-mediated controlled radical polymerization of NVI using SiNP-CPDBs.

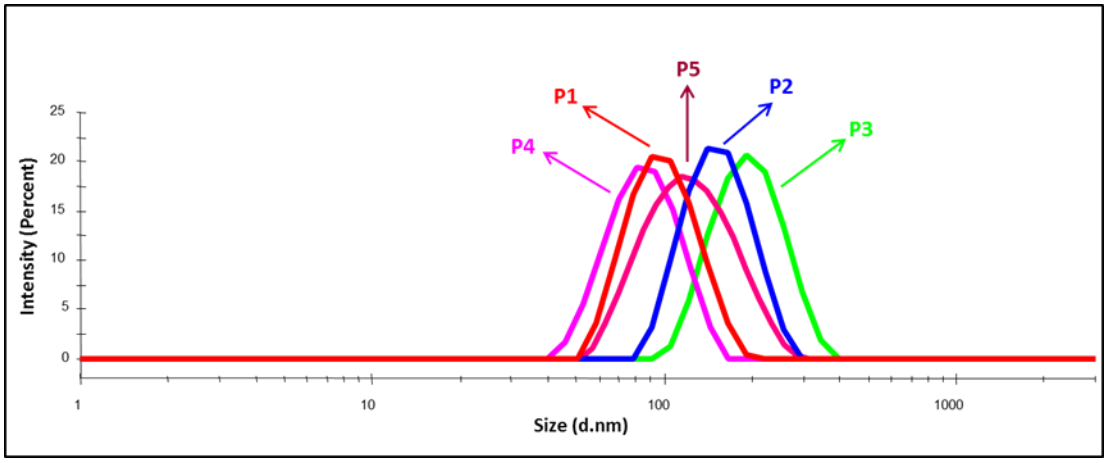

Figure 7.9. *DLS graphs of PNVI grafted SiNPs. The details of individual components are presented in the Table 7.1.*

The molecular weights and molecular weight distributions of grafted PNVI polymer chains were measured from the PNVI chains which were cleaved from PNVI grafted SiNPs by treating with aqueous HF solution. The data obtained from GPC (Fig. 7.10) about the molecular weights and molecular weight distributions of the grafted PNVI chains are tabulated in Table 7.1. The GPC curves for P4 to P5 which was synthesized from$SiNP\text{-}CPDB_L$ are unimodal and shows lower PDI values when compared to polymers P1, P2 and P3 which were synthesized from $SiNP\text{-}CPDB_H$. P1, P2 and to P_3 chains show slightly bimodal peaks and the bimodality is increased with the chain length may be due to the interchain exchanges between

the polymeric radicals on the particle surface when the density of the attached RAFT is more due to which gives relatively higher PDI values obtained in case of P1, P2 and P3 compared to P_4 to P_5. In both the cases, the PDI values are slightely on higher side as rarely be seen from RAFT (controlled radical) polymerizations. This is attributed to the use of dithiobenzoate based RAFT (CPDB) agent in our case, normally N-vinylic based monomers are polymerized using xanthate based RAFT agents but we choose dithiobenzoate RAFT agent since the ease of doing reaction on SiNP surface using this RAFT agent. Silmilar results like us obtained when Allen Jr. *et al.* polymerized the vinyl imidazole derivatives with a trithiocarbnate based RAFT reagents.[19] More importantly the polymerizations of the N-vinylic monomers gives higher PDI values than compared to the common styrenic, acrylic and methacrylic based monomers due to the highly unstable radical formed, since the formed radical is adjacent to the nitrogen atom in the reaction medium even with xanthate based RAFT agents, ATRP and NMP.[24, 52, 53] The number average degree of polymerization (DP) was calculated from $\bar{M}_n$ and included in Table 7.1 in the sample type details.

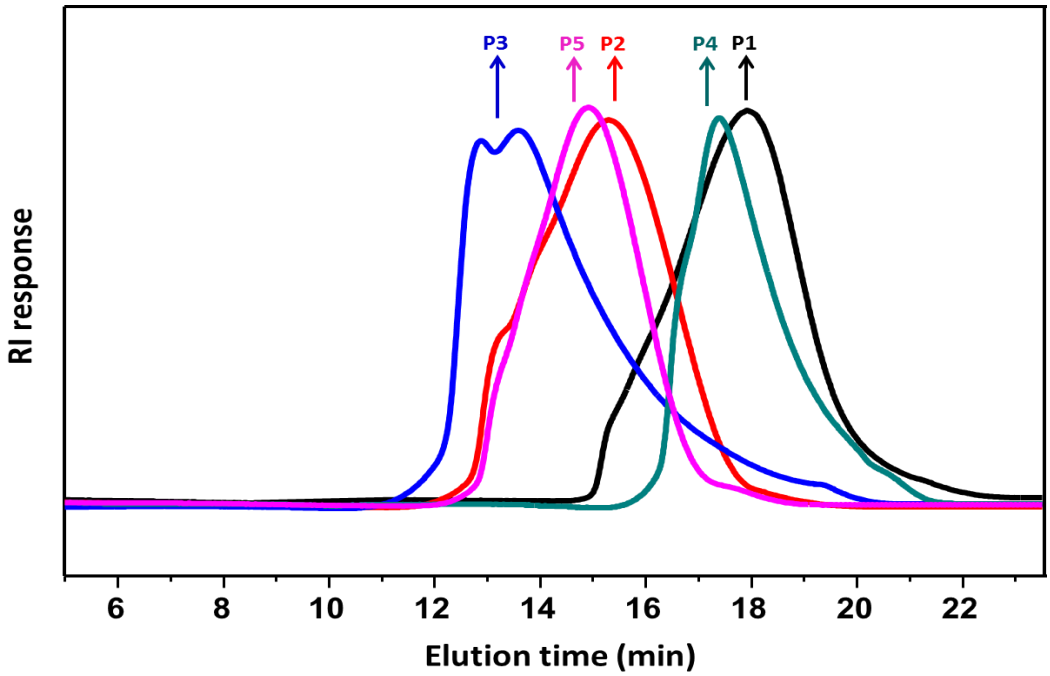

Figure 7.10. *GPC curves of PNVI chains cleaved from PNVI grafted SiNPs by using aqueous HF treatment. For sample identity refer Table 7.1.*

7.3.3 OPBI/SiNP-g-PNVI nanocomposite

The nanocomposites of OPBI are made using SiNP-g-PNVI sample as nanofiller. For the current study, we have used P4 sample as nanofiller and the preparation of nanocomposites are described in the experimental section. Two nanocomposites – 1% and 3% of SiNP-g-PNVI with respect to OPBI weight, were made and their mechanical, conductivity and leaching of PA were compared with pristine OPBI samples.

The storage modules vs temperature plots obtained from dynamical mechanical analysis of the OPBI and OPBI nanocomposite membranes are shown in Fig. 7.11. The plots clearly display a huge reinforcement of mechanical properties for nanocomposite sample across all the temperature and the strength increases with increasing loading. Of course, the reinforcement is more visible in the glassy states than the rubbery state which attributes the different nature of interaction between the OPBI and nanofiller in the glassy and rubbery regions.

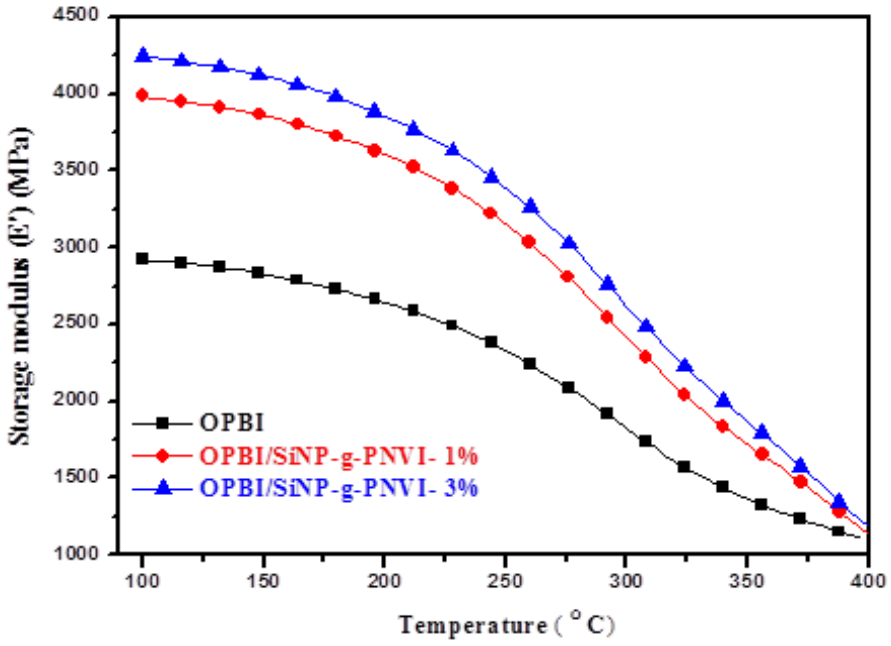

Figure 7.11. *Comparison of mechanical properties of OPBI/SiNP-g-PNVI nanocomposites with pristine OPBI. The storage modules vs temperature plots are obtained from the DMA study.*

The proton conductivities of PA doped membranes were measured as a function of temperature and plotted in Fig. 7.12 (A). The membrane PA loading of OPBI, OPBI/SinP-g-PNVI-1% and OPBI/SinP-g-PNVI-3% samples are 12.3406 (±1.516), 11.984 (±0.854) and

11.6037 (±0.395) moles/OPBI repeating unit, respectively. The higher loading of nanocomposite is due to higher basic character of the sample owing to the presence of PNVI chain. Fig. 7.12 (A) clearly shows the significant increase in proton conductivity of nanocomposite samples compared to pristine OPBI. This is due to the higher PA loading as well as the presence of extra basic site in the nanoparticle significantly increases the conductivity channels which in turn help in better and faster proton conductivity.

Fig. 7.12 (B) clearly displays the less acid leaching in case of nanocomposite than the pristine OPBI. This is because of the higher basic character of nanocomposites samples owing to the presence of PNVI chains and leaching decreases with increasing PNVI wt% in the nanocomposites.

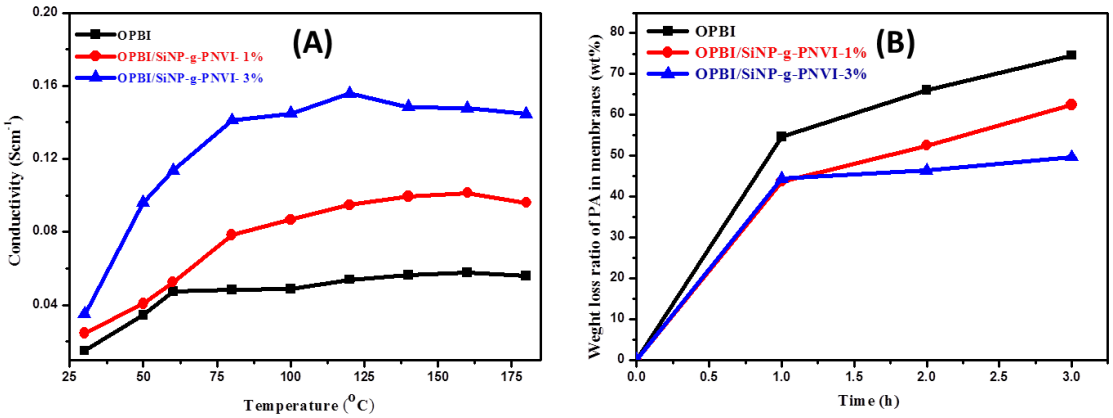

Figure. 7.12: *Proton conductivity vs temperature plots (A) and leaching study vs time plots (B) for OPBI and its nanocomposites with SiNP-g-PNVI nanofiller.*

7.4 Conclusion

In summary, we have demonstrated a simple method to covalently graft poly(N-vinyl imidazole) (PNVI) on the surface of SiNPs. Initially, CPDB RAFT agent anchored SiNPs were prepared, and then a PNVI chain was grown on the surface of SiNP using a *grafting from* RAFT polymerization. The chain length and the chain density of the PNVI on the SiNP surface have been varied. The resulting PNVI grafted SiNP core-shell particles displays narrow size distributions and the size of the PNVI chain on the particle surface can be readily controlled by changing the monomer amount in the polymerization feed. Molecular weights obtained from GPC analysis after cleaving the PNVI from the SiNPs confirms the formation of PNVI grafted SiNPs. The microscopic, spectroscopic, thermal and DLS studies

unequivocally confirm the formation of silica (core) - PNVI (shell) particles. Finally, these particles were used as nanofiller in making nanocomposite with OPBI and resulted OPBI/SiNP-g-PNVI nanocomposite display significantly higher mechanical strength than the pristine OPBI. More interestingly the acid doped nano composite display very high proton conductivity than pristine acid doped OPBI.

References

1. M. Sakurai, T. Imai, F. Yamashita, K. Nakamura and T. Komatsu, *Polym. J.*, 1994, **26**, 658.
2. V. V. Annenkov, E. N. Danilovtseva, H. Tenhu, V. Aseyev, S. P. Hirvonen and A. I. Mikhaleva, *Eur. Polym J.*, 2004, **40**, 1027.
3. S. Yuan, Q. Deng, G. Fang, J. Wu, W. Li and S. Wang, *J. Chromatography B*, 2014, **960**, 239.
4. K. Yin, Z. Zhang, L. Yang and S.-I. Hirano, *J. Power Sources*, 2014, **258**, 150.
5. H. I. Unal, O. Erol and O. Y. Gumus, *Colloids Surf. A: Physicochem. Eng. Asp.*, 2014, **442**, 132.
6. A. Bozkurt and W. H. Meyer, *Solid State Ionics*, 2001, **138**, 259.
7. C. Fodor, B. Gajewska, O. Rifaie-Graham, E. A. Apebende, J. Pollard and N. Bruns, *Polym. Chem.*, 2016, **7**, 6617.
8. S. Yuan, S. O. Pehkonen, B. Liang, Y. P. Ting, K. G. Neoh and E. T. Kang, *Corrosion Science*, 2010, **52**, 1958.
9. K. Yao, Z. Wang, J. Wang and S. Wang, *Chem. Commun.*, 2012, **48**, 1766.
10. Y. Zhou, M. Zhu and S. Li, *J. Mater. Chem. A*, 2014, **2**, 6834.
11. B. Tamami, H. Allahyari, F. Farjadian and S. Ghasemi, *Iran. Polym. J.*, 2011, **20**, 699.
12. M. Takafuji, S. Ide, H. Ihara and Z. Xu, *Chem. Mater.*, 2004, **16**, 1977.
13. M. L. Rañada, M. Akbulut, L. Abad and O. Güven, *Radiat. Phys. Chem.*, 2014, **94**, 93.
14. D. Bertin, D. Gigmes, S. R. A. Marque and P. Tordo, *Chem. Soc. Rev.*, 2011, **40**, 2189.
15. K. Matyjaszewski, *Macromolecules*, 2012, **45**, 4015.
16. G. Moad, E. Rizzardo and S. H. Thang, *Aust. J. Chem.*, 2012, **65**, 985.
17. N. Yeole, S. N. R. Kutcherlapati and T. Jana, *RSC Adv.*, 2014, **4**, 2382.
18. N. Yeole, S. N. R. Kutcherlapati and T. Jana, *J. Colloid Interface Sci.*, 2015, **443**, 137.

19. M. H. Allen Jr, S. T. Hemp, A. E. Smith and T. E. Long, *Macromolecules*, 2012, **45**, 3669.
20. S. Jana, V. A. Vasantha, L. P. Stubbs, A. Parthiban and J. G. Vancso, *J. Polym. Sc.Part A: Polym. Chem.*, 2013, **51**, 3260.
21. J. Li, H. Han, Q. Wang, X. Liu and S. Jiang, *Journal of separation science*, 2010, **33**, 2804.
22. Z. Ajji and A. M. Ali, *J. hazard. mater.*, 2010, **173**, 71.
23. F. Özmen, P. A. Kavaklı and O. Güven, *J. App. Polym. Sci.*, 2011, **119**, 613.
24. A. Chapiro, *Int. J. Rad. Appl. Ins. Part C. Rad. Phy. Chem.*, 1992, **40**, 89.
25. K. Nakabayashi and H. Mori, *Eur. Polym. J.*, 2013, **49**, 2808.
26. M. D. Green, M. H. Allen, J. M. Dennis, D. Salas-de la Cruz, R. Gao, K. I. Winey and T. E. Long, *Eur. Polym. J.*, 2011, **47**, 486.
27. R. Yokoyama, S. Suzuki, K. Shirai, T. Yamauchi, N. Tsubokawa and M. Tsuchimochi, *Eur. Polym. J.*, 2006, **42**, 3221.
28. R. Barbey, L. Lavanant, D. Paripovic, N. Schüwer, C. Sugnaux, S. Tugulu and H.-A. Klok, *Chem. rev.*, 2009, **109**, 5437.
29. S. Singha and T. Jana, *ACS App. Mater. Inter.*, 2014, **6**, 21286.
30. S. Maity, S. Singha and T. Jana, *Polymer*, 2015, **66**, 76.
31. B. Sana and T. Jana, *Eur. Polym. J.*, 2016, **84**, 421.
32. S. Singha and T. Jana, *Polymer*, 2016, **98**, 20
33. A. Lepit, N. A. Aini, N. K. Jaafar, N. Hashim, A. M. M. Ali, K. Z. M. Dahlan and M. Z. A. Yahya, *Int. J. Elec. Sci.*, 2012, **7**, 8560.
34. J. Lobato, P. Canizares, M. A. Rodrigo, J. J. Linares and J. A. Aguilar, *J. Mem. Sci.*, 2007, **306**, 47.
35. S. Ghosh, S. Maity and T. Jana, *J. Mater. Chem.*, 2011, **21**, 14897.
36. Y. Mitsukami, M. S. Donovan, A. B. Lowe and C. L. McCormick, *Macromolecules*, 2001, **34**, 2248.
37. C. L. McCormick and A. B. Lowe, *Acc. Chem. Res.*, 2004, **37**, 312.
38. N. J. Warren, O. O. Mykhaylyk, D. Mahmood, A. J. Ryan and S. P. Armes, *J. Am. Chem. Soc.*, 2014, **136**, 1023.
39. W. Stöber, A. Fink and E. Bohn, *J. Colloid and Interface. Sci.*, 1968, **26**, 62.
40. C. Li, J. Han, C. Y. Ryu and B. C. Benicewicz, *Macromolecules*, 2006, **39**, 3175.

41. D. M. Ratner, E. W. Adams, M. D. Disney and P. H. Seeberger, *ChemBioChem*, 2004, **5**, 1375.
42. E. Oh, D. Lee, Y. P. Kim, S. Y. Cha, D. B. Oh, H. A. Kang, J. Kim and H. S. Kim, *Angew. Chem. Int. Ed.*, 2006, **45**, 7959.
43. C. Bartholome, E. Beyou, E. Bourgeat-Lami, P. Chaumont, F. Lefebvre and N. Zydowicz, *Macromolecules*, 2005, **38**, 1099.
44. V. Darcos, A. Dureault, D. Taton, Y. Gnanou, P. Marchand, A.-M. Caminade, J.-P. Majoral, M. Destarac and F. Leising, *Chem. Commun.*, 2004, 2110.
45. Q. Zheng and C.-y. Pan, *Macromolecules*, 2005, **38**, 6841.
46. A. Rungta, B. Natarajan, T. Neely, D. Dukes, L. S. Schadler and B. C. Benicewicz, *Macromolecules*, 2012, **45**, 9303.
47. Y. Zhao and S. Perrier, *Macromolecules*, 2007, **40**, 9116.
48. N. G. Khaligh, *RSC Advances*, 2013, **3**, 99.
49. B. Wang, H.-J. Liu and Y. Chen, *RSC Advances*, 2016, **6**, 2141.
50. H. Mi, Z. Jiang and J. Kong, *Polymer*, 2013, **5**, 1203.
51. T. Taniguchi, Y. Kunisada, M. Shinohara, M. Kasuya, T. Ogawa, M. Kohri and T. Nakahira, *Colloids. Surf. A: Physicochem. Eng. Aspects*, 2010, **369**, 240.
52. Z. Ge, D. Xie, D. Chen, X. Jiang, Y. Zhang, H. Liu and S. Liu, *Macromolecules*, 2007, **40**, 3538.
53. Y. Guo, H. Liu, D. Tang, C. Li and Y. Zhao, *Polym. Chem.*, 2015, **6**, 2647.

Chapter 8

Summary & Conclusions

8.1. SUMMARY

This thesis entitled **''Development of Polymeric Nanostructures using RAFT Polymerization"** describes the synthesis and characterization of several polymeric nanomaterials and nanocomposites using RAFT polymerization. Applications of these newly developed nanostructured materials in the area of protein binding and polyelectrolyte membrane fuel cell have been studied. Throughout the thesis, efforts have been made in order to improve the synthetic methodologies to prepare polymeric nanomaterials with desired and controlled properties. Collectively, this thesis consists of seven chapters – an introductory chapter followed by methods and experimental chapter and five working chapters. The summary of each chapter is given below.

CHAPTER 1

This chapter deals with a brief introduction of various types of polymeric nanomaterials and their synthetic procedures in detail. In particular, it gives an overview of the variety of methods published so far that are used for the preparation of these materials. The properties and applications of different polymeric nanomaterials such as colloidal nanoparticles, graphene oxide/polymer nanocomposite and glyco polymeric nanomaterials have also been explained in detail. Throughout the discussion, it has been highlighted that the necessity of a process such as controlled radical polymerizations, which can control the preparation of these materials with desired properties. Finally, this chapter describes the scope of the thesis work.

CHAPTER 2

This chapter describes the details of materials that were used for all the working chapters and details of experimental procedures, various instrumentation techniques used for characterization of synthesized polymeric nanomaterials and nanocomposites.

CHAPTER 3

Despite the presence of bulk literature on synthesis of polymeric core-shell nanoparticles, synthesis of this type particle in a simple and one-pot method with variable particles size and core-shell dimension remains a challenging task. In this chapter a simple and robust one-pot synthesis of polystyrene (PS) nanoparticles composed of a poly(hydroxyethyl

methacrylate) (PHEMA) based macro-RAFT (reversible addition fragmentation chain transfer) agent has been developed. Initially generated hydrophilic PHEMA macro-RAFT agents were chain-extended in situ with a hydrophobic monomer (styrene) to form nanoparticles with core–shell morphology in which the PS core is covered with the PHEMA shell. Nanoparticle sizes and the dimensions (thickness) of core and shell were readily tuned by varying hydrophilic monomer (HEMA) concentration and polymerization time for the formation of a PHEMA based macro-RAFT agent. Field emission scanning electron microscopy showed the influence of molecular weight of the hydrophilic macro-RAFT agent on polymer particle size and self-assembly. The results suggested that unreacted HEMA during the nucleation process has a significant influence on the polymer morphology. In summary, we demonstrated that the current strategies can be effectively used to generate core–shell particles along with dimension tuning in a one-pot process.

CHAPTER 4

This chapter demonstrates a simple and robust one-pot method for the preparation of polystyrene (PS)/graphene oxide (GO) nanocomposite using reversible addition fragmentation chain transfer (RAFT) modified GO in surfactant-free emulsion polymerization (SFEP). The results suggested that ionic comonomer, styrene sulfonate sodium salt (SS-Na), concentration played a vital role in forming PS/GO nanocomposite. X-ray and electron diffraction studies suggested that there is no recombination of GO sheets when moderate SS-Na concentration is used, resulting complete exfoliation of GO sheets in the PS/GO nanocomposite. The formation of core–shell particles in which PS is the core and polystyrene sulfonate sodium salt (PSS–Na) is the shell, and the specific interactions between functional groups of GO and PSS–Na were attributed to the driving forces for the PS/GO nanocomposite formation. Efficient dispersibility of GO in water was expected under conditions where the ionic strength due to PSS–Na is low enough to allow polymer particle formation but high enough to provide a sufficient driving force for GO sheets to disperse and forming PS/GO sheet interface.

CHAPTER 5

Here we report a simple and one-pot method for the synthesis of glycopolymer based colloidal particles with tunable core-shell morphology using reversible addition fragmentation chain transfer (RAFT) polymerization. A hydrophilic carbohydrate functionalized monomer (called as glycomonomer) namely allyl-α-D-glucopyranoside (α-Glu) was polymerized with

the RAFT agent to yield a macro-sugar chain, which acts as a macro-RAFT agent, and then this chain was further extended by copolymerizing hydrophobic styrene monomer. The resulted polymer chains consist polystyrene (PS) as a hydrophobic chain and glycopolymer (GP) as a hydrophilic chain. Several microscopic techniques which include FE-SEM, TEM, AFM and confocal Raman imaging proved the formation of core-shell colloidal particle morphology of the synthesized PS-GP in which PS was found in the core of the particle and shell was made up of GP. The tenability in the particle size and in the core (PS)-shell (GP) dimension was achieved by altering the macro-sugar chain length and hydrophilic monomer (sugar) concentration in the polymerization feed. The formation of more number of macro-sugar chain with increasing sugar content in the feed led to the production of a large number of smaller sized micelles in the polymerization medium which yielded smaller size particles. The colloidal stability and the molecular weight of the resulted PS-GP core-shell nanoparticles were found to be dependent upon both macro-RAFT and sugar content in the reaction feed.

CHAPTER 6

Here, we report the synthesis of glycopolymer (GP) grafted silica nanoparticles (SiNP) by using Reversible Addition Fragmentation chain Transfer (RAFT) polymerization through grafting from approach. SiNP nanoparticle surface was decorated by the reaction of activated RAFT with the amino groups of the amine functionalized SiNP. Then, well-defined GP chains with control molecular weights and narrow polydispersities were grown from the RAFT agent anchored SiNP nanoparticle surface using mannosyloxyethyl methacrylate (MEMA) as a monomer and 4,4′-Azobis(4-cyanopentanoic acid) (ACP) as an initiator in two different solvents with a variation of GP chain length. The surface functionalization of GPs on SiNP nanoparticles was confirmed by fourier transform infrared spectroscopy (FTIR), nuclear magnetic resonance spectroscopy (NMR) and thermo gravimetric analysis (TGA). The mean diameter of the glyco nanoparticles (GNPs) was measured by using field emission scanning electron microscope (FE-SEM) and transmission electron microscopy (TEM). The hydrodynamic diameter was obtained by dynamic light scattering (DLS). Hydrolysis of silica cores using aqueous HF enabled characterization of cleaved polymer using GPC. The present approach is straightforward and provides carbohydrate functionalized SiNP nanoparticle. The GP grafted SiNP nanoparticles may prove to be valuable tools for further investigating glycobiological, biomedical, material science applications and especially in our case mannose

functionalized SiNP nanoparticles (GNPs) can be used as targeting cancerous cells. Furthermore, these GPNs were found to be selectively binds with a mannose specific lectin Con A and the binding of GNPs is 300-400 times higher than the only GP chain.

CHAPTER 7

Here, we report the synthesis of poly(N-vinyl imidazole) (PNVI) grafted silica nanoparticles (SiNPs) by using Reversible Addition Fragmentation chain Transfer (RAFT) polymerization through grafting from approach. The introduction of RAFT groups onto the SiNP surface was achieved by the reaction of activated RAFT (4-Cyanopentanoicacid dithiobenzoate ester of N-Hydroxy succinamide, CPDB-NHS) with the amino groups of the amine functionalized SiNP. Then, well-defined PNVI chains with controlled molecular weights and chain densities were grown from the RAFT agent anchored on the SiNP surface using N-vinyl imidazole (NVI) as a monomer and 2,2′-Azobis(2-methylpropionitrile) (AIBN) as an initiator for two different chain densities as well as with a variation of PNVI chain length on the SiNP surface. The surface functionalization of PNVI on SiNP was confirmed by Fourier transform infrared spectroscopy (FT-IR), nuclear magnetic resonance spectroscopy (NMR) and thermogravimetric analysis (TGA). The mean diameter of the PNVI grafted SiNP was measured by using field emission scanning electron microscope (FE-SEM) and transmission electron microscopy (TEM) and found to be alter slightly with the variation of PNVI chain lengths. The molecular weight of PNVI chains were obtained using GPC hydrolysis of silica cores using aqueous HF. The present approach is precious metal-catalyst free, straightforward, and provides PNVI functionalized SiNP in a simple manner. Further, SiNP-grafted-PNVI particles were used as nanofiller to prepare nanocomposites of polybenzimidazole and these PBI nanocomposites displayed better mechanical, proton conductivity and less acid leaching properties than pristine PBI.

CHAPTER 8

This chapter contains summary and conclusion of the thesis. Future scopes of the outcomes of the thesis are discussed.

8.2. CONCLUSIONS

From the above discussion in Chapter 3 to 7 on the topic ‘‘***Development of Polymeric Nanostructures using RAFT Polymerization***” the following conclusions are drawn

1. A simple and robust one-pot method for the synthesis of core–shell colloidal nanoparticles in which the PS core is covered with the PHEMA shell has been developed.
2. Nanoparticle sizes and core-shell dimensions were readily tuned by varying hydrophilic monomer (HEMA) concentration and polymerization time for the formation of a PHEMA based macro-RAFT agent which also has an influence on polymer particle size and self-assembly.
3. The microscopic analysis revealed that the synthesized colloidal nanoparticles are spherical and with narrow PDI distributions as well as they are stable for a longer duration.
4. Polystyrene (PS)/graphene oxide (GO) nanocomposite has been prepared using RAFT modified GO in surfactant-free emulsion polymerization (SFEP) in a simple and one-pot method.
5. The formation of core–shell particles in which PS is the core and polystyrene sulfonate sodium salt (PSS–Na) is the shell and the specific interactions between functional groups of GO and PSS–Na are attributed to the driving forces for the PS/GO nanocomposite formation. The ionic comonomer, SS-Na concentration plays a vital role in forming PS/GO nanocomposite.
6. An RAFT-mediated one-pot synthesis of polymeric core–shell colloidal particles in which the shell consists of the glycopolymer and polystyrene is in the core has been developed.
7. The core–shell particles display a narrow size distribution, the size of the particles and their core-shell dimensions can be readily controlled by changing the macro-sugar chain length as well as the sugar content with respect to the styrene content in the polymerization feed.
8. The controlled synthesis of well-defined core–shell colloidal particles with protein binding glycopolymers on the surface of the particles which may have potential use in designing and developing new carbohydrate-based therapeutics.

9. A simple method to covalently graft glycopolymers (carbohydrates) on the surface of silica nanoparticles has been demonstrated using *grafting from* RAFT polymerization.
10. The formed glycopolymer grafted SiNPs display narrow size distributions and the size of the GP chain on the particle surface can be readily controlled by changing the monomer amount in the polymerization feed.
11. The biochemical activity of glycopolymer grafted SiNPs shows increased binding efficiency than its linear (only glycopolymer) part.
12. Poly(N-vinyl imidazole) grafted SiNPs (SiNP-g-PNVI) has been prepared using a *grafting from* RAFT polymerization with variable chain length and the chain density of the PNVI on the SiNP surface.
13. The nanocomposite of polybenzimidazole (PBI) with SiNP-g-PNVI display significantly higher mechanical strength and proton conductivity than pristine PBI.
14. The nanocomposite membrane shows significant improvement in decreasing of phosphoric acid (PA) leaching from nanocomposite than pristine PBI.

8.3 SCOPE OF FUTURE WORK

The present thesis has addressed several issues in the development of methodologies for the synthesis and surface modification of various polymeric nanomaterials which will be useful in diverse fields ranging from biology to fuel cell using controlled radical polymerization like RAFT. Throughout this study, we have experienced several issues which need to be addressed and more importantly, this thesis work has been motivated us to think in the new directions of making nanostructured materials. We, therefore, believe that the findings from this thesis work hold the enormous scope in the field of polymer chemistry for the development of countless polymeric nanomaterials. Following are the areas which need to be addressed by researchers in future.

1. Different types of colloidal nanoparticles can be synthesized in one-pot by varying hydrophilic and hydrophobic monomers in the reaction feed and study the structure-property relationship using established methods in this thesis.
2. A series of glyconanoparticles with a variation in size and core-shell thickness can be prepared with different glyco monomers in a one-pot SFEP method and study their binding properties with corresponding proteins.

3. Efforts may be made for the synthesis of stable GO/polymer nanocomposites with the help of established methods in this thesis.
4. Varieties of block copolymer nanomaterials can be made using the methods established in this thesis.
5. Efforts can be made to prepare the glycol nanomaterials with verities of glyco monomers and study their binding properties with corresponding proteins.
6. A variety of either di, tri, and more blocks or random copolymers of glyco monomers can be synthesized with verities of glyco monomers and with a variation of chain lengths as well as densities on particle surfaces using established procedures in this thesis
7. Efforts can also be made to prepare the glycol nanomaterials with stimuli responsiveness such as pH, temperature, and light and study their interaction with proteins.
8. Efforts must be made for the preparation of varieties of nanofillers and its nanocomposite with the polybenzimidazole (PBI) matrix to improve the properties such as thermal, mechanical, acid leaching and proton conductivity.
9. Silica nanoparticles can be grafted with appropriate polymer brushes and can be used to make nanocomposites with PBI based polymers which are believed to enhance the properties of PBI greatly.
10. The effect of size and shape of nanoparticles (e.g. spheres, rods or sheets) of the same composition or different composition on the polymer properties can also be studied.
11. Nano clays can be covalently grafted with polymer brushes and can be used to prepare nanocomposites with PBI to improve properties.
12. More systematic efforts must be made to understand the usefulness of newly synthesized nanomaterials in the application side.

DEVELOPMENT OF POLYMERIC NANOSTRUCTURES USING RAFT POLYMERIZATION

ORIGINALITY REPORT

%3	%1	%2	%1
SIMILARITY INDEX	INTERNET SOURCES	PUBLICATIONS	STUDENT PAPERS

PRIMARY SOURCES

1	Yeole, Niranjan, S.N. Raju Kutcherlapati, and Tushar Jana. "Polystyrene–graphene oxide (GO) nanocomposite synthesized by interfacial interactions between RAFT modified GO and core–shell polymeric nanoparticles", Journal of Colloid and Interface Science, 2015. Publication	%1
2	Submitted to University of Aberdeen Student Paper	<%1
3	Yeole, Niranjan, S. N. Raju Kutcherlapati, and Tushar Jana. "Tunable core–shell nanoparticles: macro-RAFT mediated one pot emulsion polymerization", RSC Advances, 2014. Publication	<%1
4	Miller, Kristen P., Lei Wang, Brian C. Benicewicz, and Alan W. Decho. "Inorganic nanoparticles engineered to attack bacteria", Chemical Society Reviews, 2015. Publication	<%1

Publications & Presentations

PUBLICATIONS

1. Tunable Core-Shell Nanoparticles: Macro-RAFT Mediated One-Pot Emulsion Polymerization. Niranjan Yeole, **S. N. Raju Kutcherlapati** and Tushar Jana, ***RSC Adv.***, **2014**, *4*, 2382-2388.

2. Polystyrene-Graphene Oxide (GO) Nanocomposite Synthesized by Interfacial Interactions between RAFT Modified GO and Core-Shell Polymeric Nanoparticles. Niranjan Yeole, **S. N. Raju Kutcherlapati** and Tushar Jana, ***J. Colloid Interface Sci.,*** **2015**, *443*, 137-142.

3. Urease Immobilized Polymer Hydrogel: Long-term Stability and Enhancement of Enzymatic Activity. **S. N. Raju Kutcherlapati**, Niranjan Yeole and Tushar Jana, ***J. Colloid Interface Sci.,*** **2016**, *463*, 164-172.

4. RAFT Mediated One-Pot Synthesis of Glycopolymer Particles with Tunable Core-Shell Morphology. **S. N. Raju Kutcherlapati,** Niranjan Yeole, Madhusudhan Reddy Gadi, Ramu Sridhar Perali and Tushar Jana. ***Polym. Chem., 2017, DOI: 10.1039/c6py02202***

5. Poly(acrylamide) Hydrogel Bio-conjugated with Urease: Storage and Sensing Platform in "NanoAromoring of Enzymes: Rational Design of Polymer-Wrapped Enzymes". Konda Reddy Kunduru, **S. N. Raju Kutcherlapati**, Dhamodaran Arunbabu and Tushar Jana. Editor: C. V. Kumar, ***Elsevier***, 2017. **(Book Chapter)**

6. Glycopolymer Grafted Silicon Nanoparticles: Synthesis using *Grafting-from* RAFT Polymerization and Binding Study with Lectin. **S. N. Raju Kutcherlapati**, Rambabu Koyilapu, Umamaheswara Rao Boddu, Debparna Datta, M. J. Swamy, Ramu Sridhar Perali and Tushar Jana. *(Communicated to **Macromolecules**).*

7. Control Synthesis of Poly(N-Vinylimidazole) grafted Silica Nanoparticles using Grafting from RAFT Polymerization: Tunability of Chain Length and Density. **S. N. Raju Kutcherlapati**, Rambabu Koyilapu and Tushar Jana. *(Manuscript under preparation).*

8. Vesicular and Micellar Self-Assembly of Stimuli Responsive Poly(N-isopropylacrylamide-block-9-anthracene methylmethyacrylate) Amphiphilic diblock Copolymers. Kishor Pawar, **S. N. Raju Kutcherlapati**, Niranjan Yeole, Dilip Hundiwale and Tushar Jana. *(Communicated to **Eur. Polym. J.**).*

9. Synthesis of Poly(NIPAAm-b-NVK) Copolymer via RAFT Polymerization: Stimuli Responsive Morphology in Aqueous Media. Kishor Pawar, **S. N. Raju Kutcherlapati**, Niranjan Yeole, Tushar Jana and Dilip Hundiwale. *(Communicated to **RSC Adv.**)*.

10. Self Crosslinkable Anionic Waterborne Polyurethane Dispersions from Cotton Seed Oil Based Phosphorylated Polyol as Ionic Soft Segment. Sashivinay Kumar Gaddam, **S. N. Raju Kutcherlapati**, Aruna Palanisami. *(Communicated to **ACS Sustain. Chem. Eng.**)*.

11. Syntheses of amphiphilic block copolymers through RAFT polymerization and their application as surf-RAFT agent for the miniemulsion polymerization of styrene. Kishor Pawar, **S. N. Raju Kutcherlapati**, Niranjan Yeole, Tushar Jana and Dilip Hundiwale. *(Manuscript under preparation)*

12. Poly Quaternary Vinylimidazole Grafted Silica Nanoparticles *via Grafting-from* RAFT Polymerization and its Nanocomposite with OPBI with Improved Properties for PEM. Rambabu Koyilapu, **S. N. Raju Kutcherlapati**, Balakondareddy Sana and Tushar Jana. *(Manuscript under preparation).*

Note: Only publication numbers 1, 2, 4, 6 and 7 are included in this thesis as Chapter 3, 4, 5, 6 and 7, respectively.

CONFERENCE PRESENTATIONS

1. Poster presented on *"Well-defined core-shell nanoparticles in one-pot using RAFT polymerization"* at National Symposium on Polymers and Coatings **(NSPC-2012)**, September 7-8, 2012, IICT, Hyderabad, India.

2. Poster presented on *"Tunable core-shell nanoparticles: Macro-RAFT mediated one pot emulsion polymerization"* during Inter National conference conducted by Asian Polymer Association **(APA 2013)**, February 21-23, 2013, Punjab University, Chandigarh, India.

3. Poster presented on *"Urease Immobilized Polymer Hydrogel: Long-term Stability and Enhancement of Enzymatic Activity in Ambient Condition"* at 3rd FAPS Polymer Congress **(MACRO-2013)**, May 15-18, 2013, IISC, Bangalore, India.

4. Poster presented on *"Synthesis of Polystyrene-Graphene Oxide (PS/GO) Nanocomposites Using RAFT Polymerization"* at Recent Advances in Polymer Technology **(RAPT-2014)**, January 22-24, 2014, University of Calcutta, India.

5. Poster presented on *"Role of Ionic Co-monomer in Polystyrene-Graphene Oxide (PS/GO) Nanocomposites Synthesis Using RAFT Polymerization"* during National Symposium on Polymers and Coatings **(NSPC-2014)**, April 25-26, 2014, IICT, Hyderabad, India. **(Received best poster award)**

6. Poster presented on *"Glyconanoparticles with Tunable Core-Shell Morphology via RAFT Polymerization"* at Polymers on the Frontiers of Science and Technology **(APA 2015)**, October 29-31, 2015, Saurashtra University, Rajkot, India. **(Received best poster award)**

7. Poster Presented on *"RAFT mediated one-pot synthesis of glycopolymer particles with tunable core-shell morphology"* at 4th FAPS Polymer Congress **(4 FAPS-IPC 2015)**, October 5-8, 2015, **Kuala Lumpur. Malaysia.**

8. Oral talk presented on *"One pot method for the synthesis of glyconanoparticles with tunable core-shell morphology via RAFT polymerization"* in National symposium on Advances in Polymeric Materials **(NSAPM-2016)**, February 5-6, 2016, Sri Krishnadevaraya University, Ananthapuram, India. **(Received best oral award)**

9. Oral talk presented on *"Glyconanoparticles in one pot RAFT method"* during 13th Annual in-house Symposium **(CHEMFEST 2016)**, February 20-21, 2016, School of Chemistry, University of Hyderabad, Hyderabad, India.

10. Oral talk presented on *"Lectin Binding Glycopolymer Grafted Silica Nanoparticles using Grafting from RAFT Polymerization" during* **(ICAFM 2017)**, January 06-08 Jan 2017, Chennai, India.

11. Oral talk presented on *"Synthesis of Glycopolymer Coated Silica Nanoparticles using Grafting from RAFT Polymerization"* during **(MACRO 2017),** January 08-11 Jan 2017, Kerala, India.